Effect of Sodium Monofluorophosphate Treatment on Blast Furnace Slag Cement Paste Microstructure

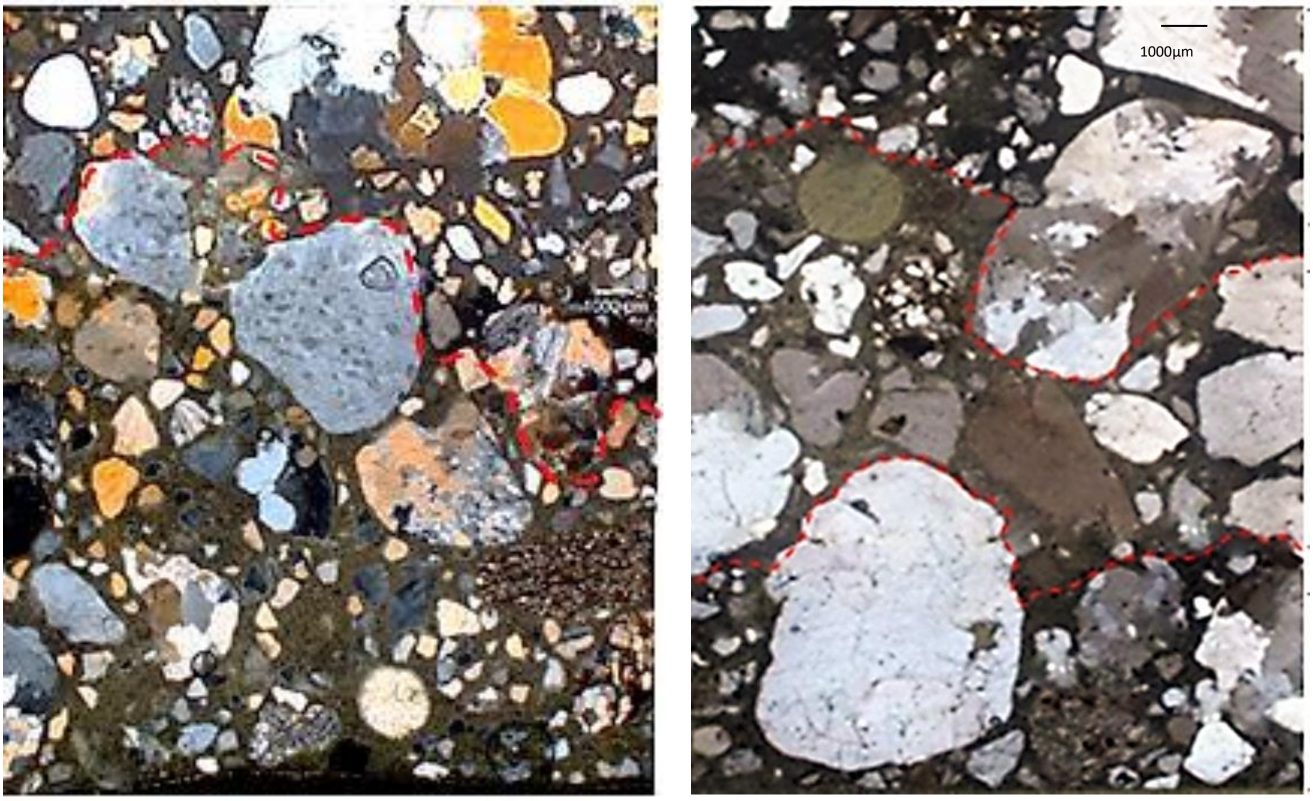

MSc Thesis

By Sawsan G.A. Hulsman-Khalil

2017

Effect of Sodium Monofluorophosphate Treatment on Blast Furnace Slag Cement Paste Microstructure

By

Sawsan G.A. Hulsman-Khalil

In partial fulfilment of the requirements for the degree of

Master of Science
In Materials Science and Engineering

At the Delft University of Technology,
To be defended publicly on Friday, January 20, 2017, at 2:00 PM

Supervisor:	Dr. O. Çopuroğlu	TU Delft
Thesis committee:	Prof. dr. R.B. Polder	TU Delft
	Dr. ir. S. Grünewald	TU Delft

Preface

This thesis presents my research on the effect of sodium monofluorophosphate treatment on slag cement paste microstructure. The research was part of the master program in Civil Engineering and Geosciences at Delft University of Technology and the experiments included has been carried out mainly in the Microlab and Stevin II lab I would like to express my gratitude towards all my thesis committee members Dr. O. Çopuroğlu, Prof. Dr. R.B. Polder and Dr. ir. S. Grünewald for their constructive comments, valuable suggestions and their inputs for helping me improve my technical writing skills. I would like to thank especially my supervisor Dr. O. Çopuroğlu for his guidance, support and motivation throughout the whole process of the work.

I am also thankful to Gerrit Nagtegaal, Arjan Thijssen and John van den Berg from Microlab for guiding and assisting me during the experiments. In addition, I would like to thank Dr. Ir. Josepha Kempl for her help to start my work and the experiments.

Further, I thank my husband and my children for their constant support and encouragement. I thank especially my daughter for her great support in helping me improve my writing and program using Matlab to analyse my data.

"*Where were you when I laid the foundation of the earth?*
Tell me, if you have understanding. Surely, you know! "
(Job 38:4)

Summary

Blast Furnace Slag (BFS) is a latently hydraulic material used as additive or substitute for Portland cement. The market share for BFS cement in the Netherlands is currently more than 60%. Previous research proved the high resistance of slag-rich concrete in aggressive environments such as exposure to acid, chloride ingress or sulphate attack, but also the poor resistance against carbonation. The carbonation of a Blast Furnace Slag (BFS) cement paste involves the conversion of calcium silicate hydrate gel (also known as C-S-H) to porous silicate hydrates. As a result, it can be expected that the strength of the matrix decreases. Consequently, the carbonated BFS concrete is vulnerable to scaling under the combined load of freezing–thawing and de-icing salt. The disintegration of the concrete surface results in a higher vulnerability to other chemical attacks decreasing its durability.

Sodium monofluorophosphate (Na-MFP) gained attention as surface treatment as a corrosion inhibitor. Recent studies revealed the recovering effect of Na-MFP on the microstructure of carbonated BFSC pastes with respect to their frost-salt scaling durability. Recently published, a study by Kempl and Çopuroğlu (2016) indicated that the impregnation of hardened carbonated cement pastes with aqueous Na-MFP resulted in a recovery of the initial pH of 98.85% and 79.81%, of an untreated cement paste for CEM I and CEM III/B, respectively. Their results brought insights on the reaction of Na-MFP solution with the cement matrix carbonated or non-carbonated.

The goal of this thesis was to investigate the influence of applying sodium monofluorophosphate (Na-MFP) on the microstructural and micromechanical properties upon a surface treatment for carbonated BFS cement with different slag concentrations. The main objective of this study is split into two parts: 1) to investigate the penetration of 25% Na-MFP solution as surface treatment into the CEM III /B cement mortar or cement paste under different curing conditions and carbonation periods, and 2) to characterize the influence of the solution on the micromechanics and microstructure of the cement paste samples. The cement types used in this study were:

1. Ordinary Portland Cement (CEM I 42,5 N) which serves as a reference
2. Blast Furnace Slag Cement with a slag content of 67% (CEM III/B 42,5 N HSR LH)
3. Ternary blended cement (SP Mix) with a slag content of 55%, 30% CEM I 52,5 R and 15% fly ash.

For the first part of the study polarized light microscopy (PLM), Scanning Electron Microscopy (SEM) with Energy Dispersive X-Ray Analysis (EDX) and stereomicroscope were used for analysing the penetration of the Na-MFP solution into the cement matrix from the surface. For the second part, analysing the effect of the Na-MFP solution on the microstructure of the cement paste the following tests was applied: Nano-indentation (NI), Mercury Intrusion Porosimetry (MIP), and Thermogravimetric Analysis/Differential Scanning Calorimetry (TGA/DSC).

The penetration results indicate that applying the Na-MFP solution once on the surface after the CEM III /B mortar sample (W/C=0.45) was carbonated was more effective than before carbonation. The penetration depth increased at increasing carbonation period. The curing methods, wet or sealed, do not show a significant influence on the penetration depth. The penetration depth for mortar samples was higher compared to the paste sample with the same water-cement ratio (W/C), cement type and carbonation period. Applying the Na-MFP solution on the surface of ternary blended cement paste, as used in the research (SP Mix), resulted in a higher resistance to carbonation compared to slag cement paste with the same W/C and carbonation period.

The results of the microstructure analysis showed that the Na-MFP solution improved the strength (the elastic modulus and the hardness), permeability (decrease in the porosity) and provided high resistance against carbonation. The study showed that applying the Na-MFP solution before carbonation increased the porosity for the CEM III/B and SP Mix cement paste especially, with W/C =0.6. The recover capillary porosity due to carbonation was 38% and 26% for CEM III/B and SP MIX cement paste, respectively.

In conclusion, the microstructural properties of the treated cement matrix were affected by the water - cement ratio in conjunction with the condition of the cement paste, whether the sample was carbonated or non-carbonated.

Abbreviations

BFS	Blast Furnace Slag
CH	Calcium Hydroxide
C-S-H	Calcium Silicate Hydrate
d	Diameter of a pore
DSC	Differential Scanning Calorimetry
EDX	Energy Dispersive X-ray analysis system
ESEM	Environmental Scanning Electron Microscope
MIP	Mercury Intrusion Porosimetry
Na-MFP	Sodium monofluorophosphate, Na_2PO_3F
NI	Nano-indentation
OPC	Ordinary Portland Cement
P	Pressure
PLM	Polarized Light Microscopy
RH	Relative Humidity
S/C	Sand-to-cement ratio
TGA	Thermogravimetric Analysis
W/C	Water cement ratio
θ	Contact angle of a liquid
ϒ	Surface tension of a liquid

Contents

List of figures

List of tables

1. Introduction

1.1. Context

Blast Furnace Slag (BFS) is a by-product of pig iron manufacturing. It is a latent hydraulic material which can exhibit hydraulic activity and can be used as an additive or as a substitute for Portland cement. Slag-bearing cement production is the second main group of cement beside Portland cement (Heinemann, 2013).

In the Netherlands, the first use of Blast Furnace Slag cement for the marine structures was during the mid-1920s. Since then intensive research has been executed result in expanding the use of the cement with a high slag content, comparable to the European CEM III /B (66-90% slag) as defined in EN 197-1 (2011) for different infrastructures including marine structures.

In a recently published report on the Dutch experience in using slag cement concrete, it is reported that in practice CEM III /B in the Netherlands contains typically about 70-72 % GGBS.
The market share for BFS cement in the Netherlands currently is more than 60% and the annual production of slag cement concrete is about 10 million cubic meters (Polder et al., 2014).

Although it has been proven that slag-rich concrete has a high resistance against aggressive environment; e.g. exposure to acid, chloride ingress and sulphate attack, it is also known that slag-rich concrete has a poor resistance against carbonation and frost-salt scaling (Çopuroğlu, 2006).

A study on the application of Sodium mono-fluorophosphate (Na-MFP) has been excluded in order to improve the frost durability of carbonated slag-rich concrete. Favorable results have been obtained with respect to healing carbonation damage in slag-rich concrete in accelerated and natural conditions. However, further characterization of the effects of Na-MFP application on the microstructure of slag-rich cementitious systems is still needed (Çopuroğlu et al., 2006).

1.2. Research background

Concrete containing blast furnace slag (BFS) is less permeable and chemically more stable than concrete with only Portland cement. The resistance to many forms of deleterious attack is enhanced, in particular: chloride related corrosion of reinforcement, sulfate-acid attack and alkali-silica reaction (Song et al., 2006).

However, previous investigations reported that concrete containing a high percentage of BFS seems to be more prone to damage caused by freeze-thaw in combination with de-icing salt than Ordinary Portland Cement (OPC) (Çopuroğlu, 2006; Polder et al., 2014).This is related to the fact that slag cement and OPC concretes perform differently when subjected to carbonation. While carbonation leads to a slight densification of the microstructure in OPC concrete, the pore structure of slag cement concrete becomes coarser.

The carbonation process leads to the conversion of all or part of the portlandite and C–S–H present in the cement paste into calcium carbonate and a liberation of porous silicate-hydrate from C–S–H (Son Tung Pham et al., 2014).

The vulnerability of BFS concrete to carbonation was attributed to the high permeability and the low CH content. Besides CH, other hydration products were also decalcified and because of the low Ca/Si ratio of these hydration products, BFS concrete is especially vulnerable to carbonation shrinkage (Elke Gruyaert et al., 2013). Consequently, carbonation (shrinkage) of the slag cement paste leads to a reduction in the solid volume, while in OPC paste an increase occurs. The carbonation of calcium hydroxide mainly leads to the formation of calcite with high specific volume while carbonation of C-S-H produces aragonite formation with lower specific volume (Çopuroğlu, 2006). As a result, it can be expected that the strength of the carbonated matrix will be reduced. Consequently, the carbonated BFS concrete is vulnerable to scaling under the combined load of freezing–thawing and de-icing salts. In conjunction with concrete surface disintegration, another type of chemical attack on the structure is possible, which can result in a dramatic decrease in durability (Chaussadent et al., 2006).

Sodium mono-fluorophosphate has been used as a corrosion inhibitor for concrete reinforcements for the last 20 years (Andrade et al., 1992; Larosa-Thomson et al., 1997). It was applied on the surface of the concrete with slag cement in the form of an aqueous solution with concentrations between 10% and 20%. The effectiveness of Na-MFP, when applied to the surface of a concrete structure is based on both its diffusion into the concrete pore network and its effect on the steel reinforcement surface (Chaussadent et al., 2006). Previous reports proved that complex interactions take place between Na-MFP and hardened Ordinary Portland Cement (OPC) paste components, especially $Ca(OH)_2$ thus producing an amorphous gel and modifying the transport properties of the concrete (Andrade et al., 1992).

A recent work by Kempl and Çopuroğlu (2016) showed that the addition of Na-MFP can recover the pH of carbonated cement pastes and can be used as a healing agent as well as a corrosion inhibitor. The results related to the effect of the of Na-MFP concentrations on the pH are presented in Table 1 (Kempl et al., 2016).

Table 1: Effect of the concentration of Na-MFP on the pH according to Kempl and Çopuroğlu (2016)

Sample Code	Treatment sequence	pH
CEM III-11	CC+10% Na-MFP impregnate.	9.4
CEM III-05	CC+20% Na-MFP impregnate.	11.4
CEM III-14	CC+25% Na-MFP impregnate.	10.2
CEM III-08	CC+45% Na-MFP impregnate.	11.7

In the light of the discussed literature, the current investigation was initiated to answer the following question: What are the effects of Na-MFP on the micromechanical and microstructure properties of slag based cementitious materials.

1.3. Aim and objectives of this research

The aim of this research is to characterize the effect of sodium mono-fluorophosphate solution on carbonated slag rich cement paste. In order to achieve this aim, and as main objectives the following was assessed:

- Carbonation depth of treated slag-rich cement systems with Na-MFP solution before or after exposure to accelerated carbonation;
- The penetration depth of Na-MFP solution into slag-rich cement systems which were treated before or after exposure to accelerated carbonation;
- Characterization of the microstructure of the different cement pastes before and after the treatment.

1.4. Research strategy

In order to reach the objectives of the research first a literature survey was conducted and secondly, lab experiments were carried out with the following focus:

1. Quantifying the carbonation depth of the treated samples using polarized light microscopy on thin sections and quantifying the penetration of the Na-MFP solution into the cement matrix using SEM/EDS;
2. Characterising the effect of the treatment on the microstructure of the cement paste using the following test methodology:
    - Nanoindentation to characterize the effect of the treatment on the mechanical properties of the slag-rich cement system microstructure;
    - MIP analysis to measure the porosity of the matrix for the cement paste samples;
    - Thermal gravimetric analysis/Differential Scanning Calorimeters (TGA/DSC) to measure the weight loss due to the dehydration of hydrated phases such as calcium hydroxide (CH) and decarbonation of calcium carbonate ($CaCO_3$).

2. Literature survey

In this chapter, first a brief history of the use of blast furnace slag cement in infrastructures, followed by its properties, durability, the carbonation resistance and the effect of slag content on the properties of cement. Secondly, brief information of ternary blended cement, its benefits and effects of concrete.

2.1. Blast furnace slag (BFS) and slag cement

Blast furnace slag cement has a long history of successful use all over the world. The use of (GGBF) slag as a cementitious material dates back to 1774 when Loriot made a mortar using GGBF slag in combination with slaked lime(Bell et al., 1995).

In 1865, commercial production of lime activated GGBF slag had been used in Germany and by 1880 (GGBF) slag was being used with Portland cement as the activator. In Europe, with its many blast furnaces and steel industries has used (GGBF) slag extensively in all manner of structures. By 1914, GGBS was being manufactured in Scotland. In Britain, over 2 million tons of GGBS is used every year.(Ecocem, 2016)

In The Netherlands, the first marine structure in which blast furnace slag cement was used for part of the concrete mixtures was the lock Noordersluis in the North Sea canal at IJmuiden built in the mid-1920. Currently, the market share for GGBS cement about 60 % and about 10 million cubic meters of slag cement concrete are produced annually (Polder et al., 2014).

2.1.1. Production and types of slag

Blast furnace slag is formed as a liquid at 1350-1550°C in the manufacture of iron; limestone reacts with materials rich in SiO_2 and Al_2O_3 associated with the ore or present in ash from the coke. Blast furnace slag contains sufficient silica and alumina and shows hydraulic properties if it is ground to obtain the fine-grained structure. The main components of slag are CaO (30-50%), SiO_2 (28-38%), Al_2O_3 (8-24%), and MgO (1-18%) by weight (Taylor, 1990). Figure 1 shows the production details of slag in the blast furnace.

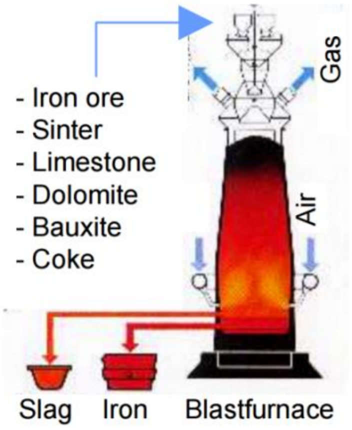

Figure 1: Blast furnace (Euroslag, 2003)

Through the production of slag, there are three main types of BFS, categorized by the way of cooling and granulation (Chen, 2006). These types are:

1. Blast Furnace Slag (BFS): It is a glassy granular material containing more than 95% of the glass. Normally, they are ground to fine powder. Grinding reduces the particle size to cement fineness, allowing its use as a supplementary cementitious material in concrete.
2. Pelletized slag contains much less glass content compared to BFS, as low as 50 percent.
3. Air-cooled slag is hard and dense and normally used for road bases, railway ballast, and asphalt paving and concrete aggregate.

Blast Furnace Slag cement (BFSC), or slag cement is commonly manufactured by integrating BS with cement clinker or by separate grinding (Divsholi et al., 2014).

In fine particle form, slag cement displays cementitious qualities similar to those of ordinary portland cement (OPC). Therefore, slag cement can be substituted for OPC in a wide range of equal mass replacement ratios (LaBarca et al., 2007).

The Slag content of slag cement varied through time as presented in Table 2.

Table 2: change of Slag content of slag cement through the years (Polder et al., 2014)

Year		Content of slag	Content of Portland	Standard (year)
Before 1933		70-85 %	30-15 %	
1933		31-85 %	69-15 %	Dutch standard N 484
1995	CEM III/A	36-65 %	64-35 %	Dutch standard NEN 3550
	CEM III/B	66-80 %	34-20%	
2011	CEM III/A	35-65 %	35-64%	NEN-EN 197-1
	CEM III/B	66-80 %	20-34%	

In practice CEM III /B in the Netherlands contains typically about 70-72% GGBS. In the 1990s, CEM III /A 52.5 R with 52-57% GGBS and increased early strength was introduced in the Netherlands, aiming at the precast industry. In 2000, separate GGBS for addition to Portland cement at concrete mixing plants has become available. This is regulated by national guidelines BRL 9325 (2006) and BRL 9340 (2007) (Polder et al., 2014). Table 3 present the European standard for a cement composition.

Table 3: European standards EN 197-1 Cement Composition

Cement Type	Designation	Notation	Clinker K	G.G.B.S. S	Silica fume D	Pozzolana		Fly ashes		Burnt Shale T	Limestone		Minor Additional consist
						Natural P	Industrial Q	Silica. V	Calcar W		L	LL	
I	Portland Cement	I	95-100										0-5
II	Portland Slag Cement	II / A-S II / B-S	80-94 65-79	6-20 21-35									0-5 0-5
	Portland Silica Fume Cement	II / A-D	90-94		6-10								0-5
	Portland Pozzolana Cement	II / A-P II / B-P II / A-Q II / B-Q	80-94 65-79 80-94 65-79			6-20 21-35 - -	- - 6-20 21-35						0-5 0-5 0-5 0-5
	Portland Fly Ash Cement	II / A-V II / B-V II / A-W II / B-W	80-94 65-79 80-94 65-79					6-20 21-35	6-20 21-35				0-5 0-5 0-5 0-5
	Portland Burnt Shale Cement	II / A-T II / B-T	80-94 65-79							6-20 21-35			0-5 0-5
	Portland Composite Cement	II / A-L II / B-L II / A-LL II / B-L	80-94 65-79 80-94 65-79								6-20 21-35	6-20 21-35	0-5 0-5 0-5 0-5
	Portland Composite Cement	II / A-M II / B-M	80-94 65-79	<--6-20--- > <---21-35-- >									
III	**Blastfurnace Cement**	**III/A** **III/B** **III/C**	**35-64** **20-34** **5-19**	**35-65** **66-80** **81-95**									**0-5** **0-5** **0-5**
IV	Pozzolanic Cement	IV/A IV/B	65-89 45-64	- -	<----------------11-35---------------- > <---------------36-55---------------->								0-5 0-5
V	Composite Cement	V/A V/B	40-64 20-39	18-30 31-50		<-------------18-30--------- > <-----------31-50------------ >							0-5 0-5

2.1.2. Properties of blast furnace slag

Physical Properties

Blast furnace slag is one of the admixtures in the production of concrete to produce a durable concrete. For a durable concrete, it is important that the concrete is dense and impermeable to liquids and gases and that it has a high resistance to the penetration of sulphates and chlorides. One of the important physical parameters of slag is the particle size (fineness) of the slag. The BS EN 15167-1 requires that the minimum specific surface area of GGBS shall be $275m^2/Kg$.

There are many research and studies that have proven that the finer the particle size the larger the pozzolanic activity of the slag particles (Binici et al., 2007). Other researchers reported that an increase in fineness of two to three times that of ordinary PC can give a better performance and properties such as bleeding, time of setting, heat evolution, high strength, and better durability (Pal et al., 2003).

Chemical Properties

The major oxides in the BFS are lime (CaO), silica (SiO_2), alumina (Al_2O_3), magnesia (MgO) and some others (SO_3, FeO or Fe_2O_3, TiO_2, K_2O, Na_2O, etc.) in minor amounts. While the oxide composition of BFS can vary from one blast furnace to another, the product from one blast furnace remains relatively consistent. Compared to the typical oxide composition of clinker, BFS generally contains less lime, more silica, alumina, and magnesia than clinker (Taylor, 1990).Table 4 present the chemical compositions of 27 blast furnace slag produced in France and Luxembourg in 1980 and their chemical compositions.

Table 4: Chemical compositions of 27 blast furnace slag produced in France and Luxembourg in 1980 (Taylor, 1990)

	Mean	**Minimum**	**Maximum**		**Mean**	**Minimum**	**Maximum**
Na_2O	0.39	0.25	0.50	TiO_2	0.55	0.49	0.65
MgO	5.99	3.63	8.66	MnO	0.64	0.34	1.31
Al_2O_3	13.29	10.26	16.01	FeO	1.24	0.29	9.32
SiO_2	33.48	31.96	37.29	S^{2-}	0.94	0.68	1.25
P_2O_5	0.13	0.00	0.34	F^-	0.16	0.06	0.31
SO_3	0.04	0.00	0.19	Cl^-	0.02	0.00	0.05
K_2O	0.70	0.44	0.98	Ign.Loss	0.42	0.00	1.04
CaO	42.24	37.92	44.38	Total	99.68		

The chemical composition of the slag plays a key role in the hydraulic activities of the slag. According to European Standard EN 15167-1, the ratio of the mass of CaO + MgO to the mass of SiO_2 must exceed 1.0. This ratio assures high alkalinity, without which the slag would be hydraulically inactive.

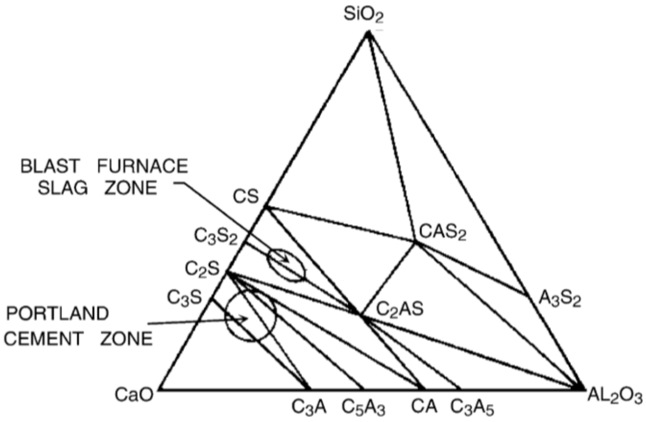

Figure 2: Ternary diagram indicating composition of PC and BFS in the CaO–SiO_2–Al_2O_3 (Pal et al., 2003)

The hydration of slag cement is an interfering process between the Ordinary Portland Cement (OPC) and the slag. The slag is activated by the alkalis and CH produced by the PC hydration and consumes a large amount of CH as well. When BFS is mixed with water, the initial hydration is much slower than PC mixed with water. The hydration of BFS consumes calcium hydroxide and uses it for additional CSH formation (Chen, 2006).

The reaction of the cement and slag:

Cement +H_2O → C-S-H + $Ca(OH)_2$ Cement hydration product

Slag +H_2O +$Ca(OH)_2$ → C-S-H Pozzolanic reaction (secondary pozzolanic)

The secondary pozzolanic reactions can result in reduced pore connectivity and make the concrete denser. The ternary diagram in Figure 2 shows the location of PC and BFS (Pal et al., 2003).

Durability of cementitious blast furnace slag products

Structural concretes containing up to 50% of slag as cementitious material are considered suitable for the same uses, in ordinary and mild exposure applications, as ordinary Portland cement (OPC) concretes of the same design strength. Rates of carbonation and permeability to gaseous species are likely to be similar (Osborne, 1999).

Slag-rich concrete with about 70% slag content has a higher durability performance compared to OPC at same condition in reducing the risk of sulphate attack, alkali–silica reactions and chloride penetration and can increase the compressive strength(Sabet Divsholi et al., 2014).

In mass concrete substantial reductions in the rate of temperature rise, overall heat release and peak temperatures in concretes can be achieved by using slag- rich concrete, thereby minimizing the risk of thermal cracking (Osborne, 1999).

On the other hand, slag-rich concrete has a poor resistance to carbonation. After carbonation attack, slag-rich concrete is vulnerable to scaling under the combined load of freezing-thawing and de-icing salt. This could lead to a surface disintegration and other attacks on the structure are more likely which can result in decrease in durability (Sisomphon et al., 2010)

Carbonation of slag cement

Carbonation attack is a common type of attack in concrete. As known from literature the process begins when CO_2 penetrates into the cement matrix, dissolving in the pore solution and produce HCO_3^- and CO_3^{2-} ions. This will react with Ca^{2+} from calcium hydroxide (CH), calcium silicate hydrate (C–S–H) and the hydrated calcium aluminates and ferro aluminates to precipitate as various forms of calcium carbonate ($CaCO_3$), silica gel and hydrated aluminium and iron oxides (Borges et al., 2009). First, a reduction of porosity is expected because CH is the first phase attacked and the volume of the carbonates (calcite) formed is 11–12% greater than the volume of CH. Therefore, an increase in the weight of carbonated samples can be expected, as well as lower porosity and higher compressive strength at early ages of carbonation (Chi et al., 2002).

The main reactions of carbonation in cement are:

$$\mathrm{Ca\,(OH)_2 + CO_2 + H_2O \rightarrow CaCO_3 + H_2O}$$

$$C - S - H + CO_2 \rightarrow CaCO_3 + H_2O + SiO_2.H_2O$$

The first reaction will cause small volume expansion and as the reaction proceeds, the second reaction will cause a serious shrinkage and reduce the strength.

The effect of the partial replacement of the OPC with slag on carbonation will concern the binding capacity of CO_2 and the porosity of the matrix. In slag cement, the quantity of CH is less than with OPC and because of that; the carbonation of slag cement transforms the C-S-H to porous silicate hydrate. This will lead to a reduction of the compressive strength in carbonated slag cement concrete if the slag content is more than 40% by weight (Sisomphon et al., 2007).

2.2. Ternary blends containing slag cement and fly ash

A ternary mixture is one that contains portland cement and two other materials in the binder. The materials included may be interground limestone or supplementary cementitious materials (SCMs) such as slag cement, fly ash, silica fume, or metakaolin (Taylor, 2014).

Fly ash is a by-product of burning pulverized coal in an electrical power generating station. Particularly, it is the unburned residue that is carried away from the burning zone in the boiler by the flue gases and then collected by either mechanical or electrostatic separators (Thomas, 2007).
Fly ash is a pozzolanic material which, when mixed with portland cement and water, will react with the calcium hydroxide released by the hydration of portland cement to produce various calcium-silicate-hydrates (C-S-H) and calcium aluminate hydrates. These pozzolanic reactions are beneficial to the concrete because it increases the quantity of the cementitious binder phase (C-S-H) which improve the long-term strength and reducing the permeability and improve the durability of the concrete (Bharatkumar et al., 2005).

Most studies look at binary blends of the powders (Portland cement + secondary/filler powder), however, a great amount of research has also been done, over the past two decades, looking at concrete with ternary and quaternary blended binders (Shams, 2014).
The main intentions behind combining different additions were to see whether it is possible to combine the benefits of each addition and, in some cases, to see whether one addition can compensate for the shortcoming of the other.
The durability of the ternary cement depends on the content of the design mixture. Li (2003) studied the influence of the combination of fly ash (FA) and ground granulated blast-furnace slag (GGBS) on the properties of high-strength concrete. The concrete (GGFAC) used in his study incorporating a combination of 15% GGBS, 25% FA and 60% OPC. Li proved that GGFAC presents an excellent behavior in both short- and long-term compressive strengths and in resistance to sulphate attack.Though HFAC has a high long-term strength, its early-age strength is low. Ordinary portland cement concrete has the lowest long-term compressive strength and is poor against H2SO4 attack (Gengying Li et al., 2003).

Another study by Hale (2008) showed that replacements rates of 15% for fly ash and 25% for slag cement improved long-term concrete properties without much sacrifice in early age properties. However, it must be noted that replacement rates of 15–20% fly ash have been shown to increase expansion related to alkali-silica reaction (ASR) (Hale et al., 2008).

The effects of high calcium fly ash in combination with slag were analysed in previous studies. Jozwiak (2012) proved in his study that concretes made with ternary cement containing both high calcium fly ash and GGBS (28.6%) showed a slight increase in carbonation depth comparable with CEM I, but when the content was 50% or more it resulted in a sudden increase of carbonation depth (Chuanlin et al., 2015).
Tikalsky et al (2007-2011) reported that from the studies and the information they gathered they claimed that there are few technical barriers to delivering ternary concrete mixtures with required performance parameters. They conclude that the effects of the mixtures could be predicted from knowledge of the effects of the individual ingredients. They also investigated the side effect and interactions between the ingredients which could lead to positive or negative synergies (Tikalsky et al., 2011; Tikalsky et al., 2007).

Polder et al (2002) tested a concretes made with composite cement according to the European standards EN 197-1, CEM V/A (S-V), containing 25% slag, 25% fly ash and 50 % OPC (see Table 6).

Their result showed that this mix combination produces low chloride migration coefficients and high resistivity (Polder et al., 2002)

In the Netherlands, there are other combinations used according to “CUR Aanbeveling 89” see Table 5. CUR Recommendation 89 indicates that the damage of ASR in concrete can be prevented by using the concrete composition they recommended (Haverkort, 2015).

Table 5: Combination of slag, fly ash and cement as found in general in the Netherlands

Slag	fly ash	CEM I 52,5R
55%	15%	30%
30%	25%	45%
70%	0%	30%
35%	5%	60%

Table 6:European standards EN 197-1 Cement Composition (Cement type V)

Cement Type	Designation	Notation	Clinker K	G.G.B.S. S	Silica fume D	Pozzolana		Fly ashes		Burnt Shale T	Limestone		Minor Additional consist
						Natural P	Industrial Q	Silica. V	Calcar W		L	LL	
V	Composite Cement	V/A	40-64	18-30		<-------------18-30--------- >							0-5
		V/B	20-39	31-50		<-----------31-50------------ >							0-5

2.3. Sodium mono-fluorophosphate (Na_2PO_3F)

The application of Sodium mono-fluorophosphate (Na-MFP) on concrete has been developed through the years. First, Na-MFP was used in the harsh Canadian winters in 1984 as an additive to road de-icing salts (sodium chloride) in order to protect reinforced concrete highway structures from the aggressive action of the chlorides (Anstice, 2000). An aqueous solution of Na-MFP is applied to structures suffering from reinforcement corrosion by means of repeated spraying, brushing or by rolling it on the concrete surface. Important applications are Na-MFP as a corrosion inhibitor and Na-MFP as a healing agent which will be explained here.

A typical commercial Na-MFP product has the composition presented in Table X (Shanghai Pengkai Chem Co. Ltd., 2015):

Table 7: Composition of a typical commercial Na-MFP product

	Chemical notation	Amount	Min/Max
Sodium mono-fluorophosphate	(Na_2PO_3F)	98 %	Min
Total phosphorus	(base on P_2O_5)	49%	Min
Total fluorine	(F)	13.15%	Min
Binding fluorine		12.90%	Min
Sodium	(Na)	31%	Min
Free fluoride	(F)	0.25%	Max
Arsenic	(As)	3 ppm	Max
Heavy metal	(Pb)	50 ppm	Max
PH value (2% water solution)		6.5 - 8.0	
Ferro	(Fe)	0.01%	Max
Loss on drying		0.15%	Max

2.3.1. Application of Na-MFP as treatment for chloride & carbonation attack

Andrade et al. (1992) studied the corrosion inhibiting action of Na-MFP in mortar contaminated with chloride. In their work, they considered either the addition of Na-MFP to the mixing water or penetration from outside. The inhibitor effect has been followed using electrochemical techniques. Their results indicated that Na-MFP may act as an inhibitor of reinforcement corrosion although it seems that the inhibition effect enhances when Na-MFP penetrates through the hardened concrete. In their experiments the concentrations of Na-MFP were 0, 0.05, 0.1 and 0.5 mol/l. The mortar samples were made from Ordinary Portland cement (OPC), w/c=0.5 and c/s = 1/3. In the fresh mortar, their analysis indicated that Na-MFP act as an anodic inhibitor in alkaline media with a ratio of Na-MFP/NaCl>1. For the hardened mortar there results showed that when Na-MFP penetrates together with chlorides, the corrosion initiation is delayed if compared to the NaCl penetration alone and in the case of immersion and drying cycles the delay heavily depends on the ratio of Na-MFP/NaCl of the wetting solution (Andrade et al., 1992).

Dillard et al. (1993) carried out a corrosion inhibition experiments with mono-fluorophosphate to compare the results with others types of inhibitor. Their results revealed that the oxygen, iron, sodium and phosphorus concentrations are lower on Na-MFP-treated reinforcing steel than the other inhibitors. Also, the expected 1:1 phosphorus to fluorine atomic ratio for PO_3F^{2-} was not found on the reinforcing steel surface. They found that the P/F ratio for the initial inhibition samples was

2.6 and that for the delayed inhibition samples was 1.6. They suggested that the loss of fluorine for adsorbed phosphate inhibitor and that a process may account for this observation is hydrolysis of Na -MFP (either partial or complete) at the reinforcing steel surface or in solution. They conclude either process would liberate fluoride and phosphate into solution and might result in subsequent adsorption of fluoride and/or phosphate (Dillard et al., 1993).

Alonso et al. (1995) investigated the protective action of Na-MFP on corrosion of reinforcing steel in concrete in carbonated environments. They used electrochemical techniques to follow the inhibitor effect. In their experiments, Na-MFP has been tested as a curative method penetrating from outside when the steel reinforcement was already corroded by carbonation. Their results showed that applying Na MFP solution with a concentration of 20% reduce significantly active corrosion.

Their explanation for the reaction process is that:

“Na-MFP hydrolysis in aqueous and neutral media to form orthophosphate and fluoride through a process like

$$Na_2PO_3F \; + \; H_2O \; \rightarrow F^- + \; H_2PO_4^- \; + \; HPO_4^{-2}$$

Therefore, the inhibiting action of Na_2PO_3F may be attributed to the formation of phosphates, and so the anodic formation of a passive layer of Fe_3O_4, Fe_2O_3, and $FePO_4.H_2O$ This mechanism implies an anodic behaviour.”

With the treatment method they used concerning the penetrating methods employed, “short” and “long” period, they proved that the effectiveness increases with the number of immersion/drying cycles, probably due to increases in the concentration of inhibitor reaching the rebar. They add that the size and distribution of the pores also influence the penetration process. They also stated in their research that the practical application of Na- MFP to real structures has shown that Na-MFP penetrates even more than 30 mm. Their conclusion was that the penetration depends on capillary absorption and the number of applications and time between saturations of concrete with the Na-MFP (Alonso et al., 1995).

In studies by Ngala (2003) on carbonated ordinary Portland cement samples, they analysed the aqueous extracts from the treated concrete samples by means of ion chromatography to determine the concentration profiles of PO_3F^{2-}, PO_4^{3-} and F^-.Their analysis revealed that negligible penetration of soluble Na-MFP ions had occurred into any of the samples. Hydrolysis products of Na-MFP (phosphate and fluoride) were present at significant depths in aqueous extracts of the carbonated concrete samples but the only fluoride was detectable in similarly obtained aqueous extracts of non-carbonated samples (Ngala et al., 2003).

2.3.2. Application of Na-MFP as a healing agent

Çopuroğlu et al. (2006) showed that Na-MFP has another benefit, namely that it improves the frost salt scaling resistance of carbonated Blast Furnace Slag Cement (BFSC) pastes. A 10% Na-MFP solution was used as a surface post-treatment compound on carbonated BFSC paste. Results of this study have shown that the treatment modifies the mineralogical structure and improves the resistance of carbonated BFSC paste against frost salt attack. Their study concludes that the technique is more effective on highly carbonated surfaces since a thick resistance zone can be created by the application. Besides that their study results in a hypothesis that the reaction between Na-MFP and vaterite/aragonite phases may lead to a resistant carbonated zone of the BFSC paste against frost salt attack (Çopuroğlu et al., 2006).

Sisomphon et al. (2007) studied the application of a 10% Na-MFP solution as a surface applied compound for carbonated blast furnace slag mortar (W/C=0.45) treatment against frost salt scaling. Their results reveal that the Na-MFP treatment reduces the pore coarsening of the matrix phase and a denser interfacial transition zone (ITZ) that was observed after the treatment. The authors' results showed that the frost scaling durability of carbonated blast furnace slag mortar was significantly improved (Sisomphon et al., 2007).

The abovementioned work revealed the high potential of using Na-MFP as a surface treatment compound to heal carbonated BFSC concrete. Sisomphon et al. (2010) studied the affectivity of using MFP as a self-healing agent in the cementitious system, which would enable autonomous self-healing of the carbonated microstructure without any external application requirement.

They studied the potential of using expanded clay lightweight aggregate impregnated with sodium mono-fluorophosphate solution which can eventually be encapsulated by a cement paste layer to produce a self-healing system in blast furnace slag cement mortars. Their results showed that the technique significantly improved the quality of the interfacial transition zone in mortars subjected to carbonation shrinkage. These results consequently promoted the durability of blast furnace slag mortars against frost salt scaling (Sisomphon et al., 2010).

Recent studies by Kempl and Çopuroğlu (2016) showed that Na-MFP can be used as a healing agent as well as a corrosion inhibitor. The results showed that the addition of Na-MFP can recover the pH of carbonated cement pastes to about 99% and 80% of an untreated cement paste for CEM I and CEM III/B, respectively, with an increasing pH proportional to the concentration of sodium in the treating agent. Additionally, they analysed the hydrolysis of Na-MFP in solutions with an electrochemical oxygen potential relevant for cementitious pore solutions and they concluded that in the pH range of cementitious products the formation of amorphous Calcium Phosphates is favoured rather than the formation of crystalline phosphates such as apatite (Kempl et al., 2016).

3. Experimental methodology

This chapter gives an overview of the experimental set-up of this study. It describes the materials, which were used in the experiments, the preparation of the samples and the way of curing, storing and treating the samples.

3.1. Materials

Three different cement types were used for the experiments of this study. The cement types had different blast furnace slag concentrations which were 67% for the ENCI CEM III/B and 55% for the ternary blended cement. The cement types were as followed:

1. Ordinary Portland Cement (CEM I 42,5 N) which serves as a reference;
2. Blast Furnace Slag Cement with a slag content of 67% (CEM III/B 42,5 N HSR LH);
3. Ternary blended cement (SP Mix) with a slag content of 55%, 30% CEM I 52,5 R and 15% fly; ash.

The origin of the cement and the manufacturers are given in Table 8 and their main chemical compositions, fineness and compressive strengths are summarised in Table 9, Table 10 and Table 11, respectively. The compressive strength results were based on the average of three tested .samples for each type of cement.

Table 8: The origin of the binder and manufactures name

Type of cement	Company name	Origin
CEM I 42,5 N	ENCI BV	Maastricht
CEM III/B 42,5 N	ENCI BV	Rotterdam
Ternary blended cement (SP Mix)		
30% CEM I 52,5 R	Dyckerhoff	Geseke
55% Slag	ORCEM	Moerdijk
15% Fly Ash	Vliegasunie	Hemweg A'dam

Table 9: Chemical compositions and fineness of cement and slag used in the experiments (Ecocem, 2016; hcmcement, 2016)

Major oxides	CEM I 42,5 N	CEM III/B 42,5 N	CEM I 52,5 R	Slag
CaO (wt.%)	63.9	45.0	66	44
SiO_2 (wt %)	20.9	27.6	21	38
Al_2O_3 (wt %)	5.5	12.2	4.5	11
Fe_2O_3 (wt %)	2.8	1.3	2.4	7
SO_3 (wt %)	3.3	3.3	3.4	
Fineness (m^2/kg)	315	376	358	400-600

Table 10: Chemical composition and fineness of fly ash (vliegasunie, 2016)

Chemical (%wt.)	Fly ash
SiO_2	58.2± 3
Al_2O_3	22.2 ± 2.8
Fe_2O_3	8.3 ± 1.4
CaO	4.0 ± 1.3
K_2O	2.3 ± 0.4
Na_2O	1.1± 0.30
MgO	1.8 ± 0.3
P_2O_5	0.5 ± 0.2
TiO_2	1.0 ± 0.1
Cl	≤ 0.01
S (as SO_3)	0.9 ± 0.30
Loss on Ignition (LOI)	3.1 ± 1.5
Fineness (m^2/kg)	300-400

Table 11: Compressive strength (MPa) of mortar for wet/sealed curing for 14 and 28 days after demolding (W/C 0.45)

	CEM I 42,5 N		**CEM III/ B 42,5 N**		**SP MIX**	
Time of test	Wet	sealed	Wet	sealed	Wet	sealed
14 days	51.1	52.0	50.5	50.4	44.5	46.5
28 days	53.9	56.7	59.1	59.4	56	60.1

3.2. Sample preparation, storage, curing, carbonation, and treatment

Two groups of samples were prepared: mortar and paste samples. First, the preparation of mortar samples will be described. This will be followed by the description of the preparation of the paste samples.

3.2.1. Mortar Samples

Mixing

Mortars samples were prepared in accordance with the European standard EN-196-1. For the mixing process and in the case of all samples, mortars were prepared with a tap water-cement (w/c) ratio of 0.45 by weight. A sand-to-cement (S/C) ratio of 3 was also adhered to, also applied by weight. Throughout the experiments norm sand (CEN standard sand, D_{max}=2mm), cement and tap water was used for the preparation of the samples.

Molds with the dimensions of 40x40x160 mm^3 (see Figure 3) were used for the preparation of the samples. The molds were first coated with RECKLI biodegradable wax then the samples were immediately cast. During casting, the molds were vibrated for about 2 min on the vibration table, after that they were covered with plastic foil to avoid evaporation of the water from the mortar matrix and were kept at a room temperature of 20°C for 48 hours. Afterwards, the samples were demoulded and cured according to either the wet or the dry curing method which is explained below.

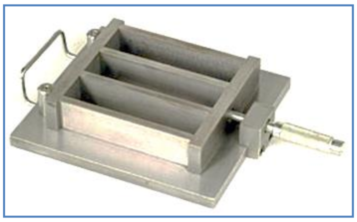

Figure 3: Mold with 3 samples 40x40x160mm3

Storage and curing

Two methods of curing were used: sealed curing and wet curing. During sealed curing, the samples were wrapped in foil and placed above water (not in water) in a closed container for 28 days. Afterwards, the samples were unwrapped and placed back in the container, again above water level, for 4 months (122 days) before being treated. In this way, the only water was available for hydration that was added during the mixture process.

During wet curing, the samples were stored under water directly after demoulding for 28 days.
This was followed by drying for three days at room temperature and then finally they were treated.

Treatment with an aqueous solution of 25 wt. % Na-MFP

The samples were treated once with an aqueous solution with 25 wt.% Na-MFP applied by means of a paint brush on the surfaces of the sample. Table 12 presents the procedures of storage, curing, carbonation and treatment of the mortar samples.

Table 12: Treatment scheme mortar samples for both wet and sealed curing samples

Sample code	Sample age at the time of treatment	Procedure of treatment, carbonation and storage	Sample age at the time of impregnation (vacuum epoxy)
R1	Wet:31 days Sealed: 125 days	Control, stored in the desiccators (50-55% RH)	Wet:31 days Sealed: 125 days
R2	Wet:31 days Sealed: 125 days	Accelerated carbonation for 14 days → storage in desiccators (50-55% RH) for 14 days	Wet:59 days Sealed: 153 days
R3	Wet:31 days Sealed: 125 days	Accelerated carbonation for 28 days → storage in desiccators (50-55%RH) for 14 days	Wet:73 days Sealed:167 days
A1	Wet:31 days Sealed:125 days	Treatment with 25% Na-MFP → storage in desiccators for 28 days → Placing in the carbonation chamber (3% CO_2-75%RH) for 14 days → storage in desiccators (50-55%RH) for 14 days	Wet:87 days Sealed:181 days
A2	Wet:31 days Sealed: 125 days	Treatment with 25% Na-MFP → storage in desiccators for 28 days → Placing in the carbonation chamber (3% CO_2-75% RH) for 28 days → storage in desiccators (50-55%RH) for 14 days	Wet:101 days Sealed:195 days
B1	Wet:31 days Sealed:125 days	Placing in the carbonation chamber (3% CO_2-75% RH) for 14 days → storage in desiccators for 14 days → Treatment with 25% Na-MFP → storage in desiccators (50-55% RH) for 28 days	Wet:87 days Sealed:181 days
B2	Wet:31 days Sealed:125 days	Placing in the carbonation chamber (3% CO_2-75%RH) for 28 days → storage in desiccators for 14 days → Treatment with 25% Na-MFP → storage in desiccators (50-55% RH) for 28 days	Wet:101 days Sealed:195 days

Table 13: Samples code

Code	Storage and Treatment
R1	Control sample
R2	Accelerated carbonation (3% CO_2,75% RH) for 14 days
R3	Accelerated carbonation (3% CO_2,75% RH) for 28 days
A1	Accelerated Carbonation for 14 days After treatment with Na-MFP
A2	Accelerated Carbonation for 28 days After treatment with Na-MFP
B1	Accelerated Carbonation for 14 days Before treatment with Na-MFP
B1	Accelerated Carbonation for 28 days Before treatment with Na-MFP

3.2.2. Paste Samples

The cement used for preparing the paste samples was also used in the mortar samples, see Table 8. Three different types of cement paste were prepared with water-cement ratios of 0.4, 0.5 and 0.6. After that, the cement pastes were cast into a plastic cylindrical container (d = 35 mm, h = 70 mm) and sealed. The samples were cured and stored at room temperature. After the curing age of 28 days, samples with a thickness of about 5 mm thickness were produced from each relevant cement paste cylinder by cutting them with the sawing machine.

Table 14 presents the procedures for storage and treatment. Samples were cut into slices of 5 mm and impregnated with Na-MFP aqueous solution with a concentration of 25% by weight.

Table 14: Treatment scheme paste samples

Sample code	Sample age at the time of treatment	Procedure of treatment , carbonation and storage	Sample age at the time of the test
R1	28 days	Control, stored in the desiccators (50-55% RH)	28 days
R2	28 days	Accelerated carbonation for 28 days →storage in the desiccators (50-55% RH) for 14 days	70 days
A: Na-MFP→ RCT28d	28 days	vacuum impregnation with 25%Na-MFP → storage in the desiccators (50-55% RH) for 28 days → Placing in the carbonation chamber (3% CO_2-75%RH) for 28 days→ storage in desiccators for 14 days	98 days
B: RCT28d→ Na-MFP	28 days	Placing in the carbonation chamber (3% CO_2-75%RH) for 28 days→ storage in desiccators (50-55% RH) for 14 days → vacuum impregnation with 25%Na-MFP → storage in desiccators (50-55% RH) for 28 days	98 days

3.3. Analytical approach and testing regime

This chapter presents the analytical procedures used for the mortar and paste samples. The first part presents the analytical part applied for the mortar samples and the second part presents the analytical part for the paste samples. This will be followed by the results obtained from each test.
A brief introduction for each lab test is presented with the information needed for this study.

Polarized light microscopy (PLM)

Introduction and test principle

Polarized light microscopy provides an analytical way to identify solid substances (whether crystalline or amorphous) with relatively high spatial resolution. It allows an estimate of chemical compositions and provides information about the history of the formation of the material (Raith et al., 2012).

PLM is a contrast-enhancing technique to evaluate the composition and three-dimensional structure of anisotropic specimens. PLM is equipped with both a polarizer, positioned in the light path somewhere before the specimen and an analyzer (a second polarizer) placed in the optical pathway between the objective rear aperture and the observation tubes or camera port. PLM uses a polarizing filter to make use of polarized light, configuring the movement of the light wave and forcing their vibration in a single direction as shown in Figure 4 (Davidson, 1988).

PLM assist in the investigation to distinguish between isotropic and anisotropic materials. When the light which has been forced to oscillate in one direction by the polarizer, passes through an isotropic material such as, glasses and cubic minerals, in thin-section, the light wave does not experience any change in vibration direction. Generally, shows a single specific refractive index and colour independent of orientation. In anisotropic materials light propagation is direction-dependent. All non-cubic crystalline substances are optically anisotropic. Light entering an anisotropic crystal is "split" into two light waves that vibrate orthogonal to each other (with exceptions applying to specific directions in the crystal). The two light waves propagate through the crystal with different velocities. This phenomenon is called double refraction (birefringent) (Roy et al., 1993).
The birefringence of anisotropic minerals can be determined in approximation by comparing the interference colors to those of the Michel-Lévy interference color charts (Raith et al., 2012; Robert, 2003).

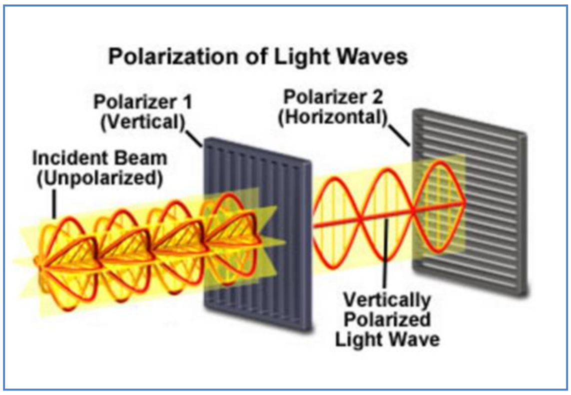

Figure 4: Polarization of light waves (Davidson, 1988)

In this study the microscope type, Leica DM-RXP was used. The focus was on studying the effect of the treatment with the aqueous solution of Na-MFP on the cement matrix of the mortar. This was done by identifying the carbonated cement mortar (yellowish interference colour) and its transformation into an amorphous material (dark colour). The samples used in this test were the wet cured samples (stored under water for 28 days).

For this analysis, thin sections were prepared by first sawing small prisms from each of the samples. Each prism slide measured 40mm x 40 mm, with a thickness of about 10 mm. The sawn specimens were then dried at 35°C and subsequently impregnated under vacuum with an epoxy resin containing a fluorescent dye. After hardening of the resin, a thin section with a surface area of about 40mm x 40 mm and a thickness of about 30 µm was prepared from each prism by grinding and polishing. Under crossed polars, this technique allowed distinguishing the carbonated and non-carbonated zones by the colour. The images obtained showed that the carbonated zones exhibit yellowish (creamy) colours due to calcite birefringence and the front can be easily determined. The carbonation depth depends on the treatment and the time exposed to accelerated carbonation.

The images present the control and carbonated samples after 14 and 28 days in comparison with samples treated with aqueous Na-MFP before or after carbonation. For the treatment and carbonation, the subsequent steps were shown in Table 12.

Scanning Electron Microscopy (SEM) with Energy Dispersive X-Ray Analysis (EDX)

Introduction and test principle

For this study, an ESEM Philips XL30, equipped with an EDS has used to analyses the penetration of aqueous Na-MFP into the sample from the surface.

Energy Dispersive X-Ray Analysis (EDX), referred to as EDS or EDAX, is an x-ray technique used to identify the elemental composition of materials. EDX systems are equipment to Electron Microscopy instruments (Scanning Electron Microscopy (SEM) or Transmission Electron Microscopy (TEM)) instruments where the imaging capability of the microscope identifies the specimen of interest. The data generated by EDX analysis consist of spectra showing peaks corresponding to the elements making up the true composition of the sample being analysed. Elemental mapping of a sample and image analysis are also possible(Wilton, 2016).

In scanning electron microscopy (SEM) an electron beam is scanning across a sample's surface. When the electrons strike the sample, a variety of signals are generated, and it is the detection of specific signals which produces an image or a sample's elemental composition. The three signals which provide the most information in SEM are the secondary electrons, backscattered electrons, and X-rays.

Secondary electrons are emitted from the atoms occupying the top surface and producing a readily interpretable image of the surface. The contrast in the image is determined by the sample’s morphology. A high-resolution image can be obtained because of the small diameter of the primary electron beam.

Backscattered electrons are primary beam electrons which are 'reflected' from atoms in the solid. The contrast in the image produced is determined by the atomic number of the elements in the sample. The image will, therefore, show the distribution of different chemical phases in the sample. Because these electrons are emitted from a specific depth in the sample, the resolution in the image is not as good as for secondary electrons (Goodge, 2016).

The EDS x-ray detector measures the relative abundance of emitted x-rays versus their energy. When an incident x-ray strikes the detector, it creates a charge pulse that is proportional to the energy of the x-ray. The charge pulse is converted to a voltage pulse (which remains proportional to the x-ray energy) by a charge-sensitive pre-amplifier. The signal is then sent to a multichannel analyser where the pulses are sorted by voltage. The energy, as determined from the voltage measurement, for each incident x-ray is sent to a computer for display and further data evaluation. The spectrum of x-ray energy versus counts is evaluated to determine the elemental composition of the sampled volume (larry D.Hank, 2015).

With EDS, it is possible to determine the concentration of each element in a sample (mass or atomic fraction).For this analysis three sealed curing mortar samples were used. The first sample exposed 14 days to accelerated carbonation followed by the treatment with aqueous Na-MFP, a second sample was treated with aqueous Na-MFP followed by exposing to carbonation 14 days and a third sample was exposed to carbonation during 28 days followed by the treatment with aqueous Na-MFP The samples were first cut to a thickness of about 10 mm then placed in the oven at 35°C for one day. After that, the samples were impregnated with low viscosity epoxy in order to obtain an optimal surface condition for the analysis with ESEM. Finally, the samples were grinded followed by polishing with 6 μm, 3 μm, 1 μm, and 0.25 μm diamond pastes.

The size of each sample was 40x40 mm and the tested area was 22.5x11.25 mm as is shown in Figure 5.The tested area was selected in this position in order to minimize the effect of the treatment from the other side on the tested area.

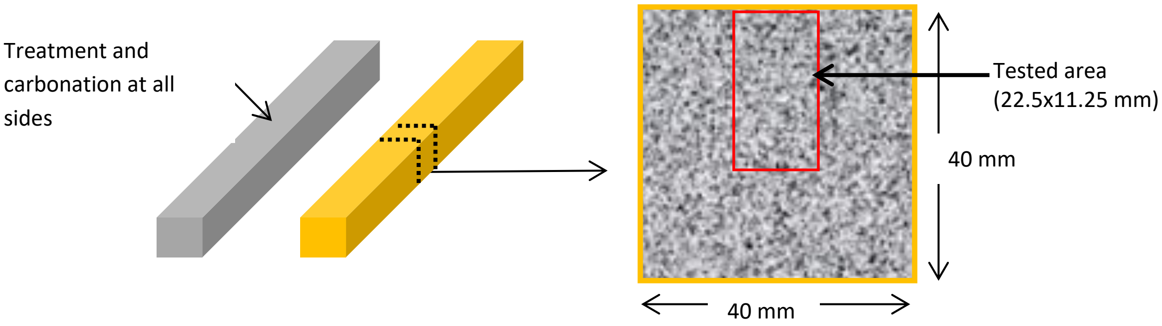

Figure 5: Sample preparation for SEM analysis, from left to right: A) samples treated and carbonated, B) sample impregnated with epoxy, a slice of 10 mm marked and C) surface of a slice of 10 mm prepared for testing with SEM.

Nanoindentation analysis

Introduction and test principle

Nanoindentation was used to characterize the nano-mechanical characterization of materials. This experimental approach provides a continuous record of the variation of the penetration depth (h) as a function of the imposed indentation load (P) into the indented specimen surface. A typical example of an indentation curve is shown in Figure 6.

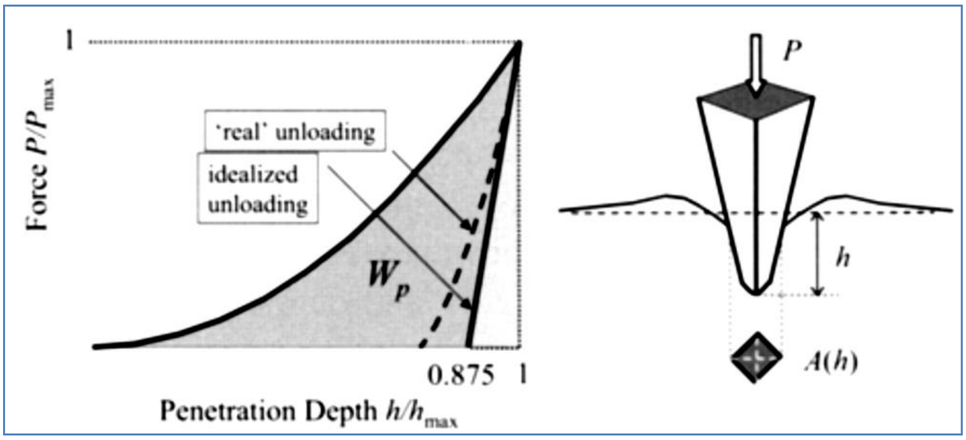

Figure 6: Principle of indentation test

The curve was generated from the loading history with initially constantly increasing loading, followed by constant holding and then constantly decreasing loading. From the initial slope of the elastic unloading in the load–depth curve, two mechanical parameters are obtained. The first one is the indentation modulus (E) and the second one is the hardness (H) (Constantinides et al., 2003).

Table 15 presents the values for the elastic modulus and hardness for portlandite (CH=$Ca(OH)_2$) and the C-S-H gel for different C/S-ratios provided by Acker (2004). These results were obtained with an ultra-high performance cementitious composite material, using a Berkovich indenter with penetration depths of about $h_{max} \approx 0.3\text{-}0.5 \times 10^{-6}$ m (Acker.P, 2004).

Table 15: Acker results for Elastic and plastic characteristics of the main constituents of a fibber-reinforced UHPC as measured using the Nanoindentation technique.

	YOUNG's modulus (GPa)	**Hardness (GPa)**
Quartz aggregate	73 ± 1.6	10 ± 0.3
Limestone aggregate	78 ± 1.4	10 ± 0.4
C_3S	135 ± 7	8.7 ± 1
C_2S	130 ± 20	8.0 ± 2
C_3A	145 ± 10	10.8 ± 1.5
C_4AF	125 ± 25	9.5 ± 3
C-S-H: C/S < 1	20 ± 2	0.8 ± 0.2
C/S > 1	31 ± 4	0.9 ± 0.3
CH	36 ± 3	1.35 ± 0.5

Zongjin (2015) presented a review on the mechanical properties of cement-based materials measured by nano-indentation see Table 16 and Table 17 (Chuanlin et al., 2015).

Table 16: Summary of the mechanical properties of C–S–H present in cement pastes obtained from nano-indentation coupled with the microstructure characterization.

w/c	Feature	C–S–H	Ca/Si (atomic)	Modulus (GPa)	Hardness (GPa)
0.4	Alite paste	IP	–	≈30	–
0.45	Cured in a water bath for a period of approximately 1 month	OP	–	25.74 ± 0.84	0.88 ± 0.36
0.2	Cured sealed at 20 °C for a period of	OP	–	≈44	≈1.3
	approximately 1 year	IP/I	–	≈50	≈1.7
0.23	Cured in moist conditions	OP	2.54 ± .35	28.9 ± 6.1	0.87 ± 0.25
	at 23 ± 1°c and 95%	IP	2.26 ± .23	39.8 ± 6.7	1.51 ± 0.38
0.4	Cured in moist conditions	OP	2.34 ± .30	25.2 ± 2.8	0.75 ± 0.26
	at 23 ± 1°c and 95%	IP	2.17 ± .19	31.6 ± 2.9	1.14 ± 0.17

Table 17: Summary of the mechanical properties of C–S–H present in blended cement pastes. Abbreviations: OP = outer product, IP = inner product, HP_1 = hydration product 1, HP_2 = hydration product 2.

Blended by	Feature	w/c	C–S–H	Modulus (GPa)	Hardness (GPa)
Nano-silica	0.3% and 0.5% replacement	0.5	HP	≈23	–
Silica fume	10% replacement; cured in moist condition	0.4	OP	25.1 ± 1.9	0.75 ± 0.09
	(23 ± 1°C and 95% relative humidity) for 90 d		IP	29.2 ± 4.1	0.93 ± 0.22
Fly ash	30% replacement; cured in moist condition	0.4	OP	22.9 ± 3.2	0.58 ± 0.16
	(23 ± 1°C and 95% relative humidity) for 90d		IP	32.5 ± 5.4	1.16 ± 0.35
		0.23	OP	26.7 ± 4.3	0.75 ± 0.21
			IP	35.5 ± 7.1	1.21 ± 0.40
Slag	50% replacement; cured in moist condition	0.4	HP_1	15.5 ± 5.8	0.41 ± 0.18
	(23 ± 1°C and 95% relative humidity) for120d		HP_2	24. 5 ± 7.3	0.81 ± 0.30
		0.23	HP_1	–	–
			HP_2	24.3 ± 7.7	0.59 ± 0.25

Nanoindentation tests were conducted using Agilent Nano Indenter G200. Numbers of indent were 100 covering an area of 1000x1000 μm^2. The spacing between the indent was 100 μm. Other input data are presented in Table 18.

Table 18: Required Inputs experiments data

Name	Value	Units
Tip Name	BT3148_22-04-15	
Calculation Inputs:		
Percent Unload In Stiffness Calculation	50	%
Perform Drift Correction	1	
Test Inputs:		
Allowable Drift Rate	0.15	nm/s
Depth Limit	2000	nm
Frequency Target	45.0	Hz
Harmonic Displacement Target	2.0	nm
Percent To Unload	90	%
Strain Rate Target	0.05	1/s

Mercury intrusion Porosimetry, MIP

Introduction and test principle

Mercury Intrusion Porosimetry (MIP) is a technique used to measure the porosity to characterize the distribution of pore sizes in cement-based materials; see Figure 7. The principle of the test is based on the premise that a non-wetting liquid (one having a contact angle greater than 90°) will only intrude pores under pressure.

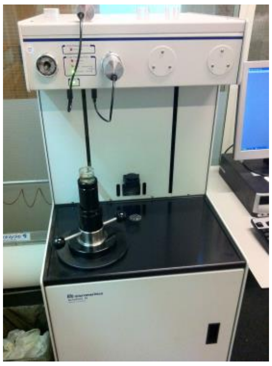

Figure 7: MIP device- PoreSizer-9320

Washburn described the relationship between the pressure and pore diameter as:

$$P = \frac{-4\gamma cos\theta}{d}$$

Where:

P pressure
ϒ the surface tension of the liquid
θ the contact angle of the liquid
d the diameter of the pore

The procedures of the test consisted of enclosing the sample in a glass tube, evacuating and pressing the mercury in the glass tube with the sample by applying incremental pressure. The mercury intruded the large pores with low pressures. At increasing pressure, the mercury can penetrate the smallest pores. Also, the penetration of the mercury into the sample depends on the continuity of the pore system in the sample.

The total porosity is determined from the total volume of the mercury intruded at the maximum pressure divided by the bulk volume of the un-intruded sample. The data from the test provided a wide range of information, such as the pore size distribution, the total pore volume or porosity, the skeletal and apparent density, and specific area of a sample.

From the previous literature, it is important to mention the limitation of the Mercury intrusion porosimetry test especially in measuring the actual pore size distributions. Wahburn assumed in his equation model that the pore shapes in hydrated cement are cylindrical pores and that the mercury is accessible to that pore. Diamond (2000) indicated in several studies that the conditions which must be met for MIP measurements to provide a valid estimation for pore size distribution cannot be reached. For this study, the obtained data from the test will be used for the purpose of microstructural investigation; comparing and evaluating the effect of the treatment with Na-MFP solution and the change in porosity and pore size distribution of equally handled samples.

Thermogravimetric analysis/Differential Scanning Calorimetry (TGA/DSC)

Introduction and test principle

Thermogravimetric Analysis (TGA) is a technique in which the mass of a substance is monitored as a function of temperature or time as the sample specimen is subjected to a controlled temperature program in a controlled atmosphere; see Figure 8. With other words, TGA is a technique in which the weight increases or decreases is measured while heating a material (PerkinElmer, 2010).

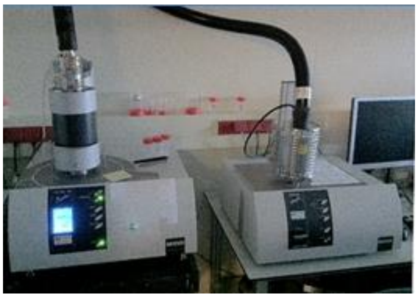

Figure 8: Thermogravimetric analyser (TG-449-F3-Jupiter)

The hydration products of cement contain chemically bound water. When the hydration products are heated to temperatures higher than 105 °C, the chemically bound water will be released. There are different phase transformations that occur in heated cementitious material, and they are not fully reversible. By applying thermal techniques; thermogravimetric analysis (TGA) and differential scanning calorimetry (DSC) phase transformations can be studied. The main phase transformations that occur in heated cementitious material are:

1. **Dehydration of calcium silicate hydrate (CSH)**

The dehydration of Calcium silicate hydrate (CSH) can be described as follows:

$(CaO)_aSiO_2(H2O)_b \rightleftharpoons (CaO)_a\ SiO_2\ (H2O)\ _{b\text{-}c}{}^{amorphous} + c.H_2O^{gas}$

The dehydration of CSH and the evaporation of water are the main reasons for the weight loss of cement paste in the temperature range from 105°C to 1000 °C.

2. Dehydration of calcium hydroxide (CH)

The dehydration of calcium hydroxide (CH) takes place at around 420°C causing a rapid weight loss which can be measured from the TG Curve. The dehydration of portlandite (CH) produces CaO and water vapor. The chemical reaction is:

$Ca(OH)_2 \rightleftharpoons CaO + H_2O^{(gas)}$

3. Decarbonation

The decarbonation of calcite ($CaCO_3$) in cement paste occurs at temperatures above 650 °C.The calcite decomposes into lime (CaO) and carbon dioxide (CO_2). The chemical reaction is:

$CaCO_3 \rightleftharpoons CaO + CO_2^{(gas)}$

Samples were crushed into fine powder and placed in the oven at 35°C for one day. The dried samples were placed into Thermogravimetric analyser as shown in Figure 8 and heated at temperatures ranging from 40°C to 1050°C, with a heating rate of 20°C /min. The gas used during the experiments was Argon.

4. Results and discussion

This section presents the test results on 1) the mortar samples for the investigation of the penetration of the Na-MFP solution (concentration 25%), followed by 2) the paste samples to investigate the microstructure of the formed product as a result of the reaction of the Na-MFP solution.

4.1. Mortar samples: Penetration analysis

4.1.1. Polarised microscopy images for mortar samples (W/C = 0.45)

Carbonation depth

To analyse the carbonation depth, cross-polarized (XPL) microscopy was used. Under (XPL) microscopy, the carbonated cement matrix appeared yellowish to light brown due to the existence of calcium carbonate ($CaCO_3$). It can be observed from the images obtained from the thin section samples as presented in Figure 10 to Figure 15 that the depth of carbonation increased with the exposure time under accelerated carbonation. The lowest carbonation depth was found for mortar samples with Portland cement (CEM I) as shown in Figure 9.

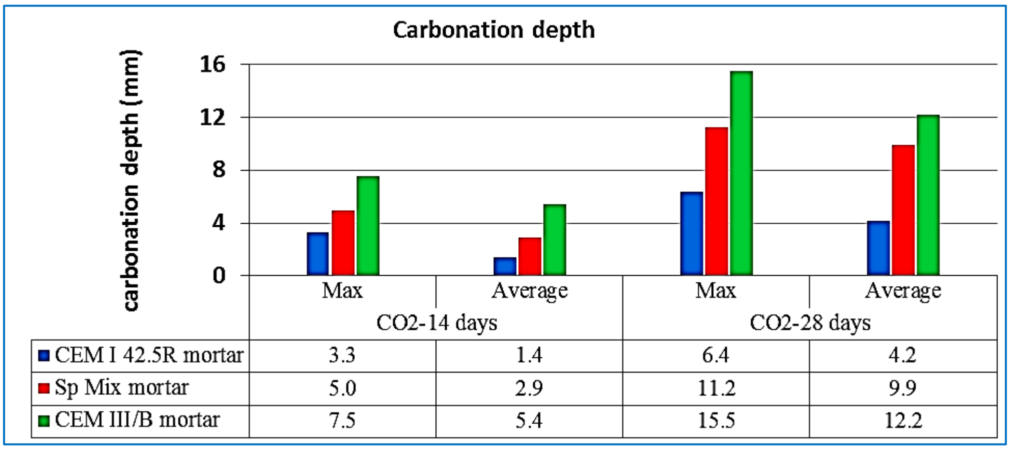

	CO2-14 days		CO2-28 days	
	Max	Average	Max	Average
🟦 CEM I 42.5R mortar	3.3	1.4	6.4	4.2
🟥 Sp Mix mortar	5.0	2.9	11.2	9.9
🟩 CEM III/B mortar	7.5	5.4	15.5	12.2

Figure 9: Carbonation depth measured from the thin sections

The carbonation depth of the CEM III/B mortar and SP Mix mortar was higher than for the CEM I mortar. The carbonation depth for CEM III/B mortar was about 50% higher than the carbonation depth of the SP Mix mortar; an explanation is the addition of the fly ash to the mix which decreased the permeability of the cement matrix. The amount of the fly ash used in the SP Mix was 15%, hence less than 50%.

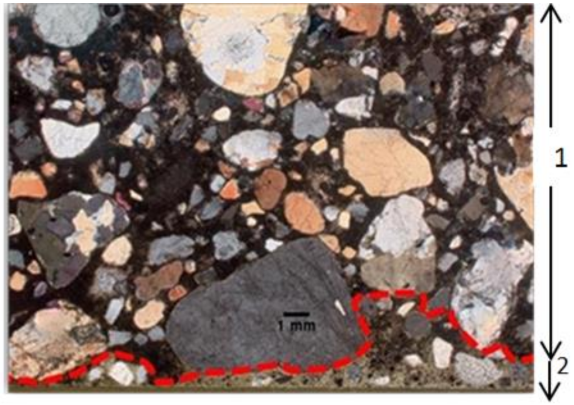

Figure 10: Photomicrographs (XPL) for CEM I 42.5R mortar exposed to accelerated carbonation for 14 days. Numbering: 1-uncarbonated part, 2-carbonated part

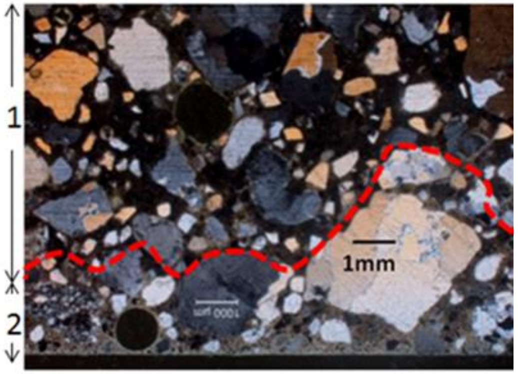

Figure 11: Photomicrographs (XPL) for SP Mix mortar carbonated for 14 days. Numbering: 1-uncarbonated part, 2-carbonated part

Figure 12: Photomicrographs (XPL) for CEM III/B mortar exposed to accelerated carbonation for 14 days. Numbering: 1-uncarbonated part, 2-carbonated part

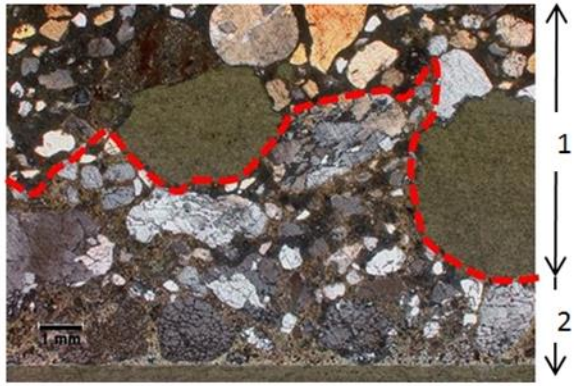

Figure 13: Photomicrographs (XPL) for CEM I 42.5R mortar exposed to accelerated carbonation for 28 days. Numbering: 1-uncarbonated part, 2-carbonated part

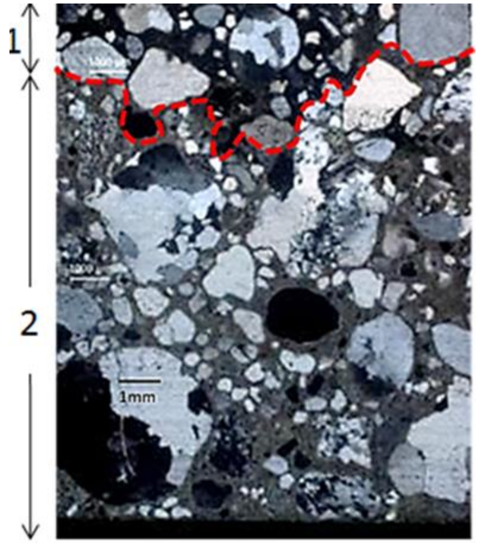

Figure 14: Photomicrographs (XPL) for SP Mix mortar carbonated for 28 days. Numbering: 1-uncarbonated part, 2-carbonated part

Figure 15: Photomicrographs (XPL) for CEM III/B mortar exposed to accelerated carbonation for 28 days. Numbering: 1-uncarbonated part, 2-carbonated part

Penetration of the Na-MFP solution into cement matrix

For the three types of mortar samples, which were treated before carbonation, the application of Na-MFP affected the samples less in comparison with the treatment after carbonation, see Table 19. These results are in agreement with what was reported in previous research: the Na-MFP solution penetrated the carbonated cement matrix forming an amorphous material which appeared as a dark layer under the XPL microscopy (Sisomphon et al., 2010).

Table 19: Depth of carbonation for CEM I 42.5R and Sp Mix mortar samples treated with Na-MFP solution (before/after carbonation) as measured from the XPL images

Treatment	**CEM I 42.5R mortar**		**Sp Mix mortar**		**CEM III/B**	
	Max	Average	Max	Average	max	average
CO_2-14 days	3	1	5	3	8	5
Na-MFP→CO_2-14 days	4	2	6	5	13	10
CO_2-14 days →Na-MFP	5	3	10	6	13 (3)*	11(2)*
CO_2-28 days	6	4	11	10	16	12
Na-MFP→CO_2-28 days	6	4	4	3	27	20
CO_2-28 days →Na-MFP	5	2	9	7	17(8)*	14(6)*

*penetration depth of the Na-MFP solution into cement matrix

Figure 16 to Figure 19 present the results for the microscopy images obtained for the thin sections of cement mortar prepared with CEM III/B (W/C = 0.45) with different types of treatments compared with the reference samples carbonated for 14 or 28 days. The carbonated area can be observed in the carbonated samples whether the exposure time for accelerated carbonation was 14 or 28 days; it is located at the bottom below the red line.

For the samples treated with Na-MFP as a surface treatment, two different behaviours were observed. For the CEM III /B mortar samples treated after carbonation (14 or 28 days), a dark layer was observed at the surface exposed to carbonation while the sample treated before carbonation this layer was not visible.

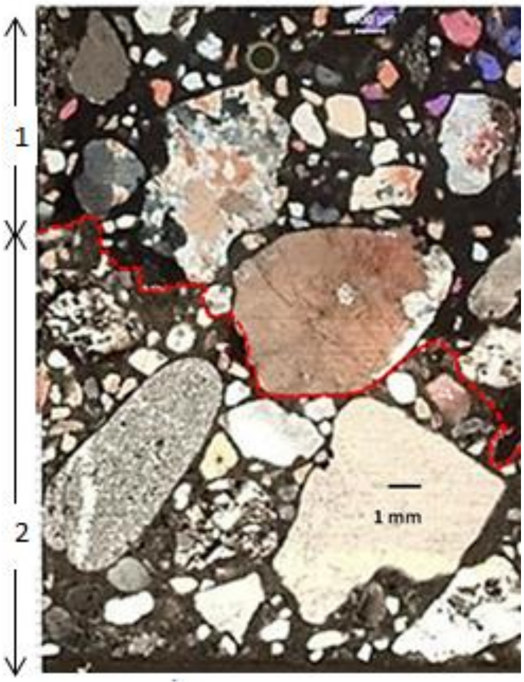

Figure 16: Photomicrographs (XPL) for CEM III/B mortar sample treated with aqueous solution of Na-MFP 25 % followed with carbonation for 14 days. Numbering: 1-uncarbonated part, 2-carbonated part

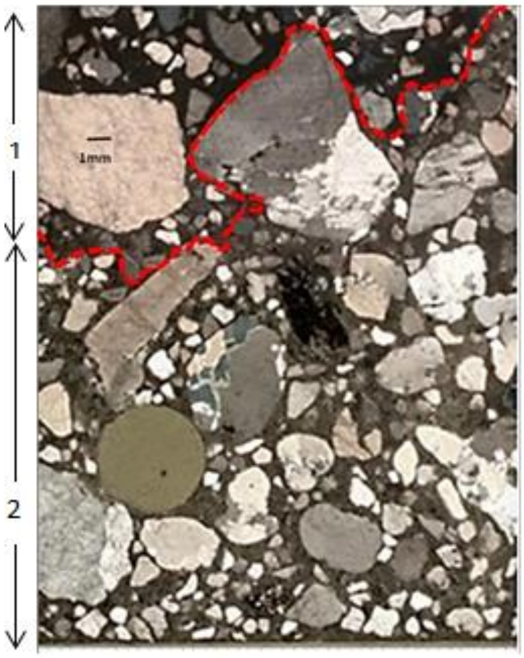

Figure 17: Photomicrographs (XPL) for CEM III/B mortar sample treated with aqueous solution of Na-MFP 25 % followed with carbonation for 28 days. Numbering: 1-uncarbonated part, 2-carbonated part

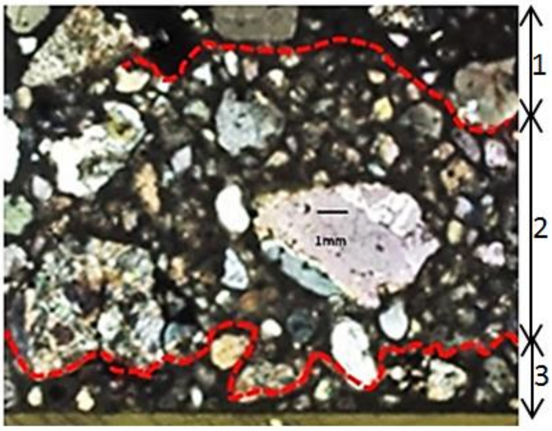

Figure 18: Photomicrographs (XPL) for CEM III/B mortar samples carbonated for 14 days followed by treatment with aqueous solution of Na-MEP 25%. Numbering: 1-uncarbonated part, 2-carbonated part, 3- part treated with Na-MFP

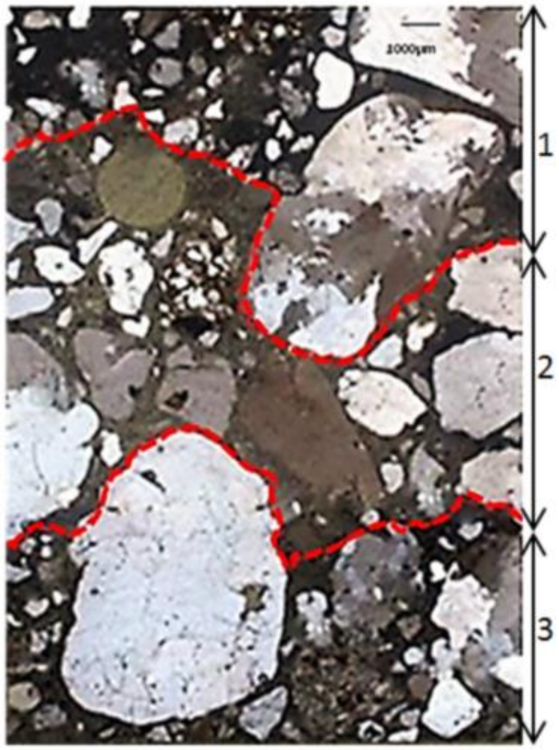

Figure 19: Photomicrographs (XPL) for CEM III/B mortar samples carbonated for 28 days followed by treatment with aqueous solution of Na-MEP 25%. Numbering: 1-uncarbonated part, 2-carbonated part, 3- part treated with Na-MFP

It is clear from these images that the surface treatment before carbonation was less effective and the penetration depth was less compared to the treatment after carbonation for the same carbonation time. The carbonation duration has an influence on the penetration depth of the solution in the cement matrix: The dark layer (amorphous) which formed as a result of the interaction of the solution with the cement matrix was thicker for the sample carbonated for 28 days than the one carbonated for 14 days. Table 19 presents the maximum and average depth for the carbonated parts as for the treated parts. This dark layer could be due to the reactions of $\mathrm{PO_3F^{2-}}$, $\mathrm{PO_4^{3-}}$ and $\mathrm{F^-}$ with $Ca(OH)_2$ and $CaCO_3$ which resulted in fluorapatite [$Ca_5(PO_4)_3F$] and carbonate fluorapatite [$Ca_5(PO_4, CO_3)_3F$] –like amorphous formations and in blocking the pore network of the cement (La Iglesia et al., 2012; Sisomphon et al., 2010).

The influence of the cement type on the penetration of the Na-MFP solution was related to the content of CH in the cement matrix. The cement matrix with low CH content became porous after exposing it to the carbonation which resulted in an increase of the permeability and facilitated the diffusion of Na-MFP solution. The Ca content of CEM I was higher compared to CEM III/B and SP MIX. While the CaO content of CEM III/B and SP Mix were comparable, the penetration of the Na-MFP solution into the SP Mix mortar was less deep than CEM III/B. This result could be attributed to the presence of the fly ash (15%) in the SP Mix mortar and its advantage in decreasing the permeability of the cement matrix. In addition, the applied treatment method could be ineffective for cement matrices with low permeability. It would be more effective to apply the solution several times on the treated surface. This would facilitate the solution to reach the pores in the carbonated cement matrix where the pH is low.

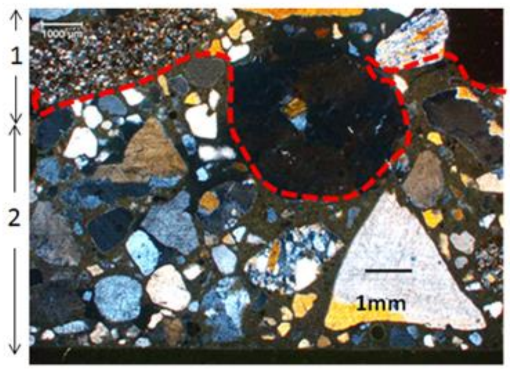

Figure 20: Photomicrographs (XPL) for SP Mix mortar sample treated with aqueous solution of Na-MFP 25 % followed by carbonation for 14 days. Numbering: 1-uncarbonated part, 2-carbonated part

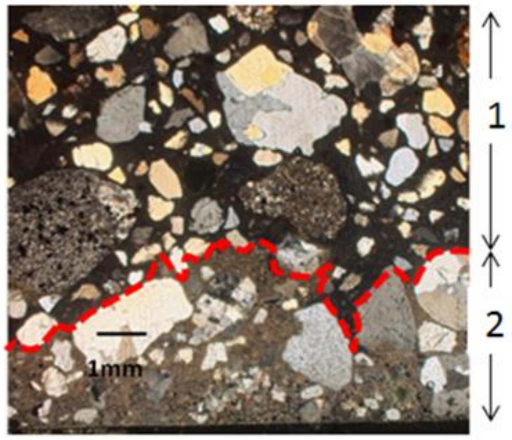

Figure 21: Photomicrographs (XPL) for SP Mix mortar sample treated with aqueous solution of Na-MFP 25 % followed by carbonation for 28 days. Numbering: 1-uncarbonated part, 2-carbonated part

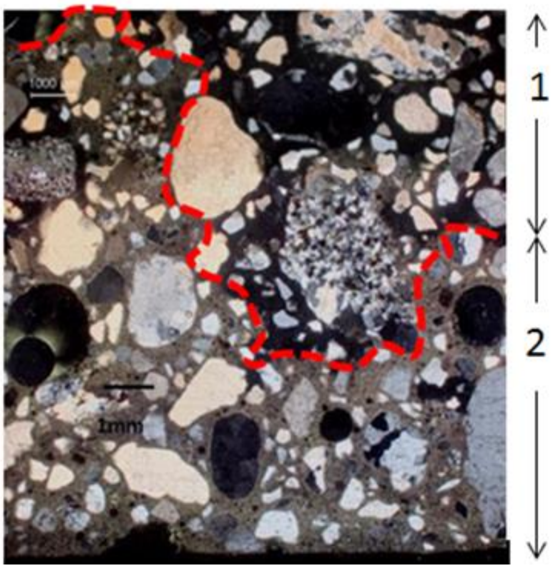

Figure 22: Photomicrographs (XPL) for SP Mix mortar samples carbonated for 14 days followed by a treatment with aqueous solution of Na-MEP 25%. Numbering: 1-uncarbonated part, 2-carbonated and treated

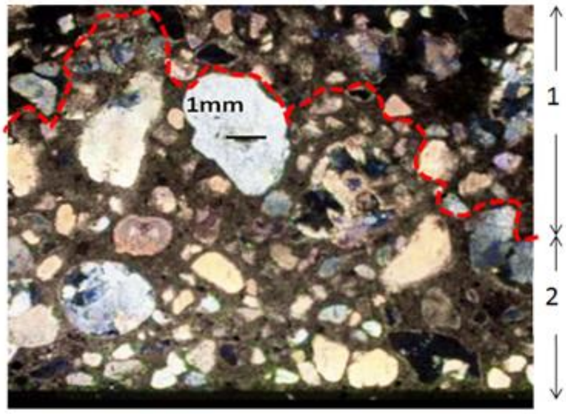

Figure 23: Photomicrographs (XPL) for SP Mix mortar samples carbonated for 28 days followed by a treatment with aqueous solution of Na-MEP 25%. Numbering: 1-uncarbonated part, 2-carbonated and treated

Figure 20 to Figure 23 show that this dark layer indicating the formation of the amorphous as a result of the reaction of Na-MFP with the cement matrix was not present. It could be that there was a very thin layer formed on the surface with a thickness of few micrometres which was not observed from the images obtained. EDX analysis was applied to the samples in order to gain more insight and to obtain data on the concentration of products formed as a result of the reaction of the Na-MFP solution with the cement matrix applying the solution before or after carbonation, an EDX analysis was applied to the samples. The results are presented in the next section.

4.1.2. Scanning Electron Microscopy (SEM/EDX) results for mortar samples (W/C =0.45)

Figure 24 to Figure 26 present the results obtained from the ESEM/EDX analysis and Table 20 presents the numerical values obtained from the measurements. The results show a high scatter in the concentration of the phosphorus at each depth. Close to the surface, at 0.5 mm, the sample treated before carbonation for 14 days showed high scatter and therefore also high standard deviation compared to treatment after carbonation. Along the measured depths, the sample treated after carbonation for 28 days showed more scatter compared to the sample carbonated for 14 days.

Scatter in the measurement is an indication for the heterogeneity of the measured section: the more scatter, the higher the heterogeneity. This heterogeneity is a result of natural irregularities within the sample itself or due to irregular reactions during carbonation and treatment. For instance due to carbonation the sample becomes more heterogeneous. This explains why higher scatter was found for carbonated sample and even more scatter if carbonation time increases.

Table 20: Concentration of P (At %) as measured by ESEM/EDX for CEM III/B Mortar (W/C 0.45) at different depth

Depth(mm)	0.5	2.5	5	7.5	10	12.5	15	17.5	20	22.5
Treatment(Na-MFP) → C_{14days}										
Average	0.98	0.36	0.32	0.32	0.37	-	-	-	-	-
STD	0.26	0.08	0.07	0.04	0.06	-	-	-	-	-
C_{14days} →Treatment(Na-MFP)										
Average	0.38	0.35	0.39	0.39	0.35	-	-	-	-	-
STD	0.10	0.04	0.03	0.03	0.06	-	-	-	-	-
C_{28days} →Treatment(Na-MFP)										
Average	0.38	0.39	0.48	0.42	0.33	0.33	0.32	0.29	0.27	0.34
STD	0.15	0.21	0.17	0.10	0.10	0.06	0.06	0.07	0.06	0.06

Figure 24 presents the results of two mortar samples mixed with CEM III/B: one was exposed to accelerated carbonation after treatment with aqueous Na-MFP (A: T → C14day) and the other one was exposed to accelerated carbonation before treatment (B: C14day → T) for 14 days. The results include the concentration of the phosphorus, P (At %), measured every 2.5 mm from the treated surface. The first measurement was taken at 0.5 mm depth which was considered being at the surface of the sample. Next measurements were taken every 2.5 mm. This type of measurement was considered an indication of the penetration depth of the Na-MFP into the cement matrix of the mortar. The images obtained from the PLM for the SP Mix indicate that the method used for applying the solution on the surface was inefficient which resulted in a limited penetration of the solution into the cement matrix. The samples used in this test were CEM III/B mortars.

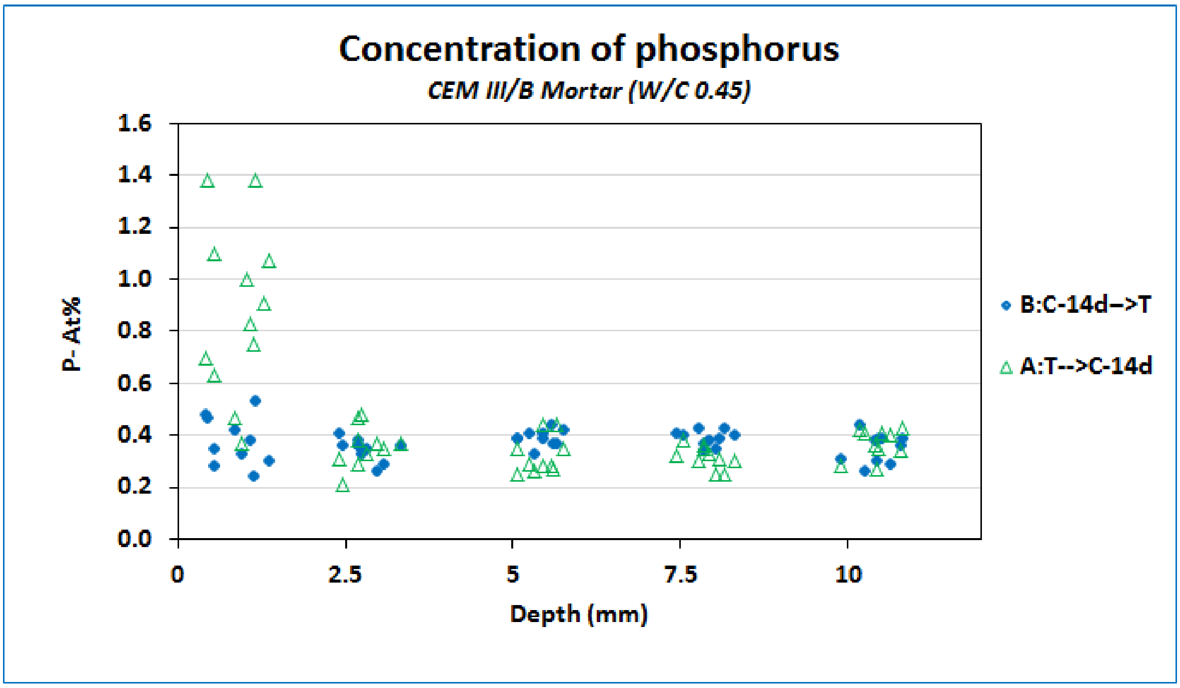

Figure 24: EDX result for two mortar samples-CEM III/B first one was carbonated for 14 days followed by treatment with aqueous Na-MFP B: C14days →T the second one was treated first with Na-MFP followed by carbonation for 14days A:T→C14days

Figure 24 shows a higher concentration of phosphorus close to the treated surface for the sample treated before carbonation compared with the sample treated after carbonation. At the depth 2.5mm to about 7.5 mm there are no significant differences in the concentration of phosphorus for the samples treatments with aqueous Na-MFP before or after carbonation for 14 days the concentration of the phosphorus decreased with the increase of the depth for both samples. At a depth of 7.5 mm it was observed that samples treated with Na-MFP solution after carbonation showed more traces of the phosphorus than the sample treated before carbonation. By comparing the value of P (At %) at depth of 7.5mm and 1mm, a slight difference between the both samples was noticed: The (B: C14day → T) sample showed a higher concentration than the (A: T → C14day) sample. This could be the result of the short carbonation duration of 14 days which was not enough to enable the penetration of the Na-MFP solution.

The effect of the carbonation duration was also tested. Figure 25 presents results obtained from the ESEM/EDX analysis for two samples both treated with aqueous Na-MFP after carbonation but one sample was carbonated for 14 days and the other sample was carbonated for 28 days. The results of the two samples presented in Figure 25 measured for depths from 0.5 to 10 mm with an interval of 2.5 mm. It was noted that the sample carbonated for 28 days indicated more tracing of Na-MFP solution than the sample carbonated for 14 days. This was clear for each depth measured: the concentration of P (At%) was higher for the sample carbonated for 28 days compared to 14 days.

This indicates the higher the sample is exposed to carbonation the larger the penetration depth of Na-MFP solution into the cement matrix due to the increase in the permeability of the cement matrix after carbonation.

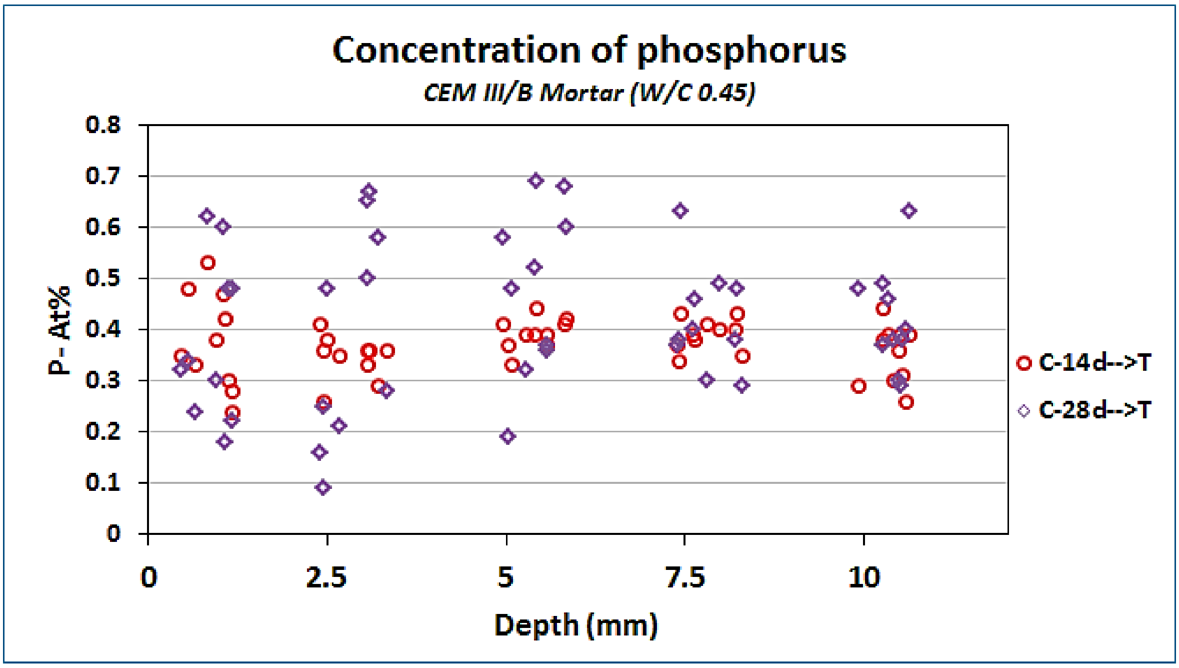

Figure 25: Result of EDX for two mortar samples-CEM III/B carbonated for 14 and 28 days followed by treatment with aqueous Na-MFP

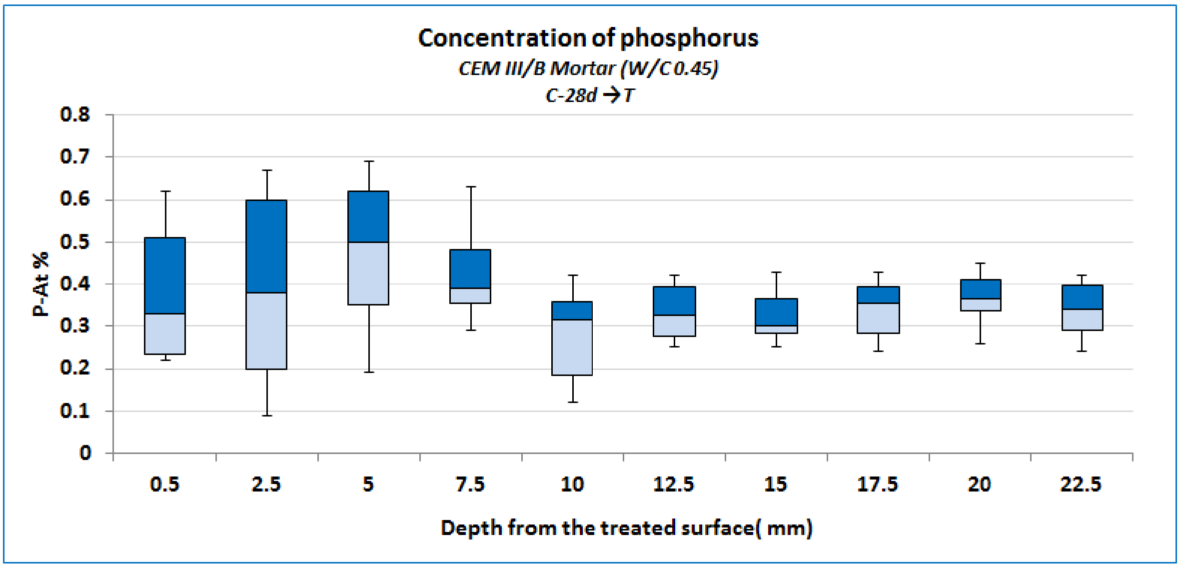

Figure 26: EDX result of mortar sample-CEM III/B carbonated for 28 days followed by the treatment with aqueous Na-MFP-the measurement was taken each 2.5mm from the treated surface.

Figure 26, present the results of the sample treated with Na-MFP solution after carbonation for 28 days. It is observed that the concentration of P (At%) as a result of the reaction of Na-MFP with the cement matrix was reduced at the depth of 12.5 mm. The lowest value of P(At%) was found at the depth of 20 mm and increased again at a depth of 22.5 mm as a result of the treatment from the other side of the surface. From these results, it was concluded that first there was a reaction between the Na-MFP aqueous and the cement matrix and second the reaction reached almost 2 cm deep into the sample from the surface.

4.1.3. Microscopy images for carbonated cement paste samples

Figure 27 to Figure 32 present the stereomicroscope images of cement paste for CEM III/B and SP Mix cement with a water-cement ratio of 0.45 tested to measure the carbonation depth. For the carbonation test, a phenolphthalein indicator solution was used. The phenolphthalein solution was applied directly on the freshly broken and cleaned parts. The carbonated parts where pH< 10 is not coloured and the carbonated parts are pink.

The method used for the treatment and carbonation was similar to the mortar samples. The numerical results are presented in Table 21. From the images and the numerical results, it was found that the maximum carbonation depth was about 2.56 mm for carbonation duration of 28 days. The treatment with Na-MFP solution after carbonation decreased the carbonation depth from 1.66 mm to 1.02 mm for cement paste CEM III/B and from 2.08 mm to 0.32 mm for cement paste SP Mix. The carbonation depth for the SP Mix paste sample is less compared to CEM III/B paste sample due to the presence of the fly ash in the mix which results in reducing the permeability and the carbonation process.

The carbonation depth for the samples treated after carbonation was less compared to the samples treated before carbonation, these results were for CEM III/B and Sp Mix cement paste. This could be due to the fact that alkali in the pore solution in the cement matrix was high (≈13.1) which delayed the reaction of Na-MFP with the cement matrix while the carbonation process was proceeding.

Table 21: carbonation depth, tested by phenolphthalein solution, for cement paste based on the stereomicroscope images for cement paste CEM III/B and SP Mix

Depth (mm)	**C_{28days}**	**T (Na-MFP) → C_{28days}**	**C_{28days} →T (Na-MFP)**
	CEM III/B Cement paste (W/C= 0.45)		
Average	0.94	1.74	0.82
Min	0.20	1.17	0.67
Max	1.66	2.05	1.02
	SP Mix Cement paste (W/C 0.45)		
Average	1.43	1.31	0.16
Min	0.62	1.01	0.09
Max	2.08	2.59	0.32

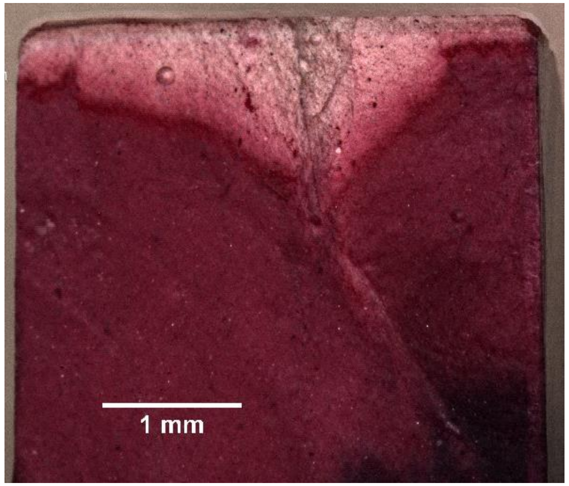

Figure 27: Stereomicroscope image of cement paste CEM III/B carbonated for 28 days

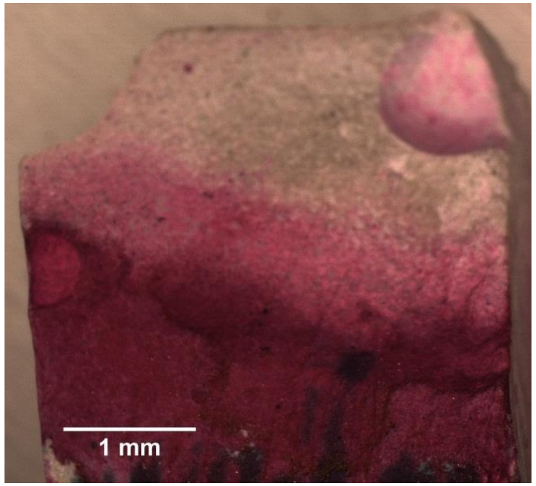

Figure 28: Stereomicroscope image of cement paste CEM III/B treated with Na-MFP before carbonation for 28 days

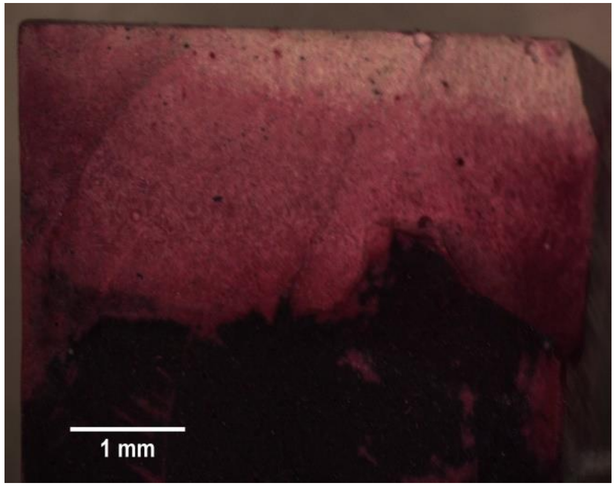

Figure 29: Stereomicroscope image of cement paste CEM III/B carbonated for 28 days before treatment with Na-MFP

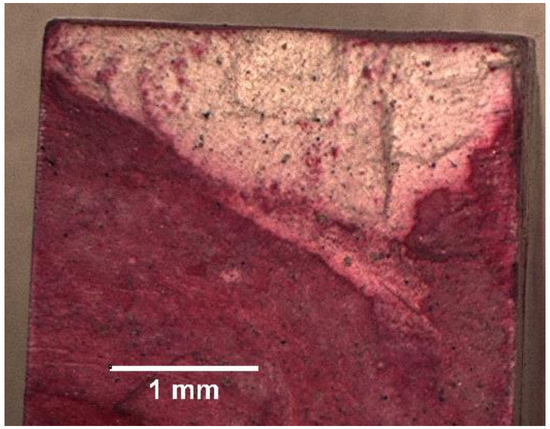

Figure 30: Stereomicroscope image of cement paste SP Mix carbonated for 28 days

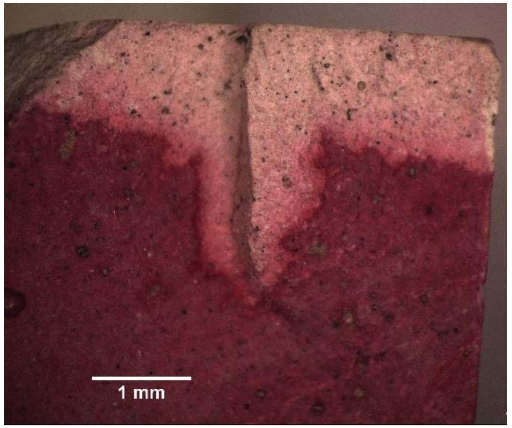

Figure 31: Stereomicroscope image of cement paste SP Mix treated with Na-MFP before carbonation for 28 days

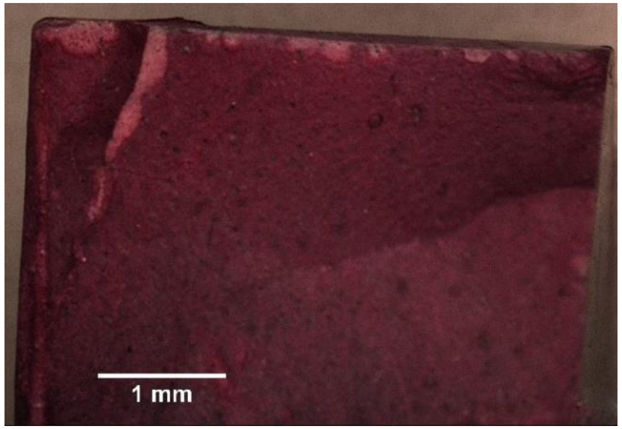

Figure 32: Stereomicroscope image of cement paste SP Mix carbonated for 28 days before treatment with Na-MFP

4.2. Paste samples: Microstructure analysis

4.2.1. Nano-indentation mechanical test results (Grid indentation analysis)

The nano-indentation technique was used to investigate the change in micromechanical properties of the paste samples through the treatment before or after being exposed to carbonation.

It is known that cementitious materials exhibit a large scatter of material properties. In order to overcome this problem, it was necessary to produce enough indents into the same material; the number depends on the accuracy of the test. For this study, the experimental set-up was 100 individual indentations performed on a grid of 10×10 indents with a spacing of 100 µm. The location of the grid was selected such that it was not located in the vanity of cracks. The data obtained from the tests were analysed in different steps.

Mean elastic modulus and hardness

1. *Effect of Carbonation*

The mean values of the elastic modulus and hardness are presented in

Table 23 and Figure 33 present the results for CEM I and SP Mix cement paste the mean elastic modulus and the hardness increased due to carbonation regardless of the water-cement ratio. The increase of the elastic modulus and the hardness for the carbonated cement paste was due to the formation of calcium carbonate as a result of the carbonation process.

As reported by Jiande (2011), the shape and pattern of calcium carbonate are microcrystalline with the scale of tens to hundreds of nanometres. Due to the formation of the microcrystalline $CaCO_3$ spherules in the calcium hydroxide crystals, the calcium hydroxide changes into $Ca(OH)_2$-$CaCO_3$ compounds. The elastic modulus and hardness of $Ca(OH)_2$-$CaCO_3$ compounds are higher than that of $Ca(OH)_2$ crystals and lower compared to $CaCO_3$ crystals (JianDe. et al., 2011).

For CEM III/B cement paste the elastic modulus and the hardness decreased with the increase of the water-cement ratio, particularly when the water-cement ratio increased to 0.6.Bertos et al. (2004) reported that the decrease in carbonation with high W/C is a result of the blockage of the pores with water in the solid and which result that there is no enough free water to promote the reaction of CO_2 and the hydration of the carbon dioxide. Also, the free water is needed to dissolve the Ca^{2+} ions from the solid that will react to form the $CaCO_3$ (Bertos et al., 2004; Johannesson et al., 2001). Add to that the carbonation of $Ca(OH)_2$ into $CaCO_3$ causes an increase of volume. The chemical reactions lead to a change of the microstructure, a decrease of the porosity, which results in a decrease in total volume involving a differential shrinkage between the surface and the bulk of the material which can lead in certain cases to cracking. An acceleration of the carbonation rate can result from this cracking (Houst, 1996). Slag cement pastes (CEM III/B with 67 % slag) have a lower Ca/Si ratio compared to CEM I, resulting in a high risk of carbonation shrinkage (Gruyaert et al., 2013). Rapid decalcification of C-S-H is expected in highly porous pastes, especially when the water content is high, which is accelerated when the Ca/Si ratio is relatively low. The addition of fly ash (SP Mix paste) in the cement mix reduces the permeability of the cement matrix , as previously reported (Ngala et al., 1997), which decrease the porosity and increases the elastic modulus compared to slag cement.

2. *Effect of treatment with Na-MFP solution on the elastic modulus and hardness*

The mean elastic modulus and the hardness for treated CEM I and SP MIX cement paste were higher compared to the non-treated carbonated and noncarbonated samples whether the treatment was before or after the carbonation and regardless the water-cement ratio. CEM III/B cement paste showed similar behaviour only with water-cement ratio 0.4 and 0.5. In the case the water-cement ratio was 0.6 the mean elastic modulus and the hardness of the treated sample after carbonation were higher compared to the carbonated and noncarbonated samples. This could be related to the reaction of the Na-MFP solution with $Ca(OH)_2$, $CaCO_3$ or porous silica which formed possibly into fluorapatite ($Ca_5(PO_4)_3F$) or carbonate fluorapatite ($Ca_5(PO_4,CO_3)_3F$) as well as unidentified amorphous formation(s) as reported by Çopuroğlu (2006).

In order to gain more insight of the effect of the treatment on the cement matrix, the elastic modulus, and the hardness were classified which will be explained in the next part of this analysis.

Table 22: The average and standard deviation of the elastic modulus for each cement paste as obtained from the nano-indentation test (indent number =100)

		Mean (±SD) Elastic modulus (GPa)		
		CEM I Cement paste		
W/C	**Control**	**C_{28days}**	**T (Na-MFP) ⟶ C_{28days}**	**C_{28days} ⟶ T (Na-MFP)**
0.4	29.19 ± 15.58	31.54 ± 13.02	38.88 ± 18.09	31.55 ± 7.34
0.5	26.11 ± 8.28	37.02 ± 21.20	36.31 ± 14.55	35.88 ± 13.53
0.6	19.85 ± 9.73	34.05 ± 10.72	33.91 ± 13.05	45.80 ± 17.21
		CEM III/B Cement paste		
0.4	25.47 ± 7.86	23.58 ± 9.24	29.36 ± 9.29	31.91 ± 11.35
0.5	17.26 ± 5.89	15.48 ± 6.51	18.53 ± 8.10	25.38 ± 10.50
0.6	26.21 ± 19.48	15.33 ± 7.88	22.84 ± 7.61	13.46 ± 4.92
		SP Mix Cement paste		
0.4	19.71 ± 11.25	18.33 ± 7.83	26.2 ± 10.21	23.86 ± 8.13
0.5	25.94 ± 11.04	28.52 ± 9.63	27.03 ± 9.11	31.55 ± 8.87
0.6	11.15 ± 5.68	17.86 ± 12.49	16.81 ± 6.71	23.11 ± 8.69

Table 23: The average and standard deviation of the Hardness for different cement pastes obtained from the nano-indentation test (indent number =100)

		Mean (±SD) Hardness (GPa)		
		CEM I Cement paste		
W/C	**Control**	**C_{28days}**	**T (Na-MFP) ⟶ C_{28days}**	**C_{28days} ⟶T (Na-MFP)**
0.4	1.08 ± 1.13	1.31 ± 1.00	1.59 ± 1.23	1.33 ± 0.46
0.5	0.83 ± 0.51	1.60 ± 1.72	1.53 ± 1.19	1.36 ± 0.80
0.6	0.74 ± 0.67	1.27 ± 0.86	1.44 ± 0.93	2.01 ± 1.48
		CEM III/B Cement paste		
0.4	0.94 ± 0.71	1.12 ± 0.81	1.28 ± 1.03	1.72 ± 1.03
0.5	0.54 ± 0.52	0.75 ± 0.69	0.85 ± 0.86	1.30 ± 1.02
0.6	1.81 ± 2.21	0.74 ± 0.64	1.05 ± 0.85	0.59 ± 0.44
		SP Mix Cement paste		
0.4	1.04 ± 1.20	0.92 ± 1.30	1.15 ± 0.93	1.19 ± 0.73
0.5	1.14 ± 0.99	1.41 ± 1.11	1.17 ± 0.74	1.65 ± 1.32
0.6	0.44 ± 0.38	1.02 ± 0.93	0.86 ± 0.58	1.19 ± 0.03

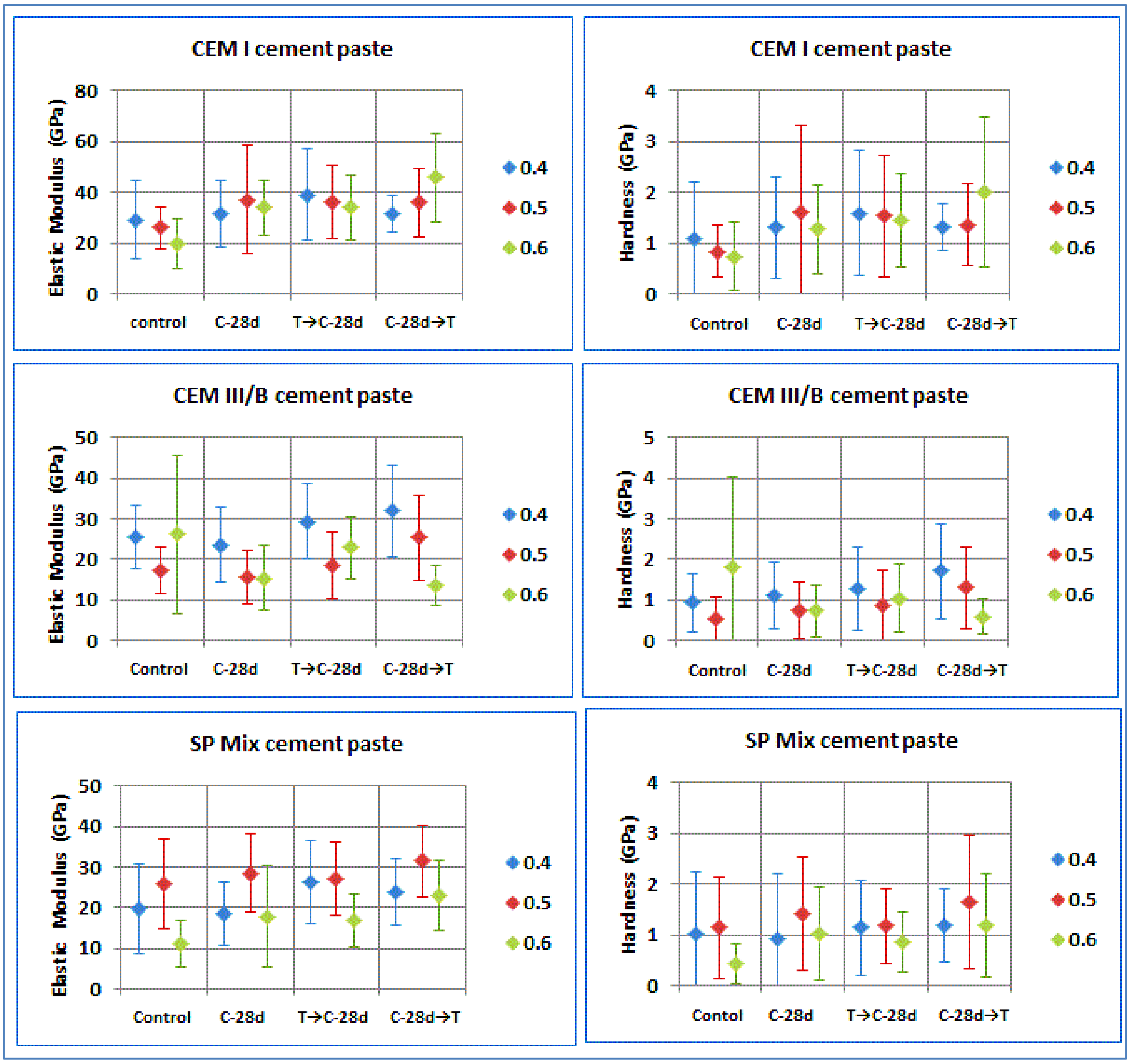

Figure 33: Mean elastic modulus (left) and hardness (right) for cement paste CEM I, CEM III/B and SP Mix with different water-cement ratio and treatments

Elastic modulus and hardness classification

Analysis method

For CEM III/B and SP Mix paste sample the data showed a change in the mechanical phase at the range of 18-35 GPa and 36-40 GPa compared to CEM I paste sample. The results were grouped into four phases in order to understand the different reactions in the cement matrix. For each phase group, the number of indents, hence the frequency, within that phase was calculated. This classification was used for the modulus and the hardness.

As discussed in Chapter 3, previous researchers reported the elastic modulus and hardness for C-S-H and CH. For the C-S-H two types were distinguished: high-density C-S-H and Low-density C-S-H which identify the inner and outer product of the hydration product, respectively. In this study, both types are listed in a single category as presented in Table 24. JianDe (2011) reported the elastic modulus and hardness for calcium carbonate to be 70 GPa and 3 GPa, respectively and for the $Ca(OH)_2$-$CaCO_3$ compounds the elastic modulus was in the range of 34–83 GPa and the hardness in the range of 1.75–4.15 GPa. Table 24 present data for the elastic modulus and hardness for a single crystal material as reported in the literature (Samandari et al., 2009; Zamiri et al., 2010). For elastic modulus lower than 18 GPa and hardness lower than 0.8 GPa are believed to be due to surface defects or porosity in the sample (Howind et al., 2011). Table 25 presents the classification of the elastic modulus as explained in Table 24.

Table 24: Classification of C-S-H and CH used in this analysis

	Elastic modulus (GPa)	**Hardness (GPa)**
C-S-H (L+H)	18 -35	0.8 -1.2
CH	36 - 39	1.3 -1.8
$Ca(OH)_2$-$CaCO_3$ (Compound)	34 - 83	1.75 - 4.15
$CaCO_3$	60 - 80	2- 4
[1]Fluorapatite ($Ca_{10}(PO_4)_6F_2$)	139.7±3.8	2.00±0.10
[2]Cement clinker	125–145 ± 25	8–10.8 ± 3
Hydroxyapatite $Ca_{10}(PO_4)_6(OH)_2$ (Side-Base)- Data for single crystal	143.56 – 150.38	6.41-7.06
[3]Cement clinker:		
C_3S	135 ± 7	8.7 ± 0.5
C_2S	130 ± 20	8 ± 1
C_3A	145 ± 10	10.8 ± 0.7
C_4AF	125 ± 25	9.5 ± 1.4
Alite	125 ± 7	9.2 ± 0.5
Belite	127 ± 10	8.8 ± 1

1-(Broz et al., 2006) 2-(Sorelli et al., 2008) 3-(Velez et al., 2001)

Overview 1: Expected reaction which affected the elastic modulus and hardness

Carbonation of Calcium hydroxide

$Ca(OH)_2 + CO_2 \rightarrow CaCO_3 + H_2O$

Carbonation of C-S-H

$(3CaO.\ 2SiO_2.\ 3H_2O) + 3CO_2 \rightarrow 3CaCO_3 + 2SiO\ .nH_2O + (3\text{-}n)\ H_2O$

(n: mass of water in the silica gel)

Reaction of Na-MFP

$$3\ \mathrm{PO_3F^{2-}} + 6\mathrm{Ca(OH)_2}_{\mathrm{(crystalline)}} \leftrightarrow \mathrm{Ca_5(PO_4)_3F}_{\mathrm{(amorphous)}} + \mathrm{CaF_2}_{\mathrm{(crystalline)}} + 6\ \mathrm{OH} + 3\ \mathrm{H_2O}$$

(Reaction of PO_3F^{2-}, PO_4^{3-} or F^- with $Ca(OH)_2$, $CaCO_3$ or porous silica which results possibly into fluorapatite ($Ca_5(PO_4)_3F$) or carbonate fluorapatite ($Ca_5(PO_4,CO_3)_3F$) as well as an unidentified amorphous formation(s)).

Table 25: The distribution of the elastic modulus (%)

Elastic Modulus (GPa)		**Control**	**C_{28d}**	**T→C_{28d}**	**C_{28d}→T**	**Control**	**C_{28d}**	**T→C_{28d}**	**C_{28d}→T**	**Control**	**C_{28d}**	**T→C_{28d}**	**C_{28d}→T**
		CEM I -W/C 0.4				**CEM III/B -W/C 0.4**				**SP Mix - W/C 0.4**			
	<18	12%	5%	5%	6%	9%	24%	3%	5%	49%	56%	14%	19%
C-S-H	**18-35**	71%	72%	42%	**64%**	77%	66%	**80%**	62%	42%	38%	72%	72%
CH	**36-39**	4%	12%	**18%**	**18%**	9%	5%	5%	**12%**	4%	3%	**6%**	4%
	>39	14%	10%	**34%**	**13%**	4%	5%	12%	**21%**	4%	3%	**8%**	4%
		CEM I -W/C 0.5				**CEM III/B -W/C 0.5**				**SP Mix -W/C 0.5**			
	<18	11%	5%	5%	5%	59%	67%	51%	18%	13%	10%	14%	6%
C-S-H	**18-35**	74%	63%	49%	54%	39%	32%	46%	**64%**	72%	68%	67%	63%
CH	**36-39**	8%	6%	7%	11%	1%	1%	0%	**9%**	5%	14%	9%	**16%**
	>39	7%	26%	**39%**	**31%**	0%	0%	3%	**9%**	9%	9%	10%	**15%**
		CEM I -W/C 0.6				**CEM III/B -W/C 0.6**				**SP Mix -W/C 0.6**			
	<18	53%	1%	13%	1%	42%	71%	15%	**83%**	89%	62%	59%	28%
C-S-H	**18-35**	40%	64%	45%	20%	33%	25%	**75%**	17%	9%	32%	39%	**67%**
CH	**36-39**	3%	21%	12%	13%	6%	1%	**6%**	0%	1%	3%	2%	**2%**
	>39	5%	13%	**31%**	**66%**	19%	3%	**4%**	0%	0%	3%	0%	**3%**

░	(3-9 %) change in the elastic modulus compared to carbonated samples
▓	(>10%) change in the elastic modulus compared to carbonated samples

Analysis of the Elastic modulus classification

The results for *CEMI cement paste samples* showed that the treatment before carbonation increased the elastic modulus for the phase > 39 GPa compared to the carbonated sample; the tests were executed for samples with water-cement ratio 0.4 and 0.5. The sample with water-cement ratio of 0.6 and a treatment after carbonation showed an increase of 53% in the elastic modulus compared with the carbonated sample.

With a high water-cement ratio, the pores were filled with a carbonated solution with a low pH which facilitated the hydrolysis of Na-MFP in HPO_4^{2-} and F^- ions and reacted with calcium to form an amorphous material. Another explanation could be that when the sample was exposed to accelerate carbonation, the $CaCO_3$ was formed filling the pores in the cement matrix. This process needed sufficient calcium and water in the pores to continue. While the formation of $CaCO_3$ continued filling the pores, it might be that there was some of the unhydrated cement that is blocked. Figure 34 and Figure 35 shows the position with high elastic modulus (104.5-114.3 GPa) which could relate to unhydrated cement or clinker.

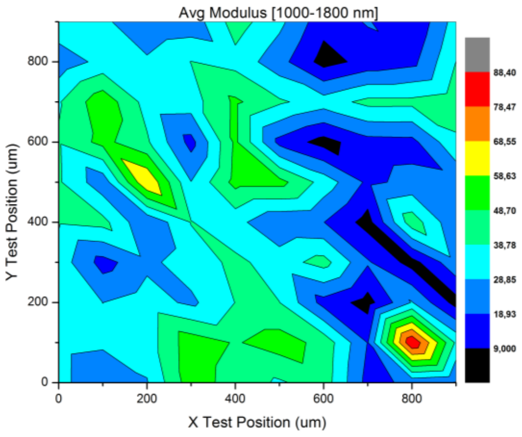

Figure 34: Cement paste CEM I W/C 0.6 –

T (Na-MFP) → C28days

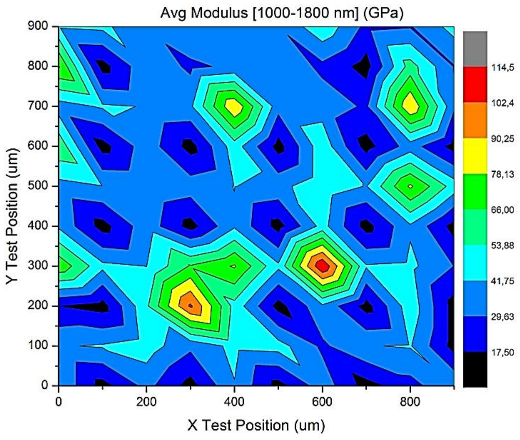

Figure 35: Cement paste CEM I W/C 0.6 –

C28days → T (Na-MFP)

The results of *CEM III/B cement paste samples* showed an increase in the elastic modulus in the phase (18-35 GPa) and a decrease in the elastic modulus lower phase (<18 GPa) for the treatment before carbonation while for the treatment after carbonation the data showed an increase in the elastic modulus with higher phase, (36-39 GPa) and (>39GPa) for water-cement ratios of 0.4 and 0.5. Figure 36 to Figure 39 show the decrease of the elastic modulus for the treatment after carbonation for water-cement ratio of 0.6 and formation a material which has a lower elastic modulus than C-S-H, the figures also show the spatial distribution of this material.

The *SP Mix cement paste samples* showed an increase in the elastic modulus for the treatment before carbonation with water-cement ratio of 0.4 and after carbonation for water-cement ratios of 0.5 and 0.6.

The reaction of Na-MFP and the formation of the amorphous material increased the elastic modulus of the cement matrix. The carbonation of the cement paste with a water-cement ratio of 0.6 followed by the treatment with Na-MFP decreased the elastic modulus.

The nanoindentation results showed that the treatment improved the elastic modulus of the cement matrix. Whether the improvement was obtained for the treatment before or after carbonation depended on the water-cement- ratio.

Considering the elastic modulus of the apatite reported in Table 24, which was higher than any values measured from the test, it was not clear whether the amorphous material formed as a result of the reaction of Na-MFP with the cement matrix was an apatite. The results gave an indication of the formation of a material improving the elastic modulus.

The treatment after carbonation gave more distributed increases in hardness compared to the treatment before carbonation. CEM III/B with water cement ratio 0.6 showed increases in the hardness in the phase <0.8 GPa while the treatment before carbonation showed a dispersed increase in the higher phases as presented in Table 26. The results showed that treatment after carbonation resulted in distributed improvement of the hardness of the cement matrix surface for CEM I and SP MIX cement paste regardless the water cement ratio but for cement paste CEM III/B was limited to lower water-cement ratios (0.4-0.5).

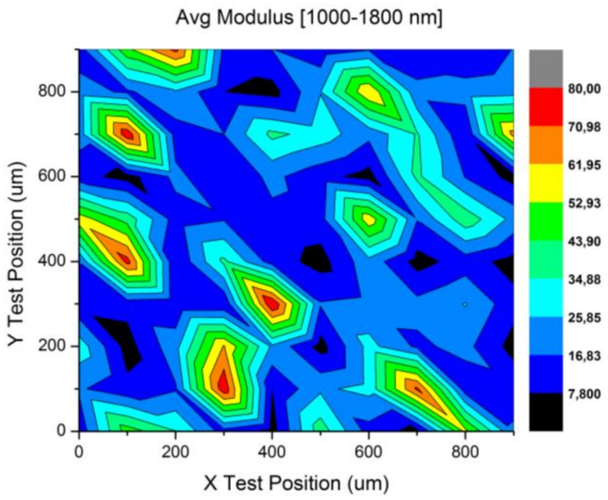

Figure 36: Cement paste CEM III/B -W/C 0.6- Control

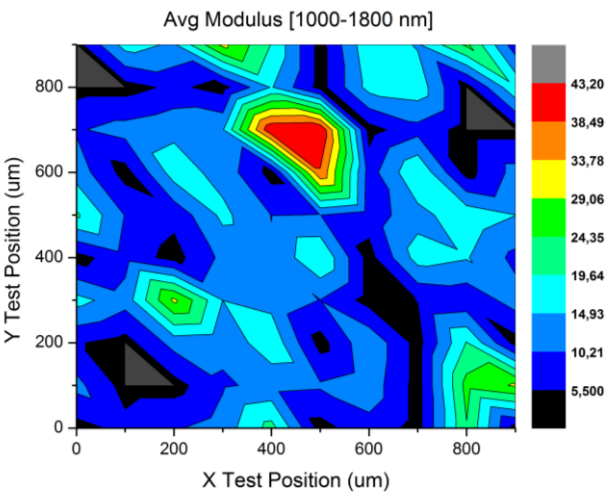

Figure 37 : Cement paste CEM III/B- W/C 0.6- C_{28days}

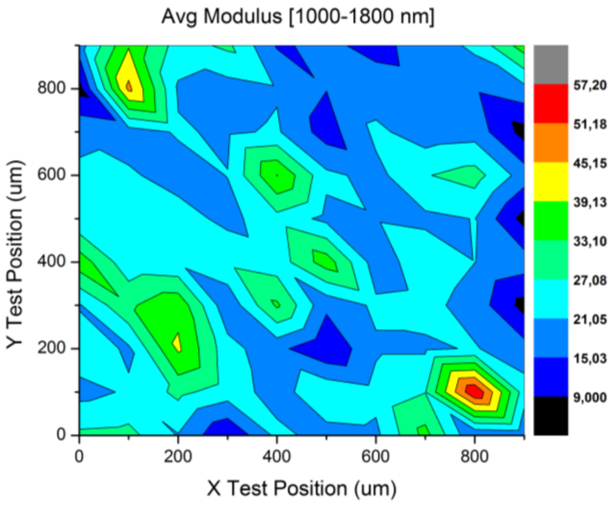

Figure 38:Cement paste CEM III/B W/C 0.6- T → C_{28days}

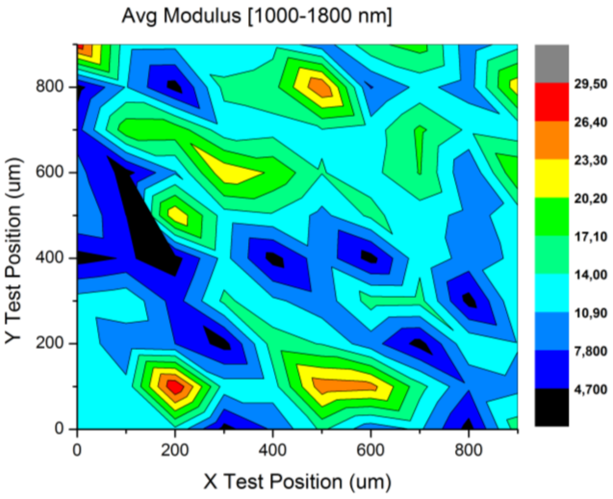

Figure 39:Cement paste CEM III/B -W/C 0.6- C_{28days} → T

Table 26: The distribution of the hardness (%)

Hardness (GPa)		Control	C_{28d}	$T\rightarrow C_{28d}$	$C_{28d}\rightarrow T$	Control	C_{28d}	$T\rightarrow C_{28d}$	$C_{28d}\rightarrow T$	Control	C_{28d}	$T\rightarrow C_{28d}$	$C_{28d}\rightarrow T$
		CEM I -W/C 0.4				**CEM III/B -W/C 0.4**				**SP Mix - W/C 0.4**			
	<0.8	62%	18%	22%	14%	47%	38%	22%	8%	61%	78%	38%	36%
C-S-H	**0.8-1.2**	21%	36%	20%	**35%**	28%	24%	42%	30%	19%	7%	36%	**27%**
CH	**1.3-1.8**	6%	37%	37%	**40%**	14%	27%	23%	**32%**	7%	3%	16%	**21%**
	>1.8	11%	9%	**21%**	11%	10%	11%	14%	**30%**	13%	12%	10%	**16%**
		CEM I -W/C 0.5				**CEM III/B -W/C 0.5**				**SP Mix -W/C 0.5**			
	<0.8	64%	44%	22%	18%	83%	68%	57%	17%	53%	18%	32%	9%
C-S-H	**0.8-1.2**	25%	29%	28%	**31%**	8%	17%	26%	**39%**	18%	43%	30%	18%
CH	**1.3-1.8**	8%	6%	20%	**32%**	7%	10%	7%	**18%**	18%	16%	22%	**39%**
	>1.8	3%	21%	**30%**	19%	1%	6%	10%	**26%**	11%	24%	16%	**34%**
		CEM I -W/C 0.6				**CEM III/B -W/C 0.6**				**SP Mix -W/C 0.6**			
	<0.8	72%	24%	28%	4%	33%	64%	26%	**77%**	85%	50%	61%	24%
C-S-H	**0.8-1.2**	17%	36%	17%	**18%**	32%	22%	**52%**	15%	12%	23%	20%	**29%**
CH	**1.3-1.8**	6%	33%	34%	**53%**	9%	10%	**7%**	5%	1%	12%	11%	**30%**
	>1.8	5%	7%	21%	**25%**	26%	4%	**15%**	3%	1%	15%	8%	**17%**

░	Increase in one phase compared to carbonated sample
▓	Increase in more than one phase compared to carbonated sample

4.2.2. Analysis of the porosity and pore size distribution

The MIP test was applied on paste samples for each cement type for different water-cement ratios. As mentioned before, the results of the MIP test are indicative values. The test techniques were kept identical for all samples; these were: sample size, drying and pressure. The values obtained were based on a single test for each sample, which for accuracy reasons will not be enough for claiming that the values obtained are reliable values. The results obtained from the tests were used to compare the porosity and the pore size distribution for each sample under systematically sampling strategy with controlled techniques.

In order to gain more insight into the pore size distribution, the measured pore size distribution from the MIP test was classified into four size ranges:

10-50 µm	Capillary pores - Large
50 nm-10 µm	Capillary pores - Medium
10-50 nm	Capillary pores - Small
2.5-10 nm	Gel pores

Table 27 presents the background of the classifications according to Mindess. Figure 40 presents the total porosity as measured by the MIP test and Table 29 presents the calculation of the total porosity compared to the capillary porosity in the range (10 nm-10 µm).

First, the effect of the carbonation was analysed, then the effect of the treatment with Na-MFP.

Table 27: The classification of the pore size is according to S.Mindess (Jennings et al., 2002):

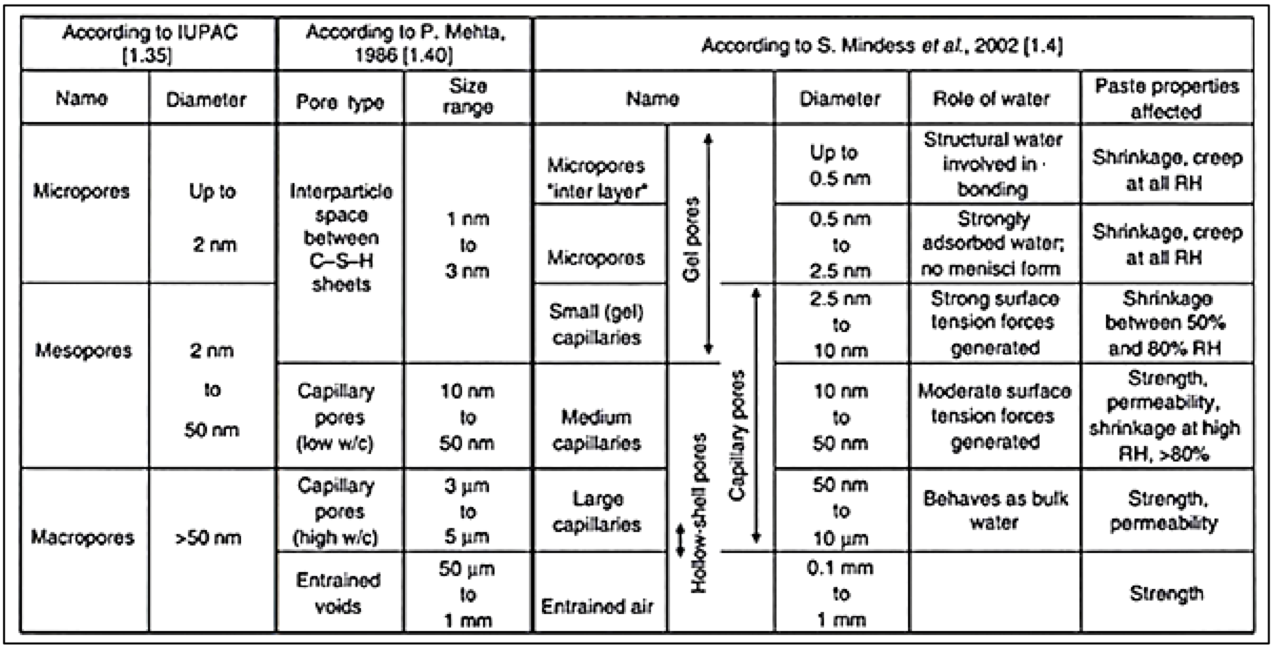

According to IUPAC [1.35]		According to P. Mehta, 1986 [1.40]		According to S. Mindess *et al.*, 2002 [1.4]				
Name	Diameter	Pore type	Size range	Name		Diameter	Role of water	Paste properties affected
Micropores	Up to 2 nm	Interparticle space between C–S–H sheets	1 nm to 3 nm	Micropores "inter layer"	Gel pores	Up to 0.5 nm	Structural water involved in bonding	Shrinkage, creep at all RH
				Micropores		0.5 nm to 2.5 nm	Strongly adsorbed water; no menisci form	Shrinkage, creep at all RH
Mesopores	2 nm to 50 nm			Small (gel) capillaries	Capillary pores	2.5 nm to 10 nm	Strong surface tension forces generated	Shrinkage between 50% and 80% RH
		Capillary pores (low w/c)	10 nm to 50 nm	Medium capillaries		10 nm to 50 nm	Moderate surface tension forces generated	Strength, permeability, shrinkage at high RH, >80%
Macropores	>50 nm	Capillary pores (high w/c)	3 µm to 5 µm	Large capillaries	Hollow-shell pores	50 nm to 10 µm	Behaves as bulk water	Strength, permeability
		Entrained voids	50 µm to 1 mm	Entrained air		0.1 mm to 1 mm		Strength

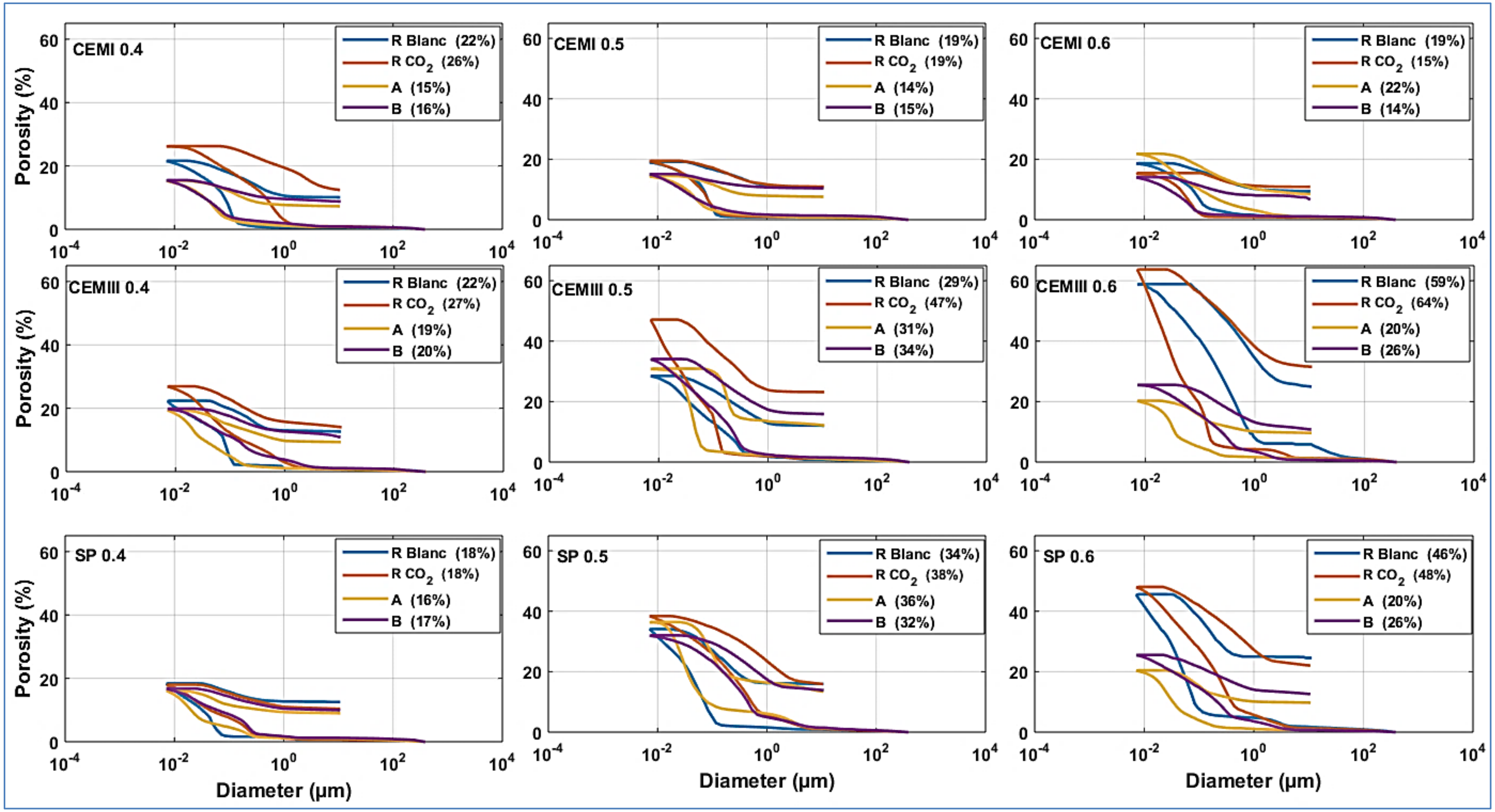

Figure 40: Total Porosity as measured by MIP Test (B:T→C$_{28d}$ and A: T→C$_{28d}$)

Effect of accelerated carbonation on the capillary porosity

Table 28: Percentage of capillary porosity for carbonated and control cement paste

Cement paste type	**W/C 0.4**		**W/C 0.5**		**W/C 0.6**	
	Control	**C_{28days}**	**Control**	**C_{28days}**	**Control**	**C_{28days}**
CEM I Paste	20%	25%	18%	18%	17%	14%
CEM III/B Paste	19%	25%	27%	39%	52%	56%
SP Mix Paste	15%	16%	30%	36%	40%	45%

Table 28 presents the results of the capillary porosity for the carbonated and control samples. The control samples of *CEM I cement paste* show a slight decrease in the capillary porosity of about (1-2%) with the increase of the water-cement ratios which was not expected. Generally the capillary porosity of the cement paste increase with the increase of the water-cement ratio. These findings could be related to the discontinuities of the pores in the sample. For the carbonated sample of CEM I cement paste with water-cement ratio 0.4 the capillary porosity increased but not when the water cement ratio increased which also not in agreement with what reported in the literature.
The results for the *CEM III/B cement paste* indicate that at increasing water cement-ratio the capillary porosities increased. In general, pastes samples made with slag blended cement showed higher porosities than those made with ordinary Portland cement this was not in agreement with the result obtained for the water cement ratio 0.4.The capillary porosity for the CEM I cement paste was higher compared to CEM III/B.

The capillary porosity of the *SP Mix cement paste*, due to the addition of Fly ash, showed decreasing compared to CEM I and CEM III/B cement paste but, at increasing the water cement the capillary porosity increased.

The results for the *carbonated CEM I paste showed* a decrease in the capillarity porosity only when the water-cement ratio was 0.6. This could be related to the decreasing volume of the permeable voids of cement paste exposed to accelerated carbonation. This might be accountable to the fact that the $CaCO3_{crystals}$ occupy more volume compared to $Ca(OH)_2$. On the contrary, calcium carbonate has a low solubility and it, therefore, promotes blocking of pores decreasing the permeability of the cement paste. CEM I cement paste had a higher calcium content compared to slag cement paste. This could result in an increase of the formation of $CaCO_3$ for the case of a higher water content (Hussaina et al., 2015).

Effect of the treatment with Na-MFP solution on the capillary porosity

Table 29: Effect of the treatment with Na-MFP solution on the capillary porosity

Cement paste	W/C 0.4				W/C 0.5				W/C 0.6			
	Control	C_{28d}	$T \rightarrow C_{28d}$	$C_{28d} \rightarrow T$	Control	C_{28d}	$T \rightarrow C_{28d}$	$C_{28d} \rightarrow T$	Control	C_{28d}	$T \rightarrow C_{28d}$	$C_{28d} \rightarrow T$
CEM I	20%	25%	14%	14%	18%	18%	13%	13%	17%	14%	20%	12%
CEM III/B	19%	25%	17%	18%	27%	39%	30%	31%	52%	56%	18%	25%
SP Mix	15%	16%	13%	15%	30%	36%	34%	30%	40%	45%	19%	24%

Table 29 presents the capillary porosity for cement pastes as measured with the MIP test. It was noted whether the treatment was before or after carbonation; a decrease in the porosity compared to the carbonated samples was obtained. Except for CEM I cement paste with a water-cement ratio of 0.6 a decrease in the porosity when the treatment was applied after carbonation.

The effect of a higher water-cement ratio on the treatment was as follows:

- With a water-cement ratio of 0.5, CEM I and CEM III /B showed more improvement in the porosity when treated before carbonation compared to the carbonated samples while the opposite was the case for SP Mix paste.
- With a water-cement ratio of 0.6, CEM III/B and SP Mix showed more improvement in the porosity when treated before carbonation compared to the carbonated sample while the opposite was the case for CEM I paste.

The improvement in the capillary porosity indicated that Na-MFP reacted with the cement matrix forming a material blocking the pores in the cement matrix. The difference between before or after carbonation varied between 1-5 % for the end results of the porosity. The porosity recovered for the carbonated CEMIII/B paste after applying the treatment were 7%, 8% and 31% for water-cement ratio 0.4, 0.5 and 0.6, respectively. See the results in Table 30.

Table 30: Covered porosity for the treatment before or after carbonation
*Change in the capillary porosity for treatment before carbonation compared to control sample
** change in the capillary porosity for treatment after carbonation compared to carbonated sample

Cement paste type	W/C 0.4		W/C 0.5		W/C 0.6	
	*($T \rightarrow C_{28d}$)	**($C_{28d} \rightarrow T$)	*($T \rightarrow C_{28d}$)	**($T \rightarrow C_{28d}$)	*($T \rightarrow C_{28d}$)	**($C_{28d} \rightarrow T$)
CEM I	6%	12%	5%	5%	-3%	2%
CEM III/B	2%	7%	-3%	8%	34%	31%
SP Mix	2%	2%	-4%	6%	21%	21%

Effect of carbonation and treatment on the pore size distribution

From the MIP measurements, the pore size distribution was analysed. These were done for several characteristic pore sizes (radii) and critical pore radius. The critical radius is the inflection point on the curve of intruded volume versus pore size that is the pore radius corresponding to the peak value in dV/dD curve. This size corresponds to the smallest pores creating a connected path in pore structure.

Figure 41 presents the critical pore size for all samples and the numerical result is presented in Table 31. The results which were underlined in the table showed a high critical pore size combared to what reported in the literatures. It is noted that the lowest critical pore size was reached when the treatment was before carbonation for all samples.

Table 31: Effect of the treatment with Na-MFP solution on the critical pore size (µm)

Cement paste	**W/C 0.4**				**W/C 0.5**				**W/C 0.6**			
	Control	**C_{28d}**	**$T\rightarrow C_{28d}$**	**$C_{28d}\rightarrow T$**	**Control**	**C_{28d}**	**$T\rightarrow C_{28d}$**	**$C_{28d}\rightarrow T$**	**Control**	**C_{28d}**	**$T\rightarrow C_{28d}$**	**$C_{28d}\rightarrow T$**
CEM I	0.095	0.543	0.045	0.073	0.073	0.073	0.045	0.045	0.095	0.073	0.036	0.073
CEM III/B	0.083	0.045	0.019	0.155	0.271	0.118	0.045	0.236	0.442	0.118	0.029	0.312
SP Mix	0.045	0.206	0.017	0.206	0.073	0.442	0.027	0.442	0.073	0.271	0.022	0.271

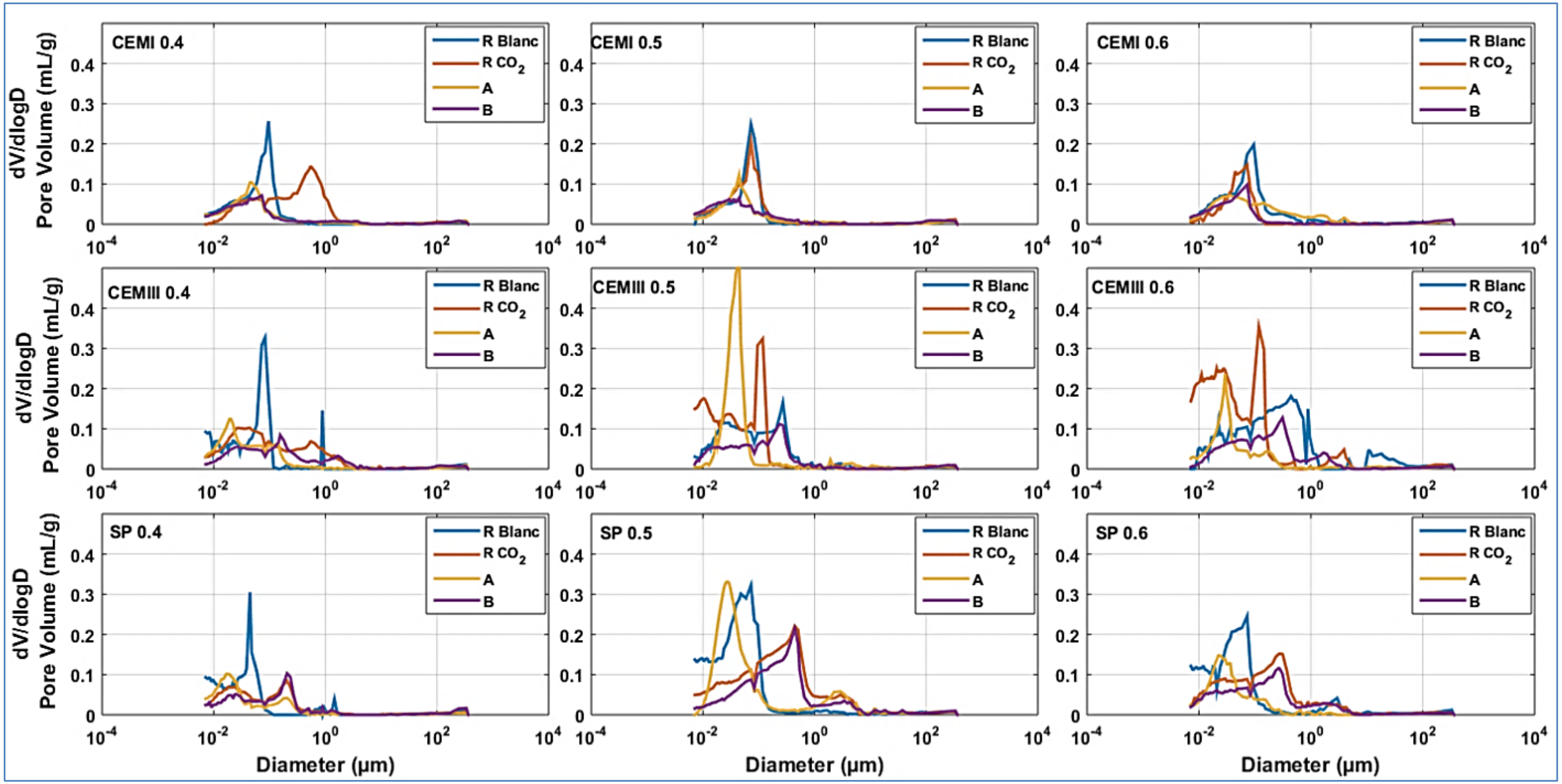

Figure 41: Critical pore size as measured by MIP Test (B: T→C_{28d} and A: T→C_{28d})

4.2.3. Thermogravimetric analysis/Differential Scanning Calorimetry (TGA/DSC)

The TGA (thermogravimetric analysis) curve presents the relationship between the temperature increase and the weight loss of a sample heated constantly from 40 to 1050 °C with a heating rate of 10°C/min. The DSC (Differential Scanning Calorimetry) curve presents the temperatures and heat flow associated with thermal transitions: phase transitions/changes, dehydration, gas evolution, melting, and crystallization.

The procedures used in this analysis and the data obtained from the tests were:

1. From the DSC curve, the onset temperatures for the phase transition zones were determined.
2. From the TGA curve, the percentages of the mass loss were calculated for the specified phase transitions temperature. The mass losses were calculated for each temperature interval for each sample.

The calculation steps and the TGA/DSC curves for each test are presented in Appendix 4. In this section, the results are summarized in tables for comparison and analyses. Table 32 present the expected mean transition.

Table 32: The expected mean transition

Peak	Approximated Temp range (^{o}C)	Process
Peak1	105-200	Dehydration of C-S-H gel and ettringite
Peak2	400-450	Dehydration of calcium hydrate(CH)
Peak3	500-800	Decarbonation of calcium carbonate ($CaCO_3$)

Overview 2: thermal stability of hydroxyapatite and calcium apatite

In previous studies on the thermal stability of the hydroxyapatite (HA), Yanming et al. (2005) and Nikčevića et al., (2004) proved that at around 800-850°C the weight loss is caused by the release of OH^- groups from the HA crystals and above 1000°C is the further decomposition of the HA (Nikčevića et al., 2004; Yanming et al., 2005).

Adolfsson et al. (1999) reported that the decomposition reactions of into tricalcium phosphate (TCP;$Ca_3(PO_4)_2$) could be divided into two steps, according to the formulae 1 and 2.

$$Ca_{10}(PO_4)_6(OH)_2 \rightarrow Ca_{10}(PO_4)_6(OH)_{2-2x}O_x + x\,H_2O \quad \text{(at about 800 °C)} \quad (1)$$

$$Ca_{10}(PO_4)_6(OH)_{2-2x}O_x \rightarrow 3Ca_3(PO_4)_2 + CaO + (1-x)\,H_2O \quad \text{(at about 1220 °C)} \quad (2)$$

Tõnsuaadu et al. (2012) investigate the thermal stabilty of diefferent type of apatite and hydroxyapatite. The most thermally stable is Fluorapatite ($CaPO_4$) with the melting point at ~1650°C which is outside the range of this study.

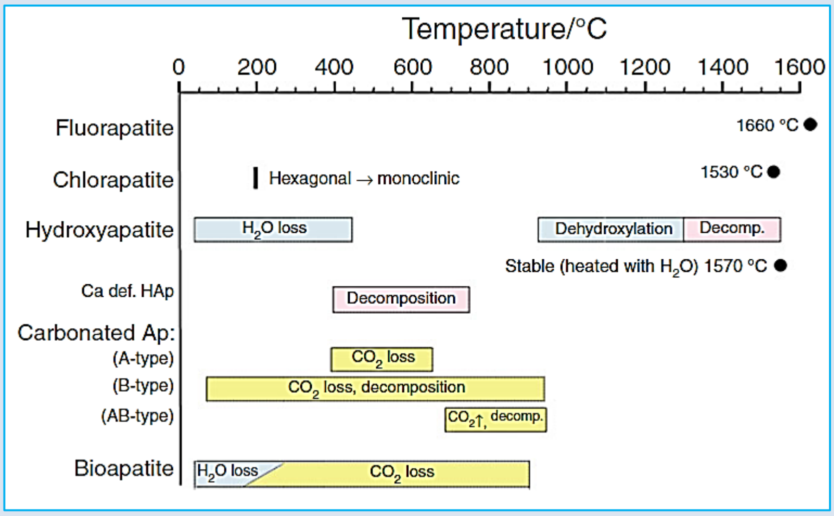

Figure 42: A review on the thermal stability of calcium apatites (Tõnsuaadu et al., 2012)

Previous studies about the thermal analysis of hydroxyapatite and calcium apatite were used to understand whether the weight loss in Peak 3 (500-800°C) and higher for the tested samples A ($T \rightarrow C_{28days}$) and B ($C_{28day} \rightarrow T$) were related to decarbonation only or a combination of decarbonation and decomposition of HA.

Analysis of the CEM I paste samples

Figure 44 shows the TGA/DSC graph of CEM I samples with water cement ratio 0.4, 0.5 and 0.6. For each water cement ratio, four samples were tested: 1) control, 2) carbonated for 28 days (C_{28days}), 3) treatment before carbonation (A: T→C_{28days}) and 4) treatment after carbonation (B: C_{28day}→T). Table 33 presents the numerical values of the results obtained from the test. The red numbers in the tables are used for explanation in the analysis.

Table 33: Result of DSC/TGA temperature interval for CEM I

CEM I Cement Paste		**W/C 0.4**		**W/C 0.5**		**W/C 0.6**	
		Temp-interval	**Mass loss**	**Temp-interval**	**Mass loss**	**Temp-interval**	**Mass Loss**
	Peaks	**(T°C)**	**(%)**	**(T°C)**	**(%)**	**(T°C)**	**(%)**
Control	Peak1	121-247	9.1(1)	121-246	6.8	104-240	9.8
	Peak2	456-550	4.9	460-558	3.5	466-516	3.2
	Peak3	722-857	1.0	701-849	3.2	717-892	2.9
C_{28days}	Peak1	125-257	4.3	93-239	8.4(2)	119-269	6.9(2)
	Peak2	459-576	2.3	469-540	2.3	458-508	1.6
	Peak3	791-916	10.7(2)	782-933	5.6	794-898	3.59
A: T→C_{28days}	Peak1	112-257	7.3	112-241	6.9	99-232	6.4
	Peak2	461-534	2.0	459-586	2.0	328-636	4.0
	Peak3	802-868	1.0(3)	817-860	0.4	780-903	0.3
B: C_{28day} →T	Peak1	94-267	9.2	100-249	11.4	119-276	10.0
	Peak2	459-622	6.6	453-557	4.3	457-581	1.4
	Peak3	622-831	2.7	742-899	3.1	750-877	3.4

Table 34: Total mass loss (%) at the end of the test for CEM I cement paste

CEM I – cement paste			
	W/C 0.4	**W/C 0.5**	**W/C 0.6**
Control	23.1(1)	21.9	23.6
C_{28days}	30.6	24.6	25.6
A: T→C_{28days}	17.4(3)	17(3)	13.9(3)
B:C_{28day}→T	25.5	22.9	24.6

The observations on the results are as follows:

1) The total mass loss for CEM I cement paste with w/c 0.4 was higher compared to cement pastes with W/C of 0.5 and 0.6. A reason is the dehydration of the C-S-H gel in Peak 1 (121-247°C) which was higher than for cement pastes with a W/C of 0.5 or 0.6. Besides that the sample showed a high mass loss of 3.94% in the beginning of the test (40-120^{o}C), see Figure 43; the sample was not dry enough and free water was released.
2) The mass loss due to the decarbonation of calcium carbonate Peak3 (791-916^{o}C) with carbonated CEM I cement paste having a W/C of 0.4 was higher compared to the carbonated cement paste with water-cement ratios of 0.5 or 0.6.
3) From Table 34 the results indicate that the treatment before carbonation showed lower mass losses compared to the treatment after carbonation for a range of test temperatures (40-1050^{o}C). The mass loss due to the dehydration of C-S-H gel and ettringite in Peak 1 and the dehydration of calcium hydrate (CH) in peak 2 was lower compared to the cement paste treated after carbonation. This could be related to the formation of a material which can discompose in temperatures higher than the given temperature in the test 1050^{o}C. Based on the studies reported by Nikčevića et al. (2004) and Adolfsson et al. (1999) and presented in Overview 2, the pyrolysis of carbonate from calcium hydroxyapatite (HA) occurs at a temperature just higher than 1050 ^{o}C. See Figure 44 where these points are identified as 1 and 2.

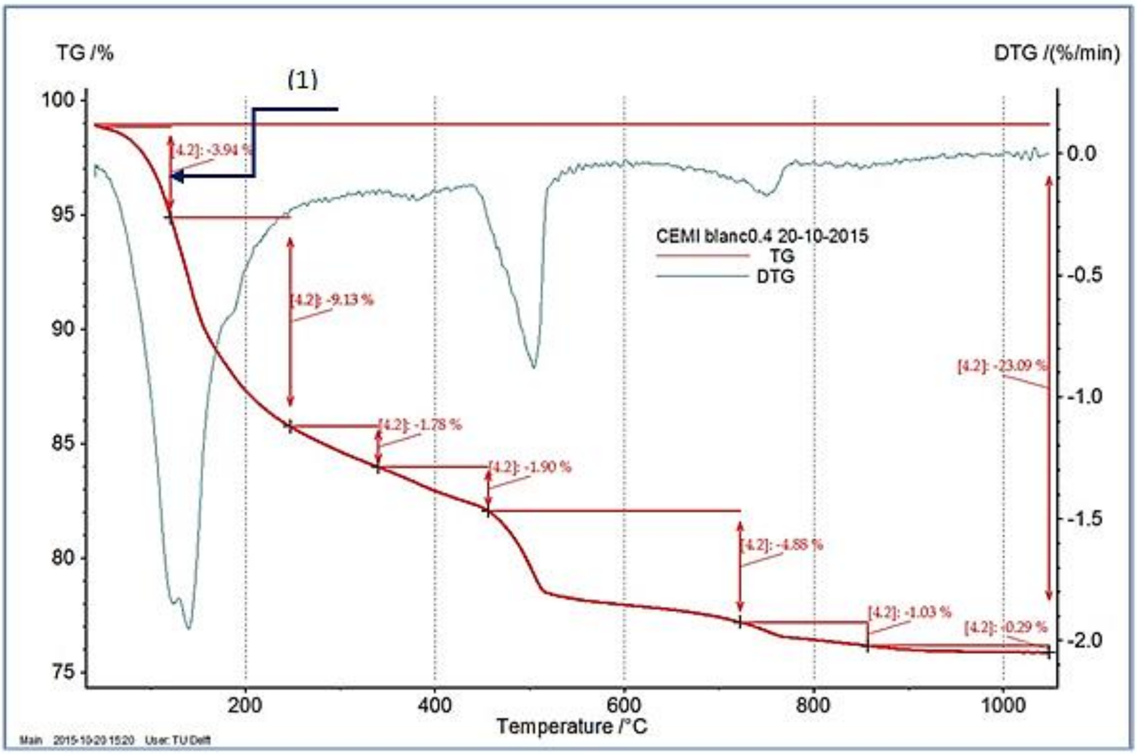

Figure 43: TG/DTG for control cement paste CEMI I -W/C 0.4

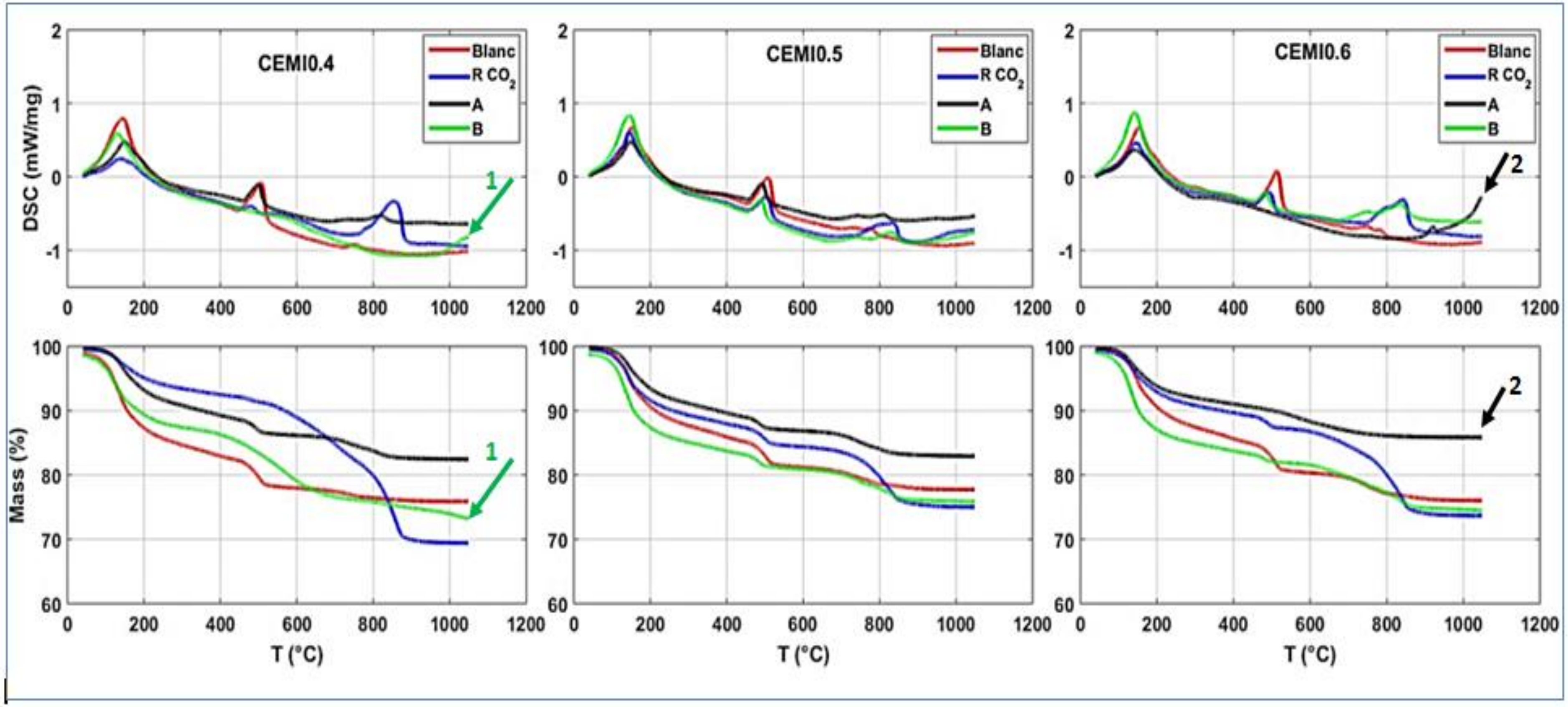

Figure 44: TGA and DSC result for CEM I cement paste for different treatments with W/C of 0.4, 0.5 and 0.6 (A: T→C_{28days} and B: C_{28day}→T)

1. Peak around 1050 °C showed mass loss which could be related to the decomposition of Apatite for B: C28day→T

2. Peak around 1050 °C with no mass loss no clear evidence of formation of Apatite for A: T→C_{28days}

Analysis for CEM III/B cement paste

Figure 45 presents the TGA/DSC results for the CEM III/B cement pastes. The analysis and observations with regard to results are as follows:

1. Peak around 900°C due to decarbonation process (decomposition of $CaCO_3$);
2. Peak around 450 ± 50 °C due to the dehydration of the CH which was clear for the control samples with different water-cement ratios but not for the treated samples regardless whether the treatment was before or after carbonation. This could be due to the reaction of Na-MFP with the CH forming calcium hydroxyapatite which will decompose at around 800 °C according to Adolfsson et al. (1999);
3. Peak around 1050°C showed mass losses, see Table 35, which could be related to the decomposition of Apatite for B: C28day→T;
4. Peak around 1050 °C with small mass losses for samples treated before carbonation which could be due to traces of apatite formation.
5. The total mass loss increased with the increase of the water-cement ratio. This was only the case for the control and carbonated cement paste samples, but not for the treated samples. The treatment after carbonation (B: C_{28day} →T) showed a slightly different mass loss of about 1%. The treatment before carbonation (A: T→C_{28days}) showed a lower mass loss around 800°C (0.1%) for a water-cement ratio of 0.4 and for the cement paste with a water-cement ratio of 0.6 the loss was around 5.0%, see Figure 46. This could be due to the decarbonation process indicated by a large peak in the range of 800-997°C followed by decomposition of another material around 1048°C which could be traces of apatite.
6. The mass loss for cement paste with a water- cement ratio of 0.4 for the sample treated before carbonation (A: T→C_{28days}) was higher compared to the samples with a water-cement ratios of 0.5 or 0.6. This might be related to the mass loss of CH indicated by a large peak around 400-762°C with a mass loss of 11.3%.

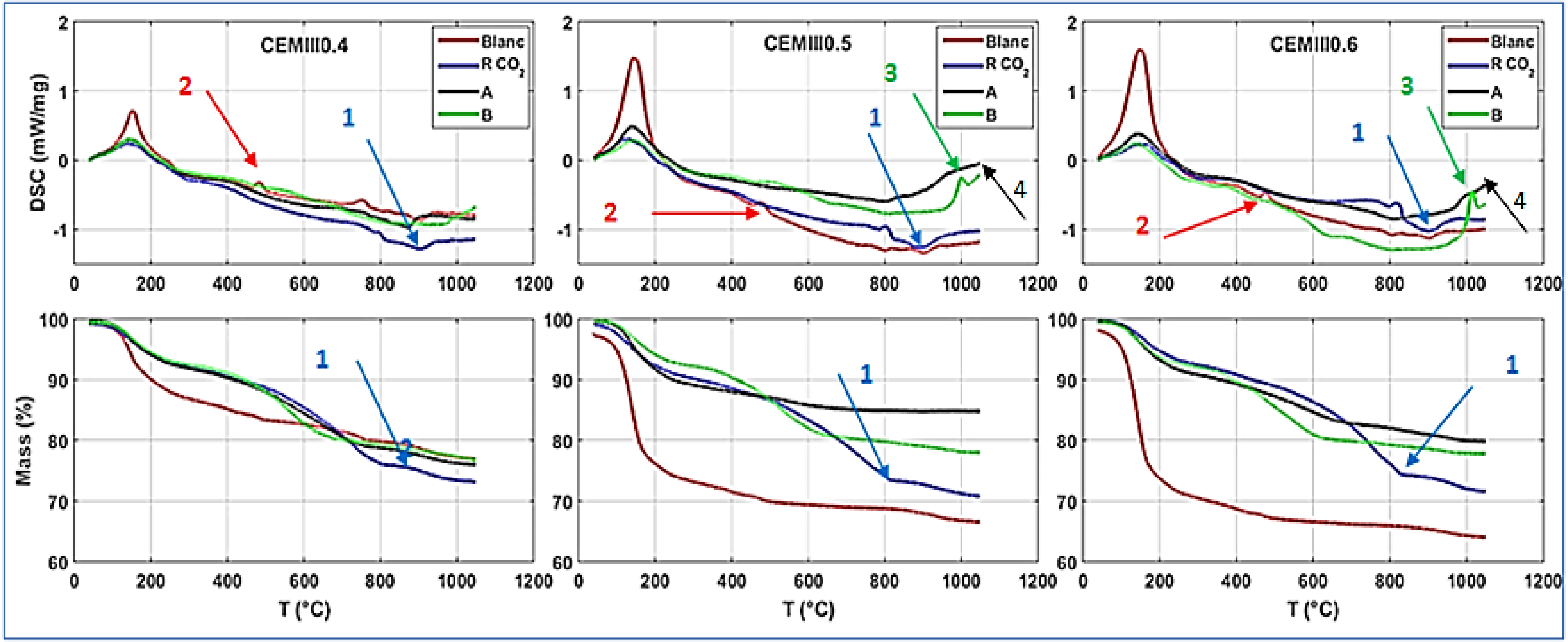

Figure 45: TGA and DSC for CEM III/B paste samples with each treatment with a W/C of 0.4, 0.5 and 0.6 (colored numbers are explained in the analysis)

Table 35: Result of DSC/TGA temperature interval for CEM III/B
(red numbers are explained in the analysis)

CEM III/B Cement Paste		**W/C 0.4**		**W/C 0.5**		**W/C 0.6**	
		Temp-interval	**Mass loss**	**Temp-interval**	**Mass loss**	**Temp-interval**	**Mass loss**
	Peaks	**(T°C)**	**(%)**	**(T°C)**	**(%)**	**(T°C)**	**(%)**
Control	Peak1	97-274	11.2	112-247	18.8	120-243	19.8
	Peak2	412-468	0.8	459-556	1.1	461-468	0.1
	Peak3	732-803	1.1	802-911	1.0	468-808	1.7
C_{28days}	Peak1	108-272	5.9	102-263	6.8	105-250	5.8
	Peak2	400-562	3.8	419-533	2.5	305-486	3.1
	Peak3	746-804	2.2	787-858	1.7	604-829	11.8
	Peak4	804-1048	3.8	858-965	1.5	993-1048	1.0
A: T→C_{28days}	Peak1	106-200	4.8	115-249	8.0	110-271	7.3
	Peak2	400-762(6)	11.3(6)	249-768	5.0	311-519	3.9
	Peak3	762-864	0.9	768-1048	0.1(4)	602-815	2.8
	Peak4	864-932	1.1			815-967	1.6
	Peak5					967-1048	0.8 (4)
B:C_{28day}→T	Peak1	110-261	5.8	112-267	6.0	101-288	6.6
	Peak2	429-700	10.3	456-549	4.4	288-637	11.9
	Peak3	700-901	1.0	632-820	1.5	637-801	1.0
	Peak4	901-1048	1.5	820- 976	1.3	801-997	1.4
	Peak5			976-1048	0.6(3)	997-1048	0.5(3)

Table 36: Total mass loss (%) at the end of the test for CEM III/B cement paste
(red numbers are explained in the analysis)

	CEM III/B-cement paste		
	W/C 0.4	**W/C 0.5**	**W/C 0.6**
Control	22.5	30.8	34.2
C_{28days}	26.1	28.5	28.4
A: T→C_{28days}	23.7(5)	14.8	19.8
B:C_{28day}→T	22.6	21.4	21.8

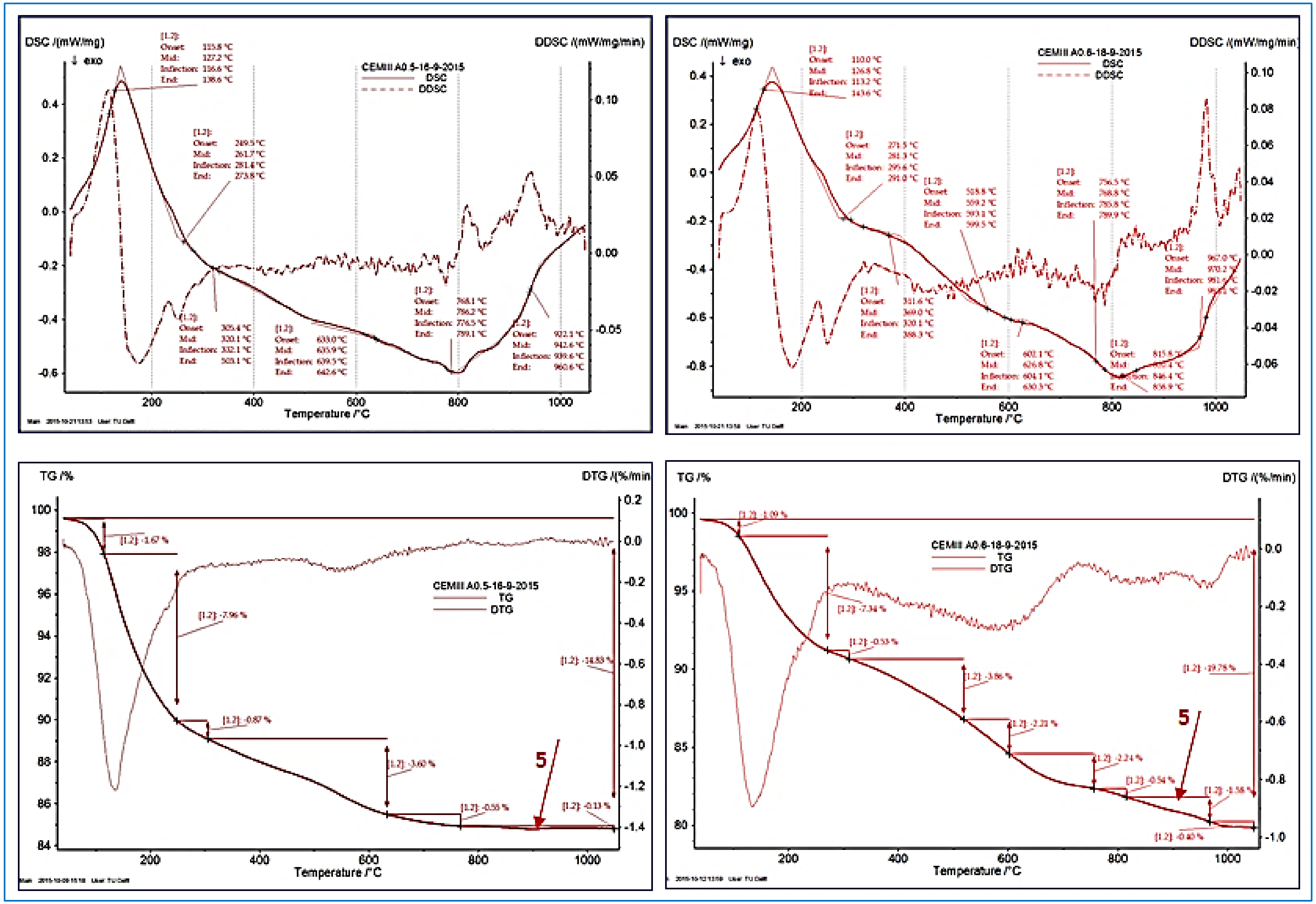

Figure 46: DCA/ TGA result for CEM III/B 0.5 left and CEM III/B right for the treatment before carbonation

Analysis for SP MIX paste samples TGA/DSC results

Figure 47 and Table 37 present the TGA/DSC results for the SP Mix cement pastes. The analysis and the observation on the results were as follows:

1. Peak around 900°C due to decarbonation process (decomposition of $CaCO_3$) and the a loss corresponds to a decomposition of CO_3^{2-} bearing minerals in FA such as calcite.
2. Peak around 450 ± 50°C due to the dehydration of the CH for the control samples and not for the treated samples. This was similar for with CEM III/B cement pastes.
3. Peak around 1050°C showed mass loss which could be related to the decomposition of apatite for B: C_{28day}→T
4. Peak around 1050 °C with small mass losses for samples treated before carbonation. This could be due to traces of the formation of apatite.
5. Control samples experienced high loss of mass due to free water at the beginning of the test (40-105 °C) which was around 4%.
6. Treatment before carbonation showed less mass loss compared to treatment after carbonation.

Table 37: Result of DSC/TGA temperature interval for SP Mix Paste samples

Cement Paste SP Mix		W/C 0.4		W/C 0.5		W/C 0.6	
		Temp-interval	Mass loss	Temp-interval	Mass loss	Temp-interval	Mass loss
	Peaks	(T°C)	(%)	(T°C)	(%)	(T°C)	(%)
control	Peak1	115-242	16.4	104-192	11.1	93-204	9.3
	Peak2	462-583	1.4	459-548	1.4	414-512	1.8
	Peak3	980	small mass loss	897-973	small mass loss	874-956	0.7
C_{28days}	Peak1	108-241	4.5	108-236	4.3	123-236	3.9
	Peak2	420-532	1.9	402-562	3.4	313-491	2.5
	Peak3	530-802	11.5	741-827	4.1	806-902	3.6
		802-922	3.3	827-973	1.5	902-1048	1.5
A: T→C28days	Peak1	108-250	6.8	108-250	6	105-272	7.6
	Peak2	300-800	5.8	457-582	3.5	441-542	1.5
	Peak3	800-1048	1.4	747-808	0.4	615-1048	2.2
B:C28day→T	Peak1	91-243	9.7	110-278	7.1	106-262	5.8
	Peak2	305-718	11.5	411-506	3.4	441-487	1.8
	Peak3	718-912	1.5	>600	Wide peak for decarbonation	745-889	0.8
		912-1048	small mass loss	901-1048	1.6	889-1048	1.4

Table 38: Total mass loss (%) at the end of the test for SP Mix cement paste
(red numbers are explained in the analysis)

SP MIX-cement paste			
	W/C 0.4	**W/C 0.5**	**W/C 0.6**
Control	26.7 (5)	22.5	21.2
C_{28days}	25.1	24	25.4
A: T⍰C_{28days}	15.5	18.8	14.7
B:C_{28day}→T	25.7 (5)	23.1	21.3

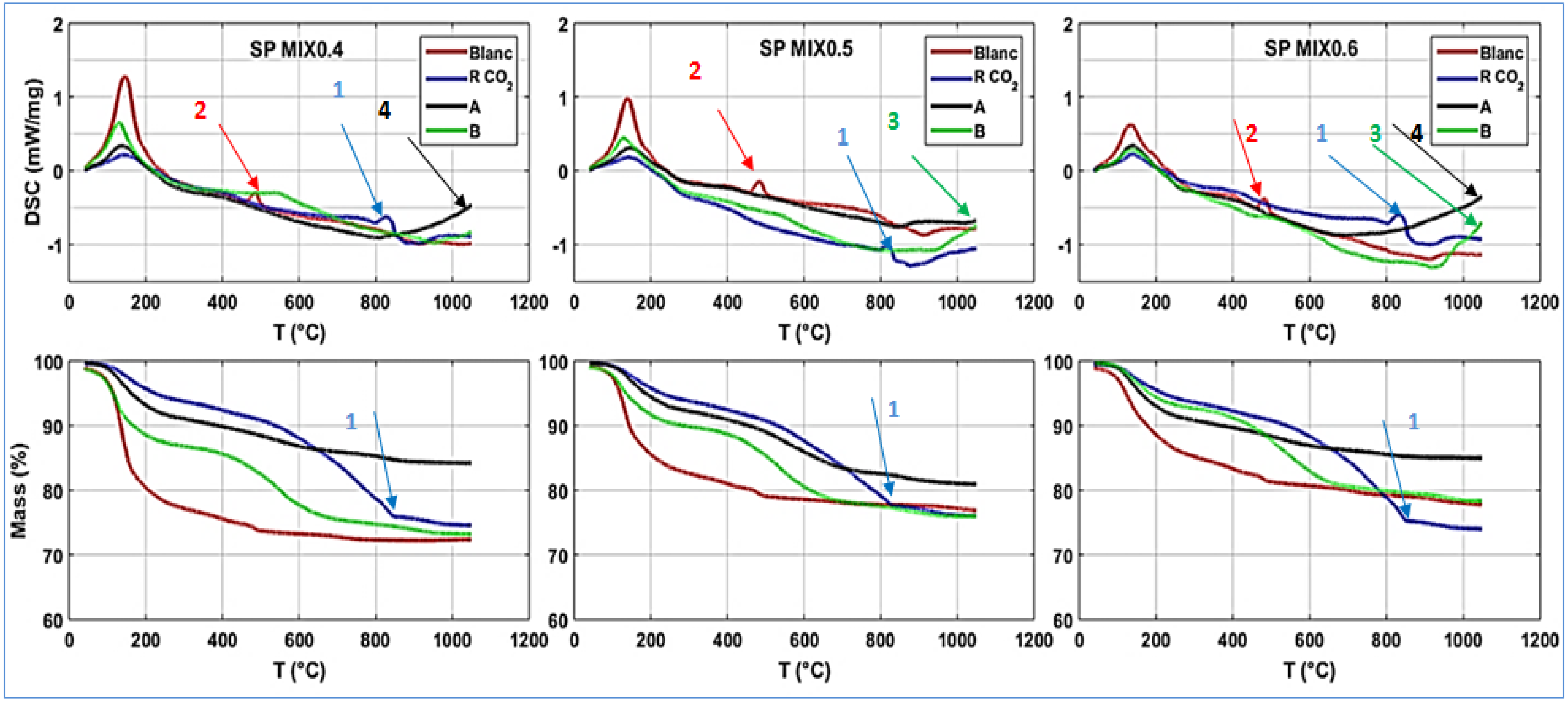

Figure 47: TGA and DSC for SP MIX Paste samples with each treatment with W/C =0.4, 0.5 and 0.6

4.3. Results overview

In this part, an overview of the results of the experiments is presented.

Table 39 presents the results obtained for the investigation of the penetration and the reactivity of the Na-MFP solution with a weight concentration of 25% into the mortar samples mixed with CEM III /B. The Na-MFP solution was applied by means of a single paint brush on the surface for wet and sealed cured mortar samples (W/C=0.45) exposed during different periods to accelerated carbonation.

Table 40 ,Table 41 and Table 42 present the results obtained from the microstructure experiments for the three types of cement. The samples were impregnated under vacuum with Na-MFP solution. The applied tests were Nano-indentation (NI), Mercury Intrusion Porosimetry (MIP), and Thermogravimetric analysis/Differential Scanning Calorimetry (TGA/DSC).

Table 39: Results overview of the penetration of the Na-MFP solution applied on the mortar samples

Test Type	Sample, storage, and treatment	Results overview
Photomicrographs XPL (Thin section around 30µm)	- Cement mortar CEM I ,CEM III/B and SP MIX - W/C = 0.45 and C/S =1:3 - Curing under water for 28 days. - Accelerated carbonation for 14/28 days (CO_2 3% &RH 65%). - Na-MFP solution applied on the surface before/after carbonation.	- The maximum penetration depth of the Na-MFP solution was about 8 mm for CEMIII/B cement mortar after the sample was exposed for 28 days to accelerated carbonation. - The reacted layer appears as a dark layer under the XPL microscope suggesting an amorphous formation. - **Detailed Results: Table 19**
Scanning Electron Microscopy (SEM/EDX) results: measuring the P(At%) concentration in different depth	- CEM III/B mortar - W/C= 0.45 - Sealed curing for 124 days. - Accelerated carbonation for 14/28 days (CO_2 3% &RH 65%) - Na-MFP solution applied on the surface after carbonation	- An clear indication of the penetration of Na-MFP solution to a depth around 10 mm for the samples treated after 14 days carbonation - Traces of phosphorus found to a depth of 20 mm for the samples treated after carbonation for 28 days. - **Detailed Results: Table 20**
Stereomicroscope images (phenolphthalein test)	- Cement paste CEM III/B and SP Mix - W/C=0.45 - Curing for 28 days in the desiccators (20 °C and RH 55%) - Accelerated carbonation for 14/28 days (CO_2 3% &RH 65%)- - Na-MFP solution applied on the surface before/after carbonation.	- Decrease in the carbonation depth for the samples treated after carbonation - Treatment after carbonation reduces the maximum carbonation depth from 1.7 mm to 1.0 mm and from2.1 mm to 0.32 for CEM III/B and SP Mix paste sample, respectively. - **Detailed Results: Table 21**

Table 40: Overview results of microstructure analysis for CEM I cement paste
(A: T (Na-MFP) → C_{28days} B: C_{28}days → T (Na-MFP) C: C_{28days} R: Control sample)

		CEM I cement paste	
W/C	**Test type**	**Results overview**	
0.4	**Nanoindentation**	*Elastic Modulus (GPa)* E(<18) : C < R, C ≈ A ≈ B E(18-39): R < C, A < B < C E(36-39): R < C, C < A ≈ B E(>39) : C < R, C < B < A	*Hardness (GPa):* H (<0.8) : C < R, A < C < B H (0.8-1.2): R < C, C < B < A H (1.3-1.8): R < C, C ≈ A < B H (>1.8) : C < R, A < B < C
	MIP: *Percentage of Capillary porosity (CP%) decreased due to the treatment A or B compared to the carbonated sample and the Critical pore size (d_{cr} µm)*	*Capillary porosity:* C-A ≈ C-B = 12%	*Critical pore size:* A_{dcr}= 0.045 µm B_{dcr} =0.073 µm C_{dcr} =0.543 µm
	TGA/DSC: *Mass loss (%) due to dehydration of (CH) and decarbonation* ($CaCO_3$) *process and (mass loss at higher temperatures)*	*M(%) due to dehydration of (CH):* R: 4.9% C: 2.3% A: 2% B: 6.6%	*M(%) due to decarbonation* ($CaCO_3$): R: 1% C: 11% A: 1% B: 3%
0.5	**Nanoindentation:**	*Elastic Modulus (GPa)* E(<18) : C < R, C≈ A≈ B E(18-39): C < R, A < B < C E(36-39): C < R, C< A < B E(>39) : R < C, C< B < A	*Hardness (GPa):* H (<0.8) : C < R, B < A < C H (0.8-1.2): R < C, C ≈ A < B H (1.3-1.8): C < R, C < A < B H (>1.8) : R < C, B < C < A
	MIP: *Percentage of Capillary porosity (CP%) decreased due to the treatment A or B compared to the carbonated sample and the Critical pore size (d_{cr} µm)*	*Capillary porosity (CP%)* C-A ≈ C-B = 6%	*Critical pore size:* A_{dcr}= 0.045 µm B_{dcr} =0.045 µm C_{dcr} =0.073 µm
	TGA/DSC: *Mass loss (%) due to dehydration of (CH) and decarbonation* ($CaCO_3$) *process and (mass loss at higher temperatures)*	*M(%) due to dehydration of (CH):* R: 3.5% C: 2.3% A: 2% B: 4.3%	*M(%) due to decarbonation (CaCO3):* R: 3.2% C: 5.6% A: 0.4% B: 3.1%
0.6	**Nanoindentation**	*Elastic Modulus (GPa)* E(<18) : C < R, C ≈ B < A E(18-39): R < C, B < A < C E(36-39): R < C, A ≈ B < C E(>39) : R < C, C < A < B	*Hardness (GPa):* H (<0.8) : C < R, A < C < B H (0.8-1.2): R < C, A ≈ B < C H (1.3-1.8): R < C , C ≈ A < B H (>1.8) : R < C , C < A < B
	MIP: *Percentage of Capillary porosity (CP%) decreased due to the treatment A or B compared to the carbonated sample and the Critical pore size (d_{cr} µm)*	**Increase in Capillary porosity :* A > C (6%) C-B = 2%	*Critical pore size:* A_{dcr}=0.036 µm B_{dcr} =0.073 µm C_{dcr} =0.073 µm
	TGA/DSC: *Mass loss (%) due to dehydration of (CH) and decarbonation* ($CaCO_3$) *process and (mass loss at higher temperatures)*	*M(%) due to dehydration of (CH):* R: 3.2% C: 1.6% A: 4% B: 1.4%	*M(%) due to decarbonation (CaCO3):* R: 2.9% C: 3.6% A: 0.3% B: 3.4%

Table 41: Overview results of microstructure analysis for CEM III/B cement paste
(A :T (Na-MFP) → C28days B :C28days → T (Na-MFP) C : C28days R: Control sample)

		CEM III/B cement paste	
W/C	**Test type**	**Results overview**	
0.4	**Nanoindentation**	*Elastic Modulus (GPa)* E(<18) : R < C, A < B < C E(18-39): C < R, B < C < A E(36-39): C < R, C ≈ A < B E(>39) : R < C , C < A < B	*Hardness (GPa):* H (<0.8) : C < R, B < A < C H (0.8-1.2): C < R, C < B < A H (1.3-1.8): R < C, A < C < B H (>1.8) : R ≈ C, C < A < B
	MIP: *Percentage of Capillary porosity (CP%) decreased due to the treatment A or B compared to the carbonated sample and the Critical pore size (d_{cr} µm)*	*Capillary porosity:* C-A ≈ C-B = 7%	*Critical pore size:* A_{dcr} = 0.019 *µm* C_{dcr} = 0.045 µm B_{dcr} = 0.155 µm
	TGA/DSC: *Mass loss (%) due to dehydration of (CH) and decarbonation* ($CaCO_3$) *process and (mass loss at higher temperatures)*	*M(%) due to dehydration of (CH):* R: 0.8% C: 3.8% A: 11.3% B: 10.3%	*M(%) due to decarbonation (CaCO3):* R: 1.1% C: 2.2% (3.8%) A: 1% (1.1%) B: 1% (1.5%)
0.5	**Nanoindentation:**	*Elastic Modulus (GPa)* E(<18) : R < C, B < A < C E(18-39): C < R, C < A < B E(36-39): C ≈ R, C ≈ A < **B** E(>39) : 0 C≈ A < **B**	*Hardness (GPa):* H (<0.8) : C < R, B < A < C H (0.8-1.2): R < C, C < A < B H (1.3-1.8): R < C, A < C < B H (>1.8) : R < C, C < A < B
	MIP: *Percentage of Capillary porosity (CP%) decreased due to the treatment A or B compared to the carbonated sample and the Critical pore size (d_{cr} µm)*	*Capillary porosity:* C-A ≈ C-B = 8%	*Critical pore size:* A_{dcr} = 0.045 *µm* C_{dcr} = 0.118 µm B_{dcr} = 0.236 µm
	TGA/DSC: *Mass loss (%) due to dehydration of (CH) and decarbonation* ($CaCO_3$) *process and (mass loss at higher temperatures)*	*M(%) due to dehydration of (CH):* R: 1.1% C: 2.5% A: 5% B: 4.4%	*M(%) due to decarbonation (CaCO3):* R: 1% C: 1.7% (1.5%) A: 0.1% B: 1.5% (1.3%) (0.6%)
0.6	**Nanoindentation**	*Elastic Modulus (GPa)* E(<18) : R < C, A < C < B E(18-39): C < R, B < C < A E(36-39): C < R, C ≈ B≈ 0 < A E(>39) : C < R, B=0, C ≈A	*Hardness (GPa):* H (<0.8) : R < C, A < C < B H (0.8-1.2): C < R, B < C < A H (1.3-1.8): R ≈ C, B < A < C H (>1.8) : C < R, B ≈ C < A
	MIP: *Percentage of Capillary porosity (CP%) decreased due to the treatment A or B compared to the carbonated sample and the Critical pore size (d_{cr} µm)*	*Capillary porosity:* C-A =38% C-B = 31%	*Critical pore size:* A_{dcr} = 0.029 *µm* C_{dcr} = 0.118 µm B_{dcr} = 0.312 µm
	TGA/DSC: *Mass loss (%) due to dehydration of (CH) and decarbonation* ($CaCO_3$) *process and (mass loss at higher temperatures)*	*M(%) due to dehydration of (CH):* R: 0.1% C: 3.1% A: 3.9% B: 11.9%	*M(%) due to decarbonation (CaCO3):* R: 1.7% C: 11.8% (1.0%) A: 2.8% (1.6%)(0.8%) B: 1.0% (.4%) (0.5%)

Table 42: Overview results of microstructure analysis for CEM III/B cement paste
(A :T (Na-MFP) → C28days B :C28days → T (Na-MFP) C : C28days R: Control sample)

		SP Mix cement paste	
W/C	**Test type**	**Results overview**	
0.4	**Nanoindentation:**	*Elastic Modulus (GPa)* E(<18) : R < C, A < B < C E(18-39): C < R, C < A ≈ B E(36-39): C ≈ R ≈ B < A E(>39) : C ≈ R ≈ B < A	Hardness (GPa): H (<0.8) : R < C, B < A < C H (0.8-1.2): C < R, C < B < A H (1.3-1.8): C < R, C < A < B H (>1.8) : C ≈ R, A < C < B
	MIP: *Percentage of Capillary porosity (CP%) decreased due to the treatment A or B compared to the carbonated sample and the Critical pore size* (*d_{cr} μm*)	*Capillary porosity:* C-A =3% C-B = 1%	*Critical pore size:* A_{dcr} = 0.017 *μm* B_{dcr} ≈ C_{dcr} = 0.206 μm
	TGA/DSC: *Mass loss (%) due to dehydration of (CH) and decarbonation* ($CaCO_3$) *process and (mass loss at higher temperatures)*	*M(%) due to dehydration of (CH):* R: 1.4% C: 1.9% A: 5.8% B: 11.5%	*M(%) due to decarbonation (CaCO3):* R: Crystallization small M% C: 11.9% (3.3%) A: 1.4% B: 1.5% (Crystallization small M%)
0.5	**Nanoindentation**	*Elastic Modulus (GPa)* E(<18) : C < R, B < C < A E(18-39): C < R, B < A ≈ C E(36-39): R < C, A < C < B E(>39) : R ≈ C, C < A < B	*Hardness (GPa):* H (<0.8) : C < R, B < C < A H (0.8-1.2): R < C, B < A < C H (1.3-1.8): C < R, C < A < B H (>1.8) : R < C, A < C < B
	MIP: *Percentage of Capillary porosity (CP%) decreased due to the treatment A or B compared to the carbonated sample and the Critical pore size* (*d_{cr} μm*)	*Capillary porosity:* C-A =2% C-B = 6%	*Critical pore size:* A_{dcr} = 0.027 *μm* B_{dcr} ≈ C_{dcr} = 0.442 μm
	TGA/DSC: *Mass loss (%) due to dehydration of (CH) and decarbonation* ($CaCO_3$) *process and (mass loss at higher temperatures)*	*M(%) due to dehydration of (CH):* R: 1.4% C: 3.4% A: 3.5% B: 3.4%	*M(%) due to decarbonation (CaCO3):* R: Crystallization small M% C: 4.1% (1.5%) A: 0.4% B: No clear peak (1.6%)
0.6	**Nanoindentation**	*Elastic Modulus (GPa)* E(<18) : C < R, B < A < C E(18-39): R < C, C < A < B E(36-39): R < C, C ≈ A ≈ B E(>39) : R=0 , A=0, C ≈ B	*Hardness (GPa):* H (<0.8) : C < R, B < C < A H (0.8-1.2): R < C, A < C < B H (1.3-1.8): R ≈ 0, A ≈ C < B H (>1.8) : R ≈ 0, A < C < B
	MIP: *Percentage of Capillary porosity (CP%) decreased due to the treatment A or B compared to the carbonated sample and the Critical pore size* (*d_{cr} μm*)	*Capillary porosity:* C-A =26% C-B = 21%	*Critical pore size:* A_{dcr} = 0.022 *μm* B_{dcr} ≈ C_{dcr} = 0.271 μm
	TGA/DSC: *Mass loss (%) due to dehydration of (CH) and decarbonation* ($CaCO_3$) *process and (mass loss at higher temperatures)*	*M(%) due to dehydration of (CH):* R: 1.8% C: 2.5% A: 1.5% B: 1.8%	*M(%) due to decarbonation (CaCO3):* R: 0.7% C: 3.6 (1.5%) A: 2.2% B: 0.8% (1.4%)

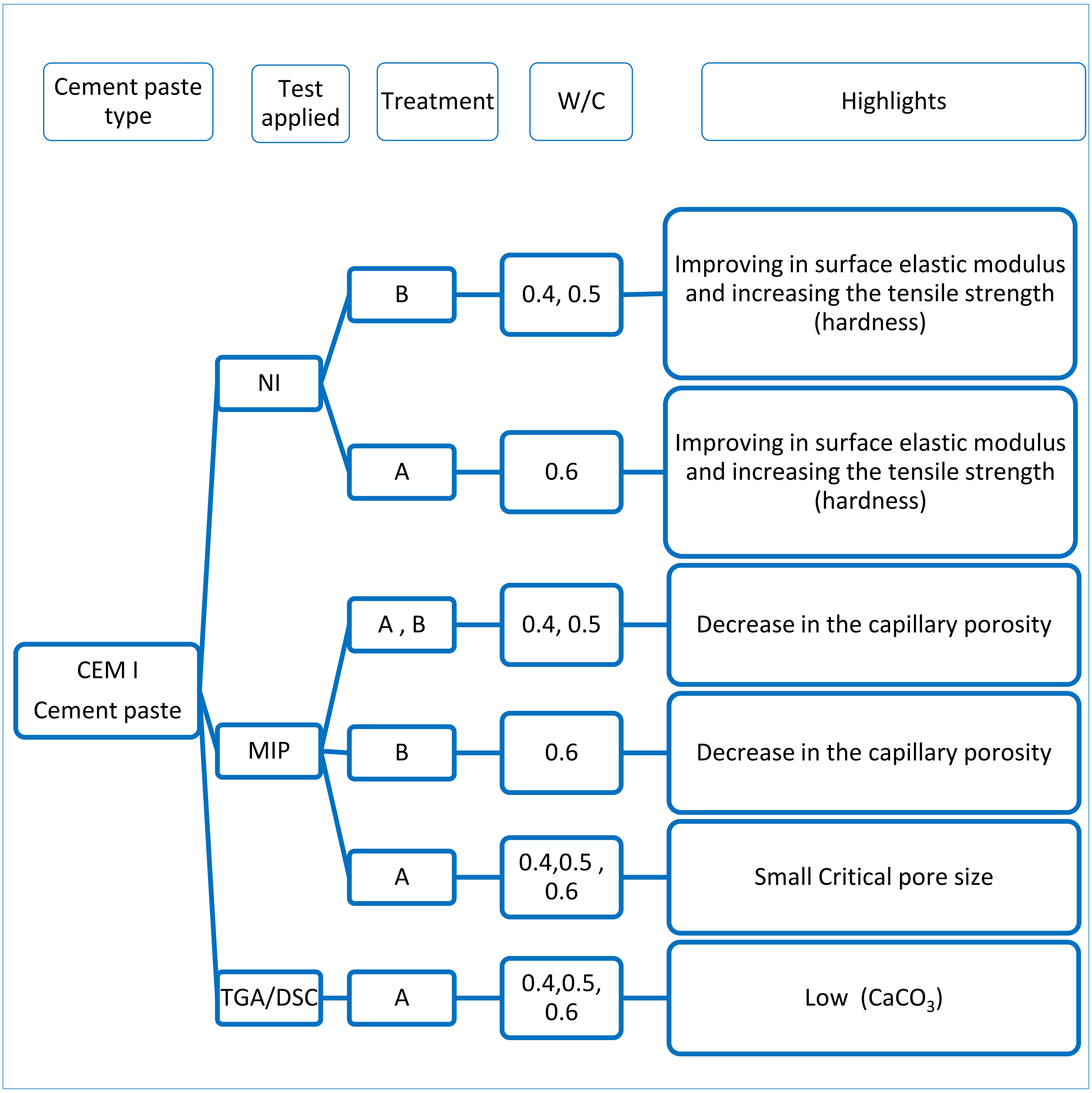

Figure 48: Highlights of the results obtained for the microstructure analysis for cement paste CEM I

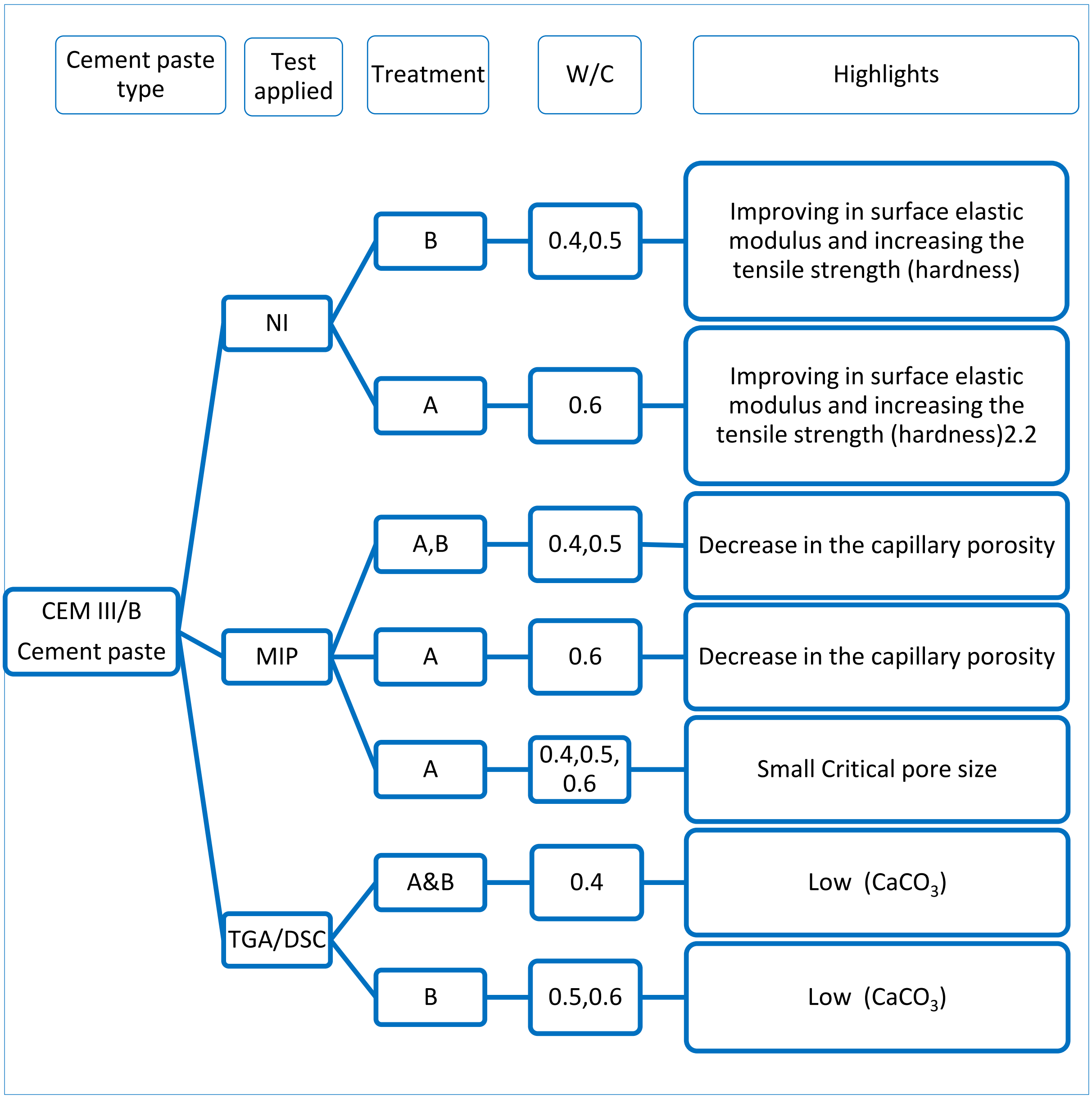

Figure 49 : Highlights of the results obtained for the microstructure analysis for cement paste CEM III/B

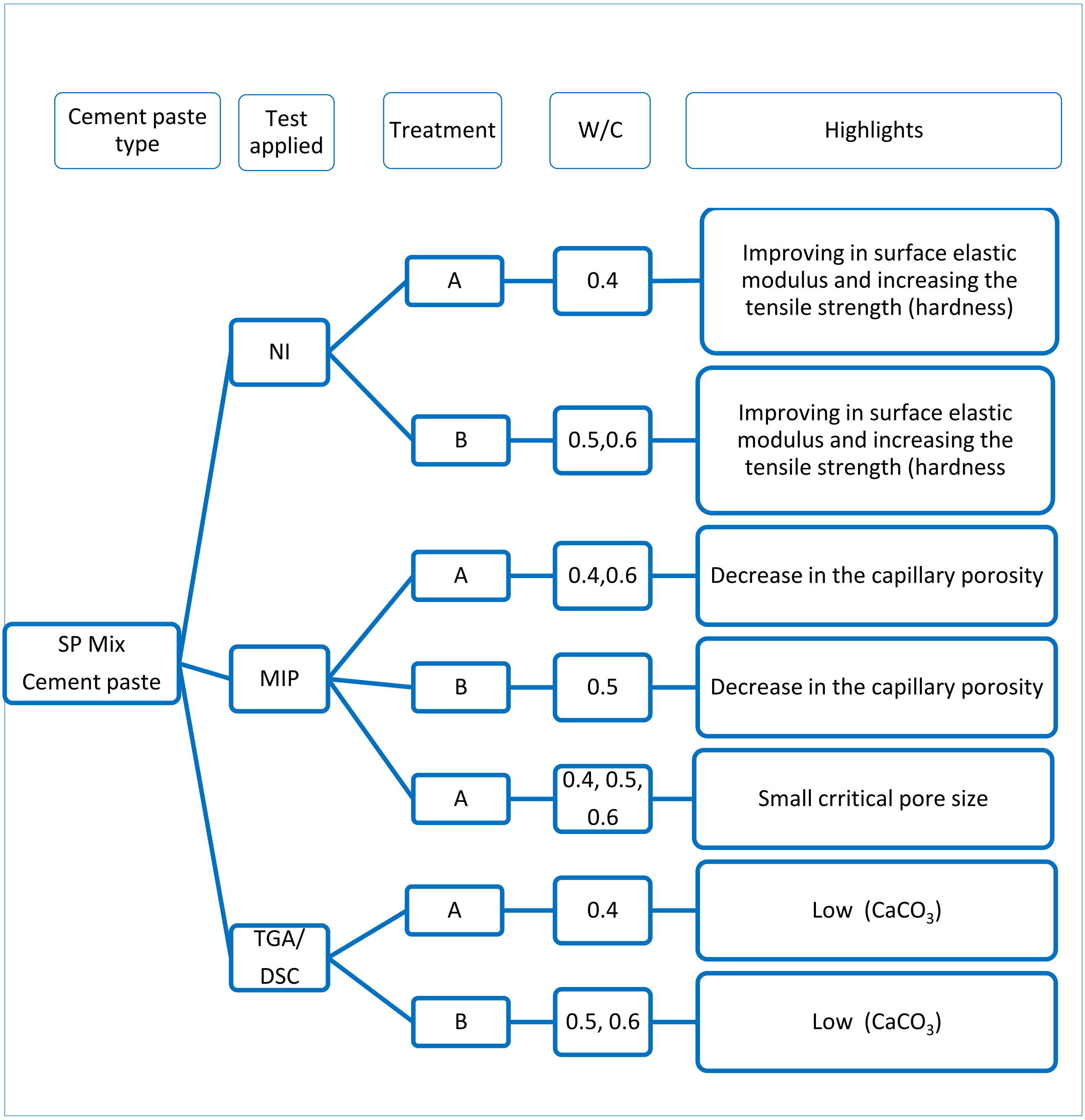

Figure 50: Highlights of the results obtained for the microstructure analysis for cement paste SP Mix

5. Conclusions

The main objective of this research was to characterise the effect of applying the aqueous sodium monofluorophosphate (Na-MFP) on the microstructural and micromechanical properties of slag cement systems. As part of the research, the most effective method of applying the Na-MFP solution (25% wt.) on the surface of slag cement mortar or paste was determined.

For the three type of cement used; CEM I 42,5 N , CEM III/B 42,5 N and Ternary blended cement (SP Mix) with a slag content of 55%, 30% CEM I 52,5 R and 15% fly ash, the study indicates that applying the Na-MFP solution on carbonated surfaces provide a higher penetration of the solution than before carbonation, regardless the curing method used; wet, sealed or in a dissectors (20 °C and RH 55%). Applying the Na-MFP solution on the carbonated surface improved the surface by forming a product that blocking the pores in the cement mortar/paste and it showed as a dark layer under the XPL microscope suggesting an amorphous formation. Decreasing the permeability of the surface will increase the surface resistance against carbonation and other environmental attacks.

The second part of the study focused on the effect of the Na-MFP solution (25% it.) on the micromechanical and microstructural properties of paste samples with different slag contents and the different water-cement ratio (W/C). The reaction of the solution with the cement matrix was significantly affected by the water-cement ratio, slag content and the condition of the cement paste at the time the solution was applied; whether this sample was carbonated. or not carbonated. The conclusions of the study are as followed:

1- Micromechanical properties; *the elastic modulus and hardness*

The Na-MFP solution reacts with the carbonated cement matrix improving the elastic modulus and the hardness of the cement paste. The study indicates that this applied to CEM III /B and CEM I with W/C of 0.4 and 0.5 and for the cement paste SP Mix with W/C of 0.5 and 0.6 when the Na-MFP solution was applied after carbonation. When the Na-MFP solution was applied before carbonation, the elastic modulus and the hardness of cement paste with CEM I, CEM III/B for a W/C of 0.6 and for the cement paste with SP Mix with a W/C of 0.4 was improved.

2-Porosity

The capillary porosity for CEM I, CEM III /B cement pastes with a W/C of 0.4 and 0.5 was improved when the Na-MFP solution applied on the cement paste before or after carbonation. This indicates that the solution reacts with the cement matrix forming a product (amorphous material) blocking the pores in the cement matrix.

The decreases of the capillary porosity of CEM I cement paste compared to the carbonated samples were 12% and 5% for W/C = 0.4 and 0.5, respectively while for CEM III/B cement paste the decreases in the capillary porosity were 7% and 8% for W/C = 0.4 and 0.5, respectively.

Applying the Na-MFP solution before carbonation on cement paste that has a high water-cement ratio can result in an increase in the capillary porosity. The capillary porosity for CEM I cement paste with a W/C of 0.6 increased after applying the Na-MFP solution compared with the carbonated sample. The decrease in the capillary porosity was only 2% when the Na-MFP solution was applied after carbonation.

The capillary porosity of CEM III/B cement paste with W/C=0.6 improved when the Na-MFP solution was applied after carbonation.

The decrease in the capillary porosity for the SP Mix (with 15% fly ash) cement paste was not significant for the samples with a W/C of 0.4 and 0.5 but the samples with a W/C of 0.6 the decrease in the capillary porosity for the samples treated after carbonation was 26% compared to the carbonated sample.

The lowest critical pore size was reached with the treatment before carbonation. This was the case for all cement paste samples with different slag contents and W/C ratios. The critical pore size for the SP Mix cement paste was lower compared to CEM I and CEM III/B cement paste. This result was due to the presences of the fly ash in the cement mix.

3-Thermal analysis; carbonation resistance

The content of $CaCO_3$ was low in the cement matrix for the samples treated before carbonation for CEM I cement pastes (W/C=0.4, 0.5 and 0.6). For CEM III /B and SP Mix cement paste with W/C=0.4 a low $CaCO_3$ content in the cement matrix was reached when the treatment was applied before carbonation. With higher water –cement ratios (W/C= 0.5 and 0.6) a low $CaCO_3$ content was reached when the treatment was applied after carbonation.

The low content of $CaCO_3$ in the cement matrix showed that the treatment increased the resistance against carbonation.

The analysis of the microstructure showed that the reaction of the Na-MFP and the formation of the amorphous products were affected by the slag content as was proven in previous research. This study showed that the reaction also was affected by the water -cement ratio in conjunction with the condition of the cement paste, whether the sample was carbonated or non-carbonated.

6. Recommendations

The experiments showed favourable results with regard to of sodium monofluorophosphate (Na-MFP) on the surface of slag content cement in order to increase the resistance against carbonation. However, further research it is recommended to obtain more information on the chemical composition of the amorphous gel formed as a result of the reaction of Na-MFP solution with the cement matrix; after or before carbonation.

The penetration test showed that applying the treatment on the surface of the CEM III/B and SP MIX cement pastes tests before carbonation increased the carbonation depth. This result is not in agreement with what was obtained from the microstructure analysis based on the TGA/DSC tests. The method used in applying the Na-MFP solution can play a role which needs further studies.

The effect of applying the Na-MFP solution before carbonation and repeated again after carbonation is an important topic, especially in the highly carbonated environments. Also, the influence of fly ash which was used in the SP Mix needs further research since the finesse and content of calcium of the fly ash could affect the results of the microstructure analysis.

7. Literature

Acker.P. (2004). Why Does Ultrahigh-Performance Concrete (UHPC) Exhibit Such Low Shrinkage and Such Low Creep? *, 220*, 14.

Alonso, et al. (1995). Na_2PO_3 As Inhibitor Of Corroding Reinforcement In Carbonated Concrete. *Cement and Concrete Research, 26*(3), 405-415.

Andrade, et al. (1992). Preliminary Testing of Na2P03F as a Curative Corrosion Inhibitor for Steel Reinforcements in Concrete. *Cement and Concrete Research*, 869-881.

Anstice. (2000). Corrosion inhibitors for the rehabilitation of reinforced concrete.

Bell, et al. (1995). *Ground Granulated Blast-Furnace Slag as a Cementitious Constituent in Concrete*. Retrieved from

Bertos , et al. (2004). A review of accelerated carbonation technology in the treatment of cement-based materials and sequestration of CO_2. *Journal of Hazardous Materials, B 112*, 13.

Bharatkumar, et al. (2005). Effect of fly ash and slag on the fracture characteristics of high performance concrete. *Materials and Structures, 38*, 36-72.

Binici, et al. (2007). The effect of fineness on the properties of the blended cements incorporating ground granulated blast furnace slag and ground basaltic pumice. *Construction and Building Materials, 21*(2007), 1122–1128.

Borges, et al. (2009). Carbonation of CH and C–S–H in composite cement pastes containing high amounts of BFS. *Cement and Concrete Research, 40*.

Broz, et al. (2006). Microhardness, toughness, and modulus of Mohs scale minerals. *American Mineralogist, 91*, 4.

Chaussadent, et al. (2006). Effectiveness conditions of sodium monofluorophosphate as a corrosion inhibitor for concrete reinforcements. *Cement and Concrete Research, 36*, 556-561.

Chen. (2006). *Hydration of Slag Cement: Theory, Modeling and Application*: University of Twente, The Netherlands.

Chi, et al. (2002). Effects of carbonation on mechanical properties and durability of concrete using accelerated testing method. *J. Mar. Sci. Technol., 10*(1), 14-20.

Chuanlin, et al. (2015). A review on the mechanical properties of cement-based materials measured by nanoindentation. *Construction and Building Materials, 90*, 11.

Constantinides, et al. (2003). On the use of nanoindentation for cementitious materials. *Materials and Structures, 36*, 6.

Çopuroğlu. (2006). *The characterisation, improvement and modelling aspects of Frost Salt Scaling of Cement-Based Materials with a High Slag Content.* (Doctor), Delft University of Technology.

Çopuroğlu, et al. (2006). Effect of sodium monofluorophosphate treatment on microstructure and frost salt scaling durability of slag cement paste. *Cement and Concrete Research, 36*, 1475-1482.

Davidson. (1988). Specialized Microscopy Techniques. Retrieved from https://micro.magnet.fsu.edu/primer/techniques/index.html

Dillard, et al. (1993). *Concrete Bridge Protection and Rehabilitation: Chemical and Physical Techniques* Retrieved from Washington:

Divsholi, et al. (2014). Durability Properties and Microstructure of Ground Granulated Blast Furnace Slag Cement Concrete. *International Journal of Concrete Structures and Materials*, 157-164.

Ecocem. (2016). CHEMICAL CHARACTERISTICS. Retrieved from http://www.ecocem.fr/en/products/#751

Elke Gruyaert, et al. (2013). Carbonation of slag concrete: Effect of the cement replacement level and curing on the carbonation coefficient – Effect of carbonation on the pore structure. *Cement & Concrete Composites, 35*(2013), 9.

Euroslag. (2003). Technical Leaflet No. 1.

Gengying Li, et al. (2003). Properties of concrete incorporating fly ash and ground granulated blast-furnace slag. *Cement and Concrete Composites, 25*, 7.

Goodge. (2016, July05, 2016). Energy-Dispersive X-Ray Spectroscopy (EDS). Retrieved from http://serc.carleton.edu/research_education/geochemsheets/techniques/SEM.html

Gruyaert, et al. (2013). Carbonation of slag concrete: effect of the cement replacement level and curing on the carbonation coefficient–effect of carbonation on the pore structure, . *Cement and Concrete Composites, 35*(1), 10.

Hale, et al. (2008). Properties of concrete mixtures containing slag cement and fly ash for use in transportation structures. *Construction and Building Materials*(22), 11.

Haverkort. (2015). *UITWERKING CUR AANBEVELING 89 Mengsels van portlandcement, slak en/of poederkoolvliegas* Retrieved from

hcmcement. (2016). Retrieved from http://www.hcmcement.nl/pdf/portland01/Gebr%20Seibel%20Erwitte%20CEM%20I%2052,5%20N%20productinformatie%2020150101.pdf

Heinemann. (2013). *Historic Concrete.* (Doctor), TU Delft.

Houst. (1996). The Role of Moisture in the Carbonation of Cementitious Materials. *Internationale Zeitschrift für Bauinstandsetzen, 2*(1), 18.

Howind, et al. (2011). *Mapping of mechanical properties of cement paste microstructures.* Paper presented at the 13th International Congress on the Chemistry of Cement, Madrid, España.

Hussaina, et al. (2015). An Experimental Investigation of Accelerated Carbonation on Properties of Concrete *Engineering journal, 20*(2), 10.

Jennings, et al. (2002). Cements as Porous Materials *Handbook of porous solids*: Wiley-VCH.

JianDe., et al. (2011). Application of nanoindentation to investigate chemomechanical properties change of cement paste in the carbonation reaction. *Science China Technological Sciences*.

Johannesson, et al. (2001). Microstructural changes caused by carbonation of cement mortar. *Cement and Concrete Research, 31*(6), 7.

Kempl, et al. (2016). EH-pH- and main element analyses of Blast Furnace Slag Cement paste pore solutions activated with sodium monofluorophosphate -Implications for carbonation and self-healing. *Cement and Concrete Composites, 71* 14.

La Iglesia, et al. (2012). Reaction between sodium monofluorophosphate and portlandite and impact on steel reinforcement corrosion inhibition. *Construction and Building Materials, 37*, 5.

LaBarca, et al. (2007). *Effects of Ground Granulated Blast Furnace Slag in Portland Cement Concrete – Expanded Study* (WHRP 07-01). Retrieved from Madison , :

Larosa-Thomson, et al. (1997). Sodium silicate applications for cement and concrete. . *Proc. 10th Int. Congr. On the Chemistry of Cement, Gothenburg, 3.3*.

larry D.Hank. (2015). *HANDBOOK OF ANALYTICAL METHODS FOR MATERIALS* Plymouth, USA: Materials Evaluation and Engineering.

Ngala, et al. (1997). Effects of carbonation on pore structure and diffusional properties of hydrated cement pastes. *Cement and Concrete Research, 27*(7), 13.

Ngala, et al. (2003). Corrosion inhibitor systems for remedial treatment of reinforced concrete. Part 2: sodium monofluorophosphate. *Corrosion Science*(45), 1523–1537.

Nikčevića, et al. (2004). Mechanochemical synthesis of nanostructured fluorapatite/fluorhydroxyapatite and carbonated fluorapatite/fluorhydroxyapatite. *Journal of Solid State Chemistry, 177*(7), 10.

Osborne. (1999). Durability of Portland blast-furnace slag cement concretes. *Cement and Concrete Composites, 21* 11.

Pal, et al. (2003). Investigation of hydraulic activity of ground granulated blast furnace slag in concrete. *Cement and Concrete Research, 33*, 1481-1486.

PerkinElmer. (2010). Thermogravimetric Analysis (TGA).

Polder, et al. (2014). *Slag cement concretethe -The Dutch experience*. Retrieved from

Polder, et al. (2002). “Characterisation of chloride transport and reinforcement corrosion in concrete under cyclic wetting and drying by electrical resistivity”,. *Cement and Concrete Composites, 24*, 9.

Raith, et al. (2012). *Guide to thin section microscopy*

Robert. (2003). Rediscovering Polarized Light Microscopy. *American laboratory*.

Roy, et al. (1993). *Concrete Microscopy* (SHRP-C-662). Retrieved from Washington, DC:

Sabet Divsholi, et al. (2014). Durability Properties and Microstructure of Ground Granulated Blast Furnace Slag Cement Concrete. *International Journal of Concrete Structures and Materials, 8*(2), 8.

Samandari, et al. (2009). Micromechanical properties of single crystal hydroxyapatite by nanoindentation. *Acta Biomater., 5*, 7.

Shams. (2014). *The Use of Ternary Blended Binders in High-Consistence Concrete.* (Doctor of Philosophy), University College London, London.

Shanghai Pengkai Chem Co. Ltd. (2015). Sodium Monofluorophosphate. Retrieved from http://chlorides7.sell.curiousexpeditions.org/pz5412ad2-sodium-monofluorophosphate.html

Sisomphon, et al. (2010). Properties of carbonated blast furnace slag mortars after Na_2FPO_3 treatment. *ScienceAsia, 36*, 233-230.

Sisomphon, et al. (2007). Carbonation rates of concretes containing high volume of pozzolanic materials. *Cement and Concrete Research, 37*, 1647–1653.

Son Tung Pham, et al. (2014). Effects of Carbonation on the Microstructure of Cement Materials:Influence of Measuring Methods and of Types of Cement. *International Journal of Concrete Structures and Materials, 8*(4), 6.

Song, et al. (2006). Studies on the corrosion resistance of reinforced steel in concrete with ground granulated blast-furnace slag—An overview. *Journal of Hazardous Materials, 138*(2), 8.

Sorelli , et al. (2008). The nano-mechanical signature of Ultra High Performance Concrete by statistical nanoindentation techniques. *Cement and Concrete Research*(38), 10.

Taylor. (1990). *Cement Chemistry*. London: ACADEMIC PRESS LIMITED.

Taylor. (2014). *The Use of Ternary Mixtures in Concrete* (InTrans Project 05-241). Retrieved from Iowa State University Research Park

Thomas. (2007). Optimizing the Use of Fly Ash in Concrete. *Portland Cement Association*.

Tikalsky, et al. (2011). *Development of performance properties of ternary mixtures: laboratory study on concrete* Retrieved from Iowa State

Tikalsky, et al. (2007). *Development of Performance Properties of Ternary Mixtures: Phase I Final Report*. Retrieved from

Tõnsuaadu, et al. (2012). A review on the thermal stability of calcium apatites. *Journal of Thermal Analysis and Calorimetry, 110*(2), 647-659. doi:10.1007/s10973-011-1877-y

Velez, et al. (2001). Determination by nanoindentation of elastic modulus and hardness of pure constituents of Portland cement clinker. *Cement and Concrete Research, 31*(4), 555-561. doi:http://dx.doi.org/10.1016/S0008-8846(00)00505-6

vliegasunie. (2016). Retrieved from http://www.vliegasunie.nl/engels/fly_ash_composition.php

Wilton. (2016). Retrieved from http://www.intertek.com/analysis/microscopy/edx/

Yanming, et al. (2005). Thermal and chemical stability of fluorohydroxyapatite ceramics with different fluorine contents. *Biomaterials, 26*(11), 6.

Zamiri, et al. (2010). Mechanical properties of hydroxyapatite single crystals from nanoindentation data. *The mechanical behavior of biomedical materials, 4*, 7.

Appendice

Content

1. Appendix: Images of mortar samples

1.1 Images for blanc and samples exposed to accelerated carbonation for14 days

Condition	CEMI	CEMIII	SP Mix
Blanc *Photo original size:* *h:14.08mm* *w:18.78mm*	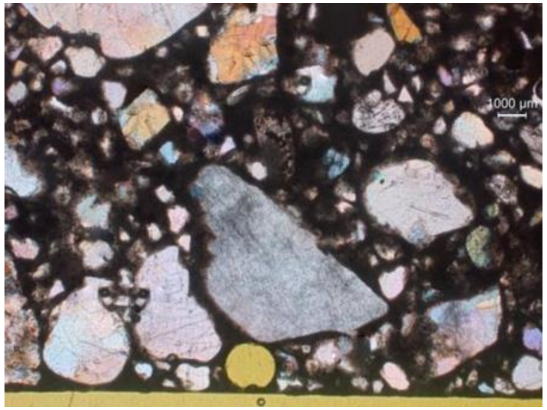	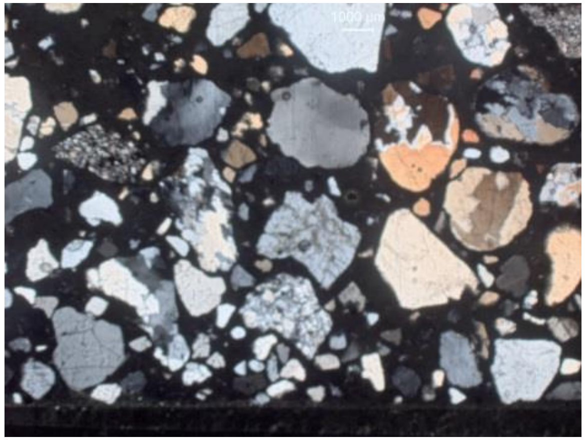	
Accelerated Carbonation-14 days *Photo original size:* *h:14.08mm* *w:18.78mm*	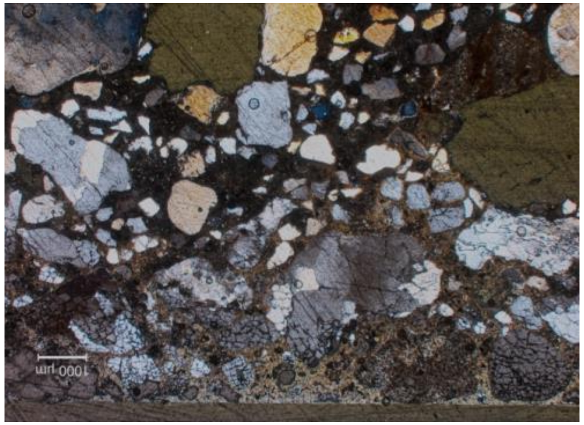	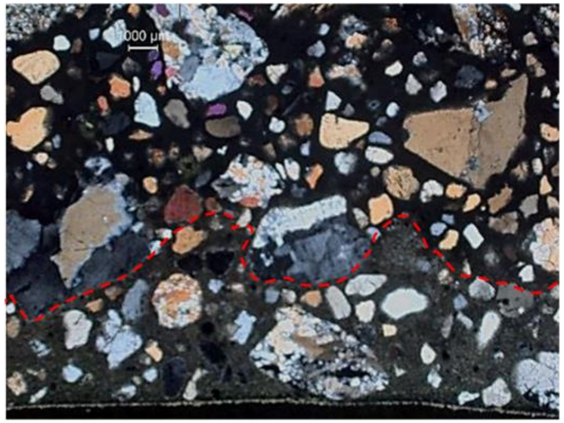	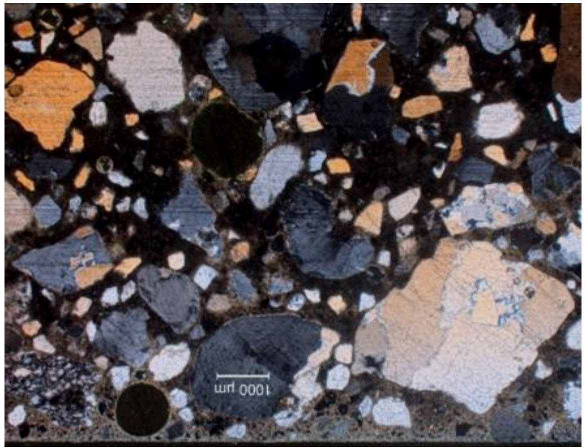

1.2 Images for samples treated with Na-MFP followed by exposition to accelerated carbonation for 14 days

Condition	CEMI	CEMIII	SP Mix
Na-MFP→ RCT_{14days} ***Photo original size:*** ***h:14.08mm*** ***w:18.78mm***	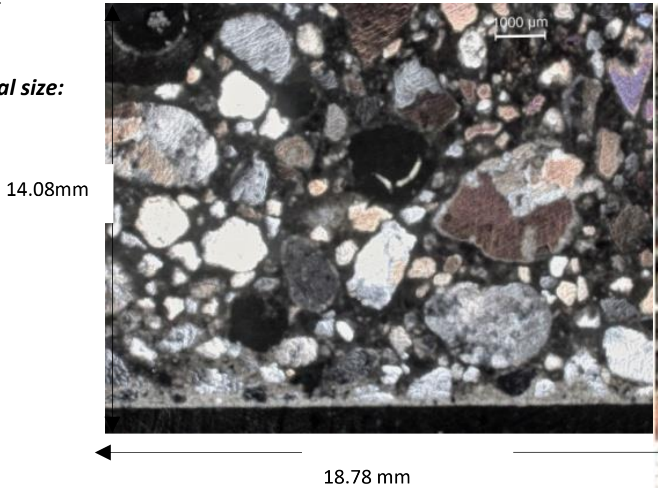	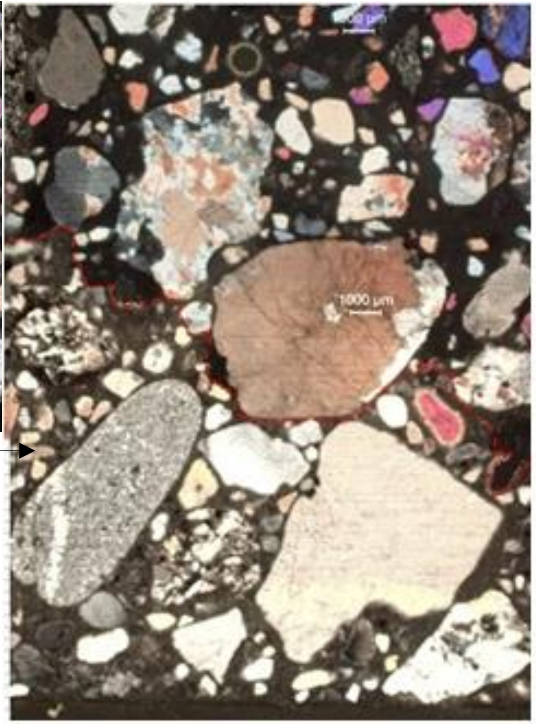	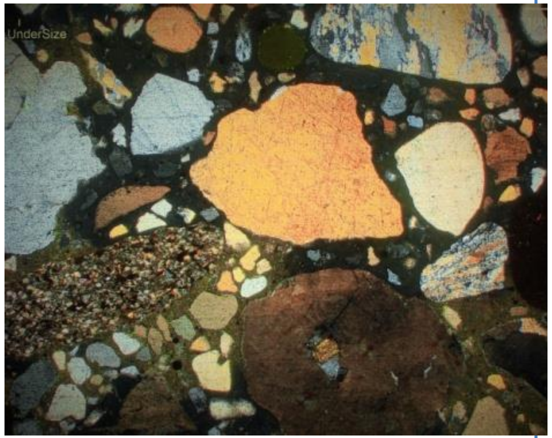 

1.3 Images for samples exposed to accelerated carbonation for 14 days followed by treatment with Na-MFP

Condition	CEMI	CEMIII	SP Mix
RCT$_{14d}$→ Na-MFP ***Photo original size:*** ***h:14.08mm*** ***w:18.78***	14.08mm 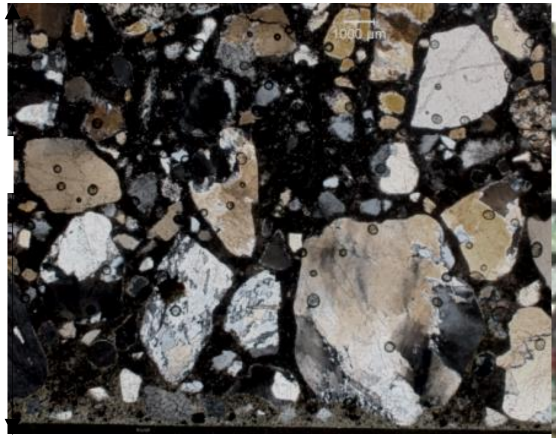 18.78 mm	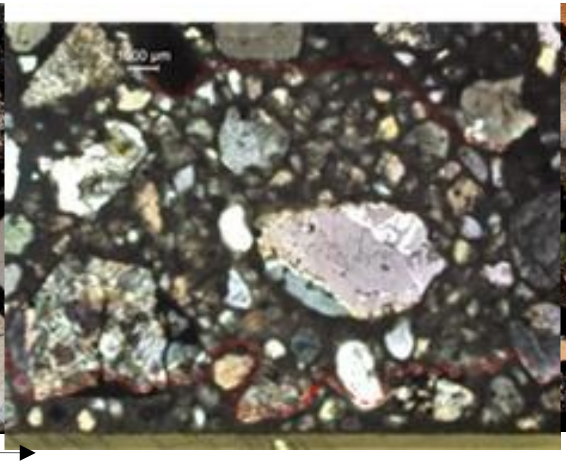 	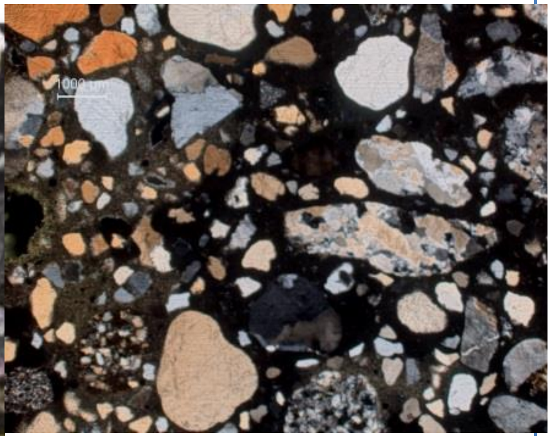 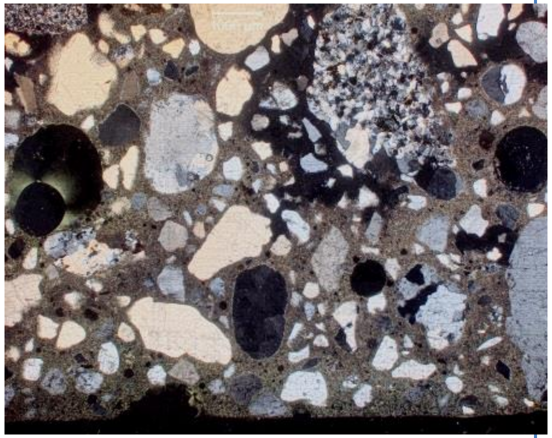

1.4 Images for samples treated with Na-MFP followed by exposition to accelerated carbonation for 28 days

Condition	CEMI	CEMIII	SP Mix
Na-MFP → **RCT$_{28d}$** ***Photo original size:*** ***h:14.08mm*** ***w:18.78m***	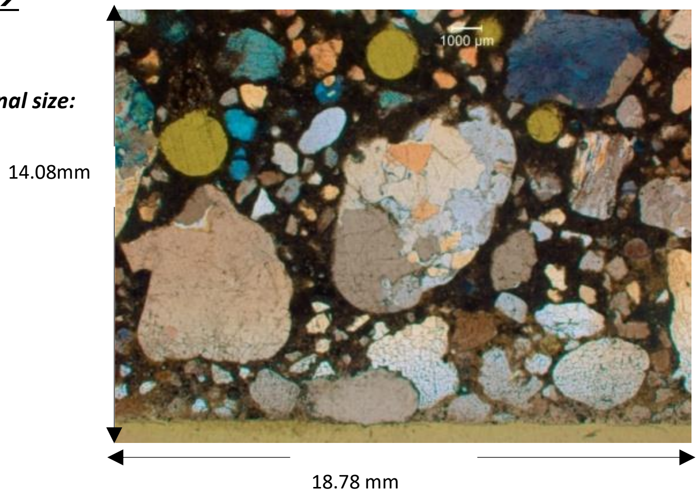	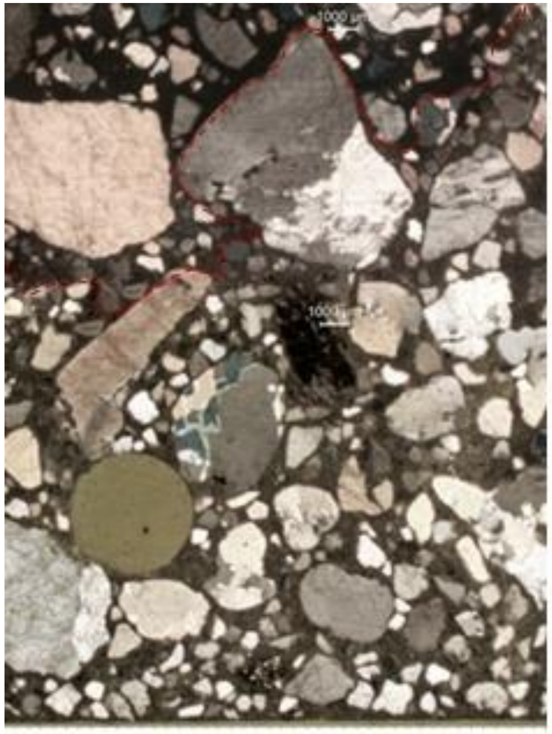	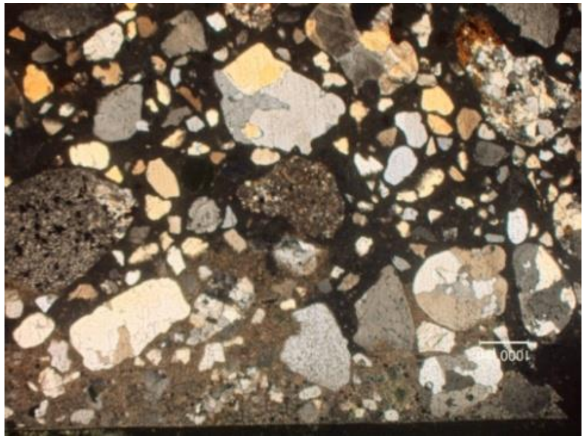

1.5 Images for samples exposed to accelerated carbonation for 28 days followed by treatment with Na-MFP

Condition	CEMI	CEMIII	SP Mix
RCT$_{28d}$→ Na-MFP ***Photo original size:*** ***h:14.08mm*** ***w:18.78mm***	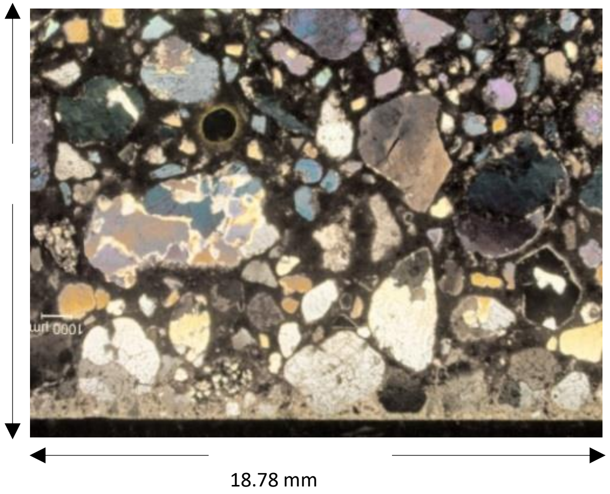	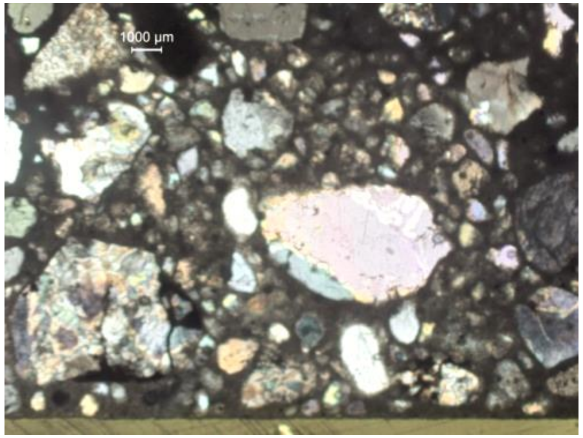	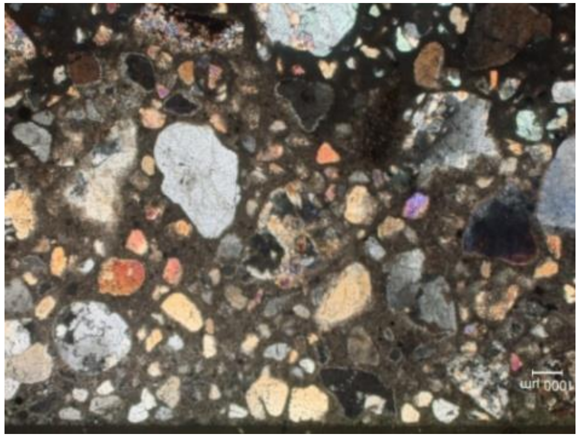

2. Appendix : Result of ESEM/ EDX analysis for CEM III

1.6 Result for paste samples-CEMIII treated with Na-MFP solution after and before exposing to carbonation for 14 days

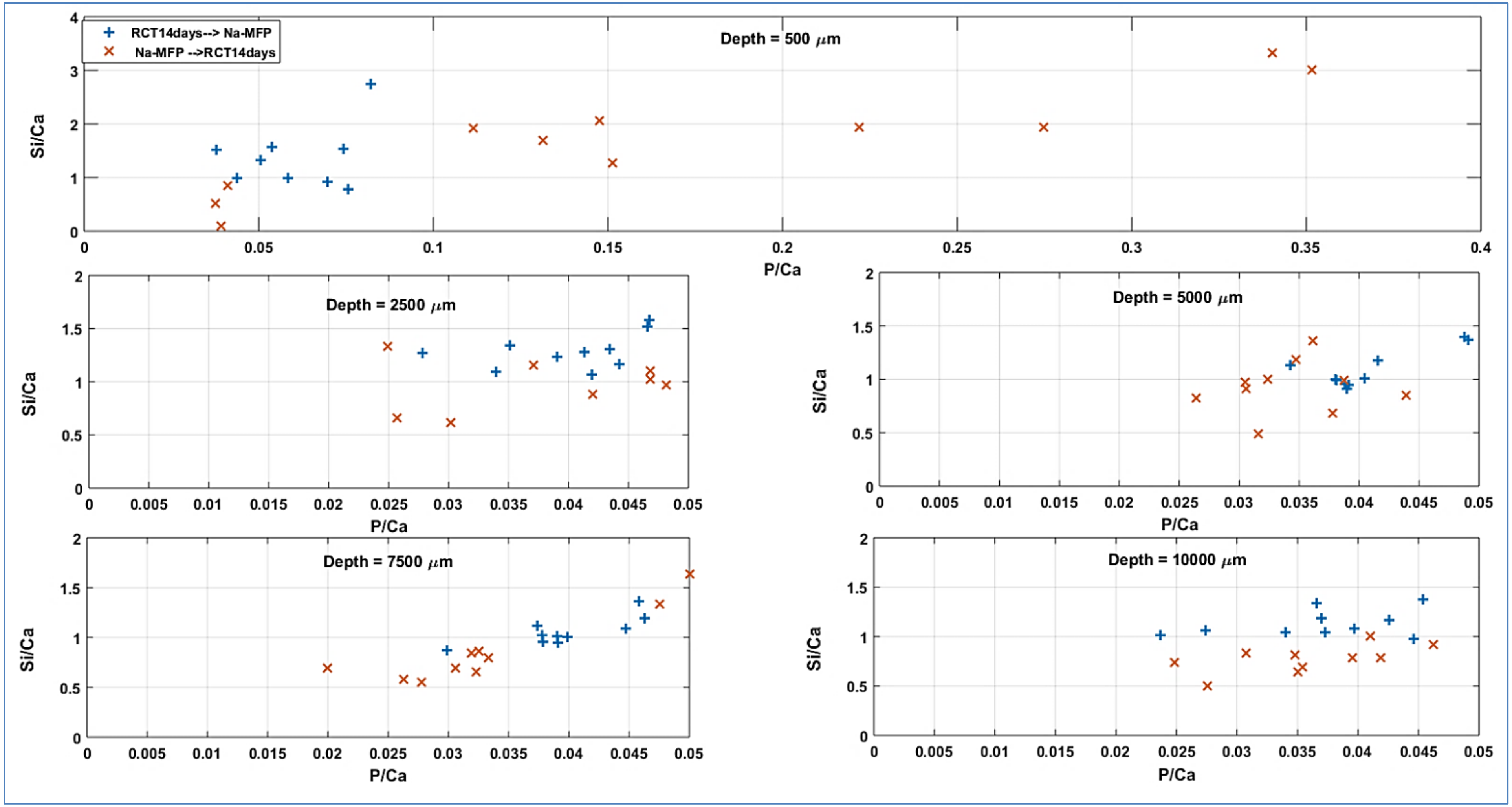

1.7 Paste samples-CEM III treated with Na-MFP solution after 14/28 days

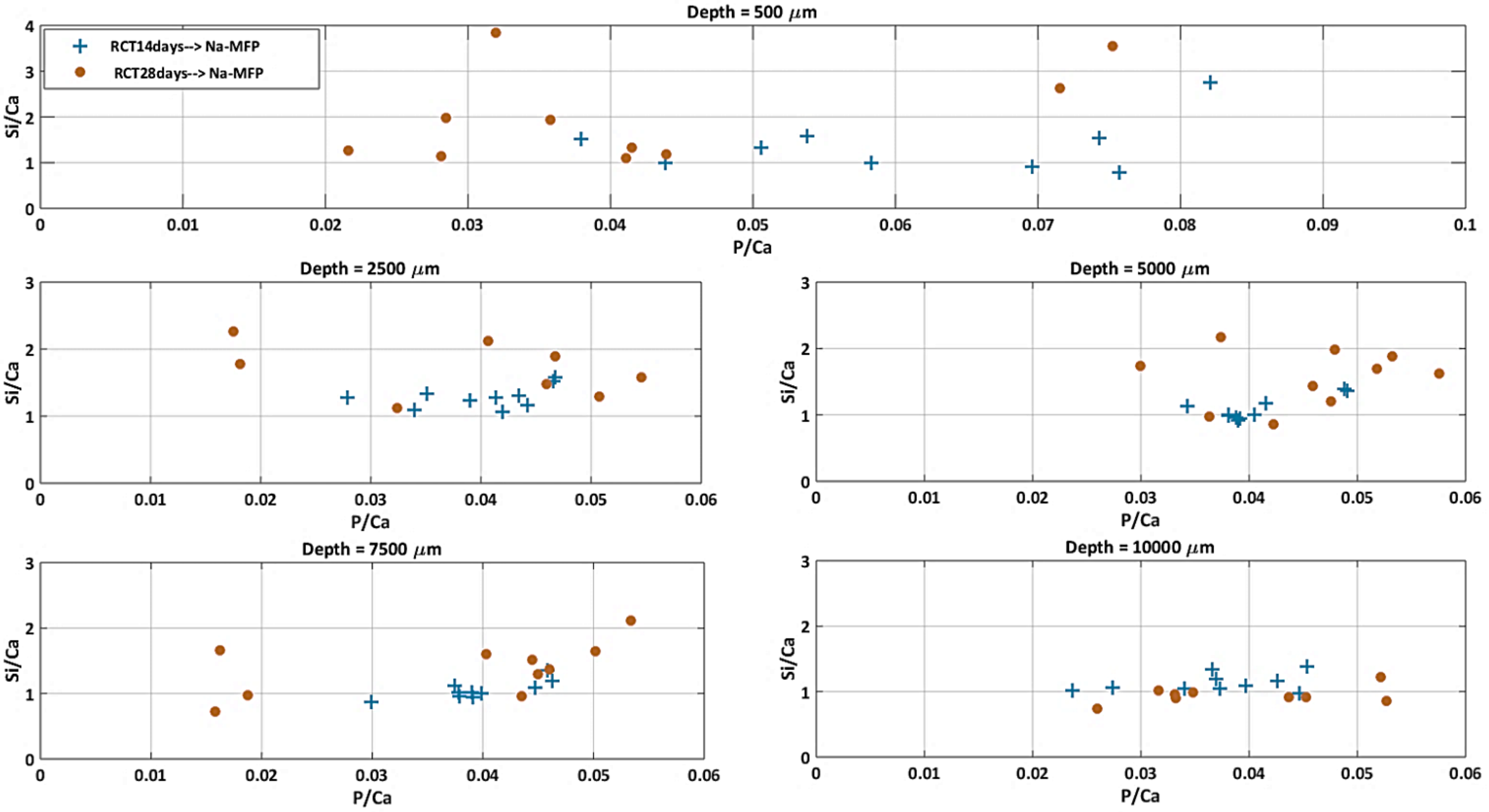

1.8 ESEM/EDX result for paste sample-CEM III treated with Na-MFP solution after carbonation for 28 day (500-7500 µm)

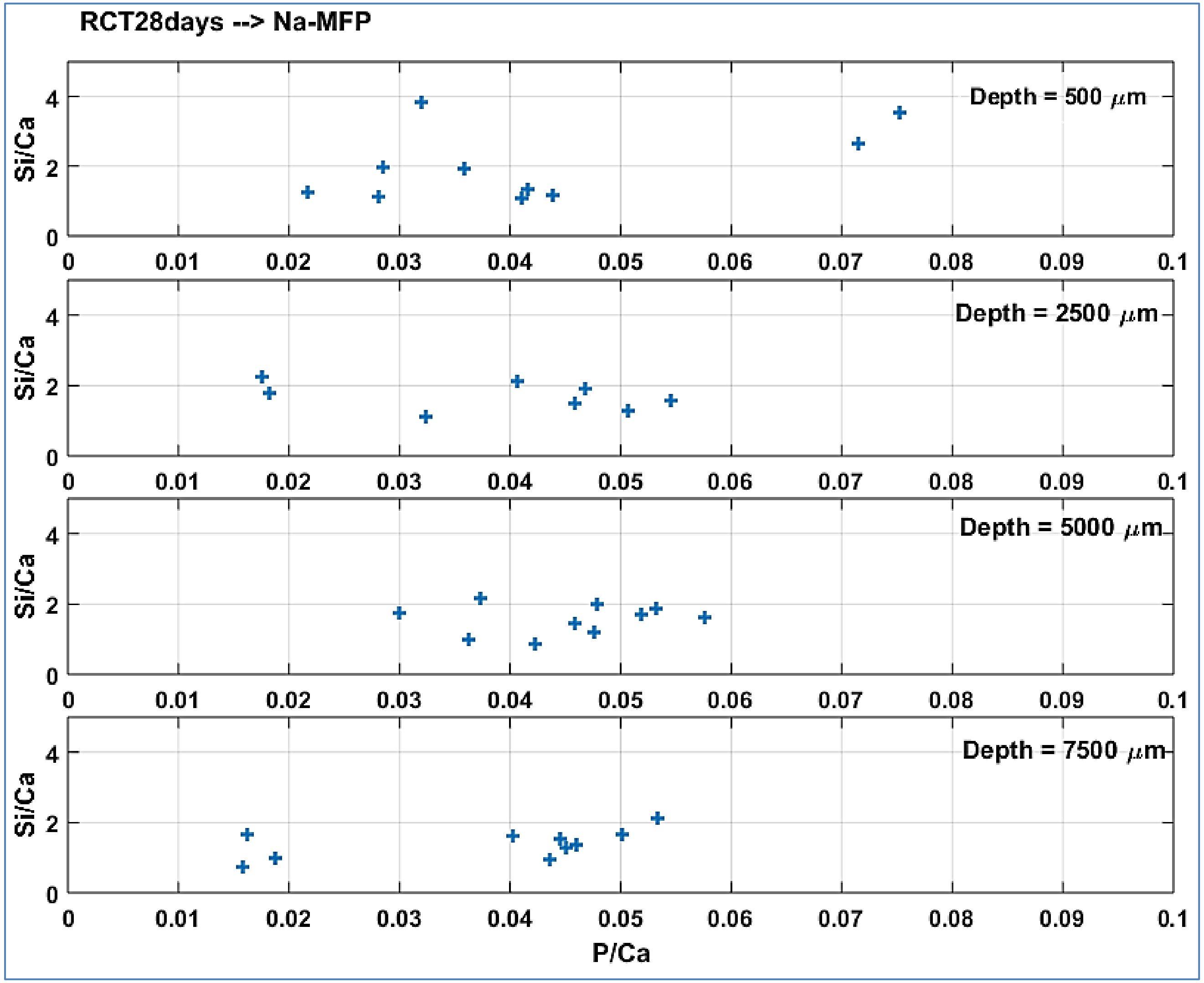

1.9 ESEM/EDX result for paste sample CEM III treated with Na-MFP solution after carbonation for 28 day (10000-15000 µm)

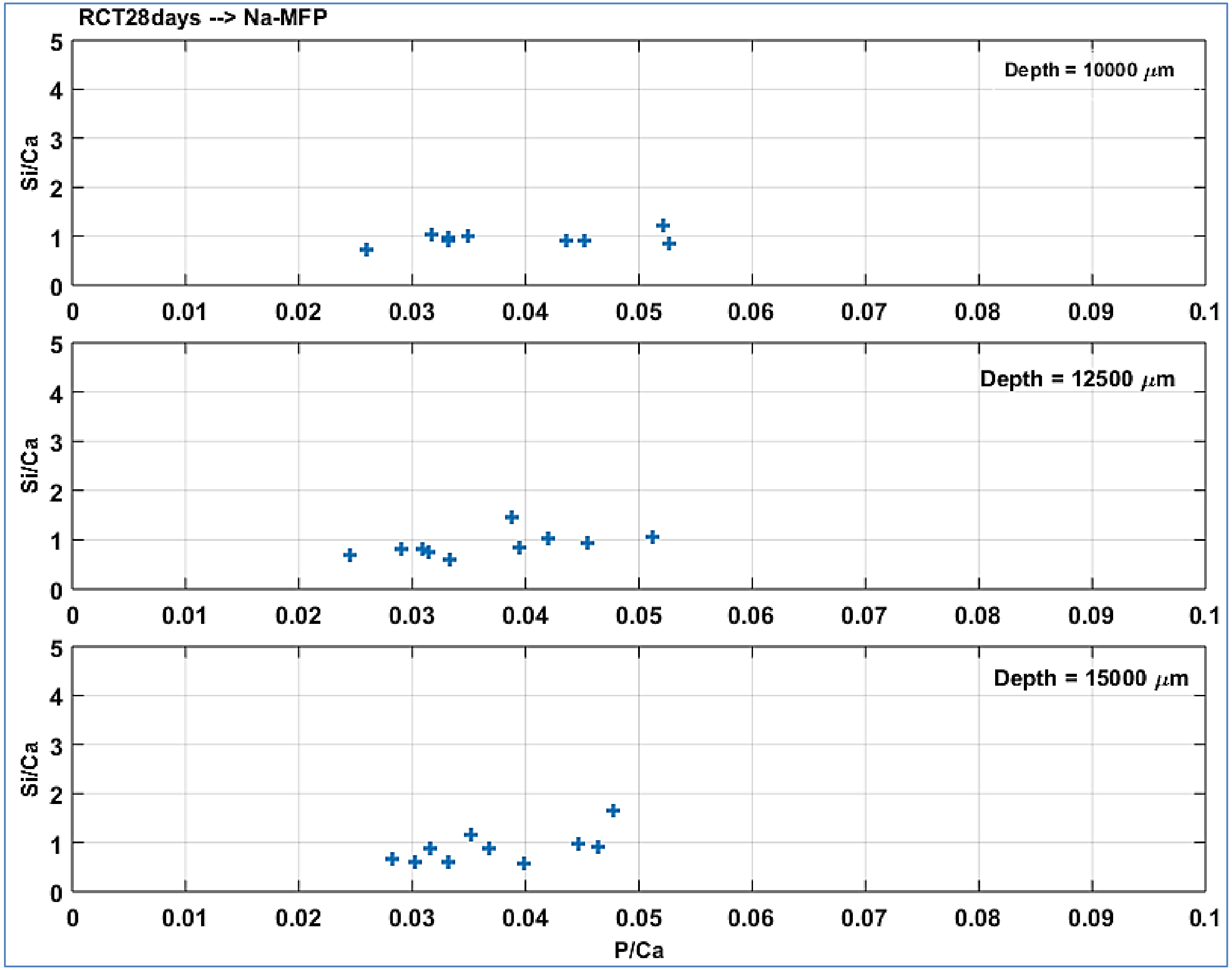

1.10 ESEM/EDX result for paste sample CEM III treated with Na-MFP solution after carbonation for 28 day (17500-22500 µm)

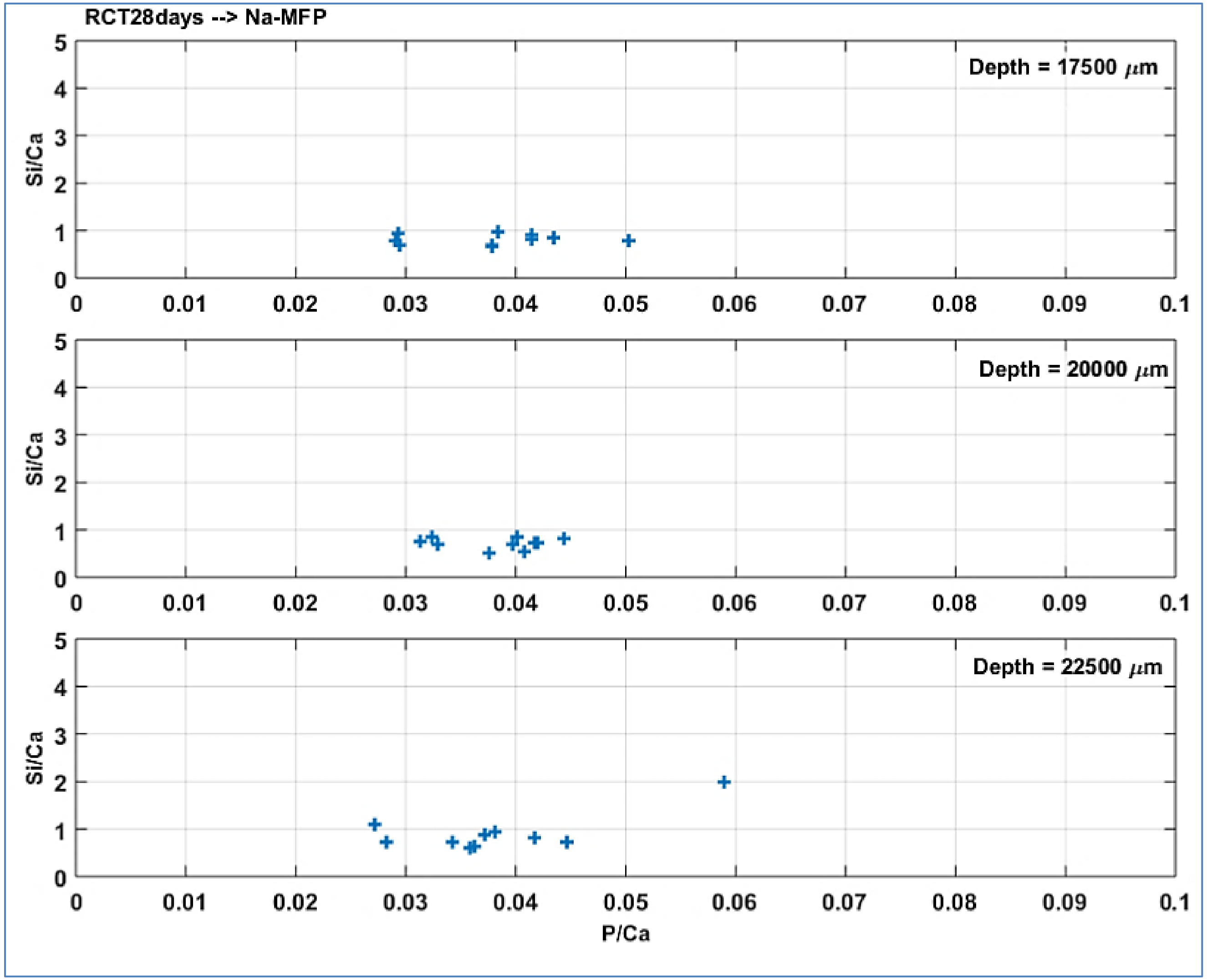

3. Appendix: Nanoindentation test

1.1. CEMI Paste samples

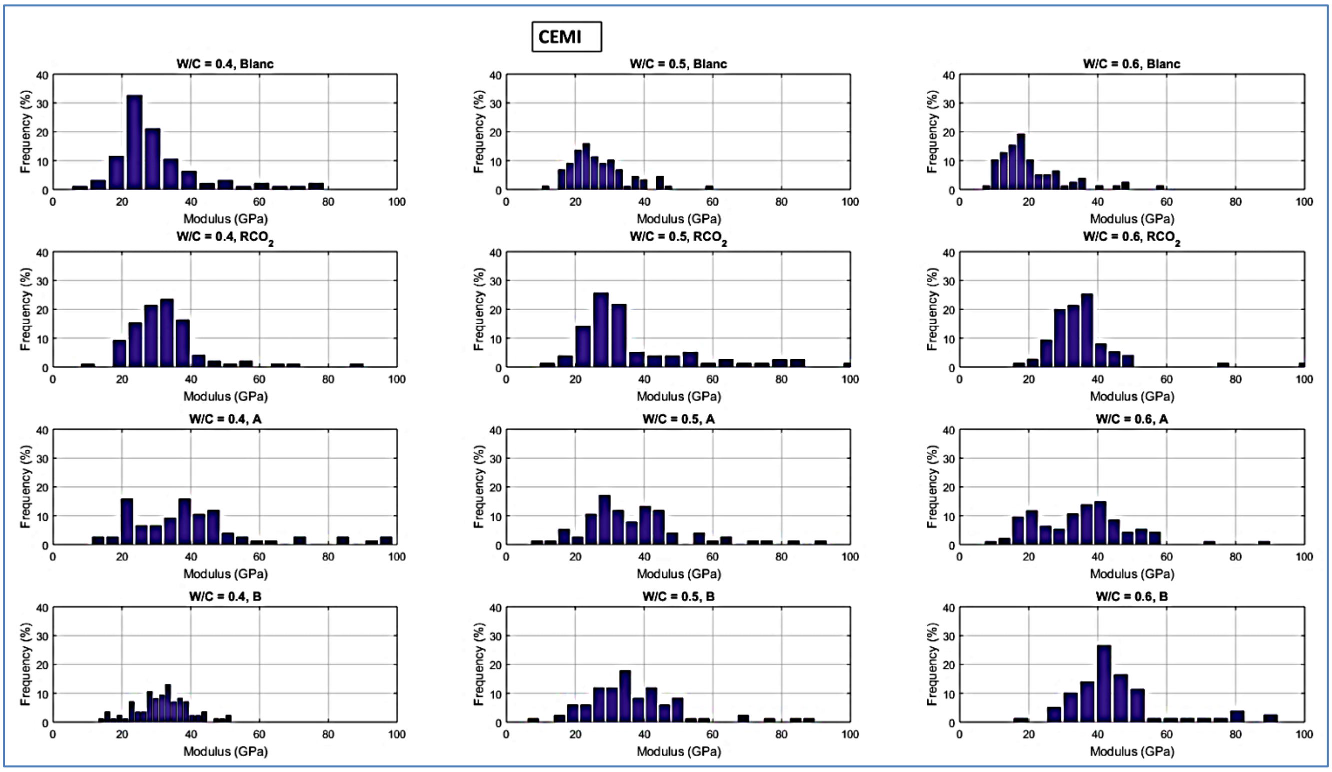

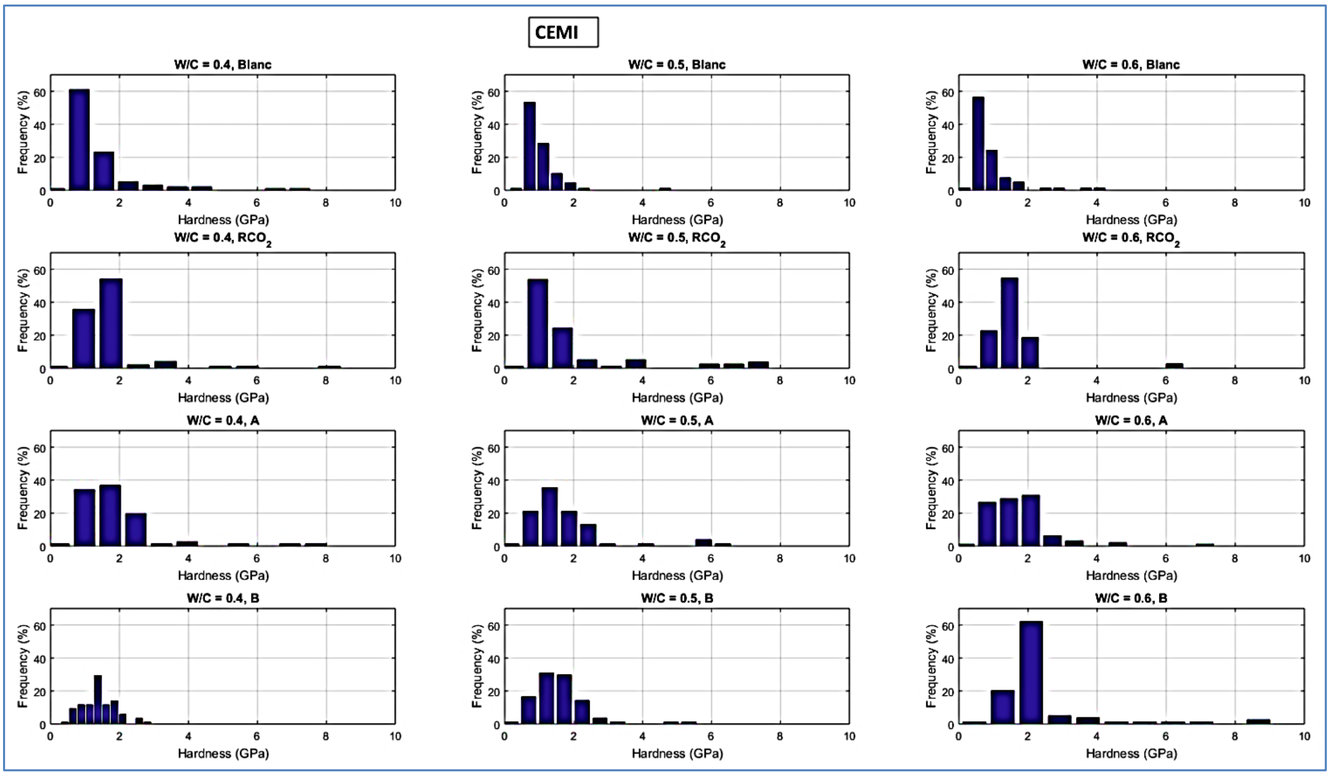

1.2. CEM III paste samples

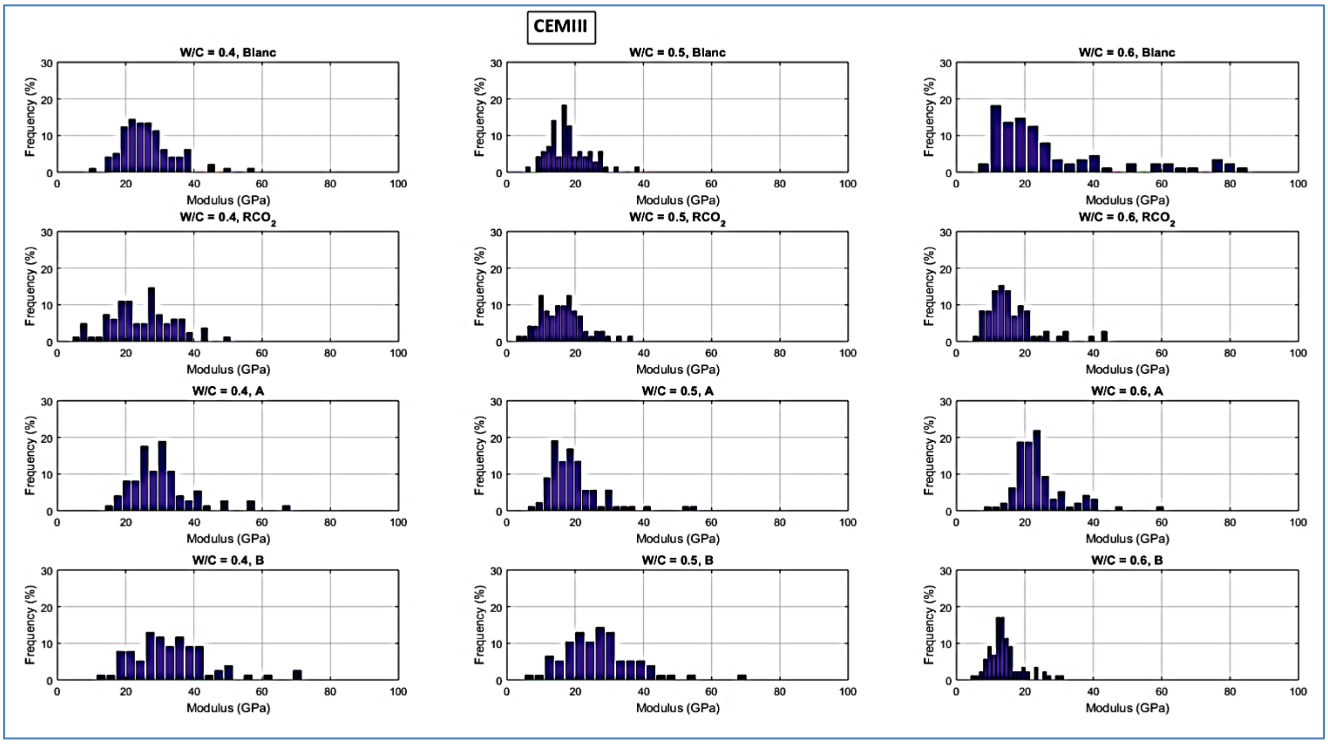

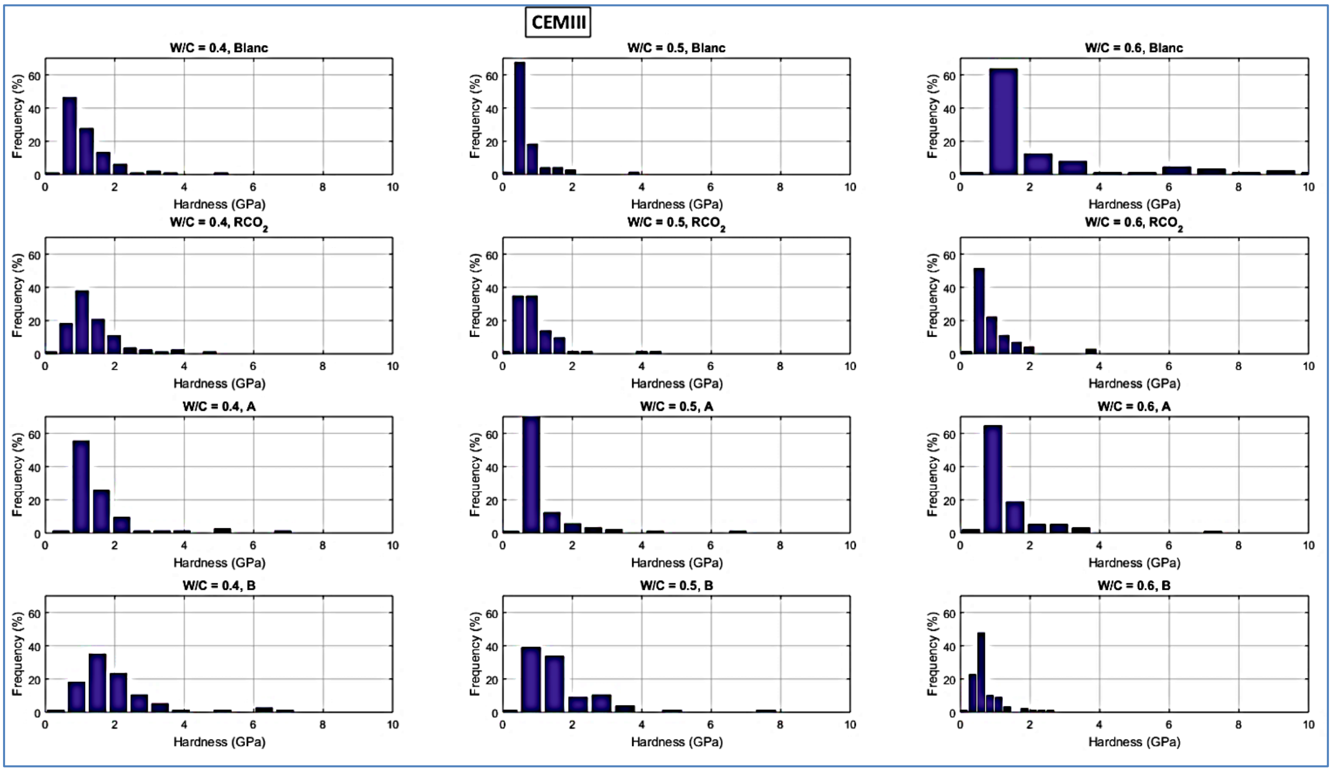

1.3. SP MIX paste samples

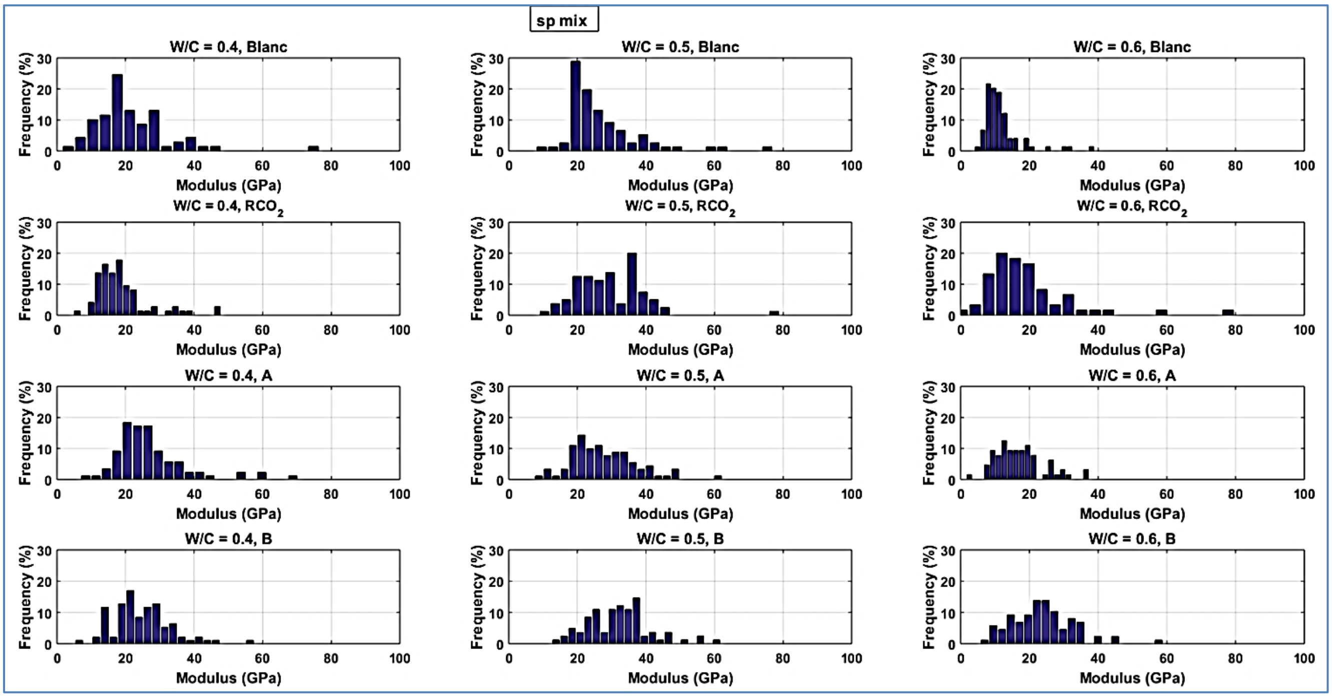

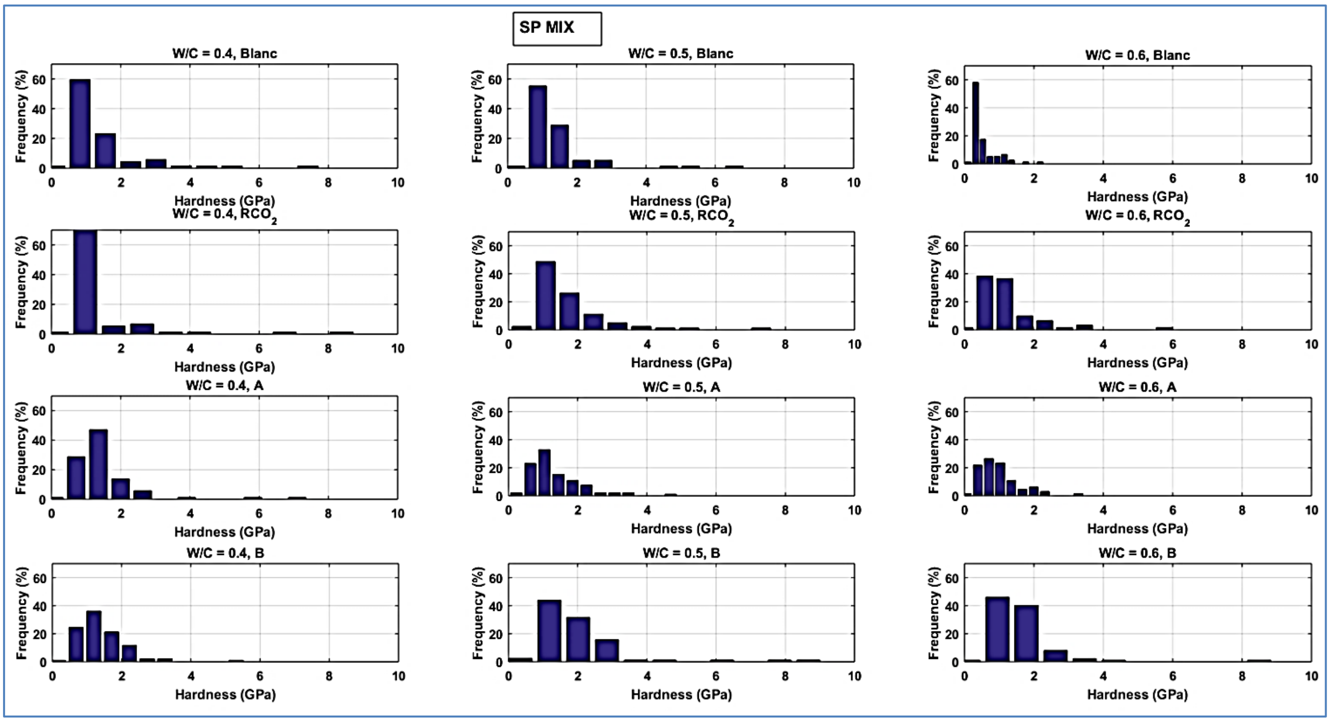

1.4. CEM III 0.4 Blanc

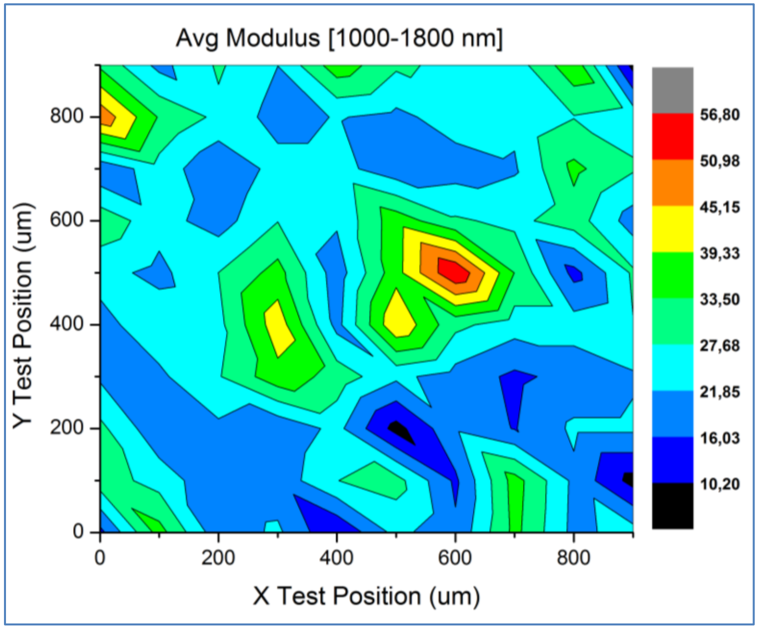

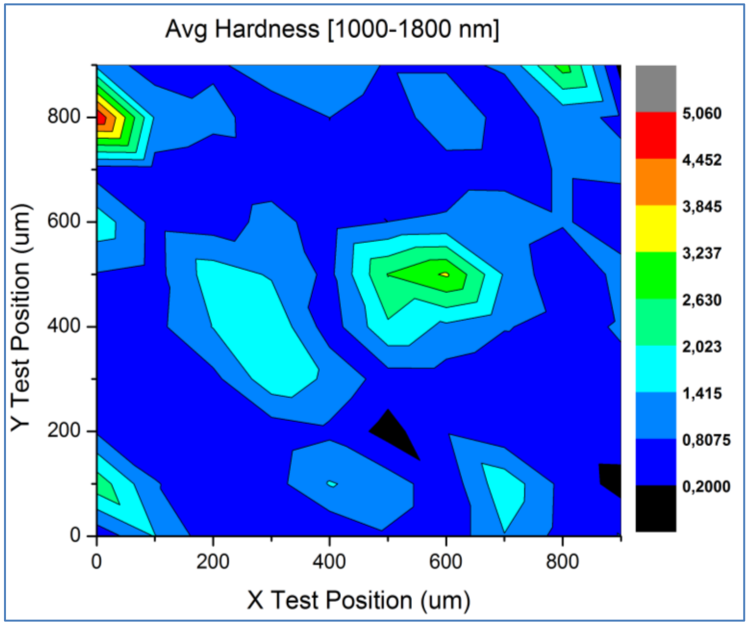

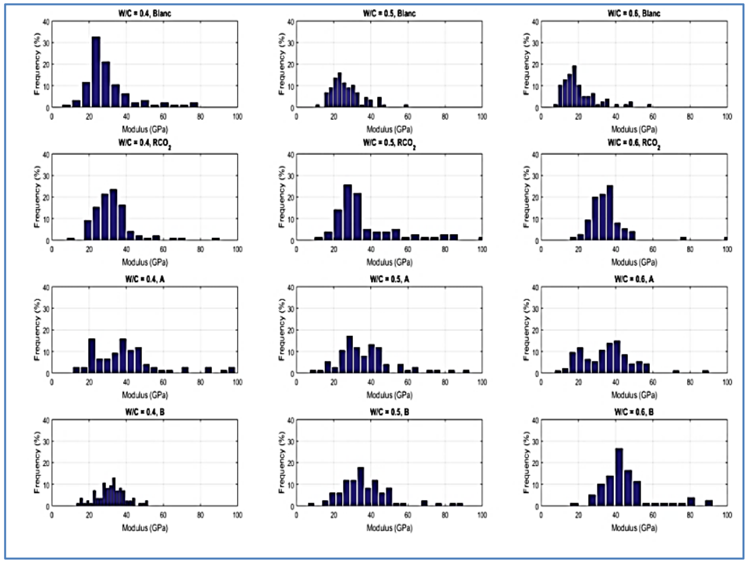

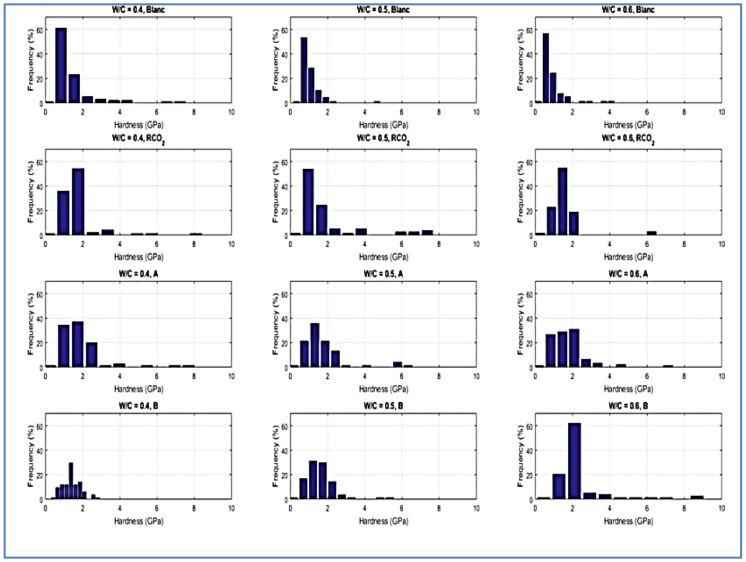

1.5. CEM III 0.4 RCO$_2$ -28 days

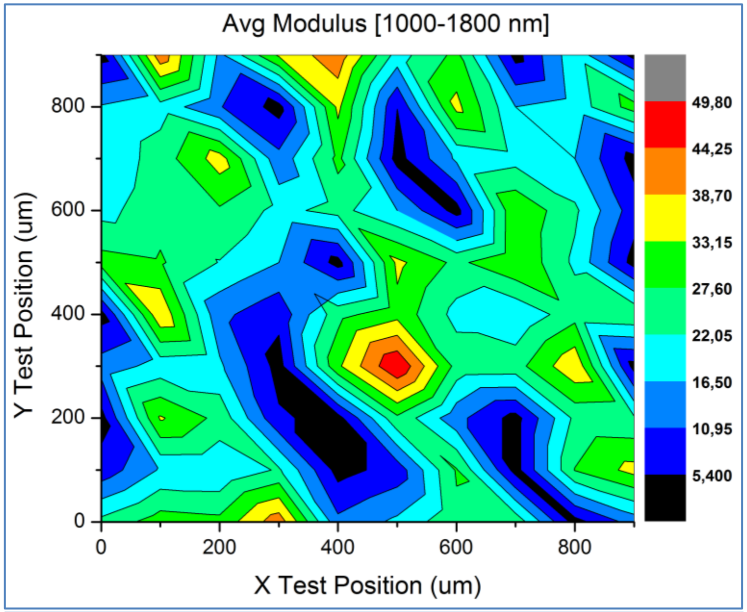

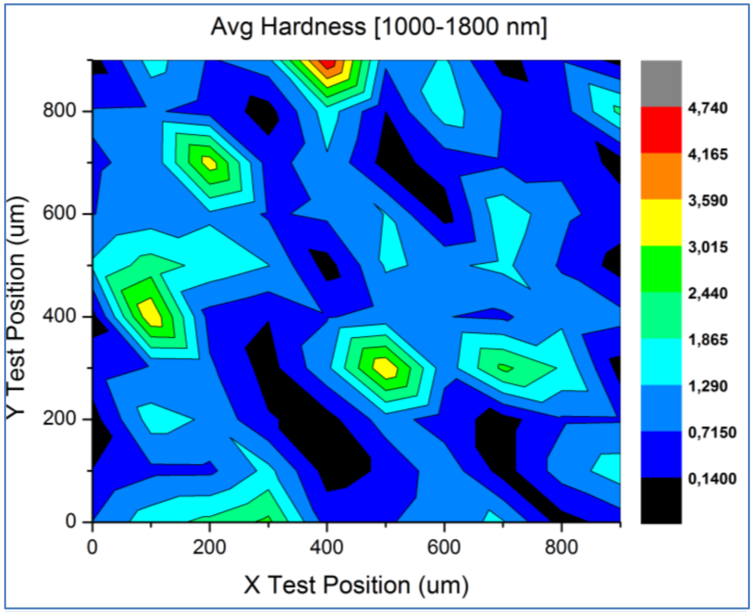

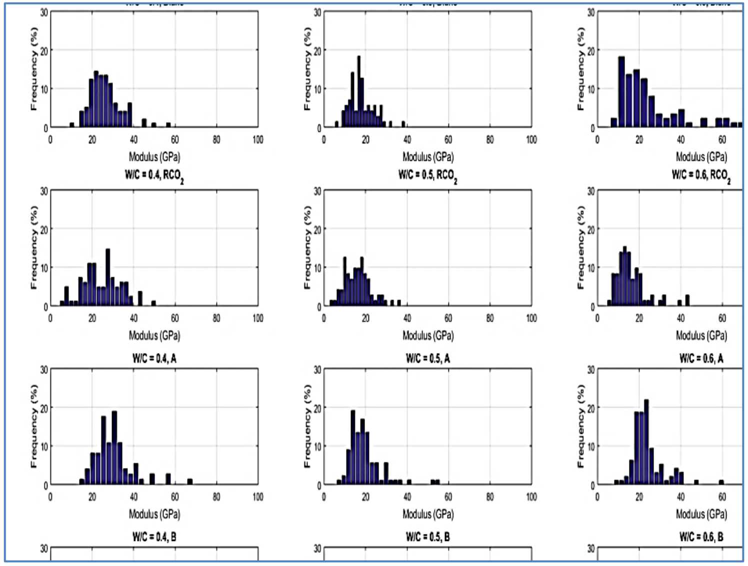

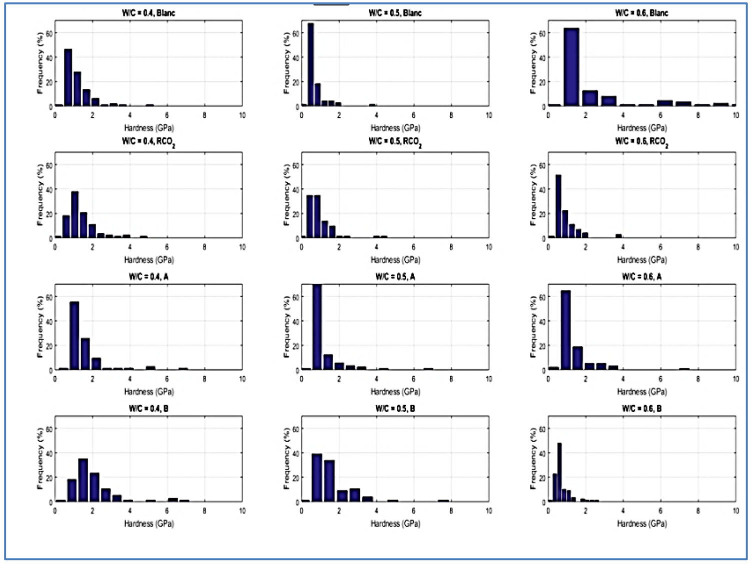

1.6. CEM III 0.4 A

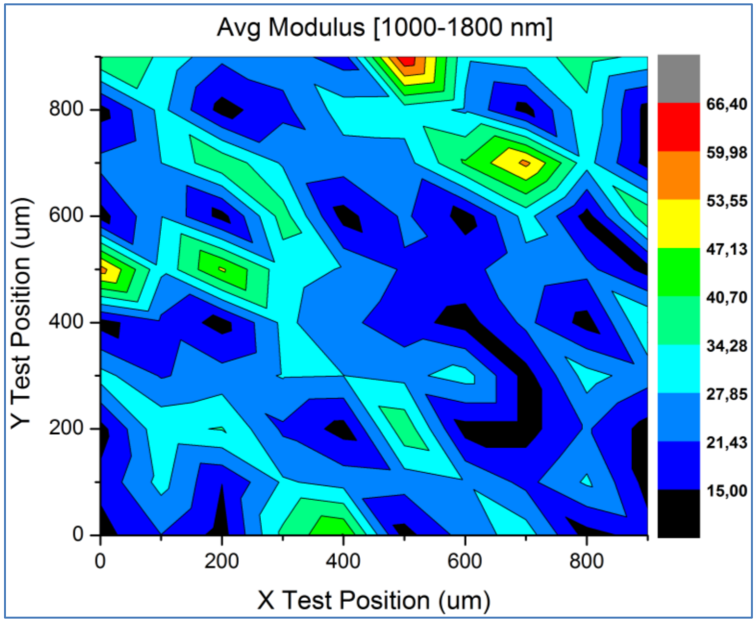

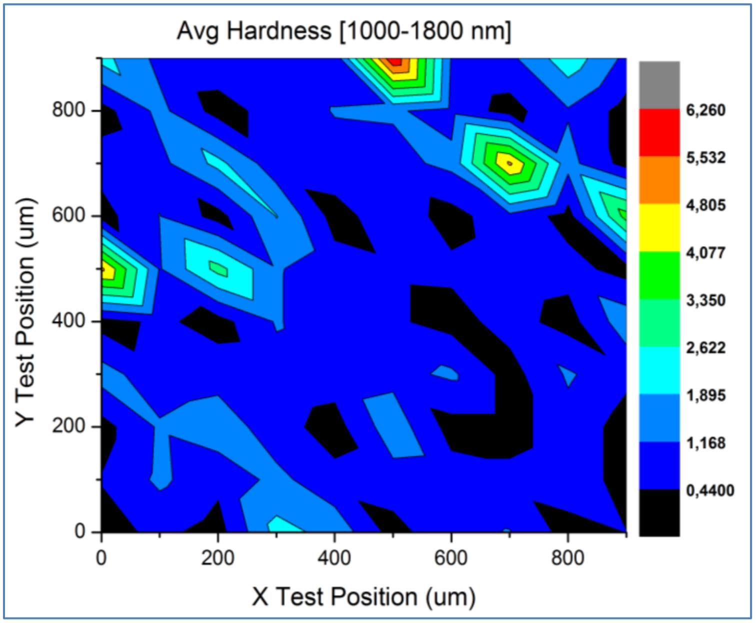

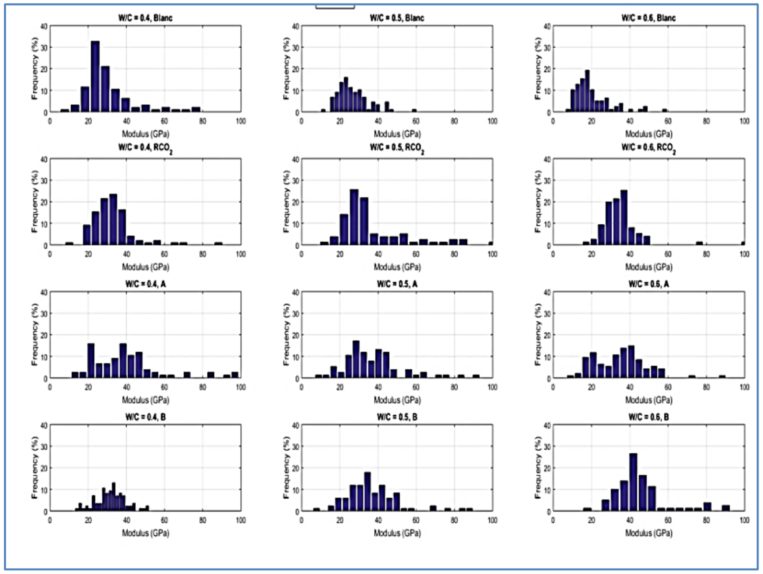

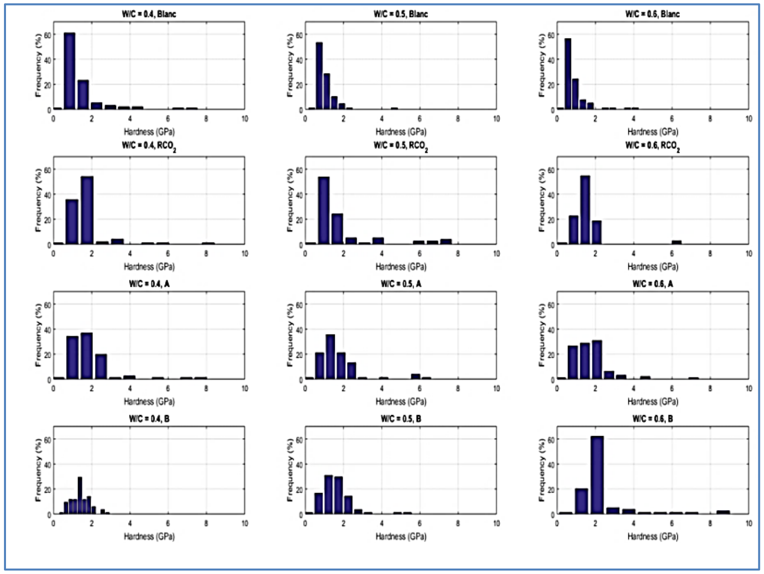

1.7. CEMIII 0.4 B

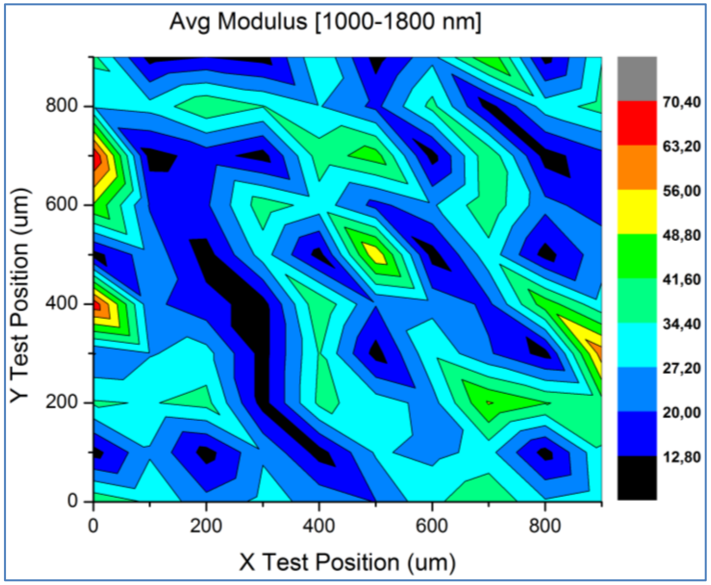

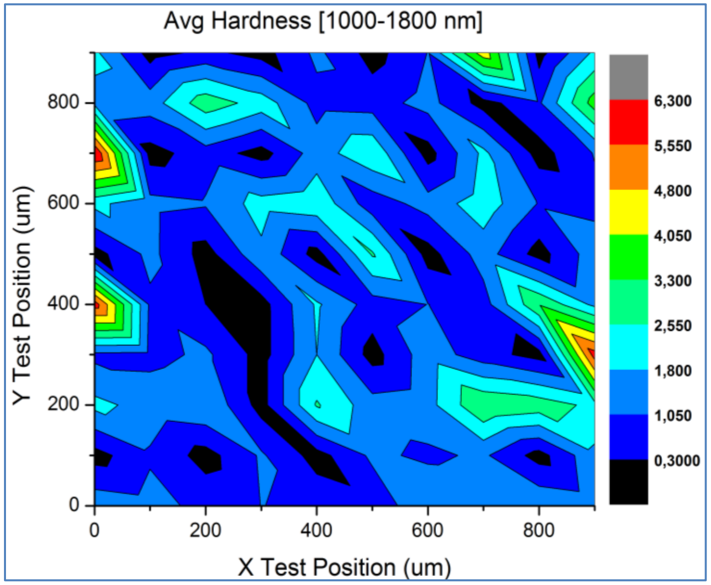

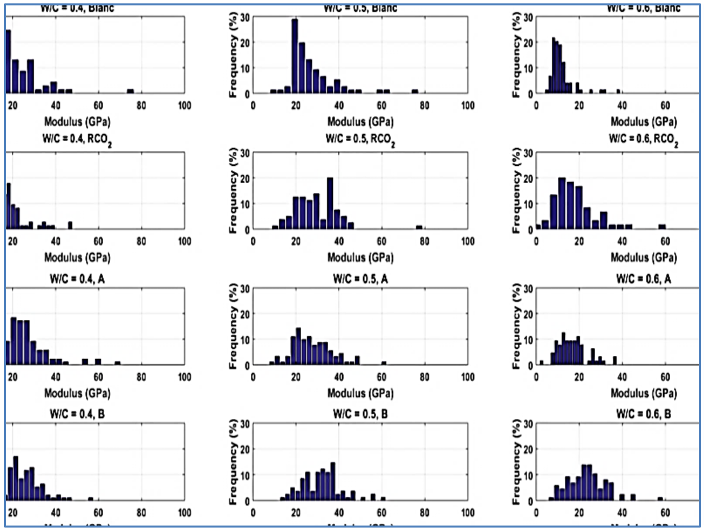

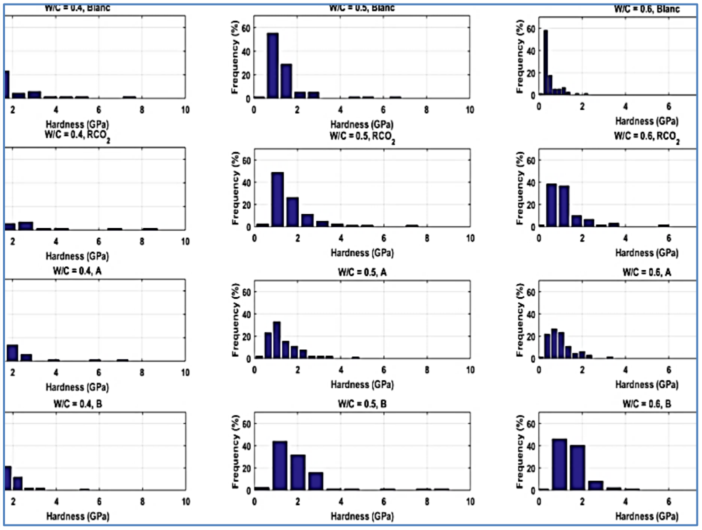

1.8. CEMIII 0.5 Blanc

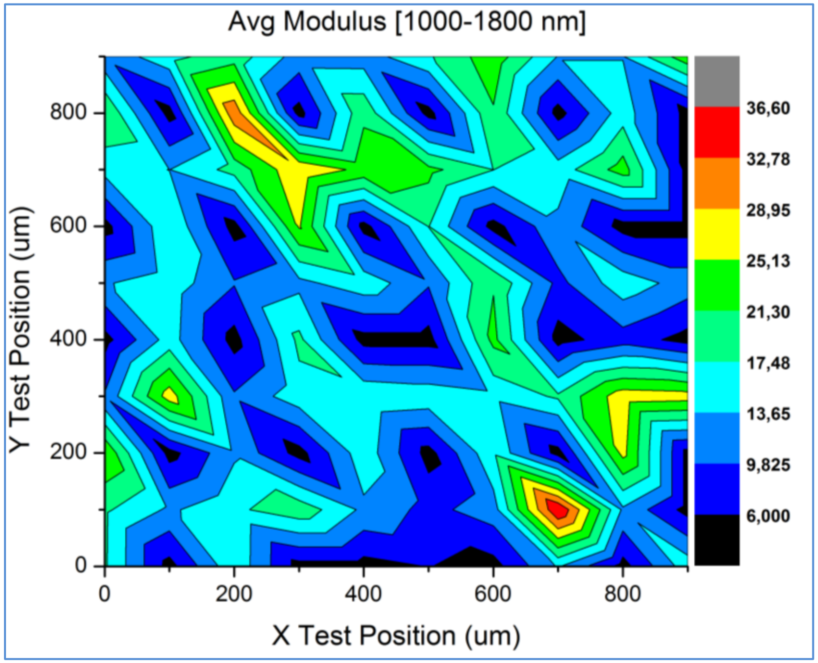

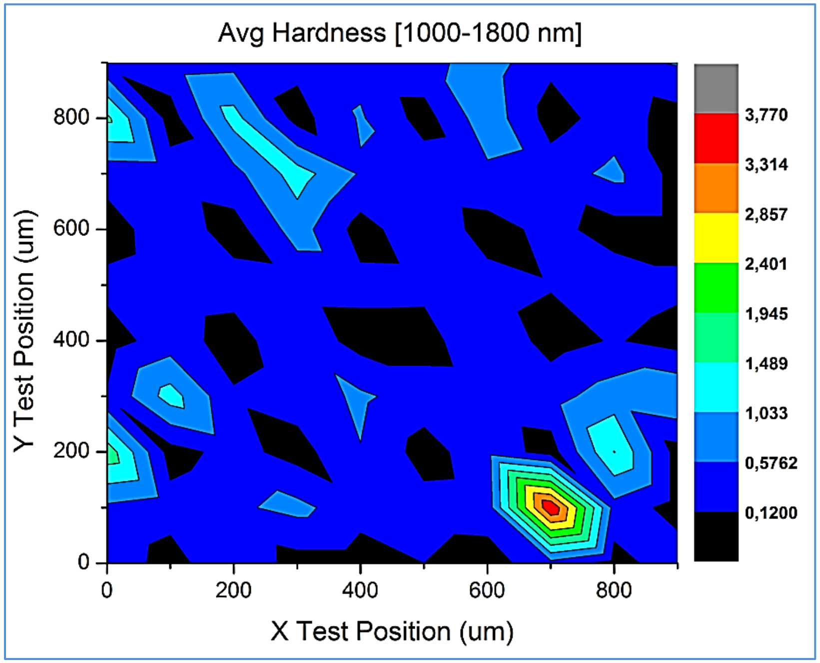

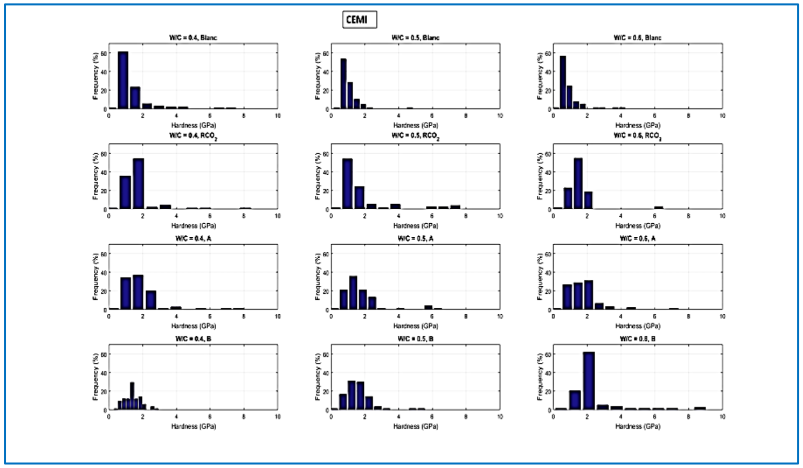

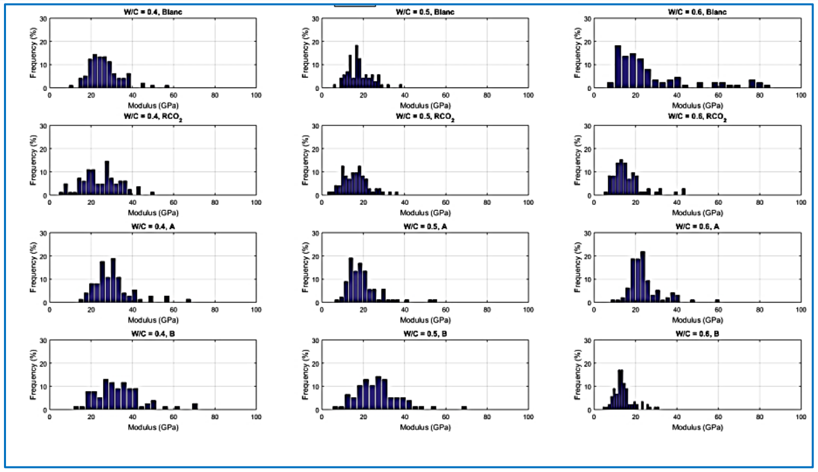

1.9. CEM III 0.5 RCO_2-28 days

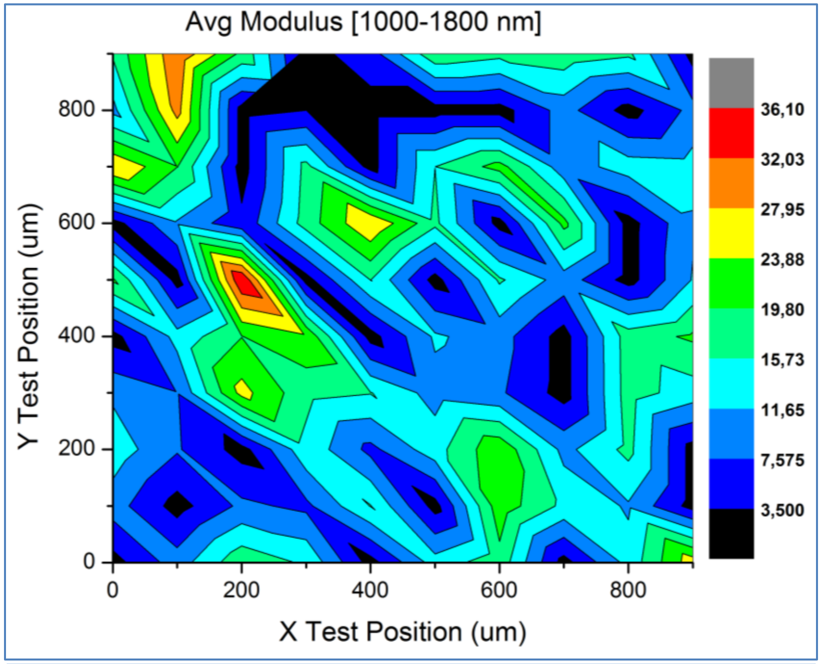

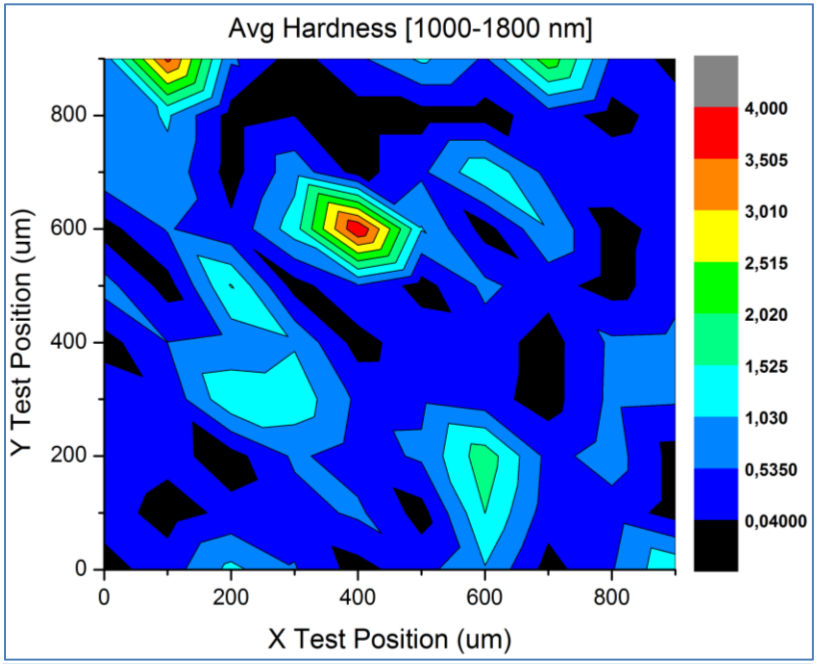

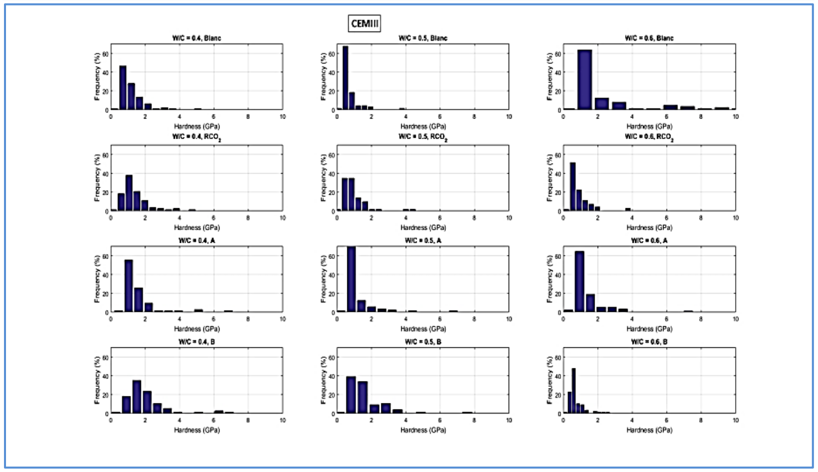

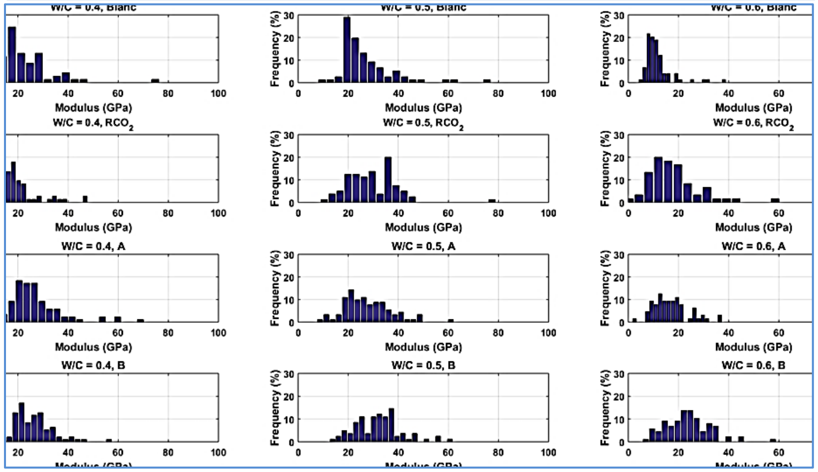

1.10. CEM III 0.5 A

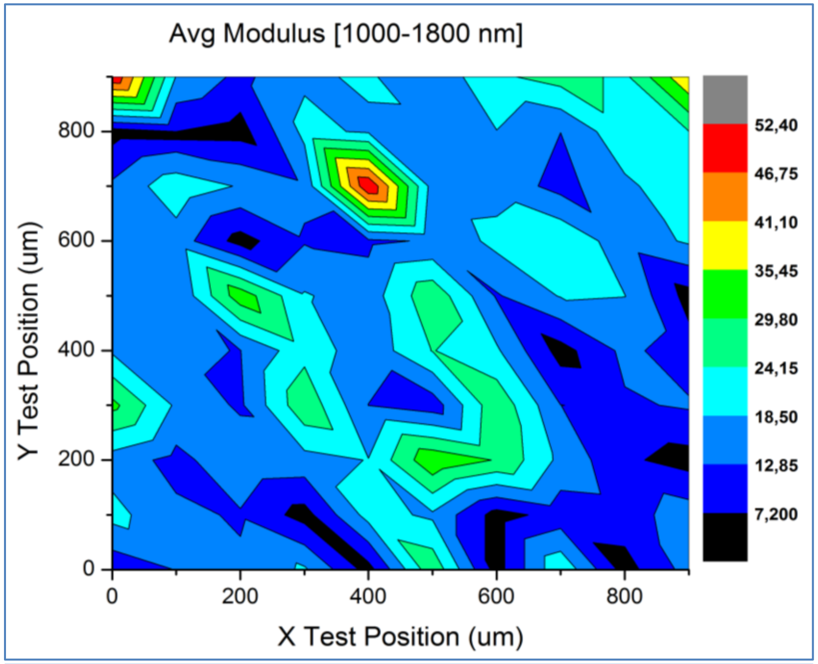

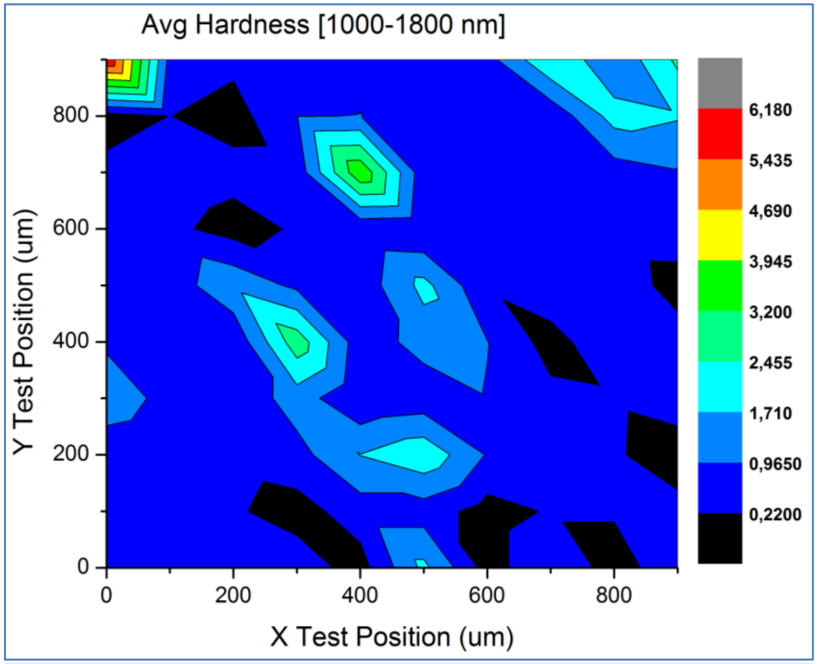

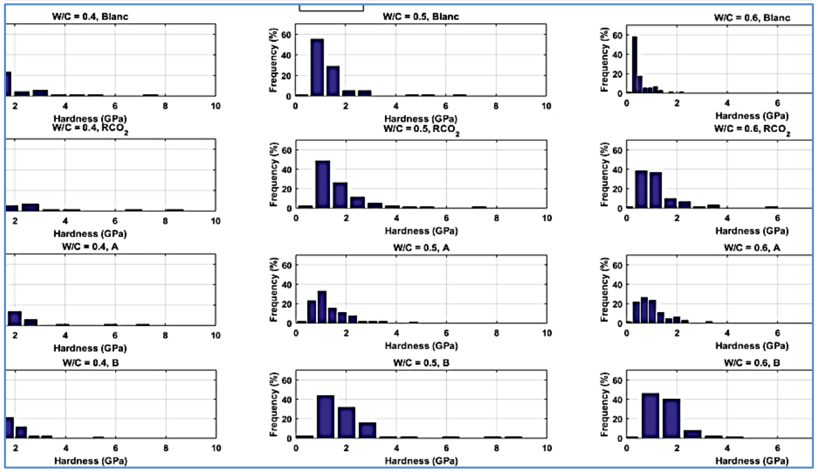

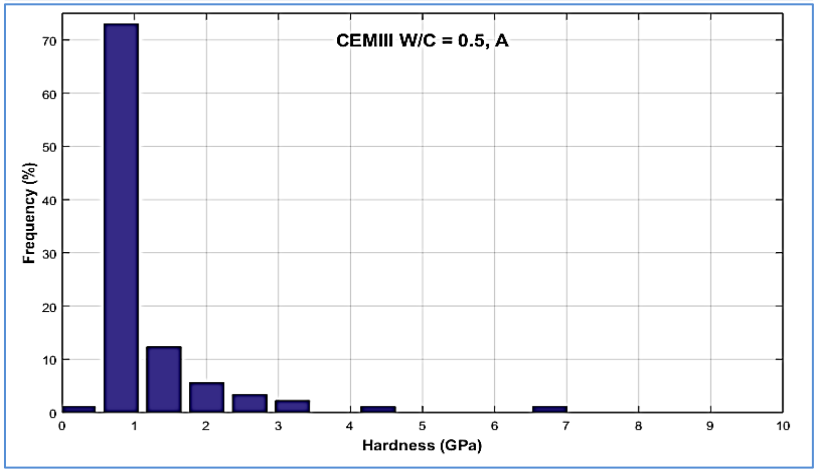

1.11. CEM III 0.5 B

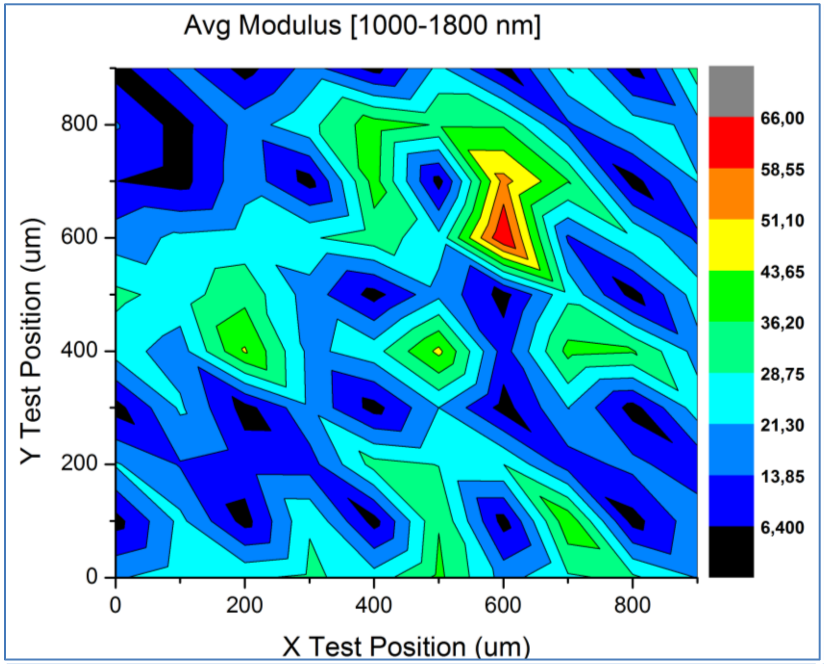

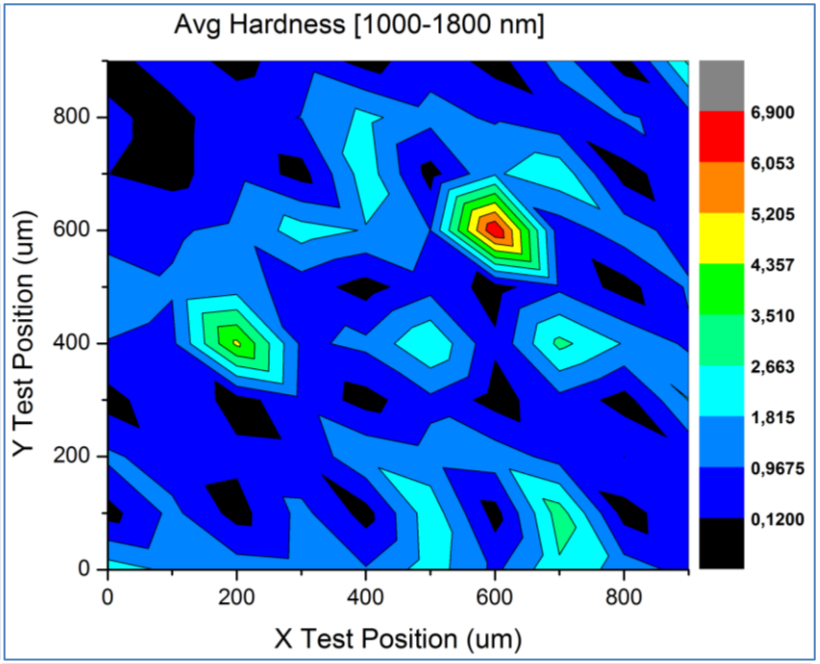

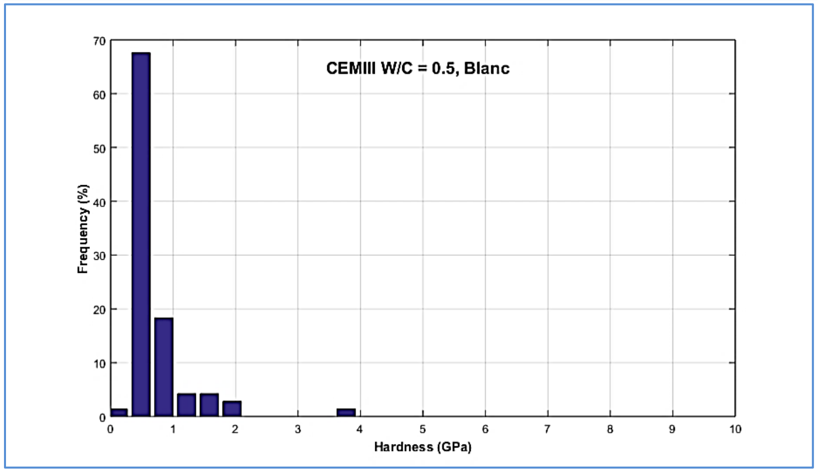

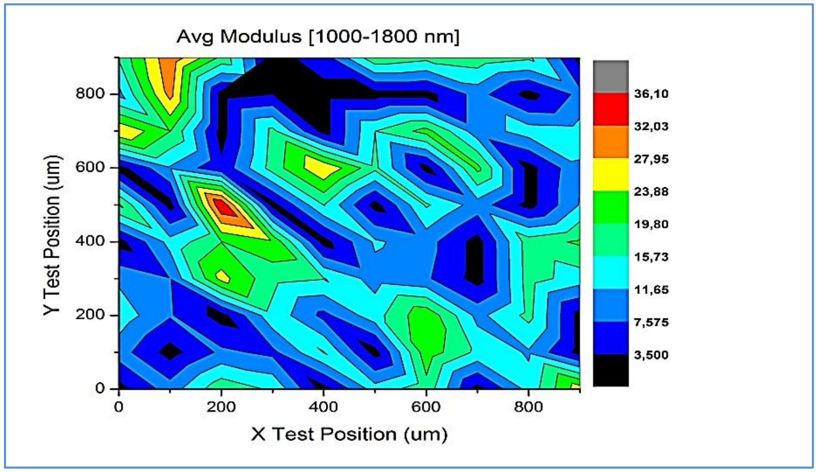

1.12. CEM III 0.6 Blanc

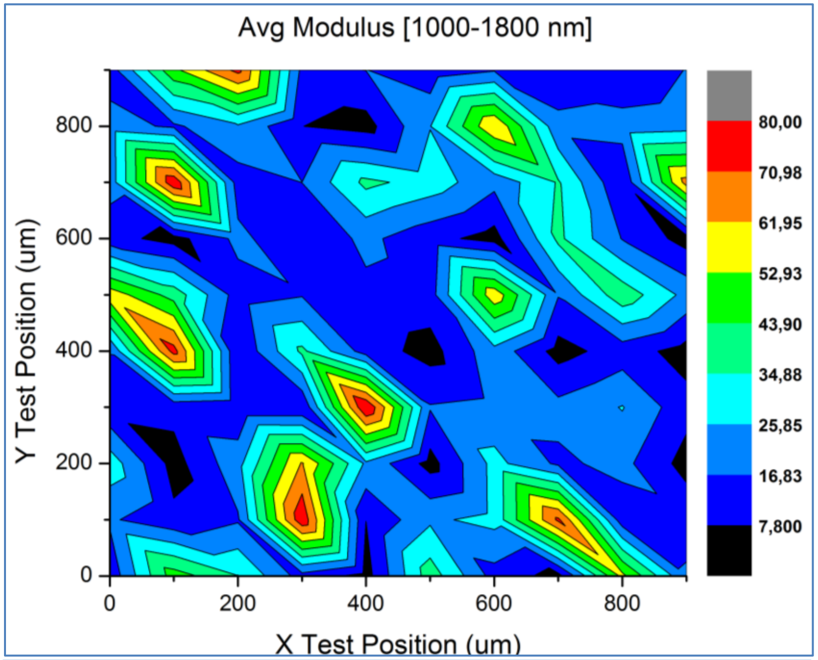

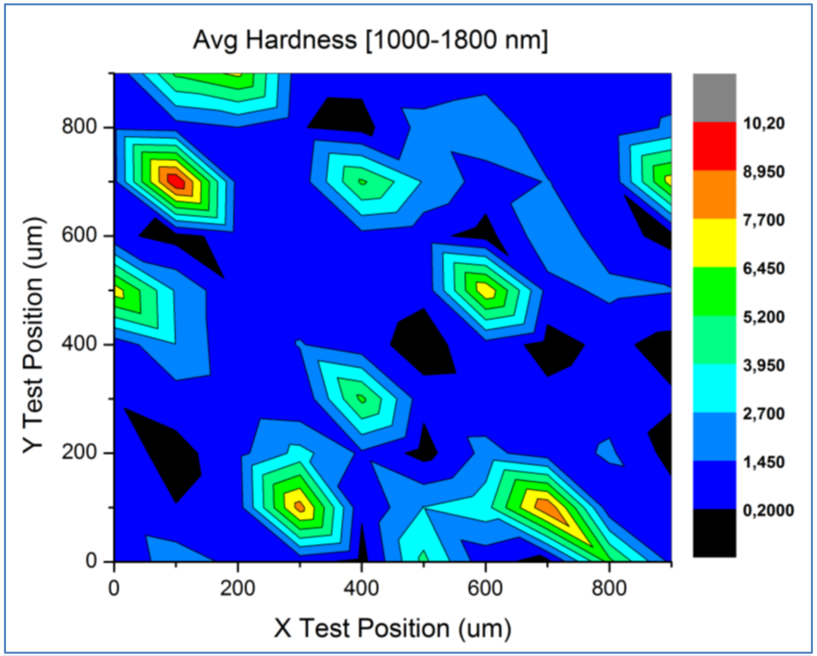

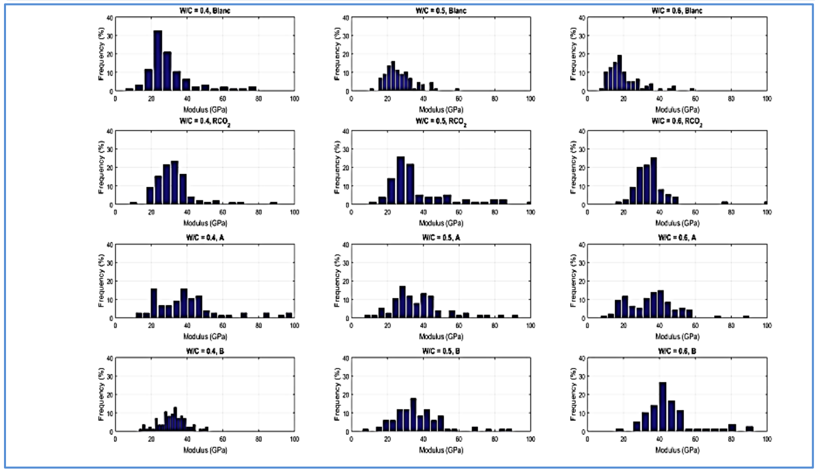

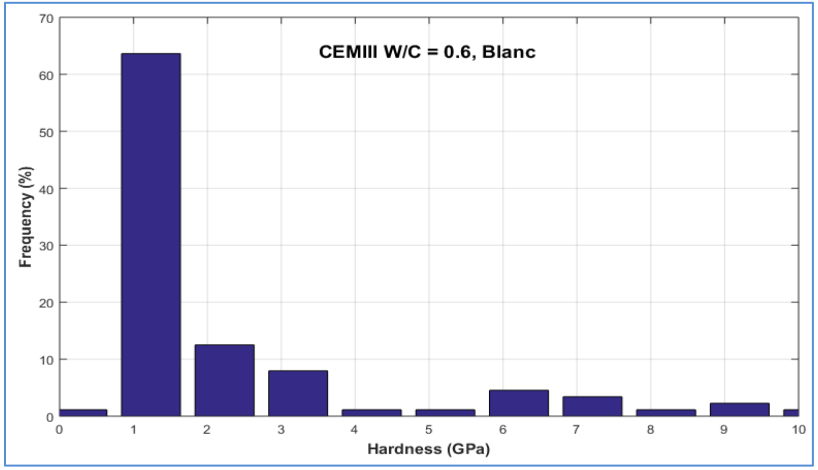

1.13. CEMIII 0.6 RCO_2-28 days

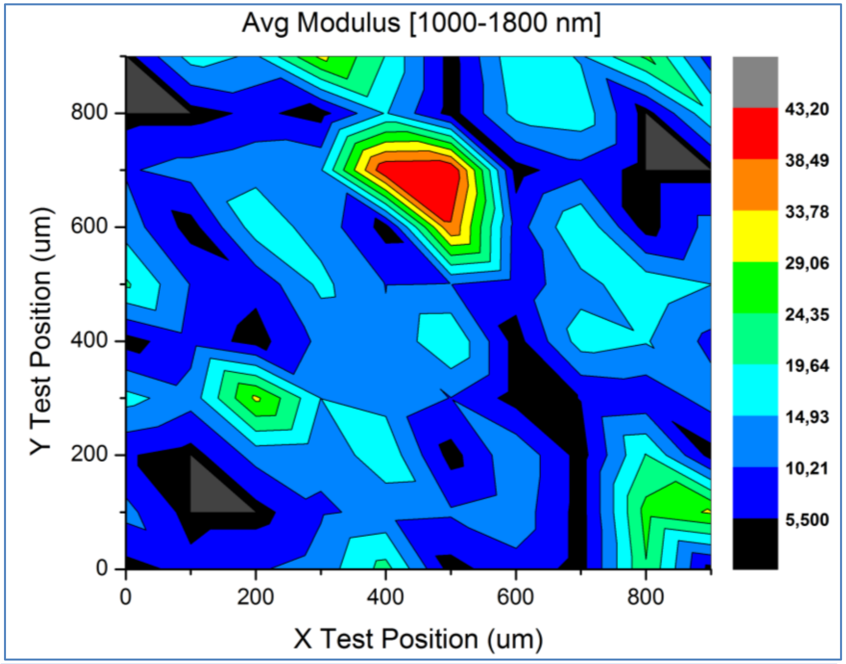

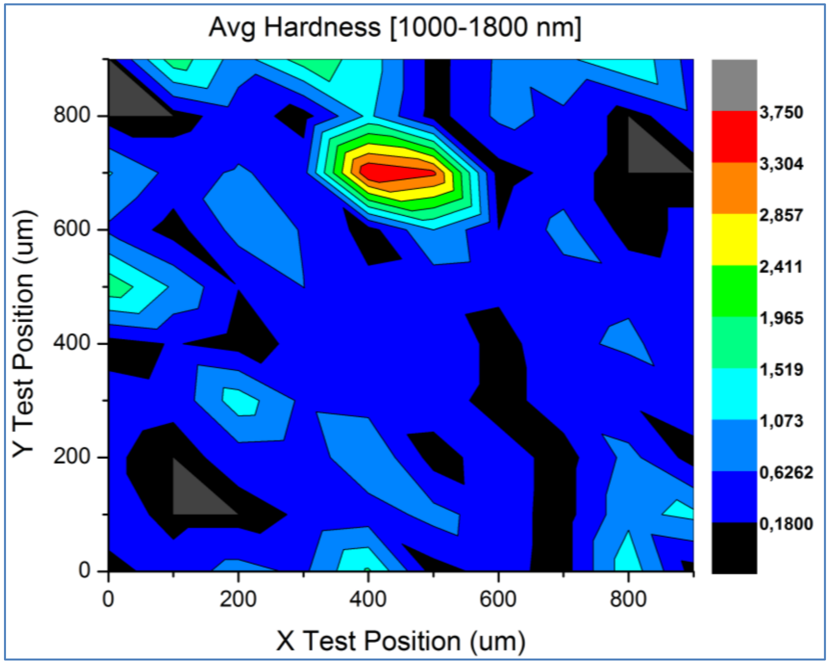

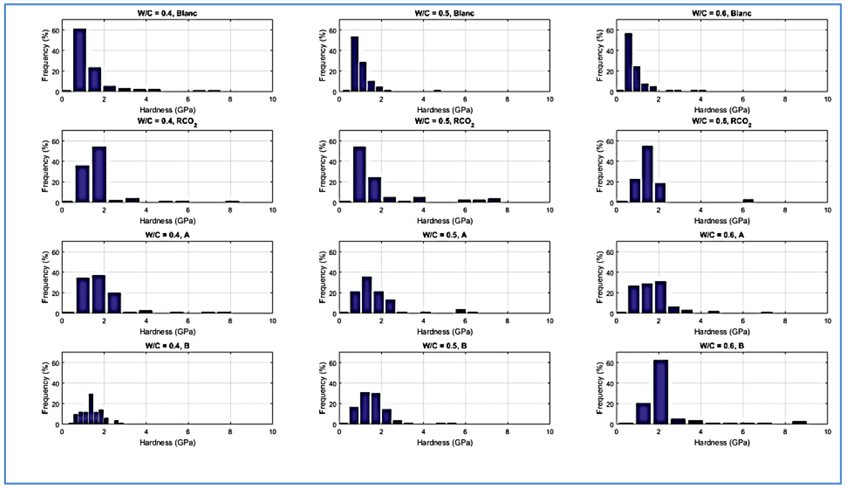

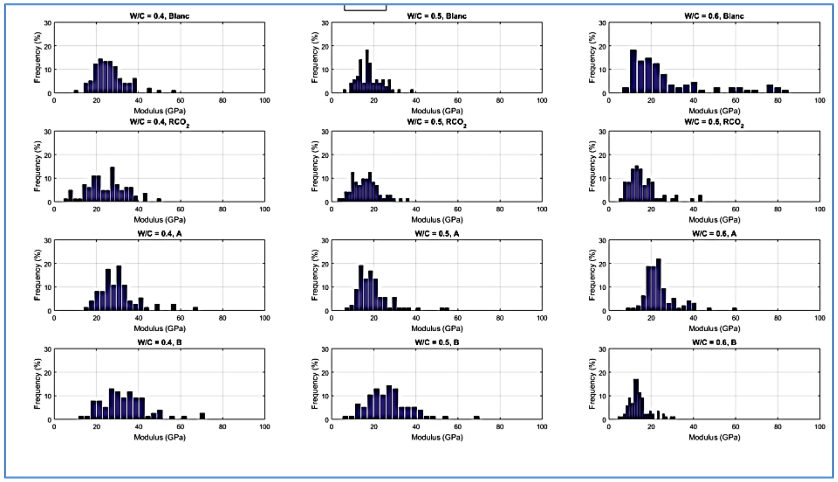

1.14. CEM III 0.6 A

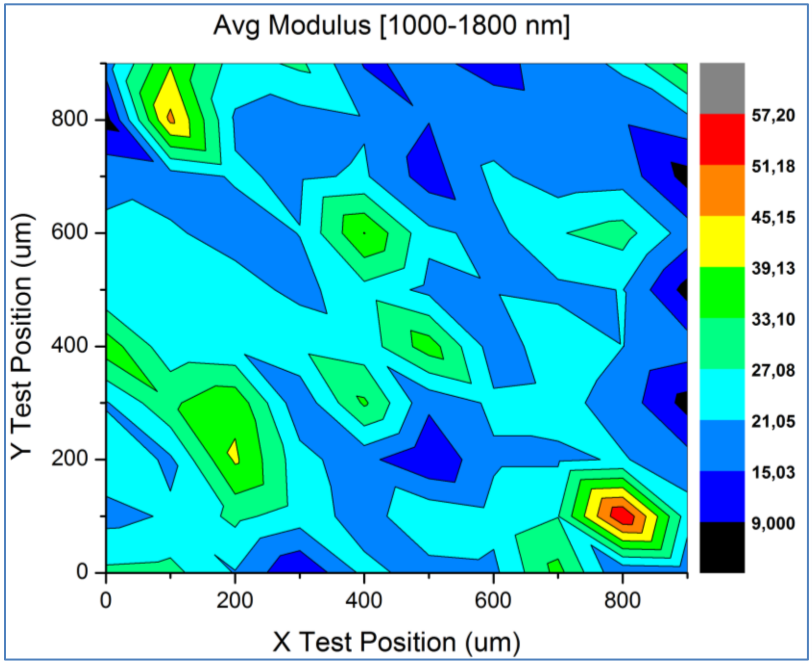

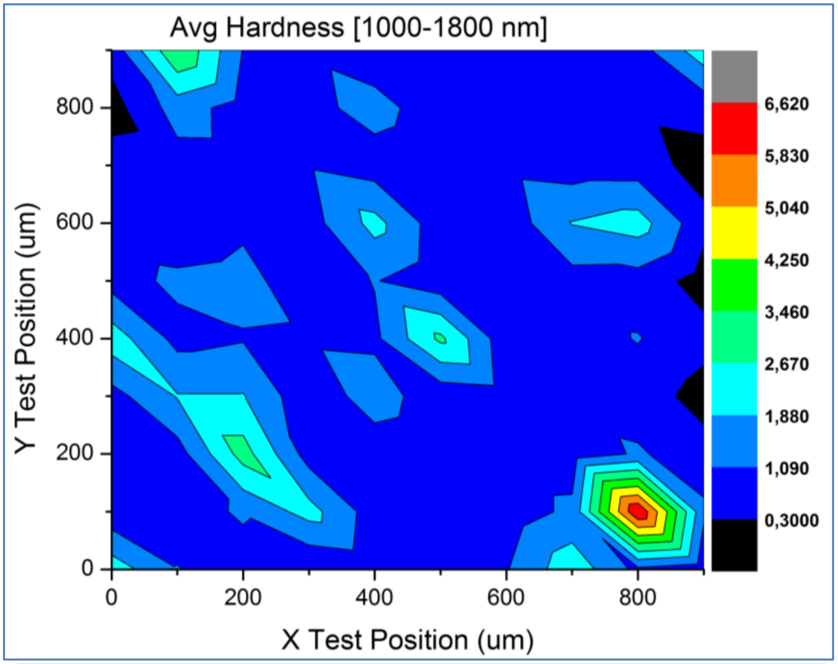

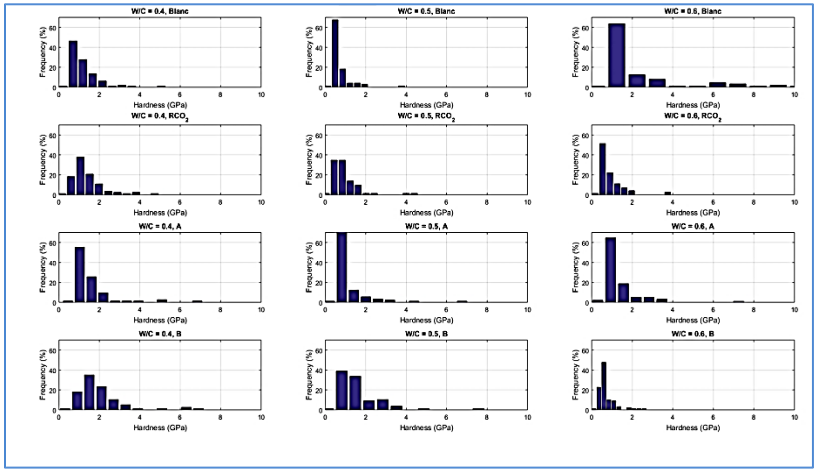

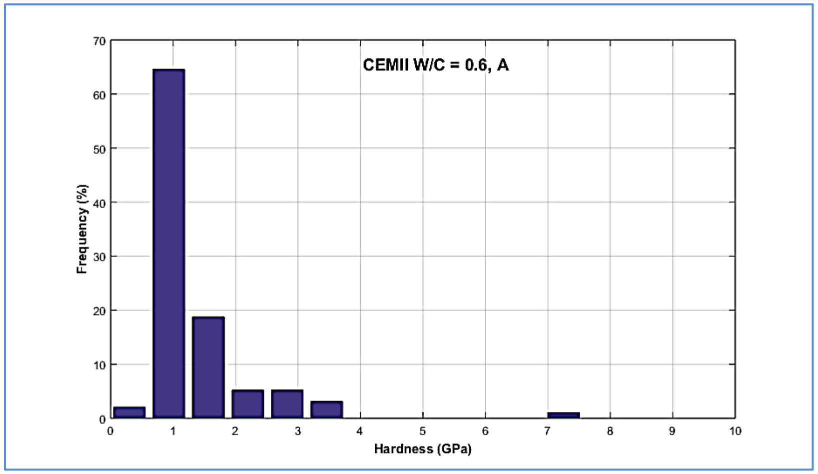

1.15. CEMIII 0.6 B

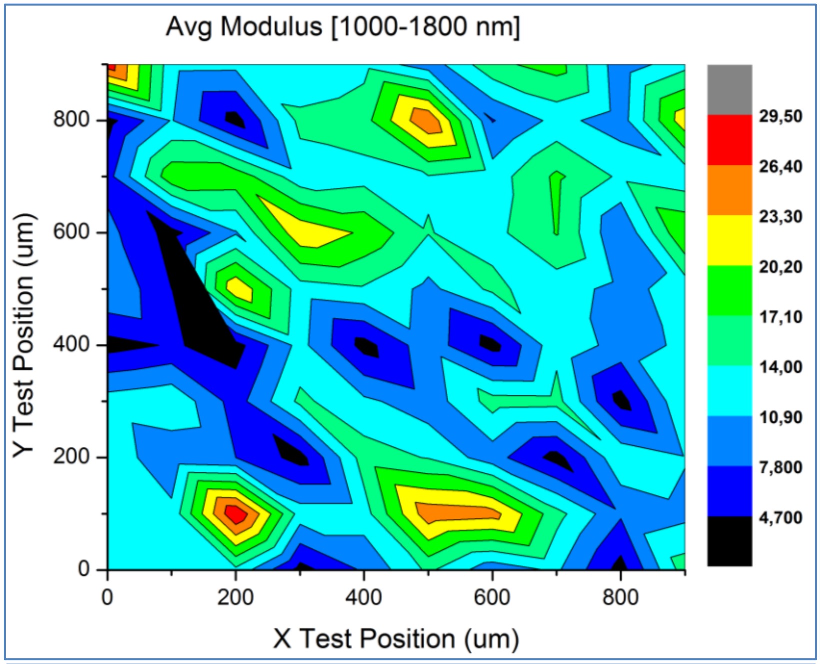

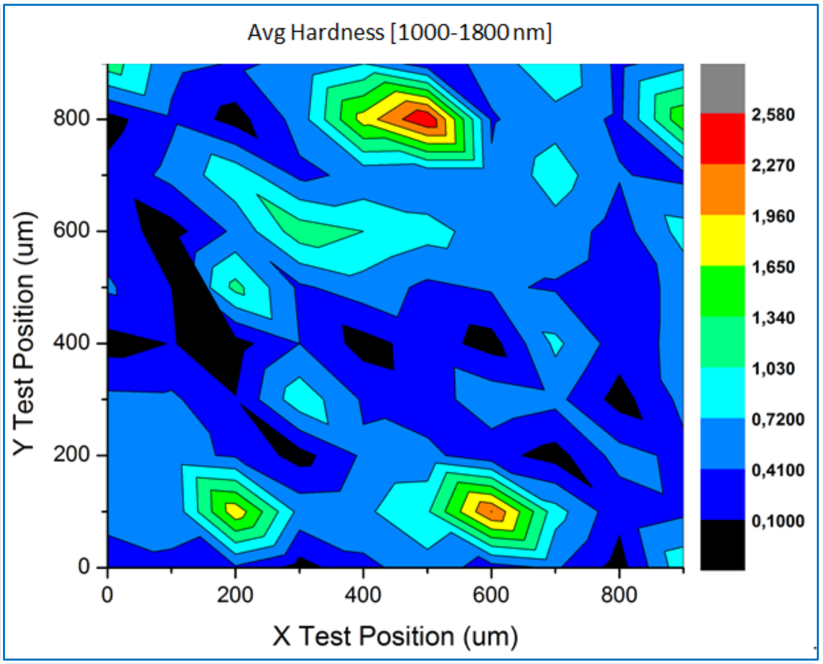

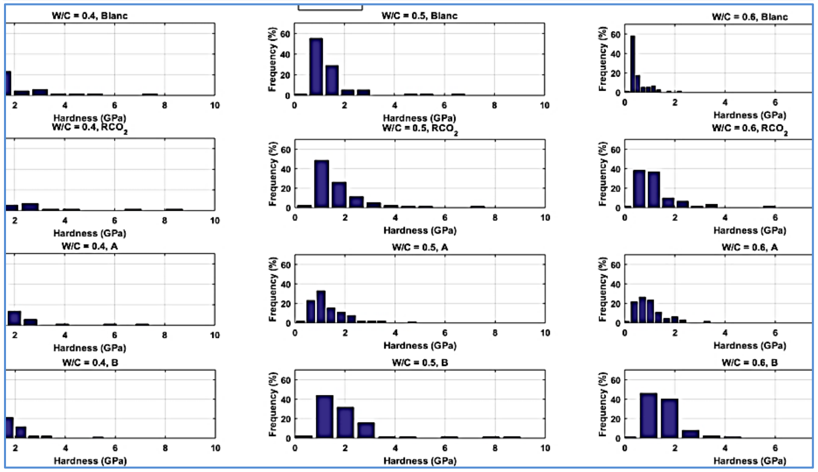

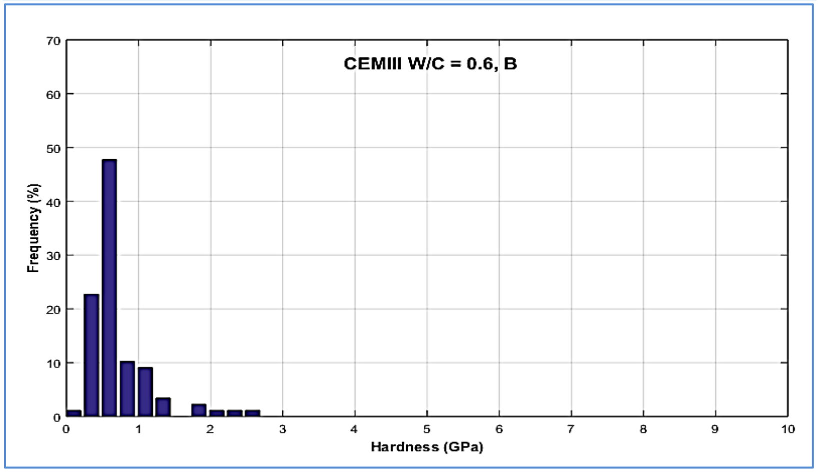

1.16. Classification of elastic modulus

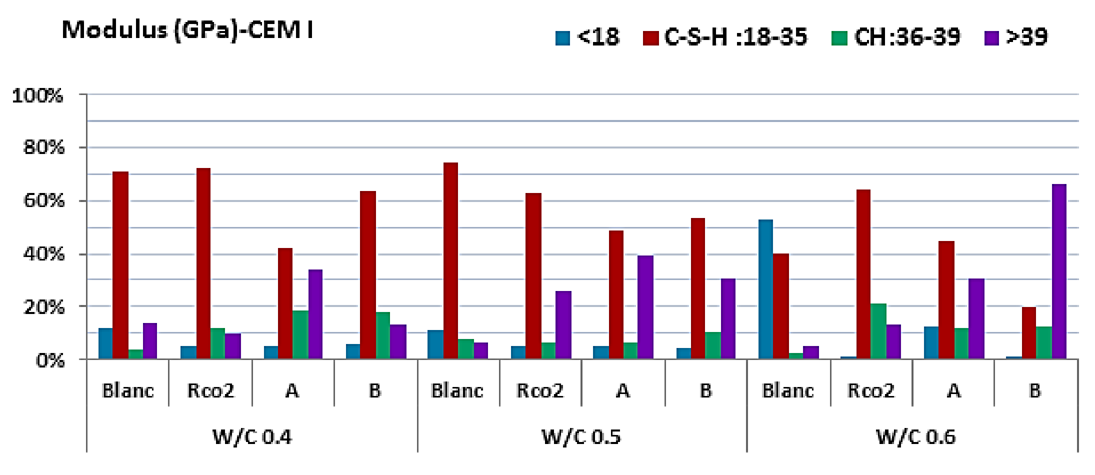

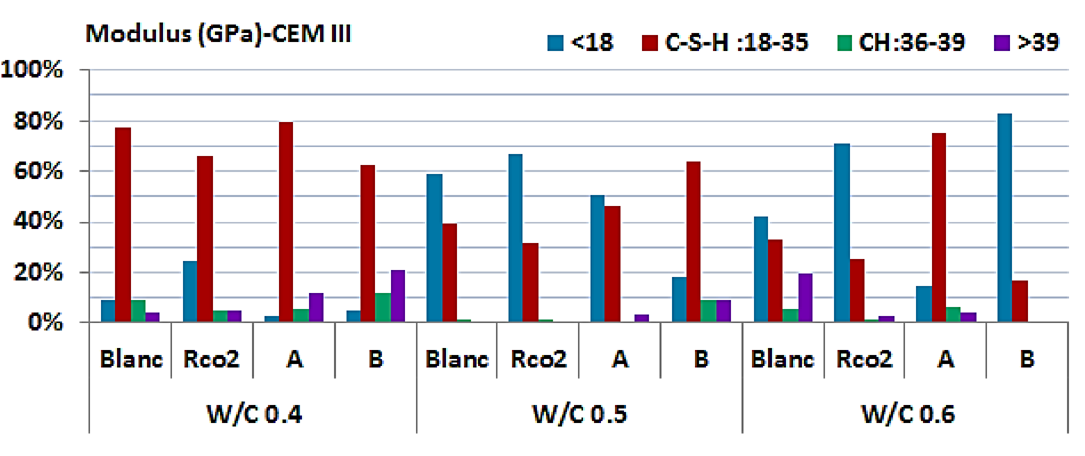

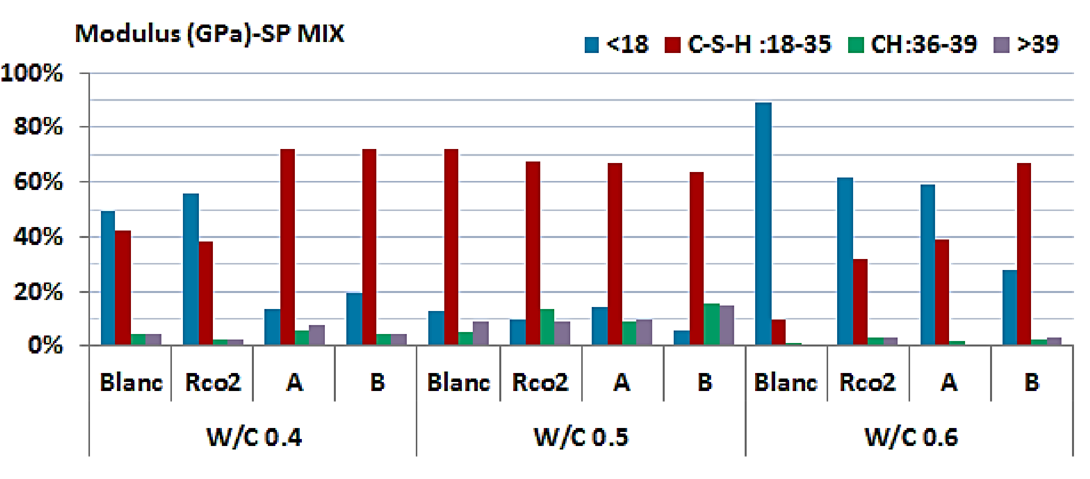

	Modulus (GPa)
	<18
C-S-H	18-35
CH	36-39
	>39

1.17. Classification of Hardness

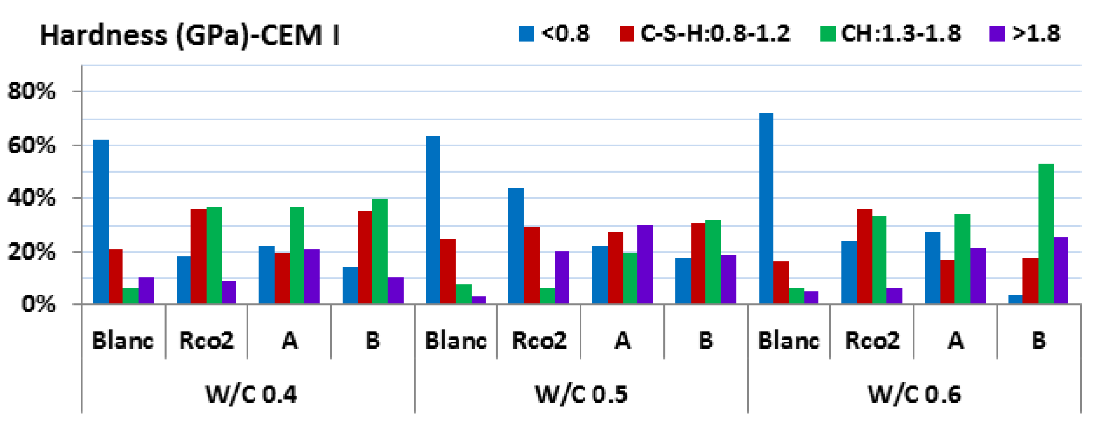

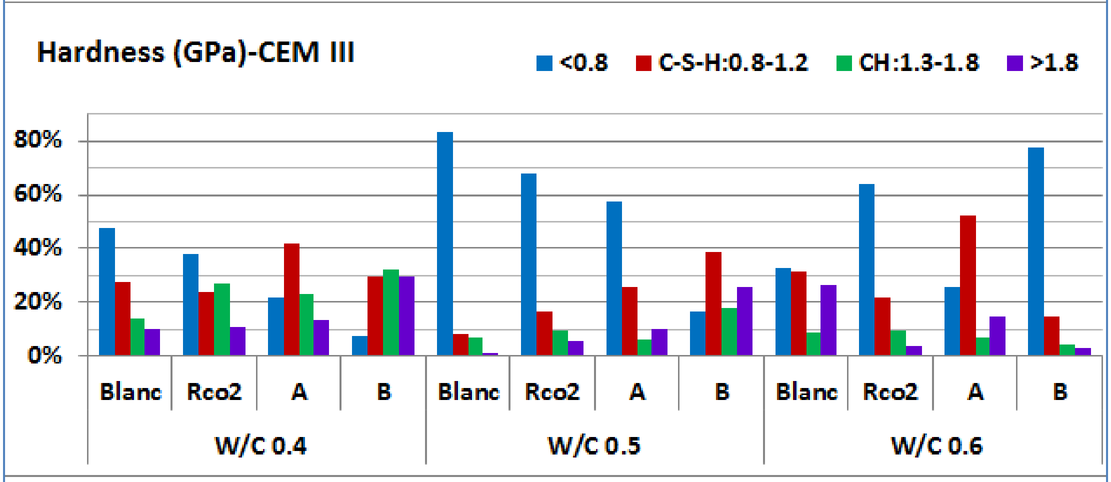

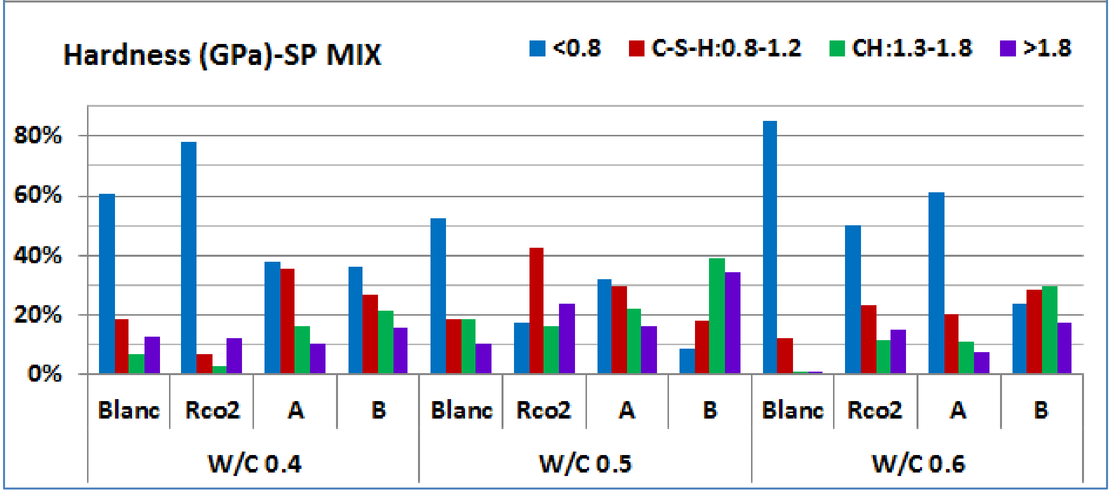

	Hardness (GPa)
	<0.8
C-S-H	0.8-1.2
CH	1.3-1.8
	>1.8

4. Appendix: Result of the Mercury Intrusion Porosimetrytests

1.11 Porosity and critical diameter for paste samples with different treatments with the same W/C ratio

Water cement ratio 0.4

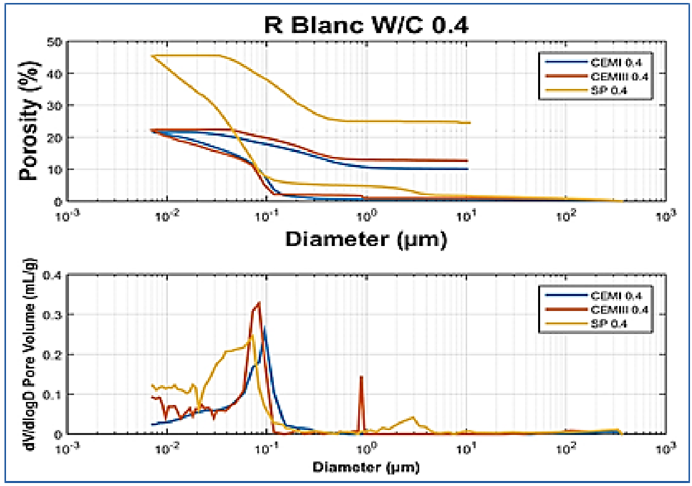

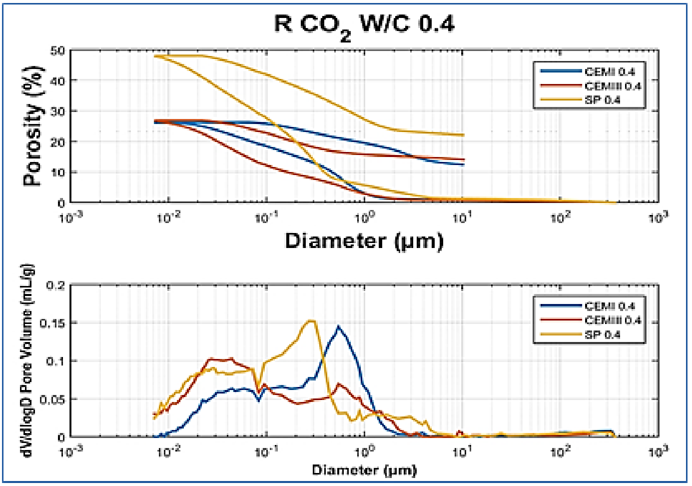

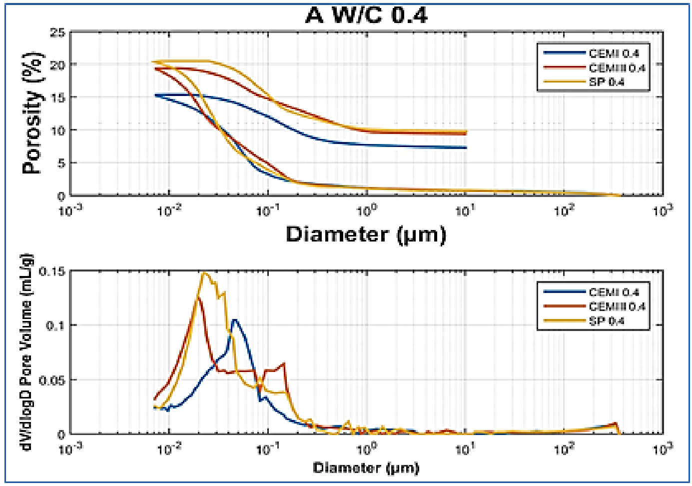

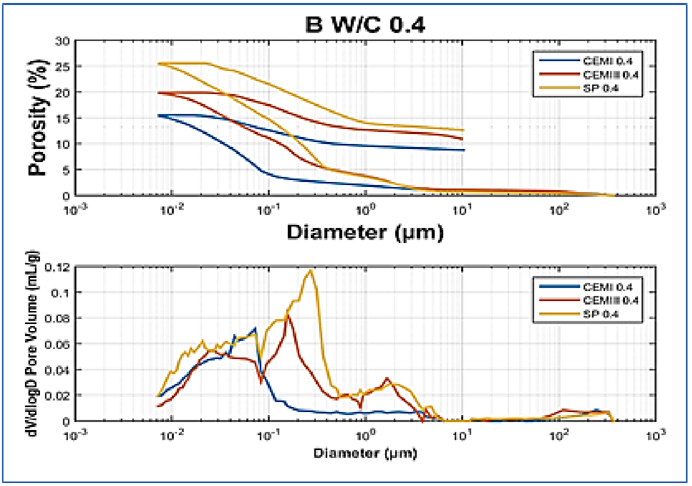

Water cement ratio 0.5

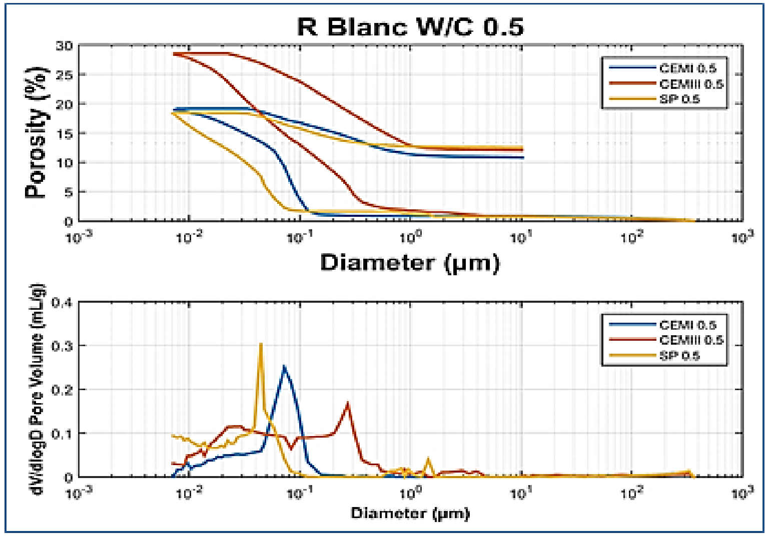

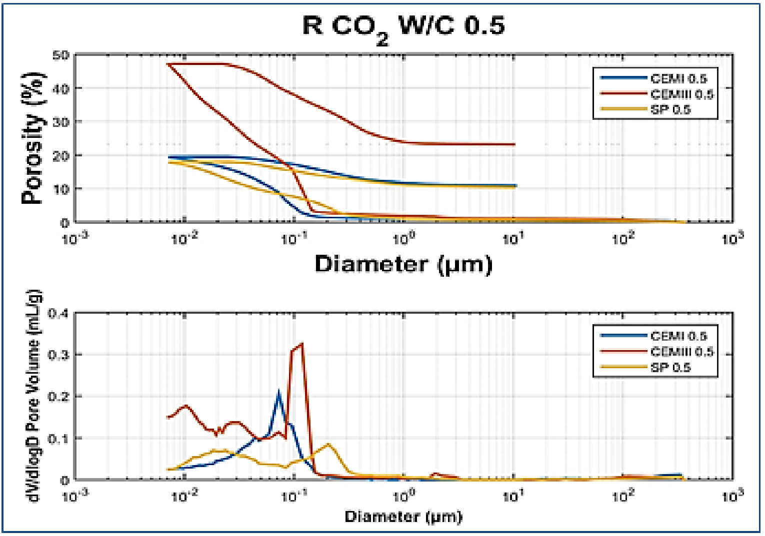

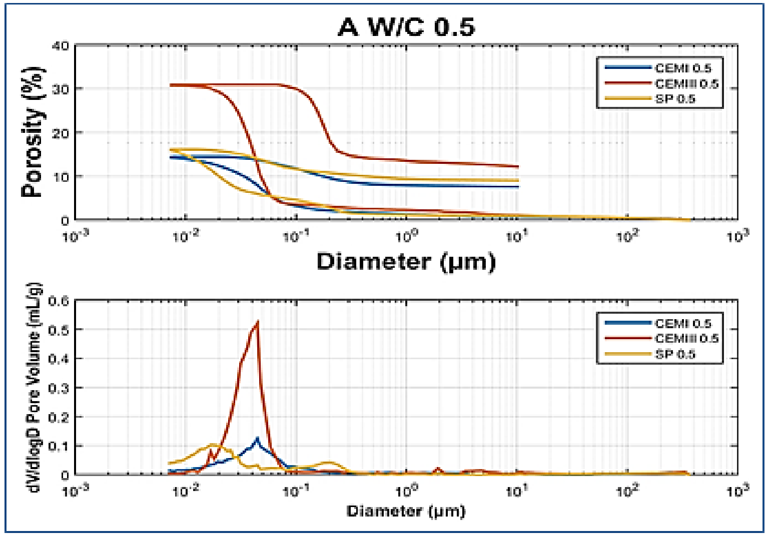

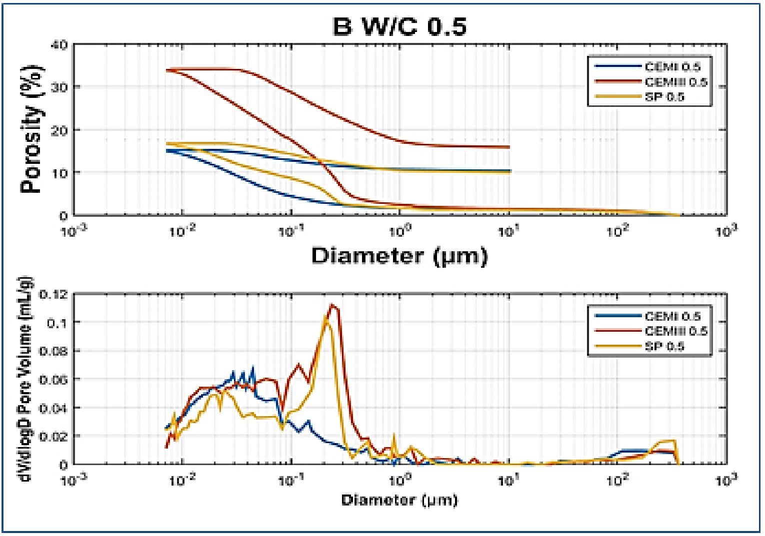

Water cement ratio 0.6

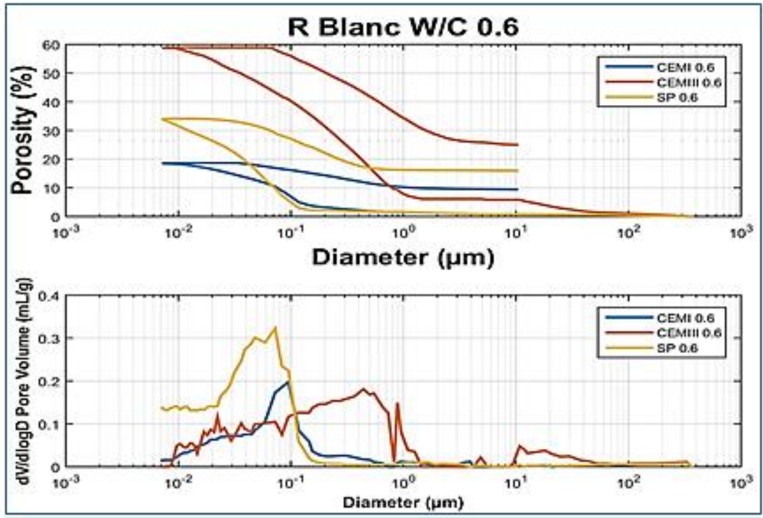

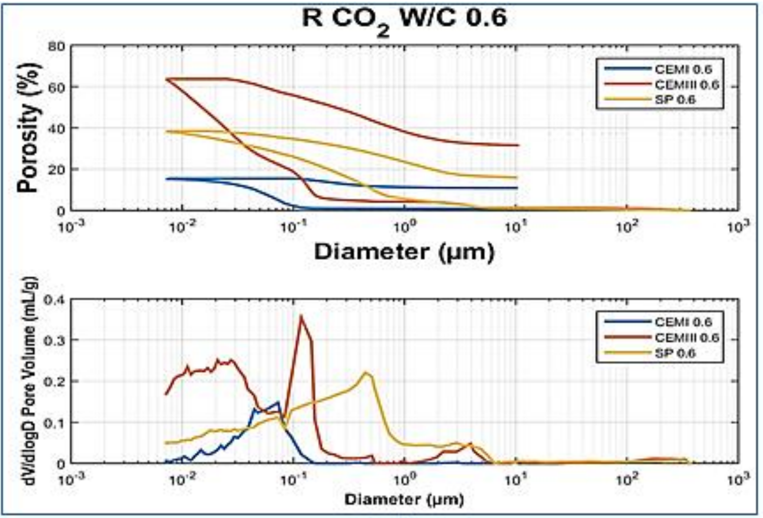

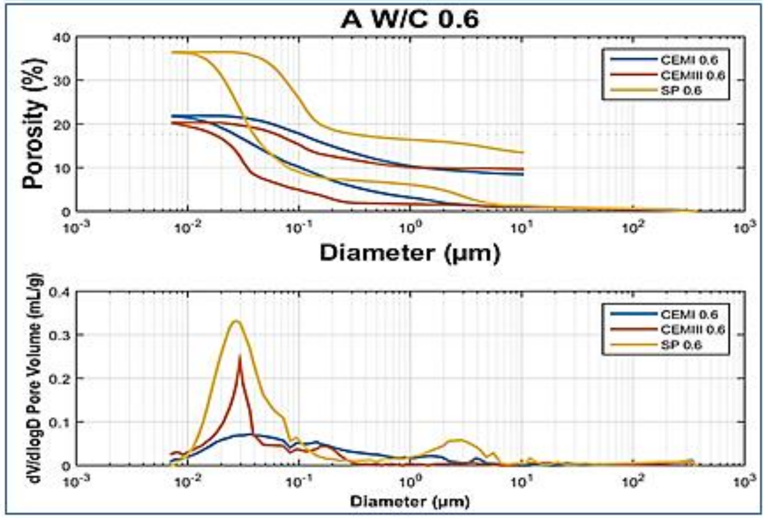

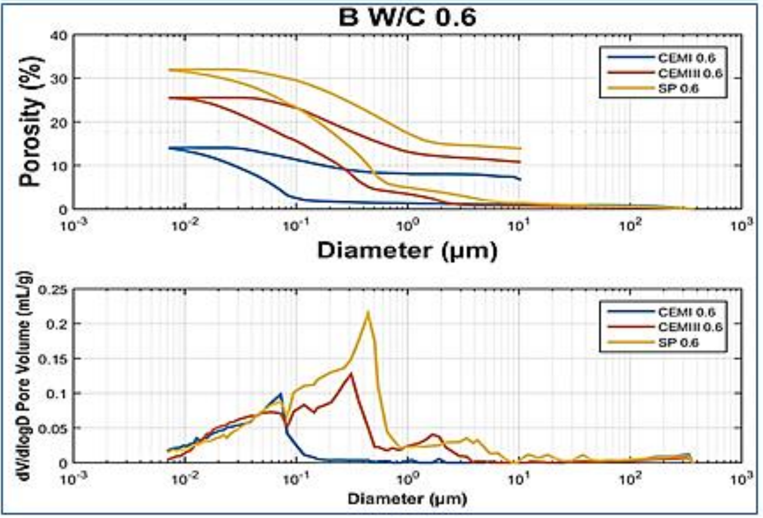

1.12 Porosity and critical diameter for paste with different treatments with the same cement type

CEM I

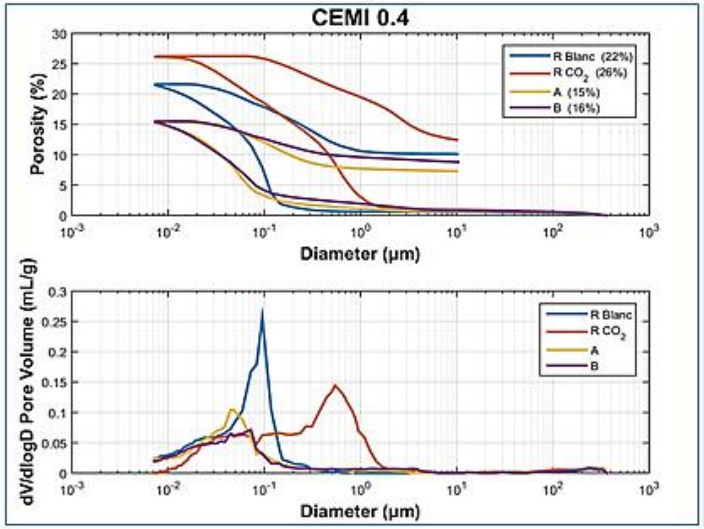

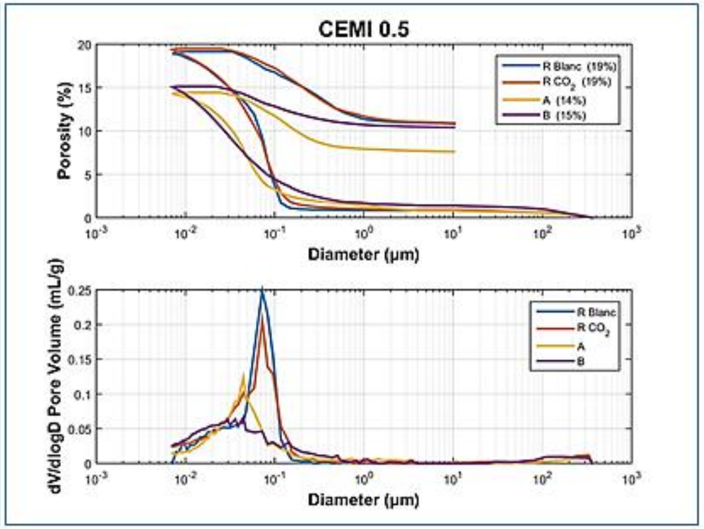

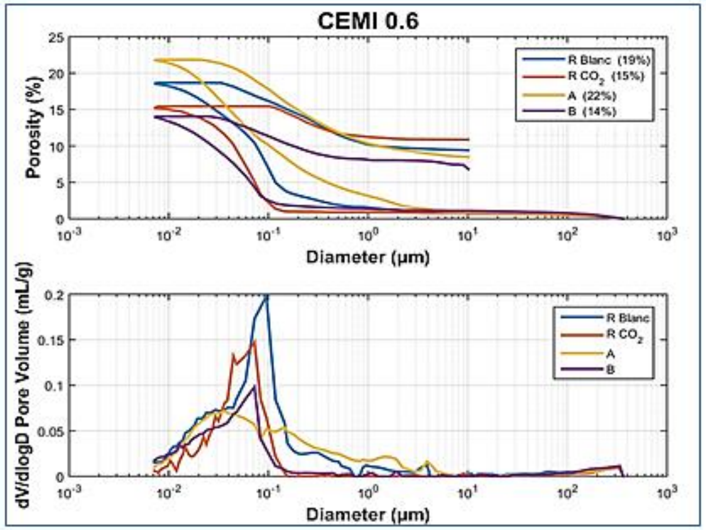

CEM III

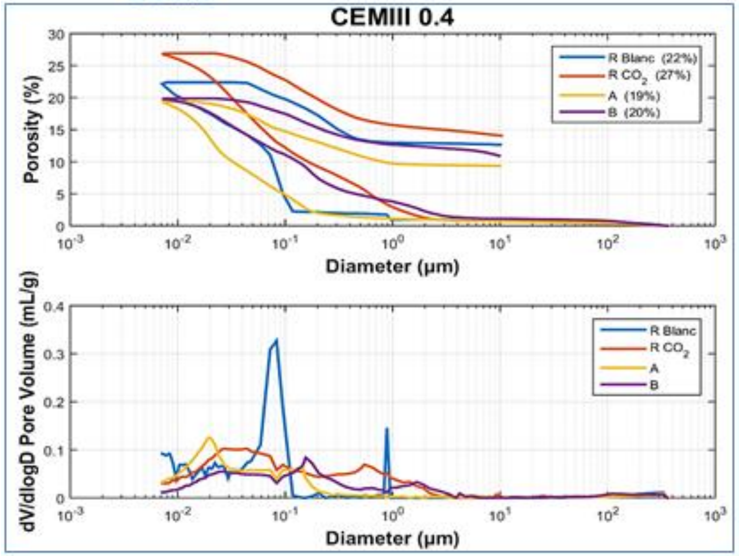
CEMIII 0.4
Porosity (%)
30
25
20
15
10
5
0
Diameter (µm)
10^{-3}
10^{-2}
10^{-1}
10^{0}
10^{1}
10^{2}
10^{3}
R Blanc (22%)
R CO$_2$ (27%)
A (19%)
B (20%)
dV/dlogD Pore Volume (mL/g)
0.4
0.3
0.2
0.1
0
R Blanc
R CO$_2$
A
B
Diameter (µm)

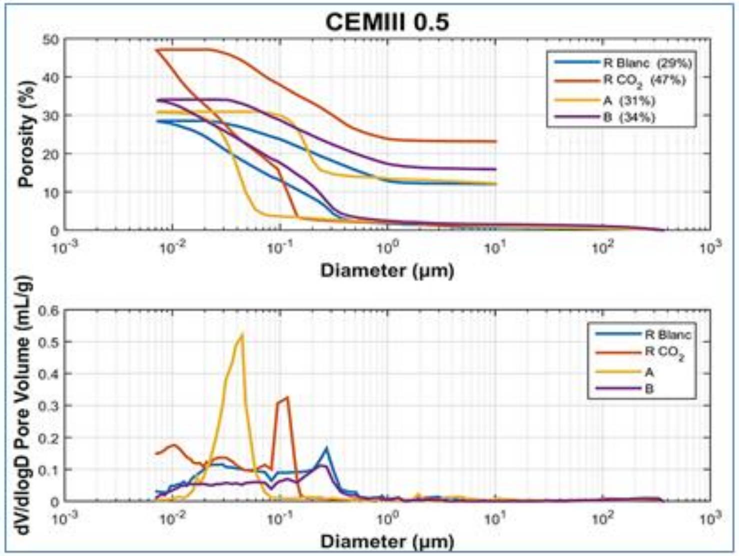
CEMIII 0.5
Porosity (%)
50
40
30
20
10
0
Diameter (µm)
10^{-3}
10^{-2}
10^{-1}
10^{0}
10^{1}
10^{2}
10^{3}
R Blanc (29%)
R CO$_2$ (47%)
A (31%)
B (34%)
dV/dlogD Pore Volume (mL/g)
0.6
0.5
0.4
0.3
0.2
0.1
0
R Blanc
R CO$_2$
A
B
Diameter (µm)

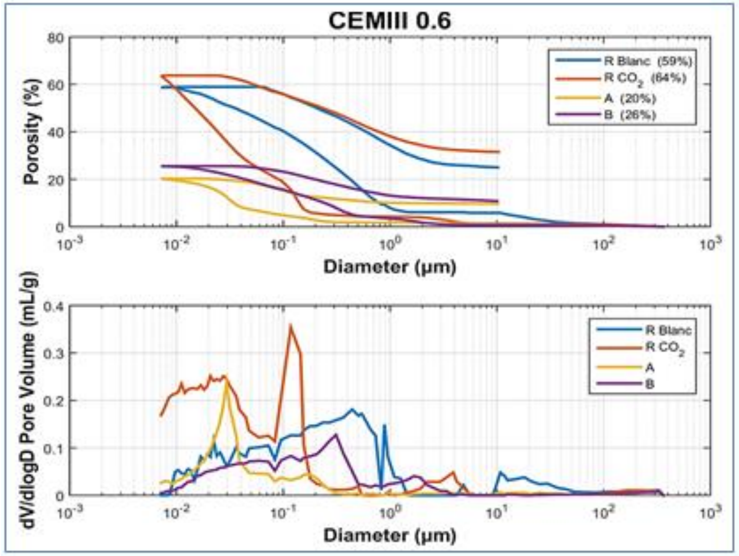
CEMIII 0.6
Porosity (%)
80
60
40
20
0
Diameter (µm)
10^{-3}
10^{-2}
10^{-1}
10^{0}
10^{1}
10^{2}
10^{3}
R Blanc (59%)
R CO$_2$ (64%)
A (20%)
B (26%)
dV/dlogD Pore Volume (mL/g)
0.4
0.3
0.2
0.1
0
R Blanc
R CO$_2$
A
B
Diameter (µm)

SP MIX

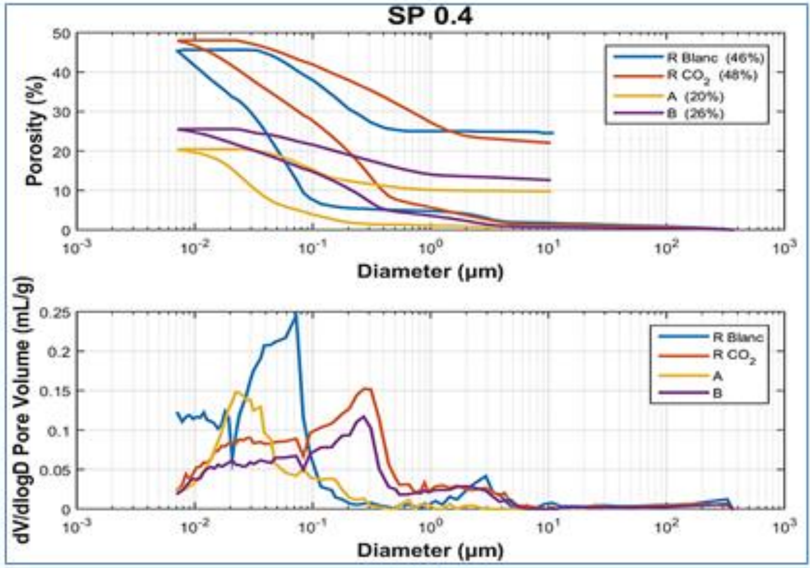
SP 0.4
Porosity (%)
Diameter (μm)
R Blanc (46%)
R CO$_2$ (48%)
A (20%)
B (26%)
dV/dlogD Pore Volume (mL/g)
Diameter (μm)
R Blanc
R CO$_2$
A
B

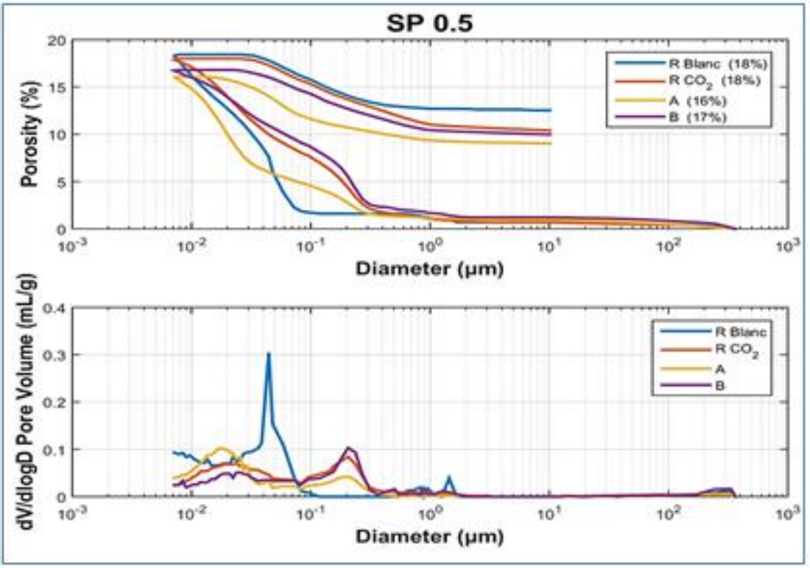
SP 0.5
Porosity (%)
Diameter (μm)
R Blanc (18%)
R CO$_2$ (18%)
A (16%)
B (17%)
dV/dlogD Pore Volume (mL/g)
Diameter (μm)
R Blanc
R CO$_2$
A
B

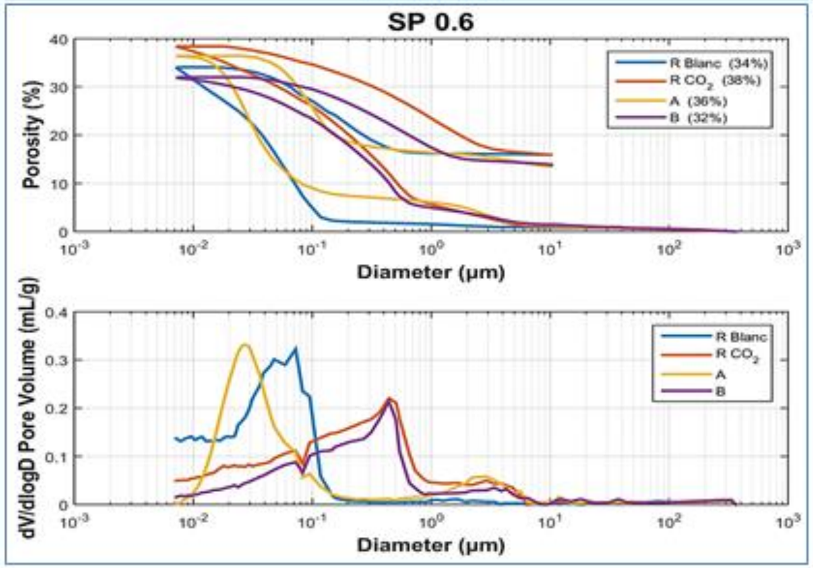
SP 0.6
Porosity (%)
Diameter (μm)
R Blanc (34%)
R CO$_2$ (38%)
A (36%)
B (32%)
dV/dlogD Pore Volume (mL/g)
Diameter (μm)
R Blanc
R CO$_2$
A
B

1.13 Total porosity

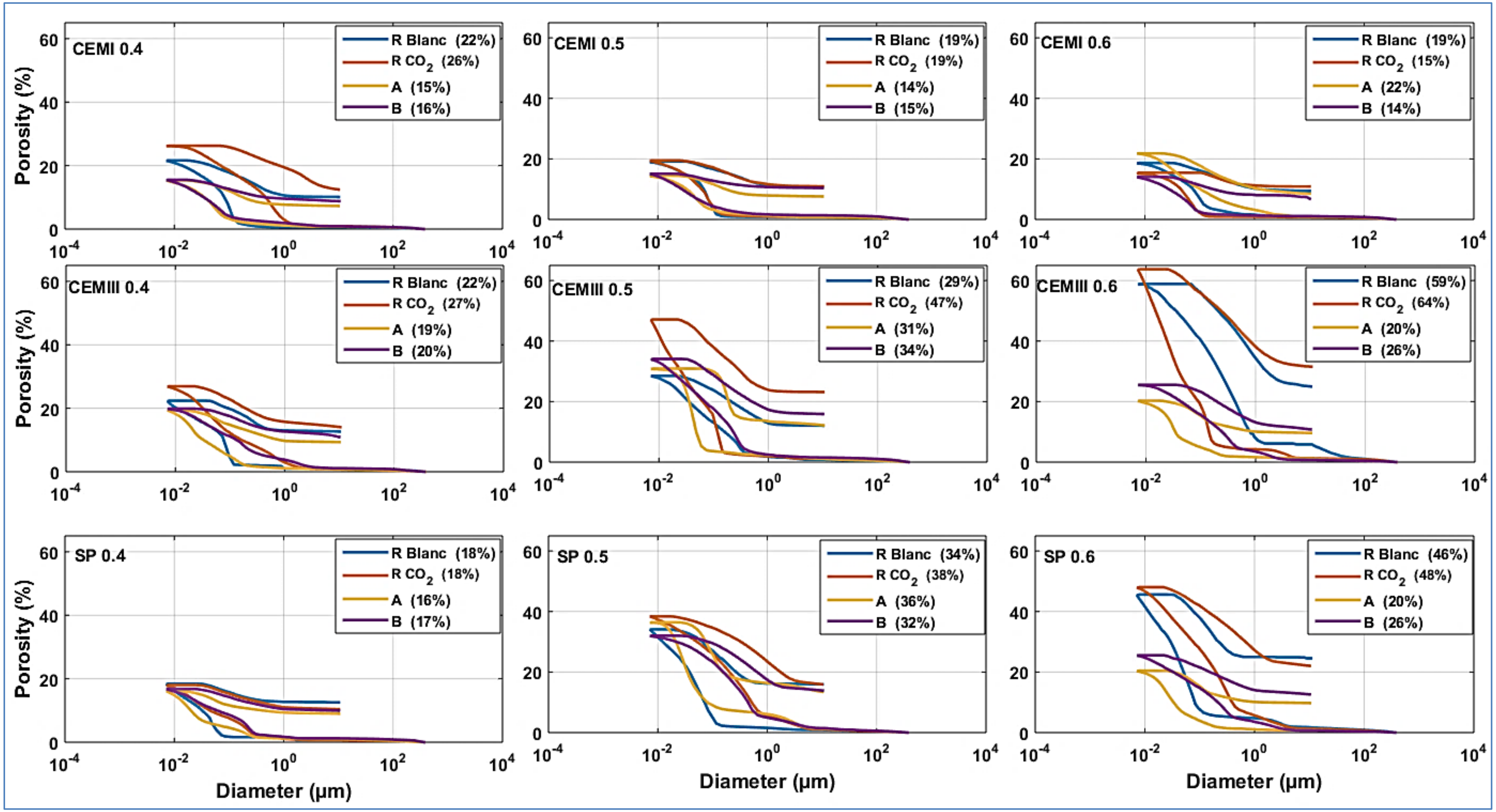

1.14 Critical diameter size

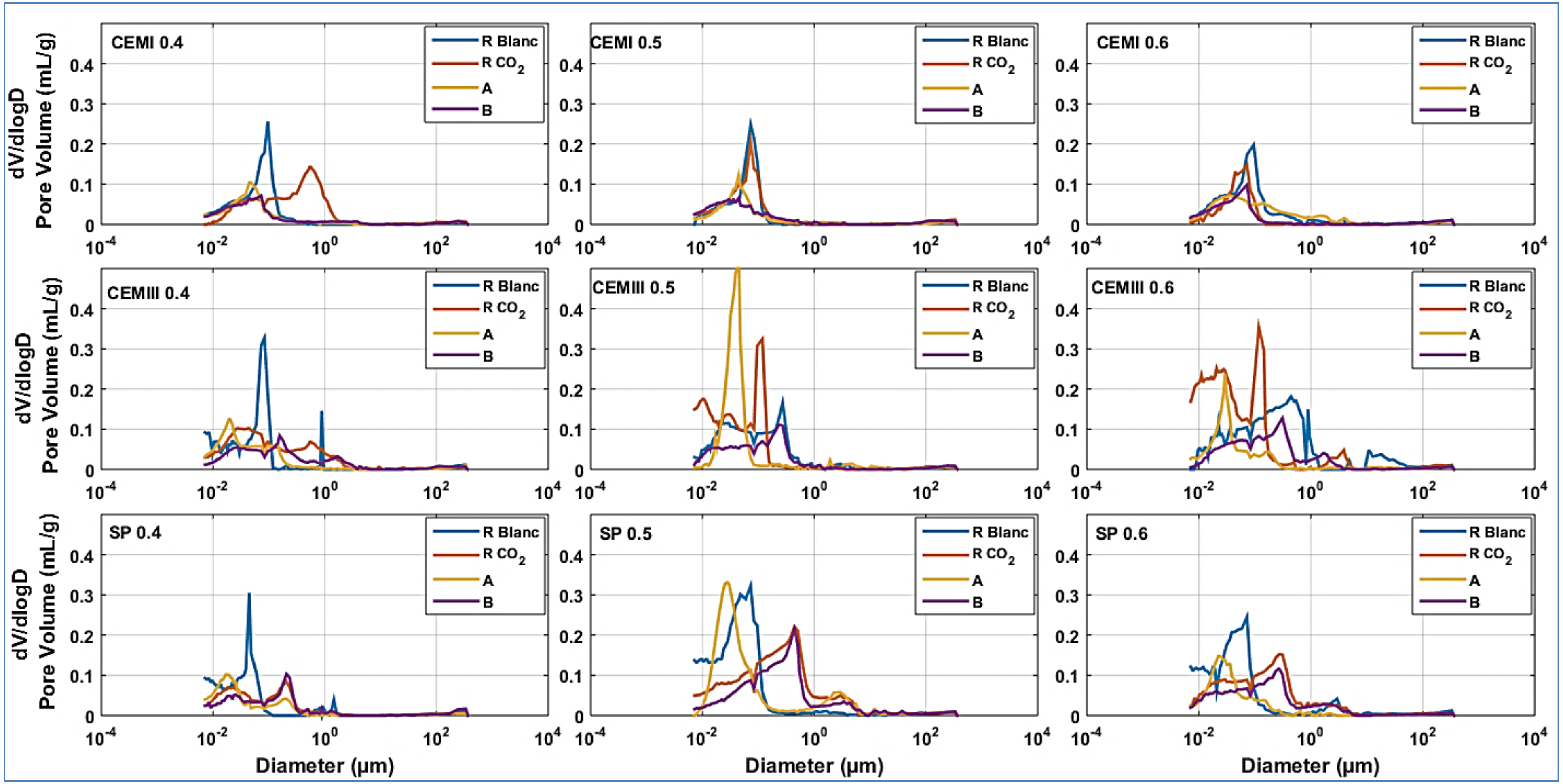

1.15 Calculation of the pore size distribution and capillary porosity

Pore size distribution	**CEMI W/C 0.4**				**CEMI W/C 0.5**				**CEMI W/C 0.6**			
	Blanc	**RCO2**	**A**	**B**	**Blanc**	**RCO2**	**A**	**B**	**Blanc**	**RCO2**	**A**	**B**
10-50 µm	0.6%	0.9%	0.7%	0.9%	0.8%	0.9%	0.8%	1.4%	0.8%	0.7%	0.9%	1.3%
50nm-10 µm	12.6%	19.9%	5.3%	6.1%	11.0%	9.7%	4.7%	4.9%	10.9%	7.6%	11.7%	4.6%
10-50 nm	7.4%	5.2%	8.4%	7.4%	6.5%	8.0%	8.3%	7.8%	6.4%	6.3%	8.6%	7.3%
2.5-10 nm	0.9%	0.1%	0.9%	1.0%	0.5%	0.8%	0.5%	0.9%	0.5%	0.6%	0.5%	0.9%
Total porosity	**21.5%**	**26.1%**	**15.3%**	**15.3%**	**18.9%**	**19.4%**	**14.3%**	**15.1%**	**18.6%**	**15.2%**	**21.7%**	**14.0%**
	CEMIII W/C 0.4				**CEMIII W/C 0.5**				**CEMIII W/C 0.6**			
	Blanc	**RCO2**	**A**	**B**	**Blanc**	**RCO2**	**A**	**B**	**Blanc**	**RCO2**	**A**	**B**
10-50 µm	1.0%	0.7%	0.7%	1.1%	0.8%	1.1%	1.1%	1.5%	5.8%	1.3%	1.1%	0.7%
50nm-10 µm	11.7%	14.7%	6.5%	11.9%	15.4%	19.5%	4.3%	19.7%	39.5%	23.3%	5.5%	17.6%
10-50 nm	7.1%	10.3%	10.6%	6.3%	11.1%	19.6%	25.2%	11.3%	12.9%	32.6%	12.8%	6.9%
2.5-10 nm	2.4%	1.1%	1.5%	0.6%	1.1%	6.7%	0.2%	1.4%	0.5%	6.4%	0.8%	0.2%
Total porosity	**22.2%**	**26.8%**	**19.3%**	**19.8%**	**28.5%**	**47.0%**	**30.8%**	**33.8%**	**58.7%**	**63.5%**	**20.2%**	**25.5%**
	SP MIX W/C 0.4				**SP MIX W/C 0.5**				**SP MIX W/C 0.6**			
	Blanc	**RCO2**	**A**	**B**	**Blanc**	**RCO2**	**A**	**B**	**Blanc**	**RCO2**	**A**	**B**
10-50 µm	1.7%	1.3%	0.8%	0.7%	0.7%	0.7%	1.0%	1.2%	0.8%	1.0%	0.5%	1.5%
50nm-10 µm	15.3%	29.0%	5.1%	16.5%	3.1%	8.4%	4.5%	8.9%	12.2%	28.2%	6.1%	24.8%
10-50 nm	24.2%	15.6%	13.7%	7.4%	12.2%	7.7%	8.8%	5.7%	17.7%	7.7%	14.8%	5.1%
2.5-10 nm	4.1%	1.8%	0.8%	0.8%	2.3%	1.1%	1.7%	1.0%	3.3%	1.4%	14.9%	0.5%
Total porosity	**45.3%**	**47.7%**	**20.3%**	**25.4%**	**18.3%**	**17.9%**	**16.0%**	**16.7%**	**34.0%**	**38.4%**	**36.3%**	**31.9%**

1.16 Relation between total porosity and capillary porosity for the same type of cement with different W/C ratio and treatment

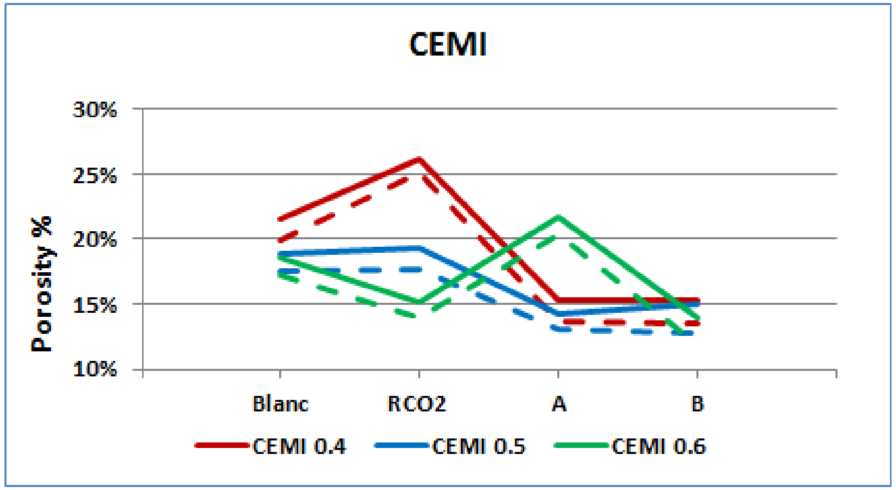

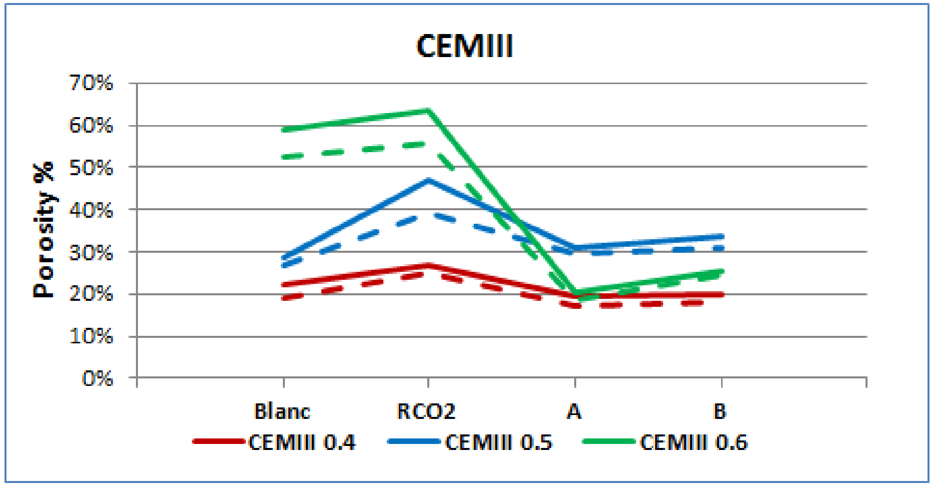

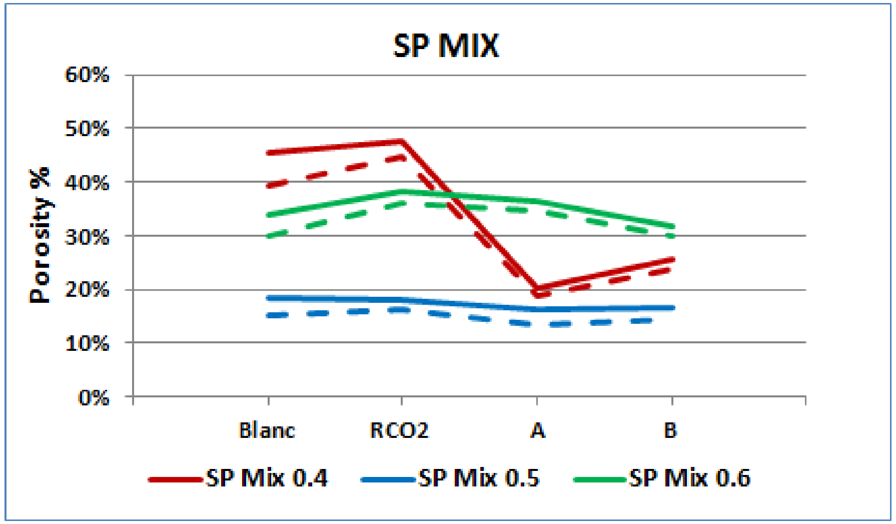

Capillary porosity (10nm-10µm) ----------
Total porosity ______

1.17 Relation between total porosity and capillary porosity for each type of cement with the same W/C ratio and different treatment

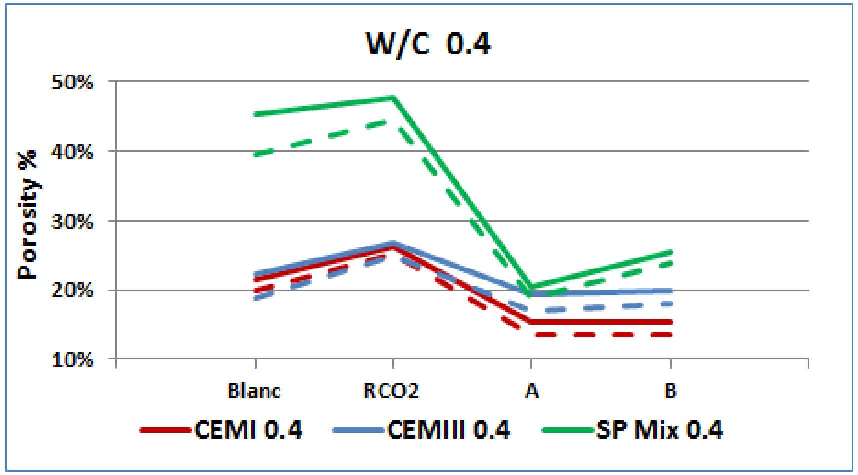

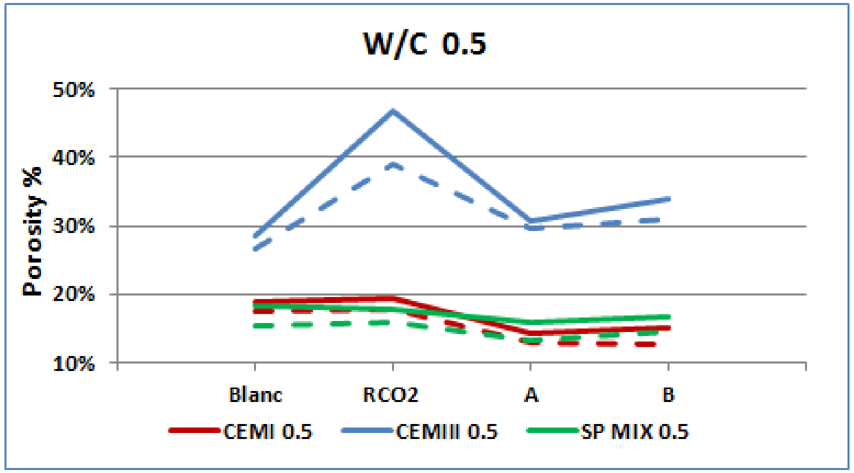

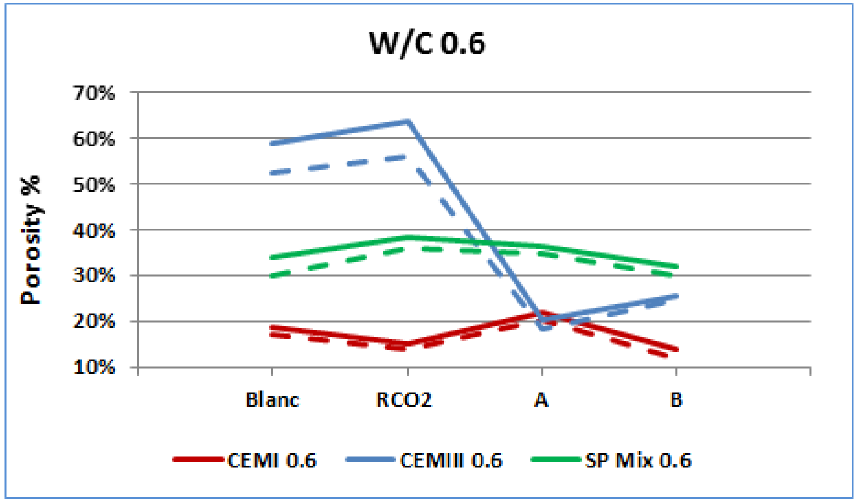

Capillary porosity (10nm-10µm) ---------
Total porosity ———

5. Appendix: Thermalgravimetric analysis/Differential Scanning Calorimetry (TGA/DSC)

1.18 Cement paste mixed with CEM I and different water- cement ratio

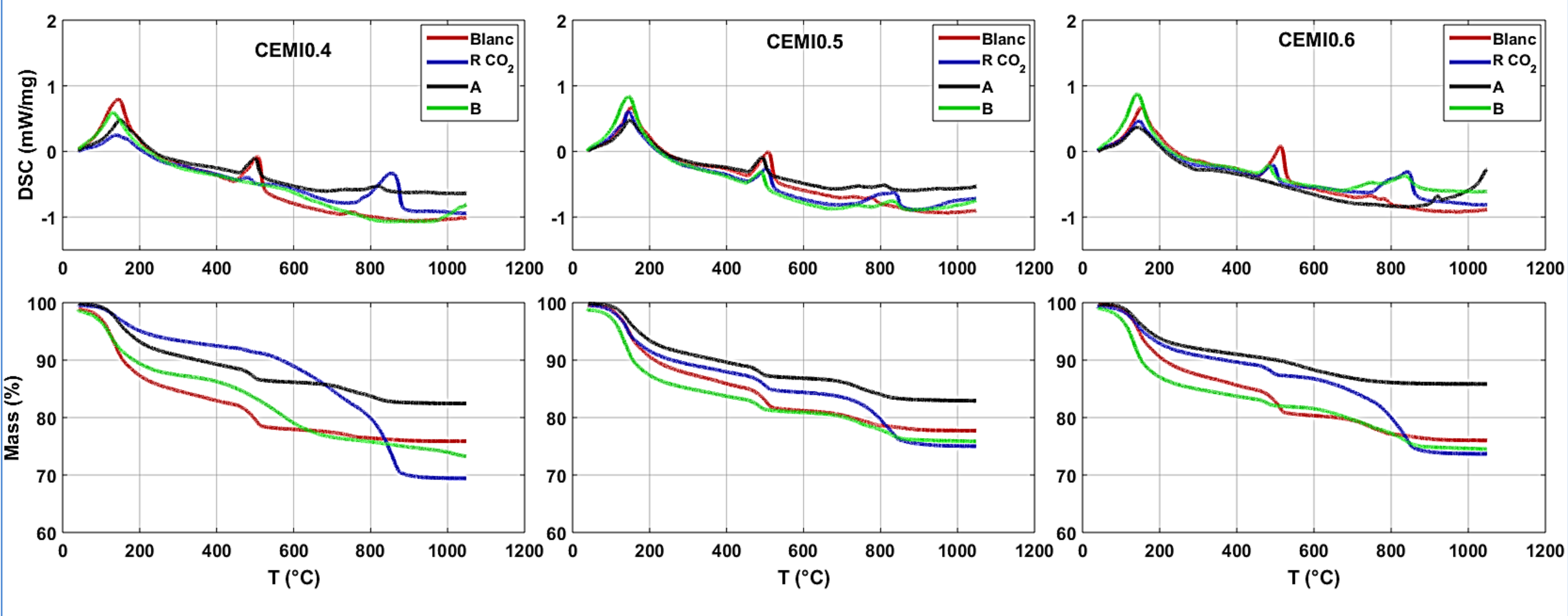

1.19 Cement paste mixed with CEM III and different water- cement ratio

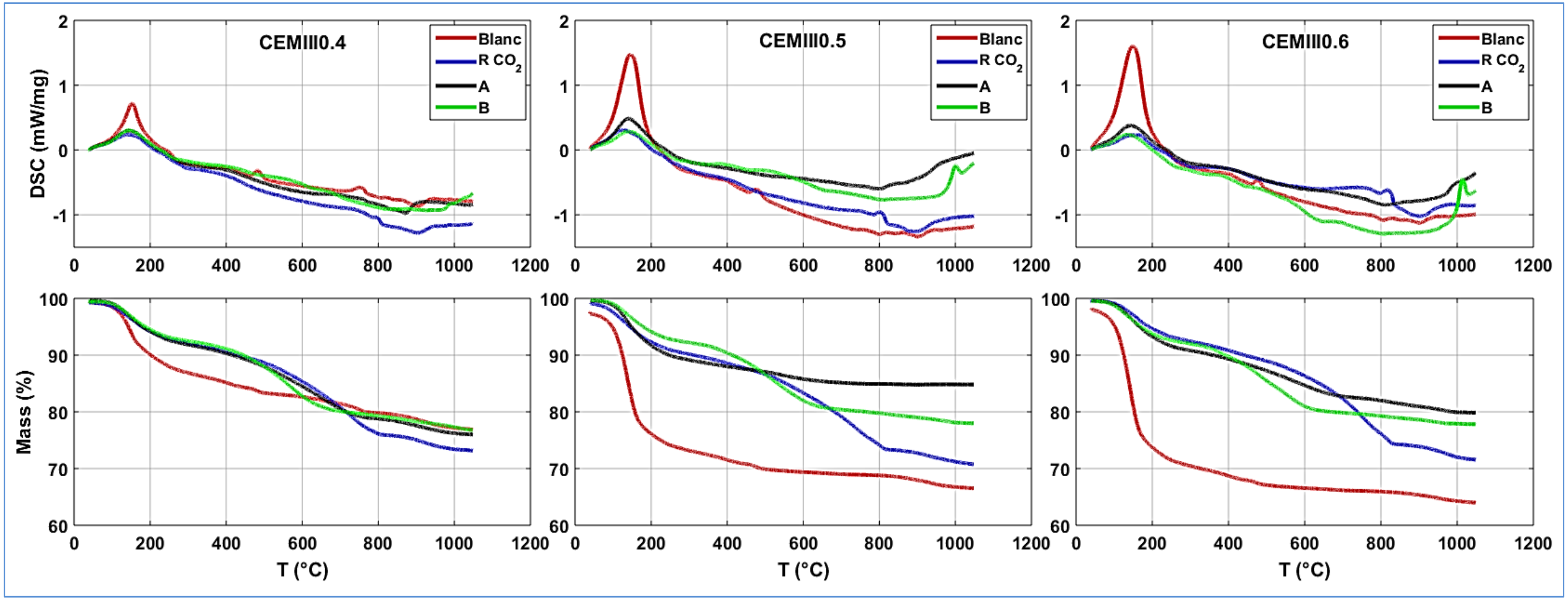

1.20 Cement paste mixed with SP MIX and different water- cement ratio

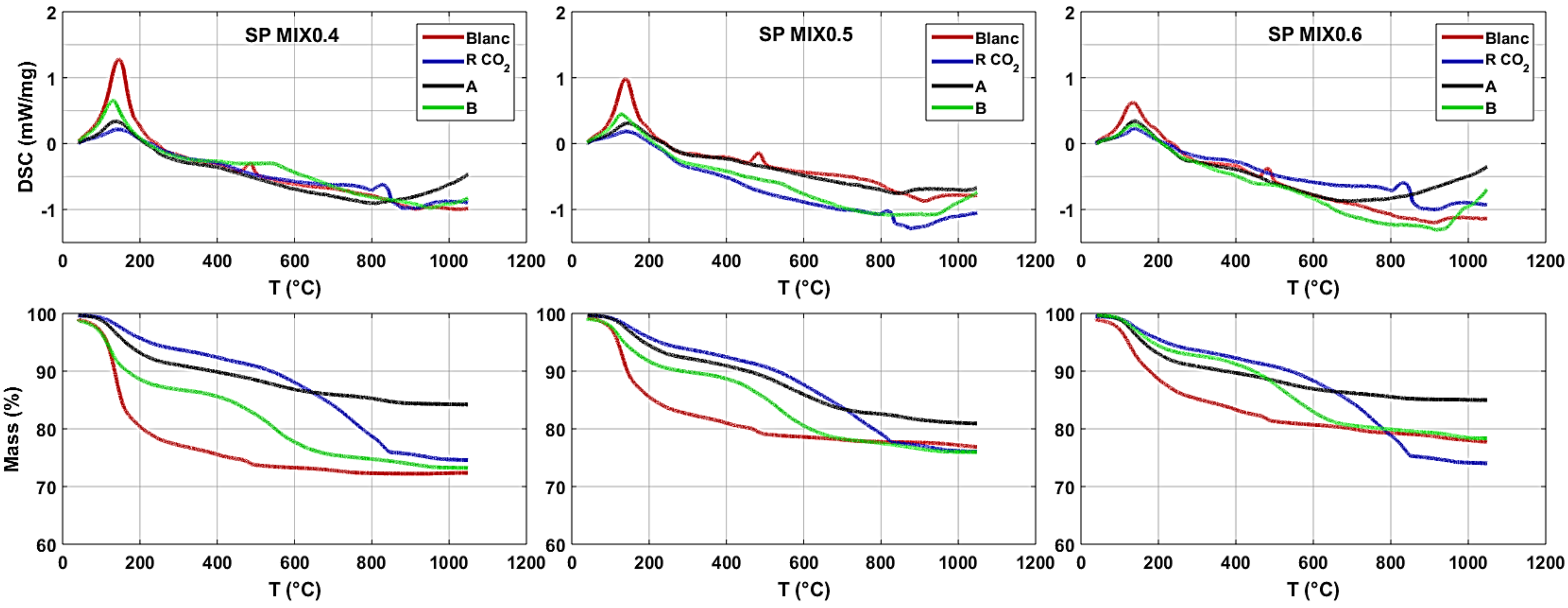

1.21 Analyzing data from TGA/DSC Test: onset points and mass changes

CEM I W/C 0.4

R: Blanc

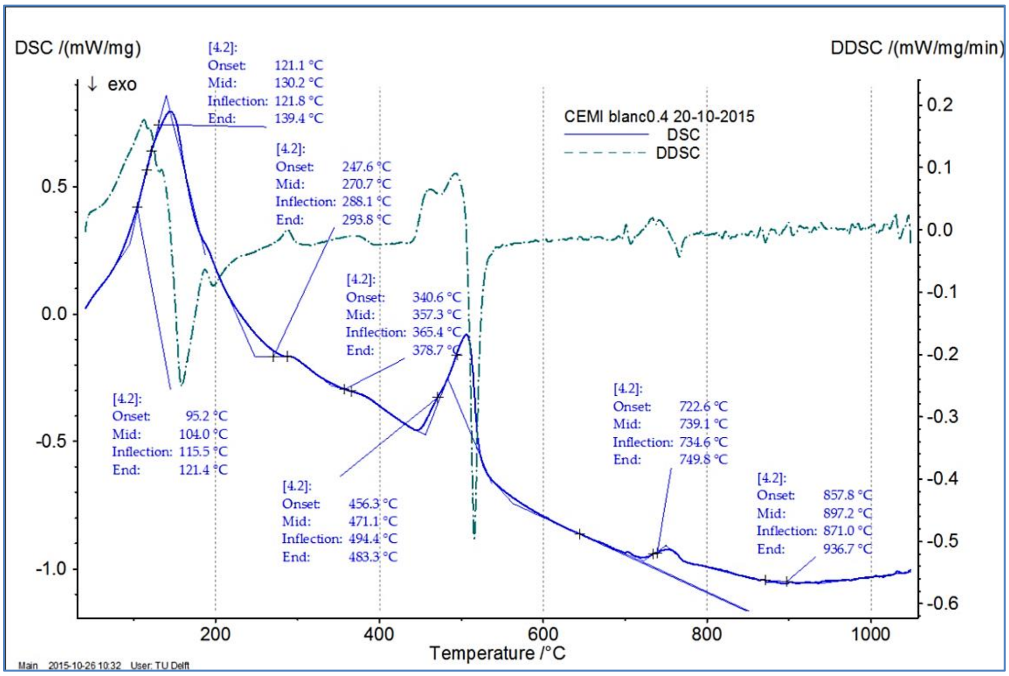

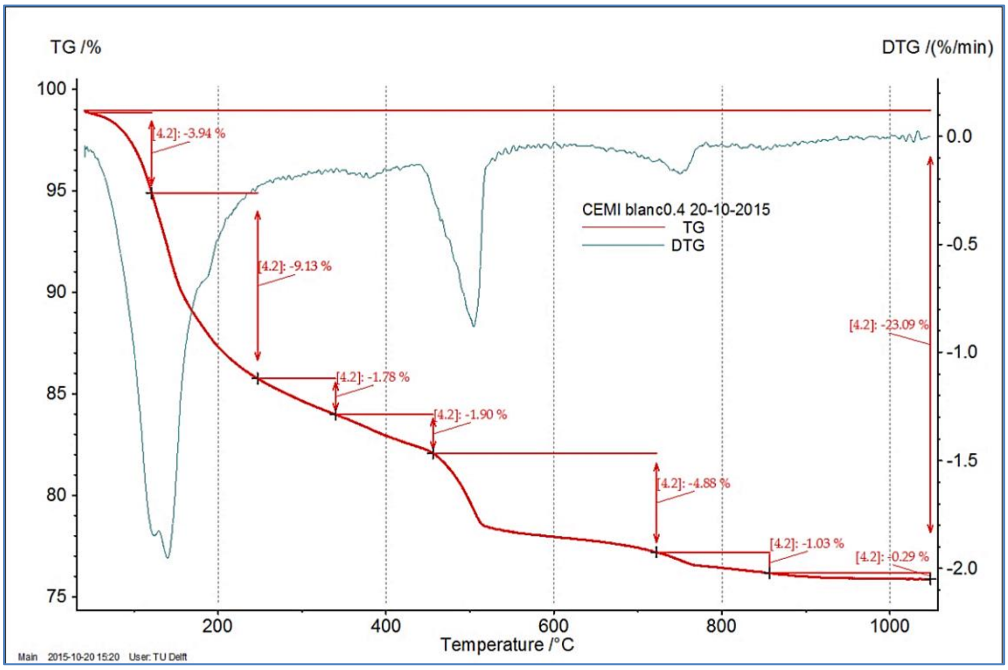

CEM I W/C 0.4

R1CO2: RCT28d

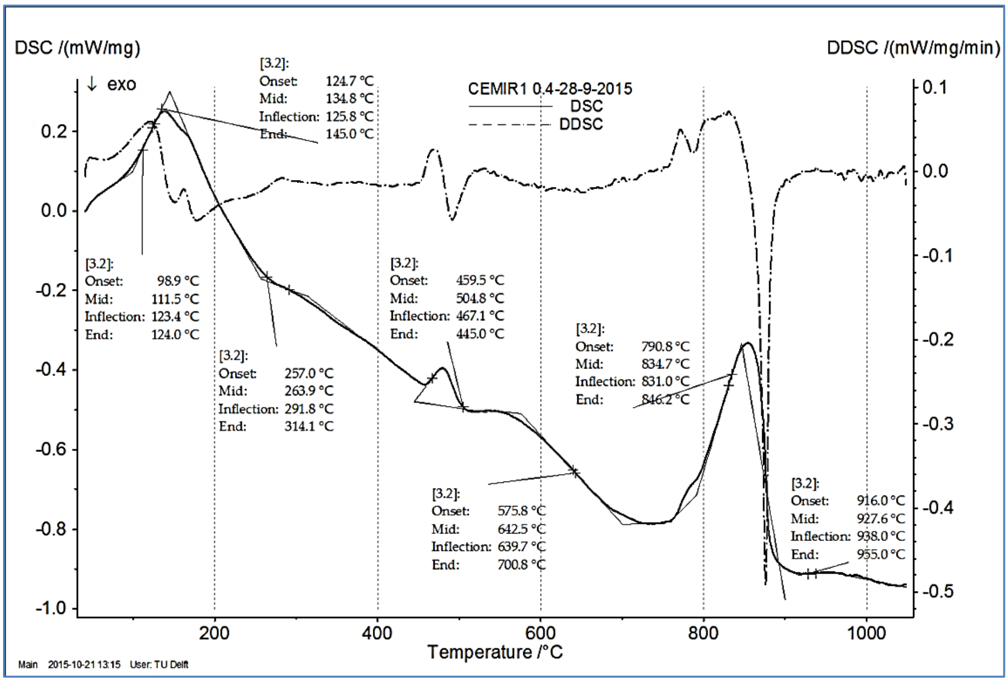

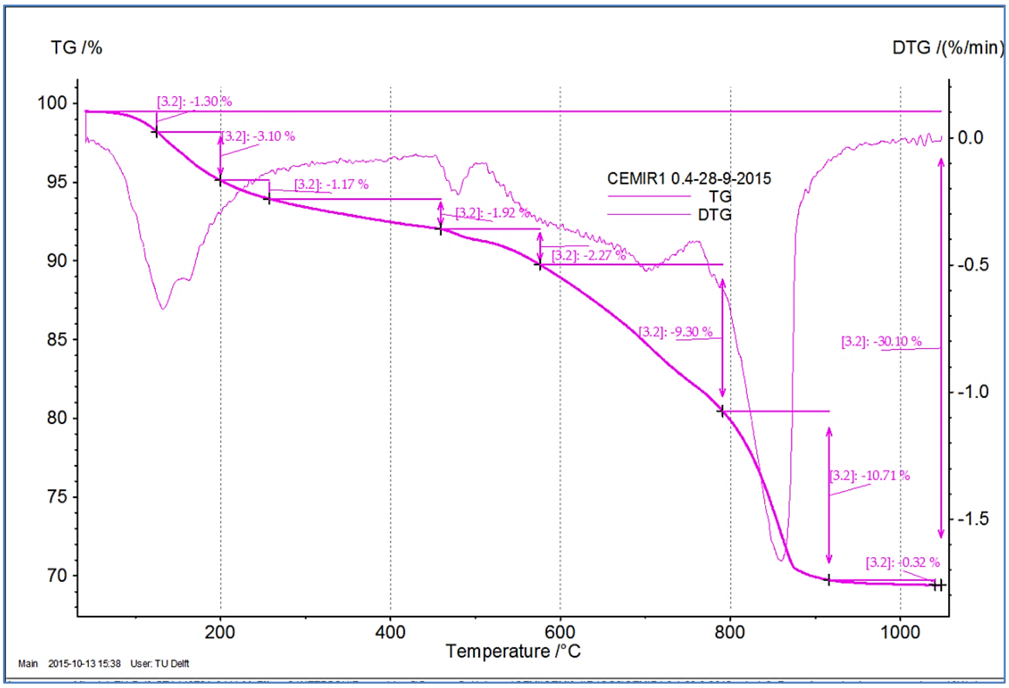

CEM I W/C 0.4

A: Na-MFP → RCT28d

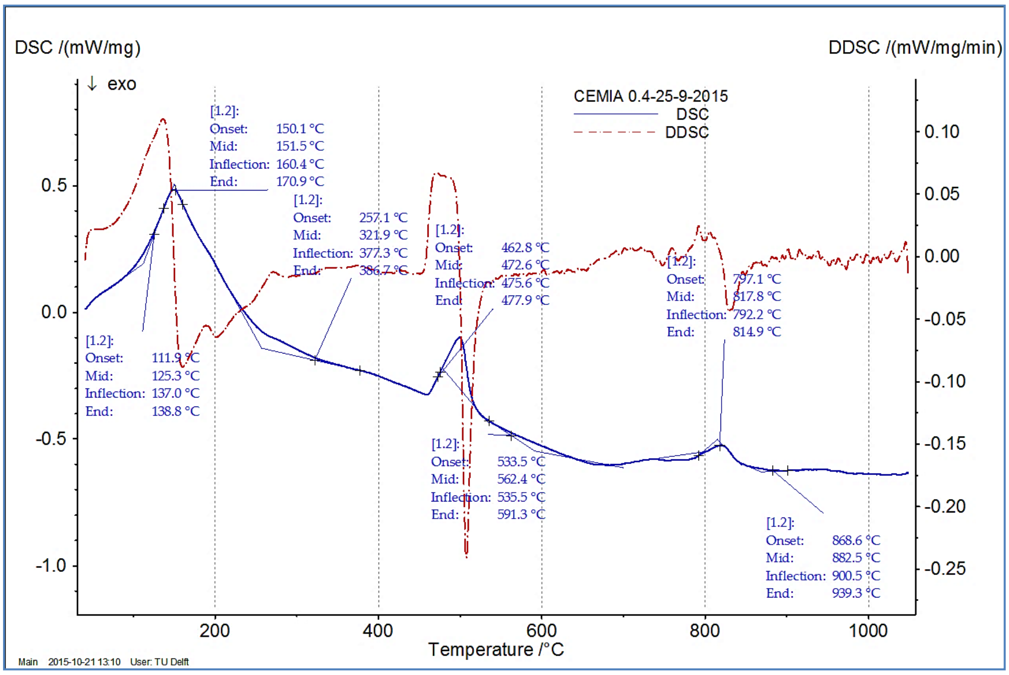

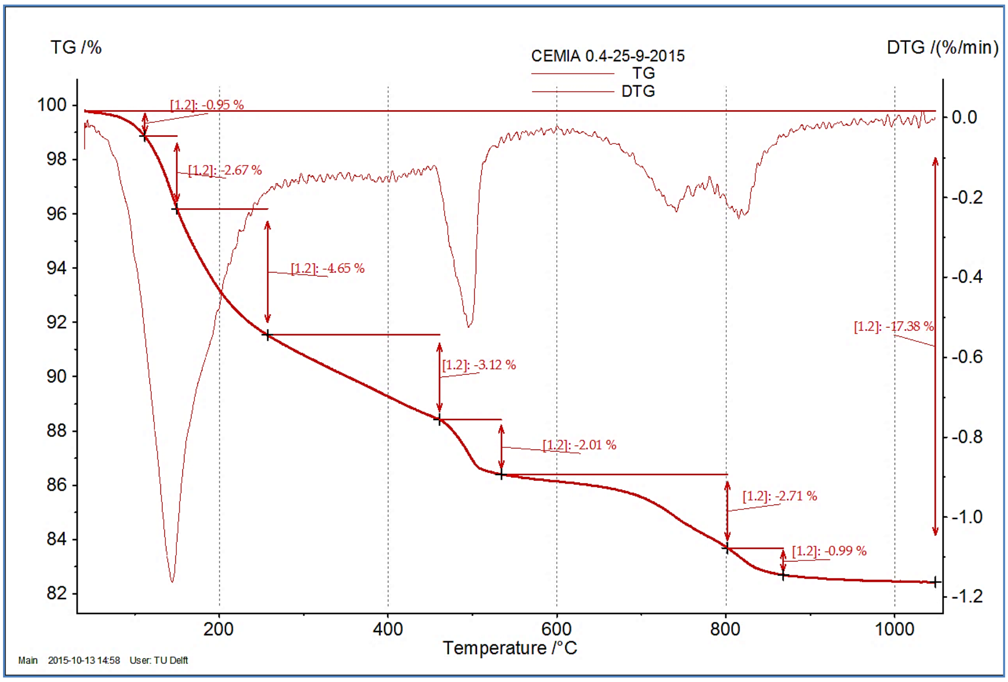

CEM I W/C 0.4

B: RCT28d →Na-MFP

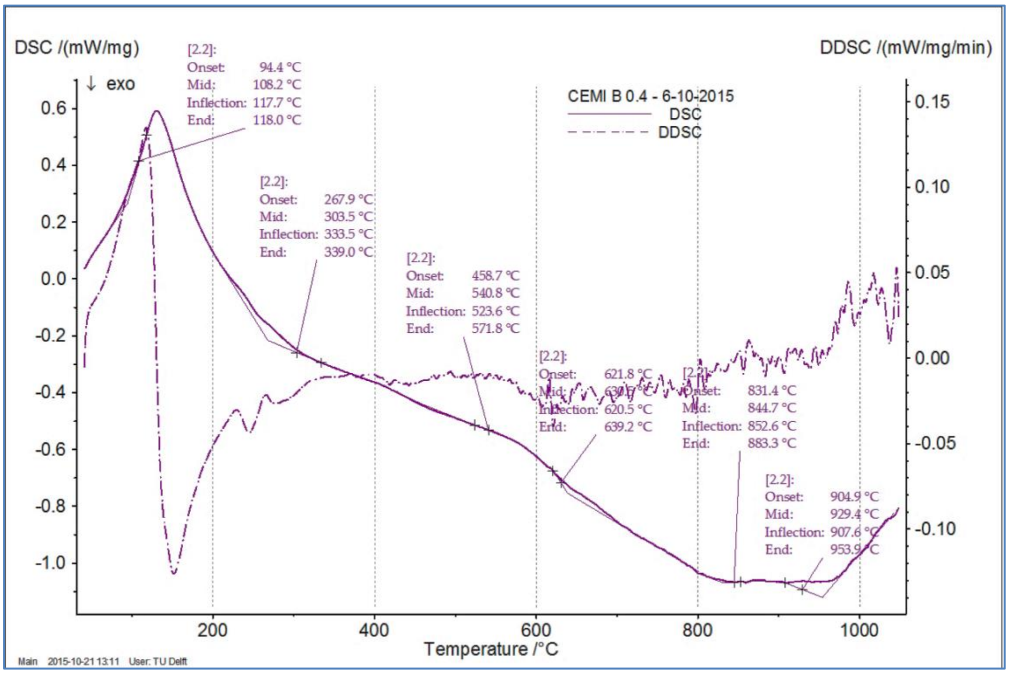

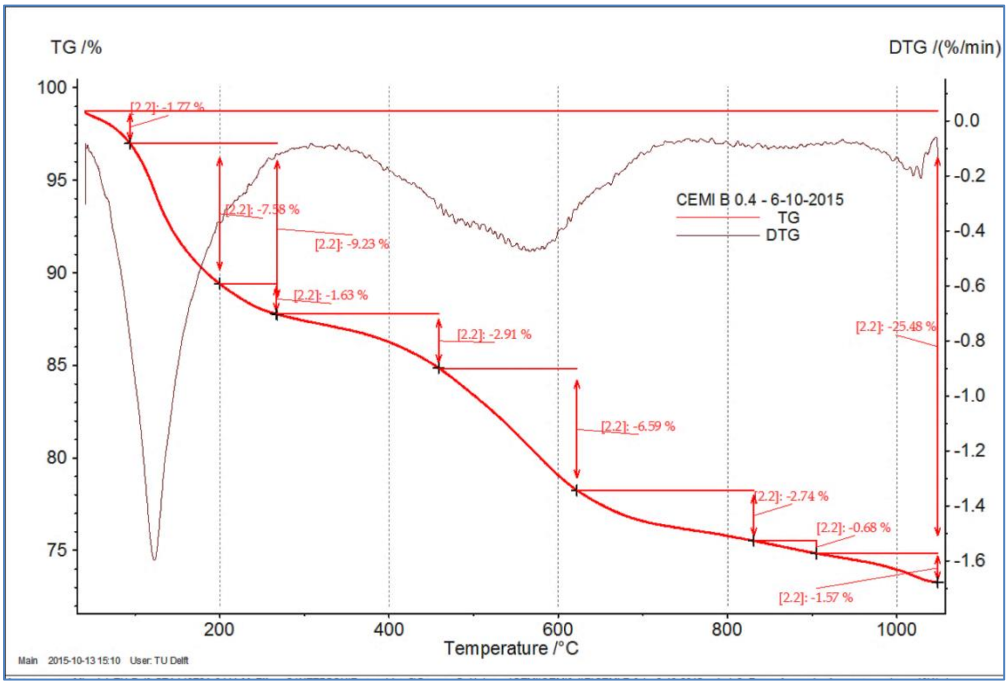

CEM I W/C 0.5

R: Blanc

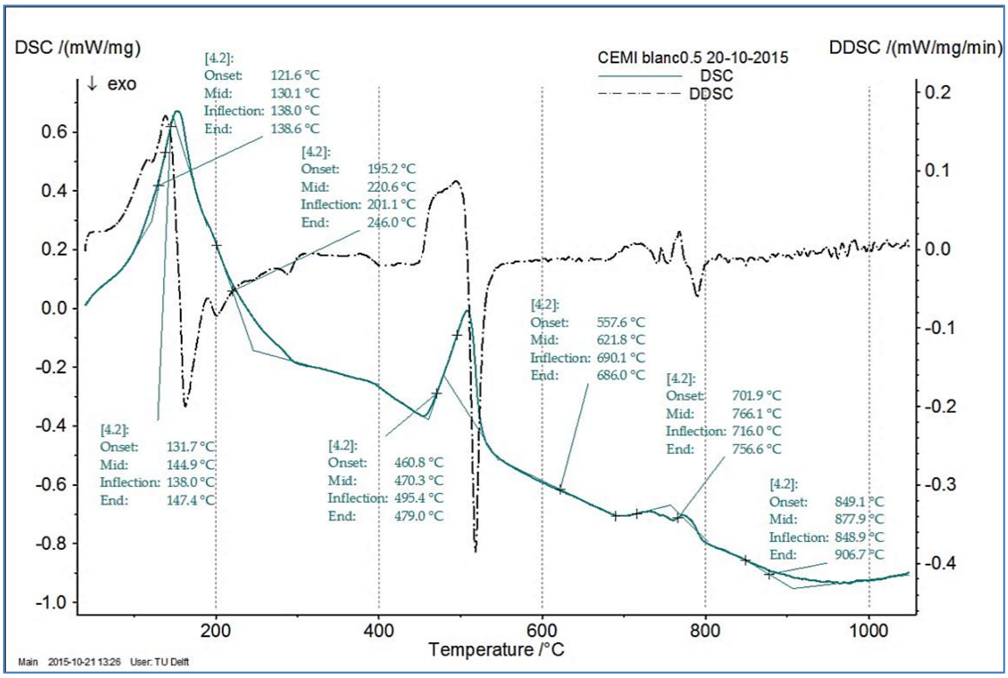

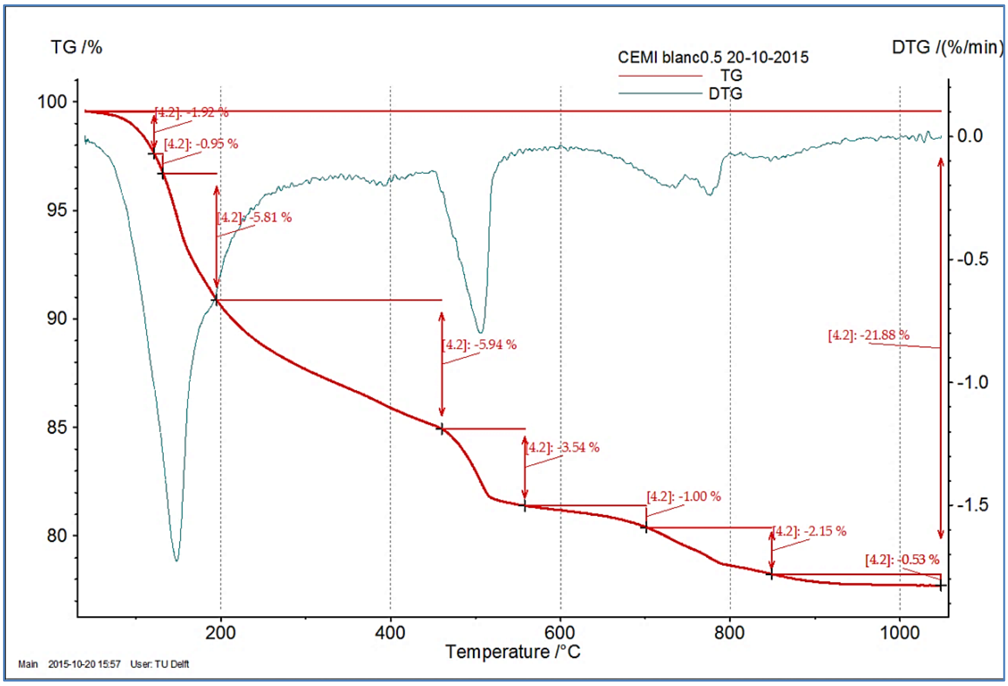

CEM I W/C 0.5

R1CO2: RCT28d

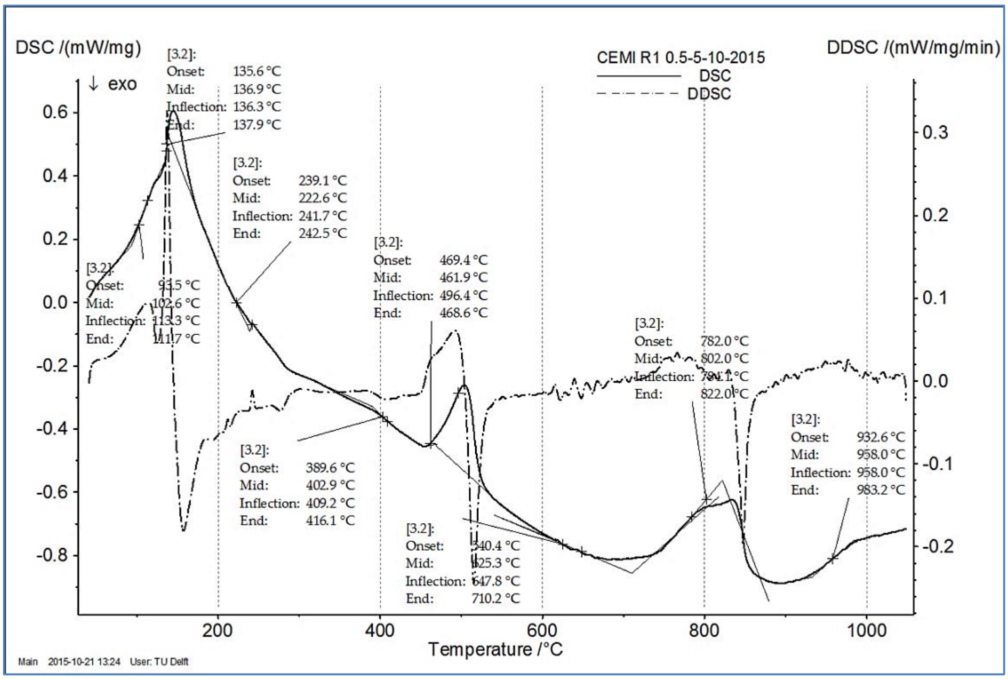

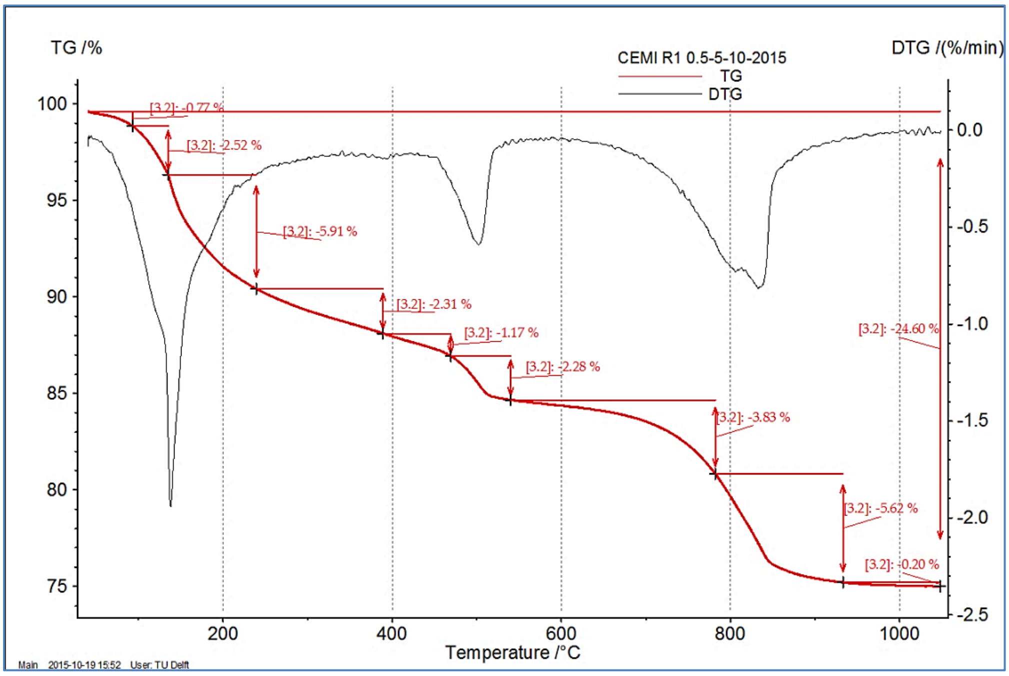

CEM I W/C 0.5

A: Na-MFP → RCT28d

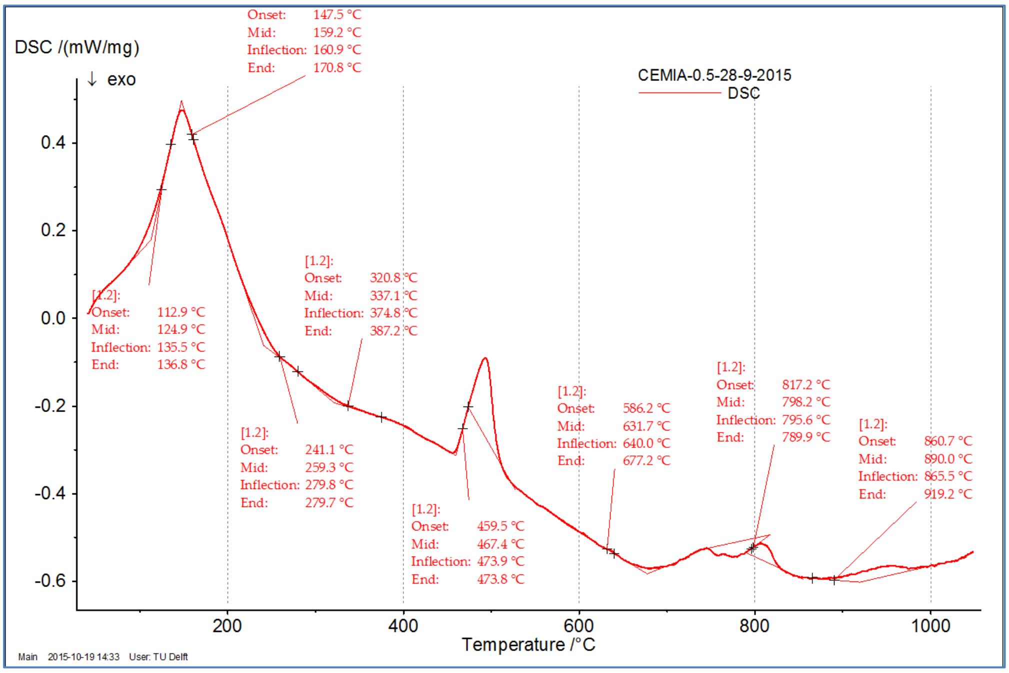

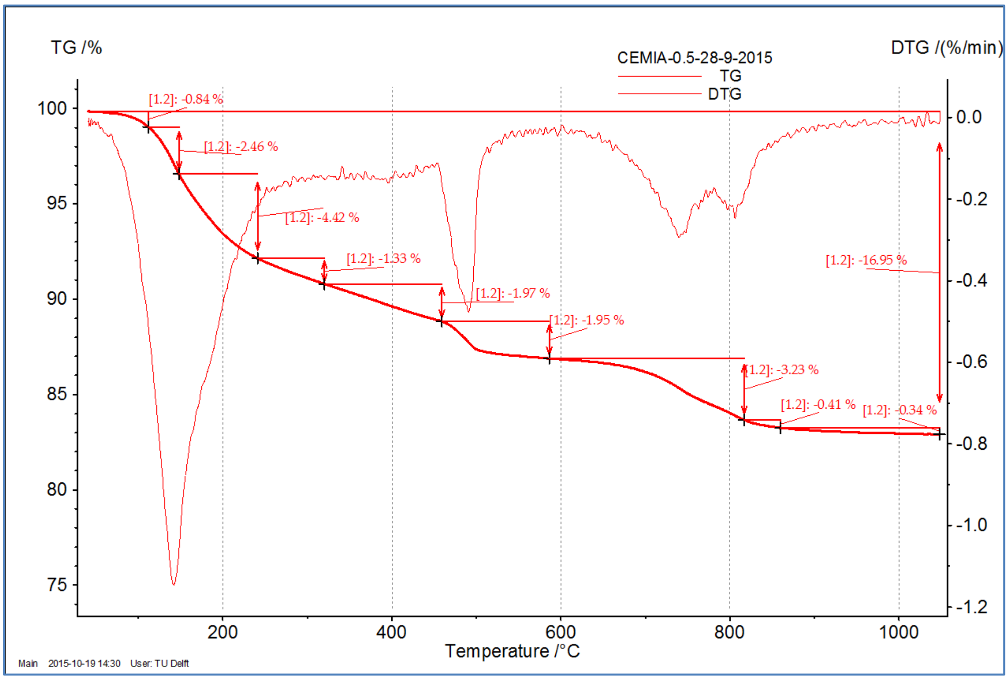

CEM I W/C 0.5

B: RCT28d → Na-MFP

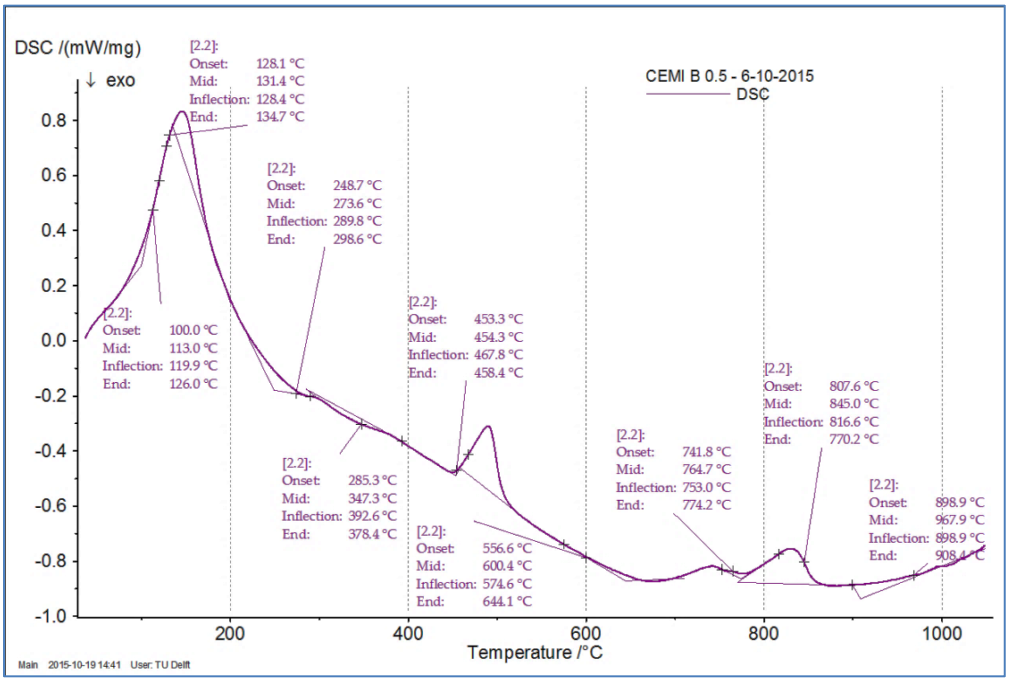

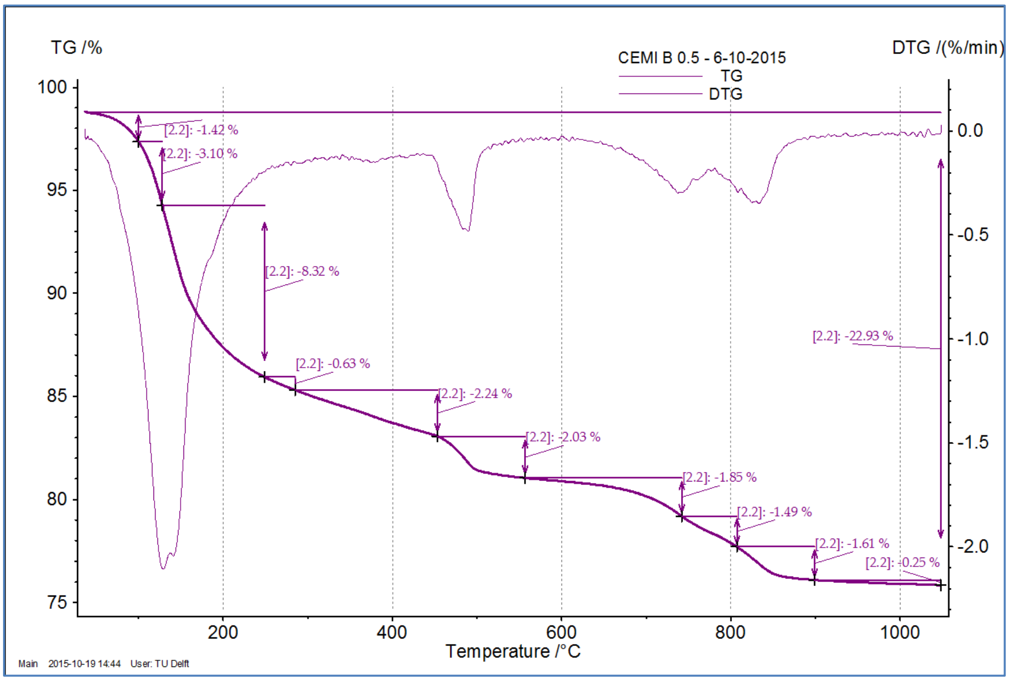

CEM I W/C 0.6

<u>R: Blanc</u>

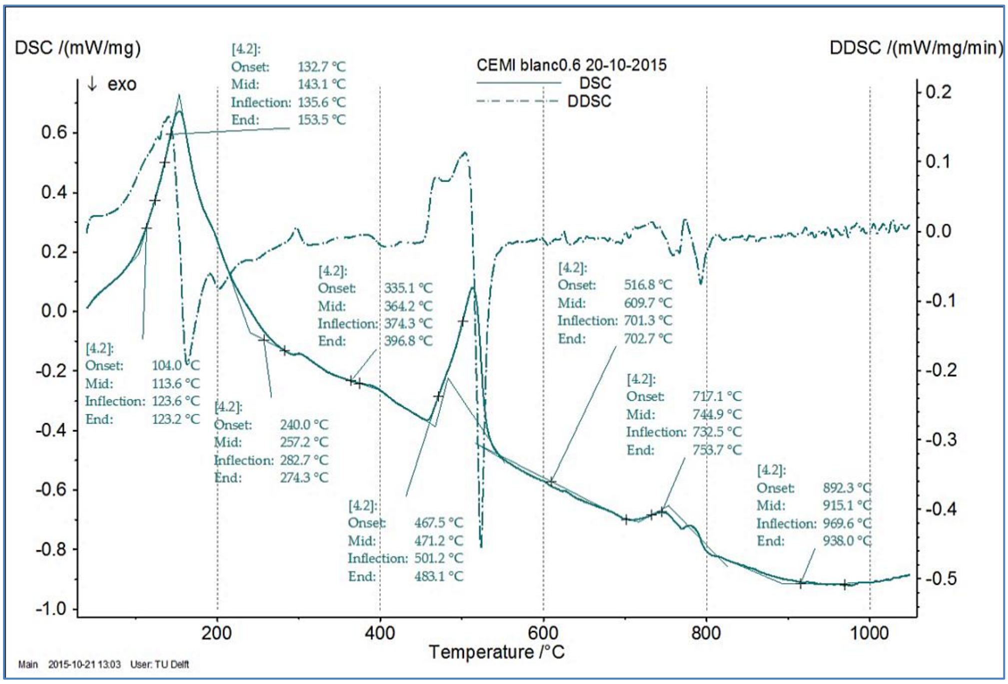

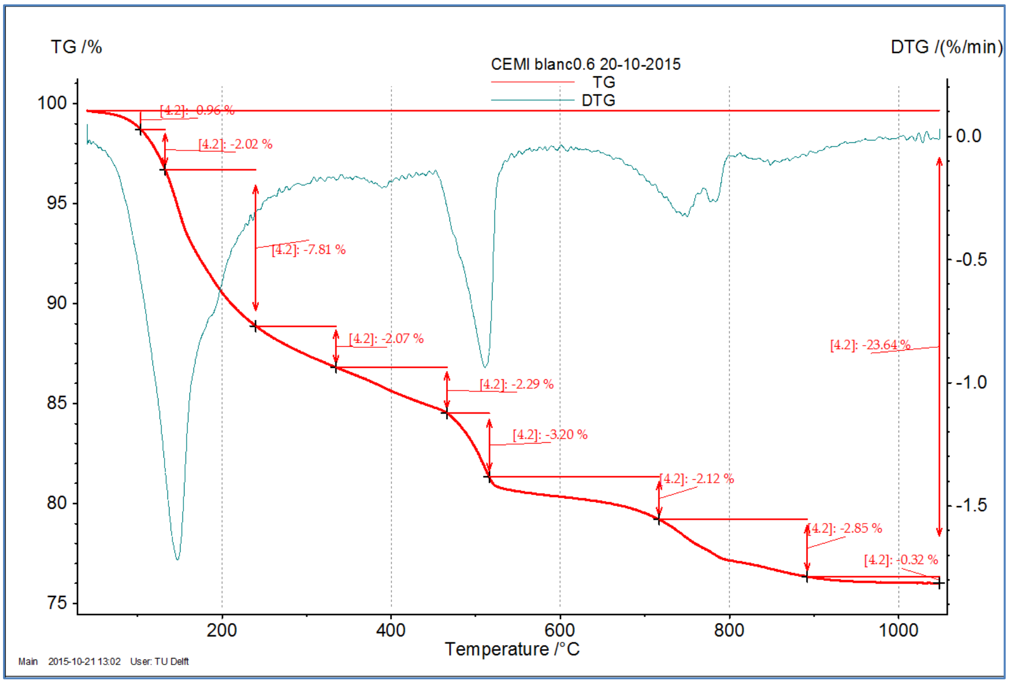

CEM I W/C 0.6

R1CO$_2$: RCT$_{28d}$

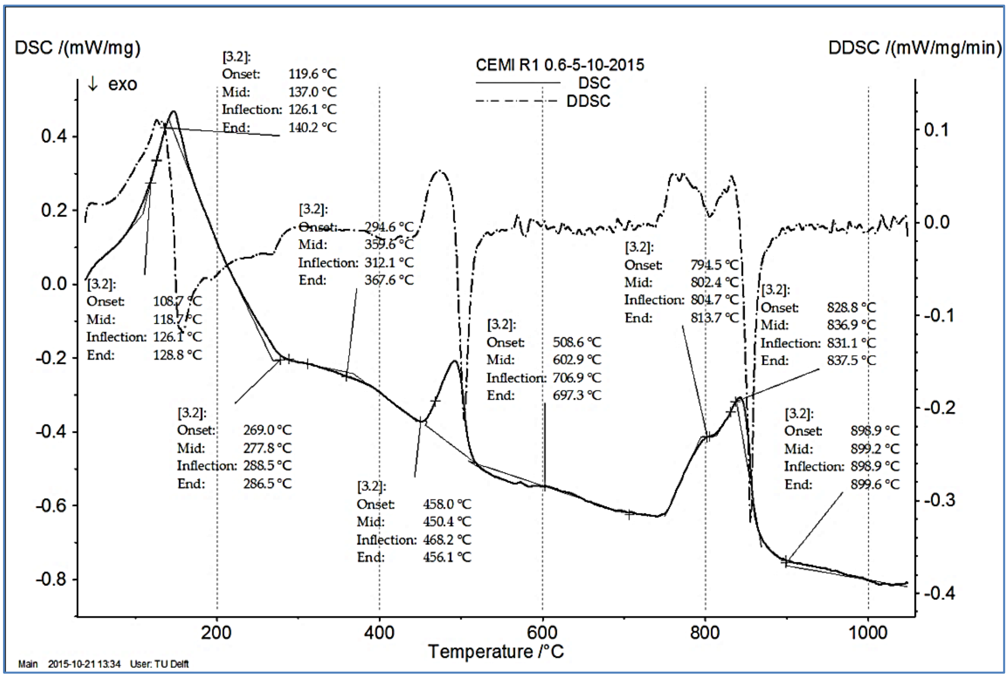

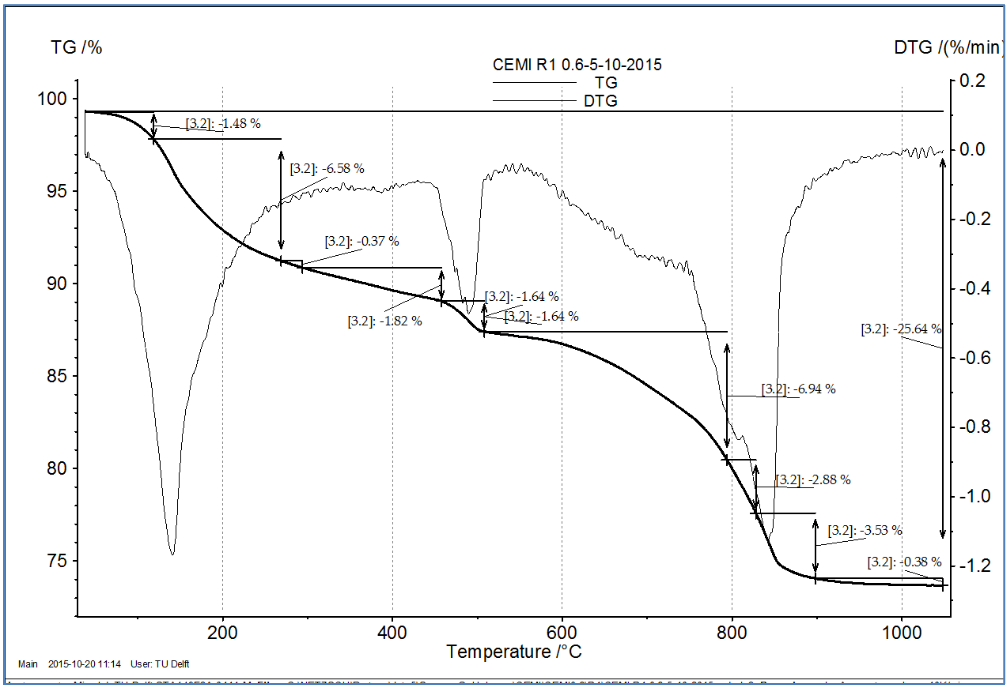

CEM I W/C 0.6

A: Na-MFP→RCT28d

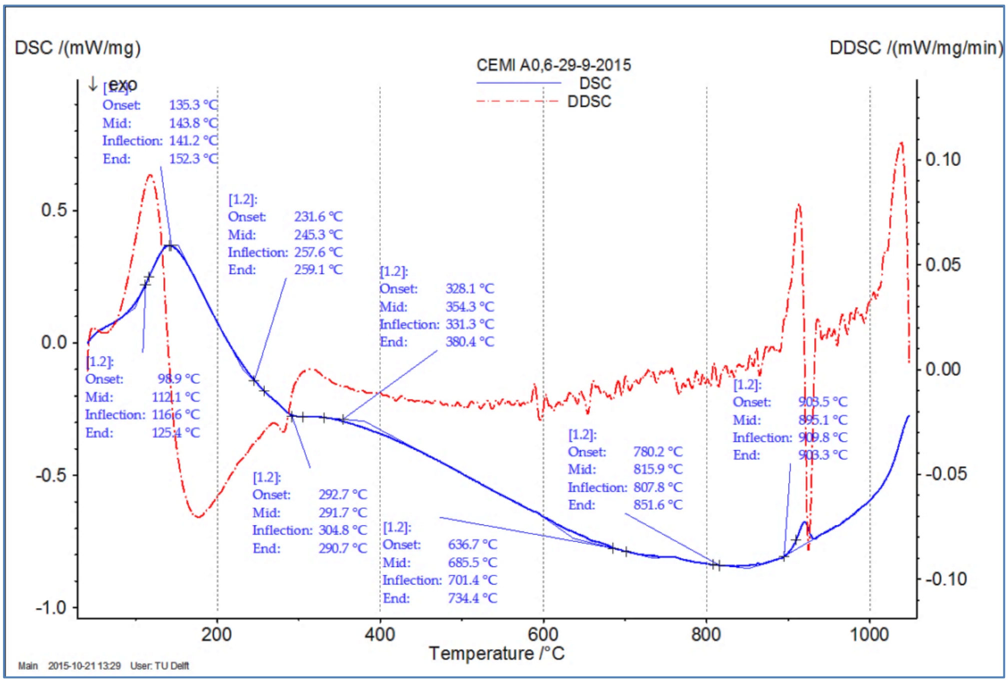

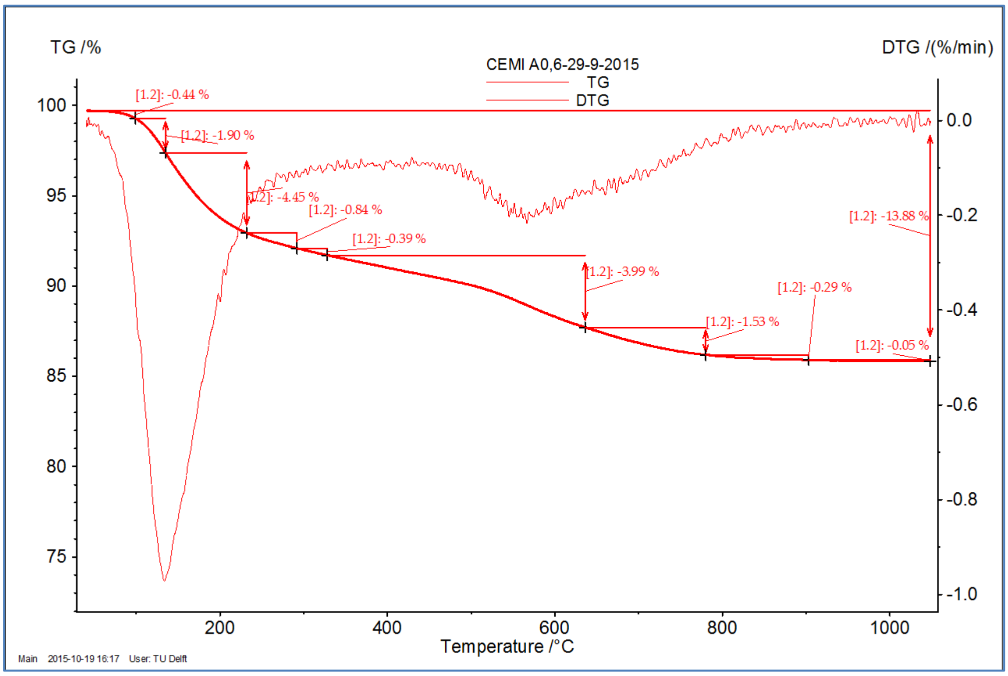

CEM I W/C 0.6

B: RCT28d → Na-MFP

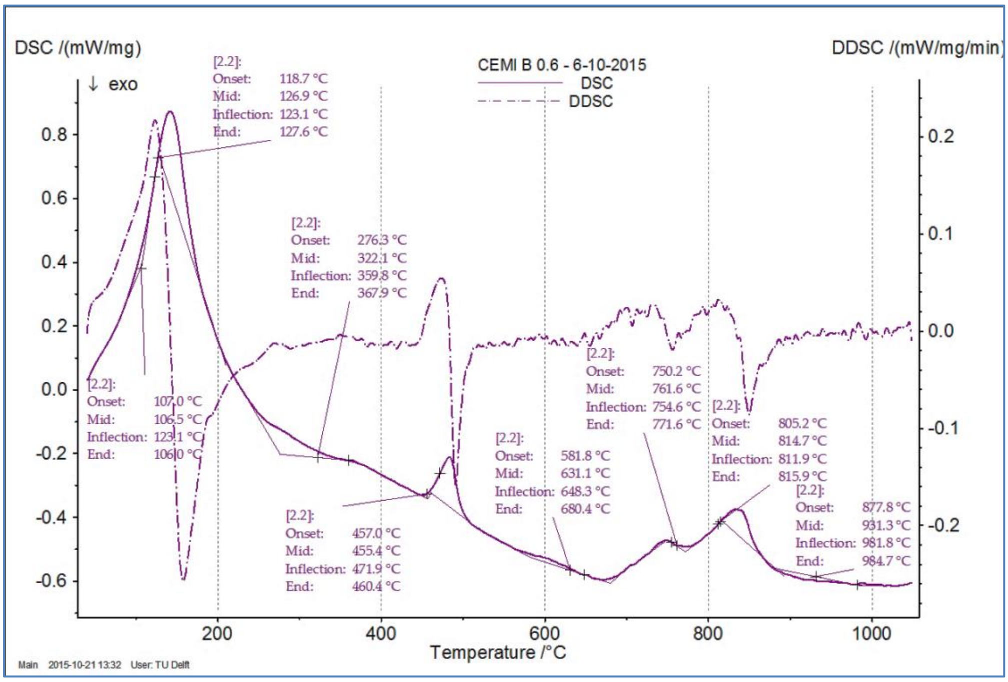

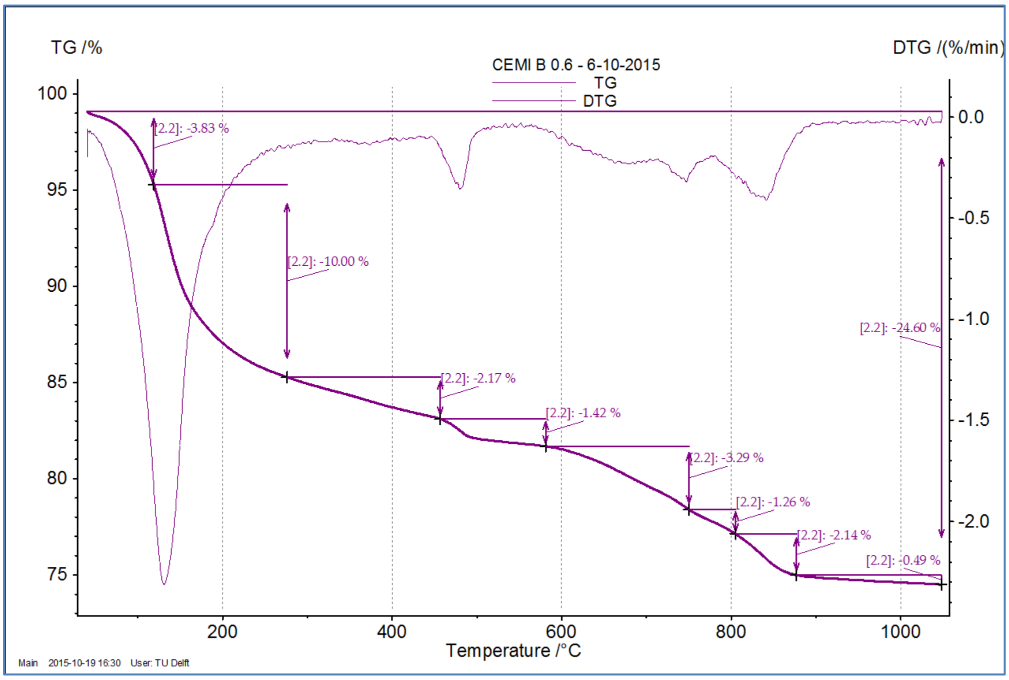

CEM III W/C 0.4

R: Blanc

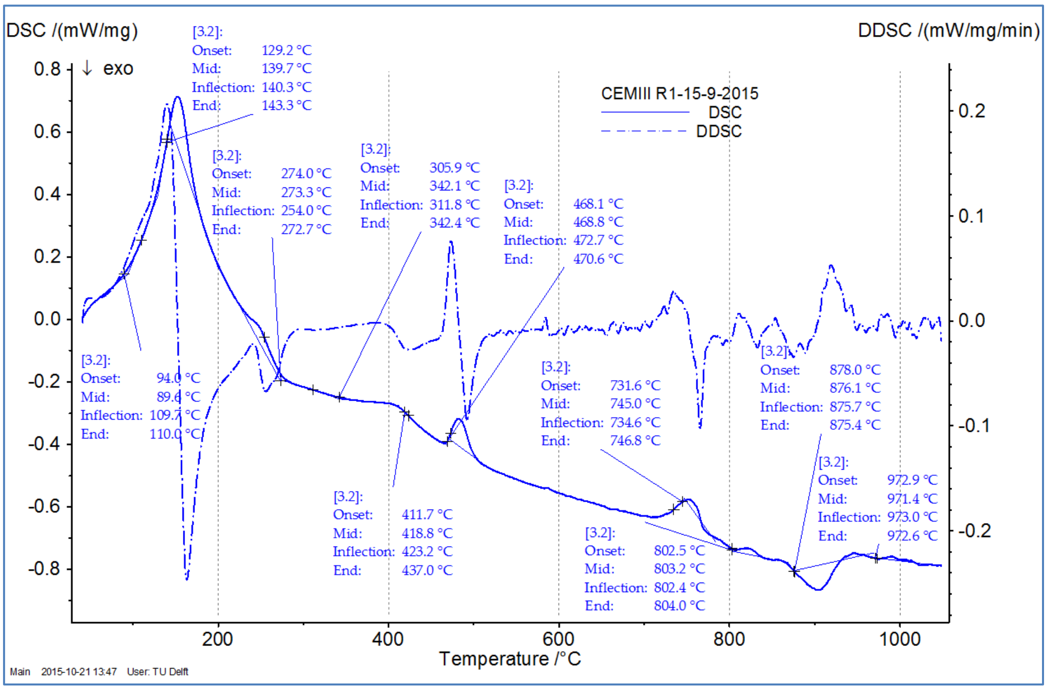

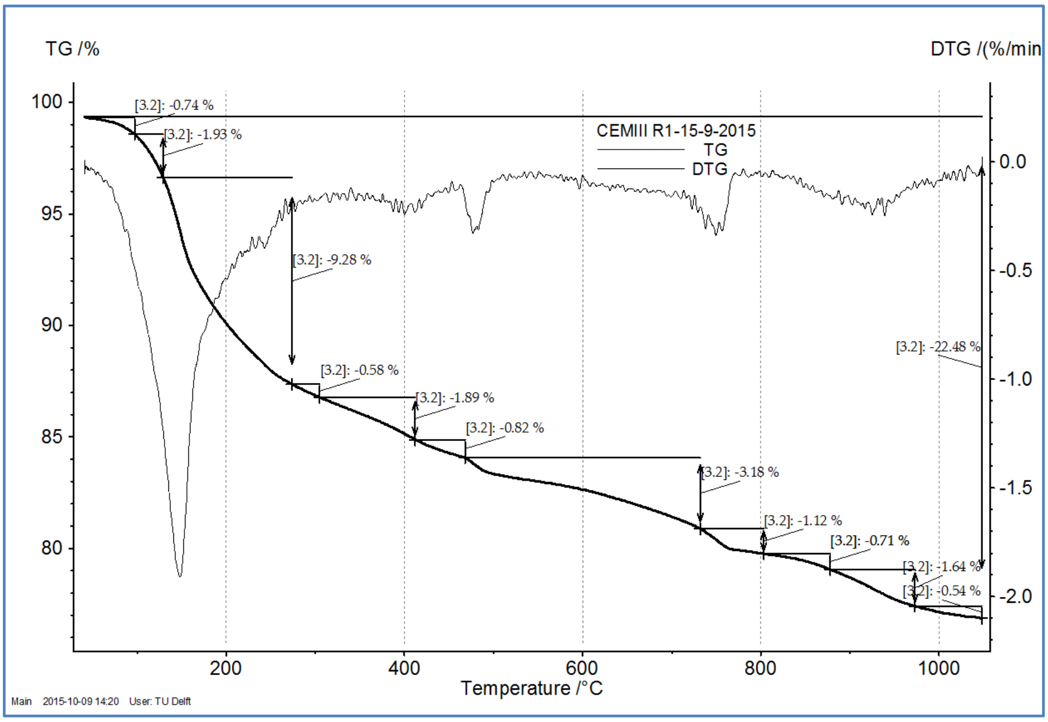

CEM III W/C 0.4

R1CO$_2$: RCT$_{28d}$

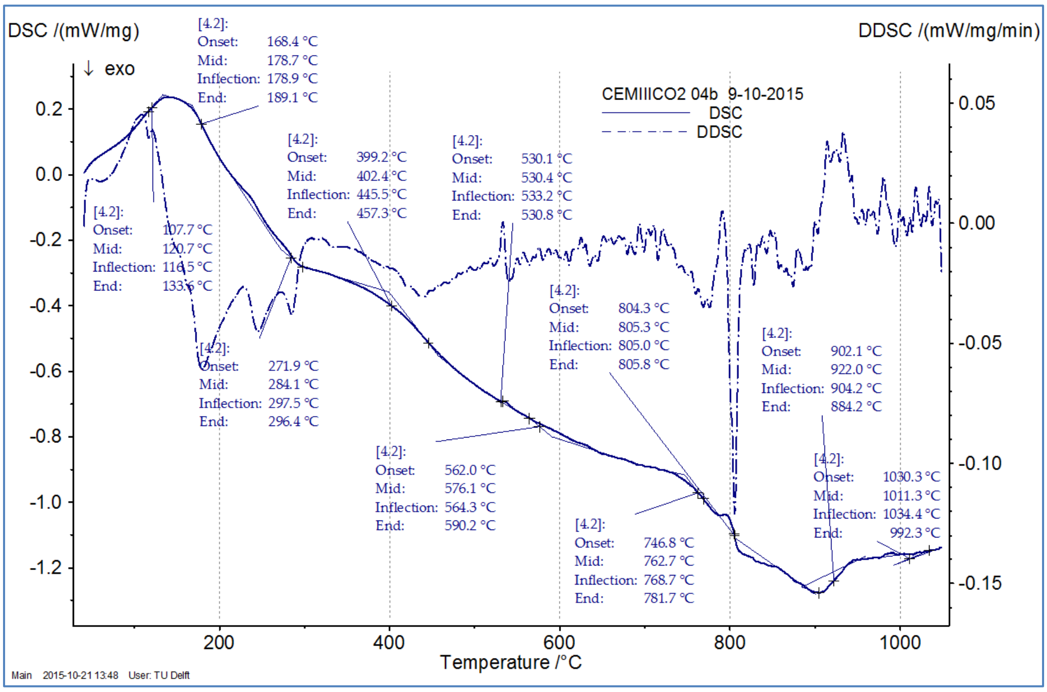

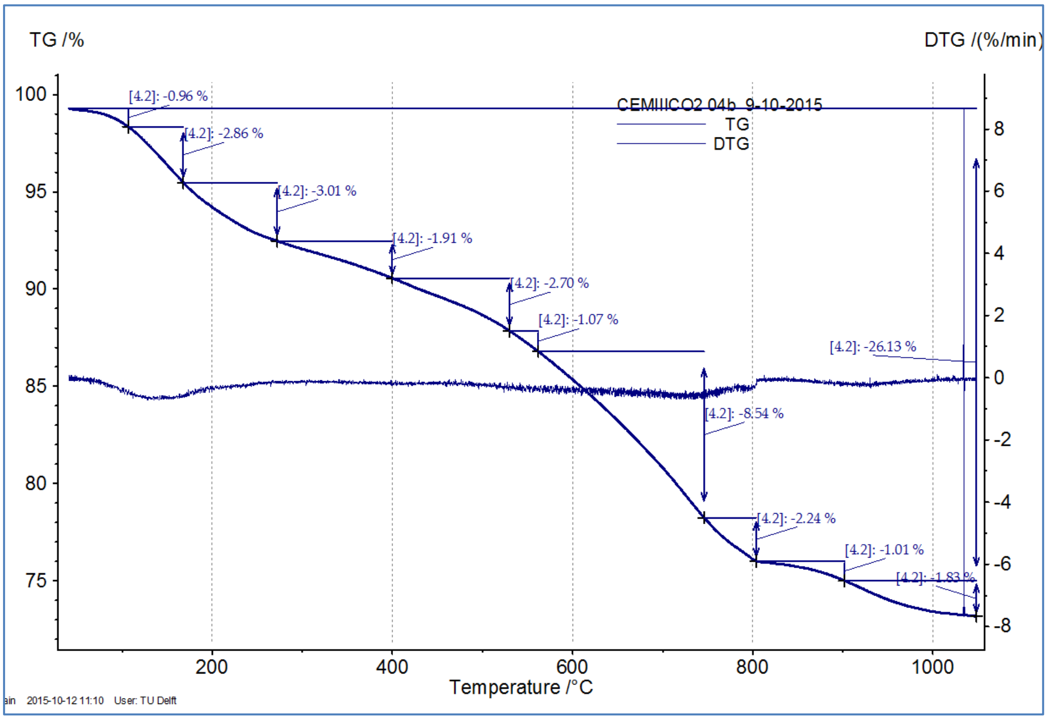

CEM III W/C 0.4

A: Na-MFP → RCT28d

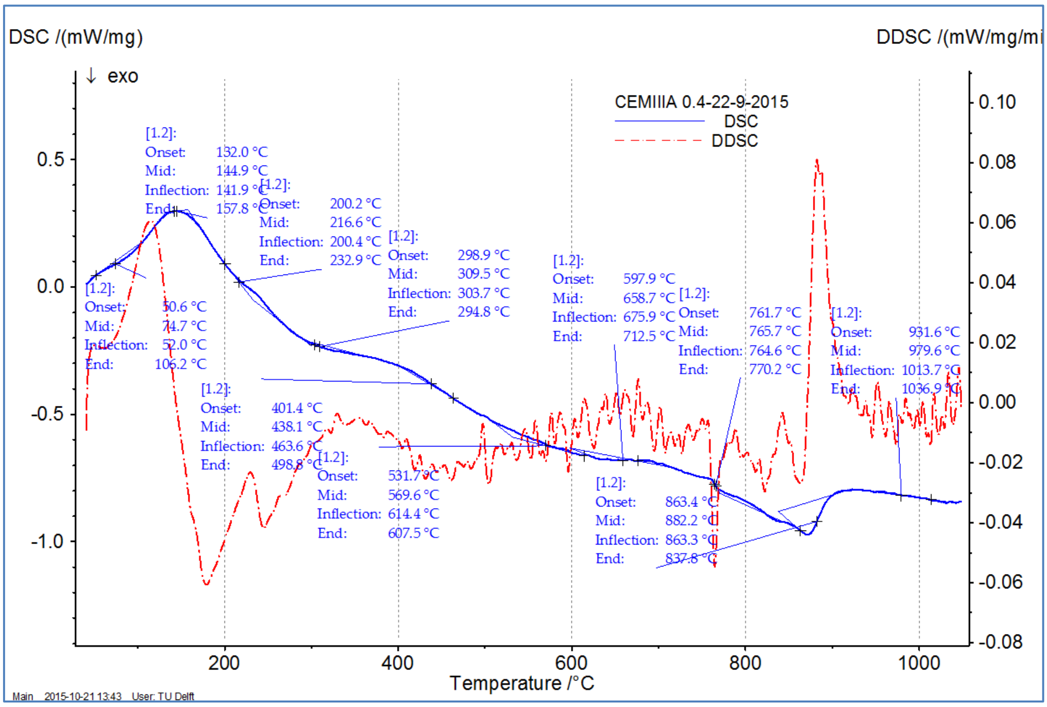

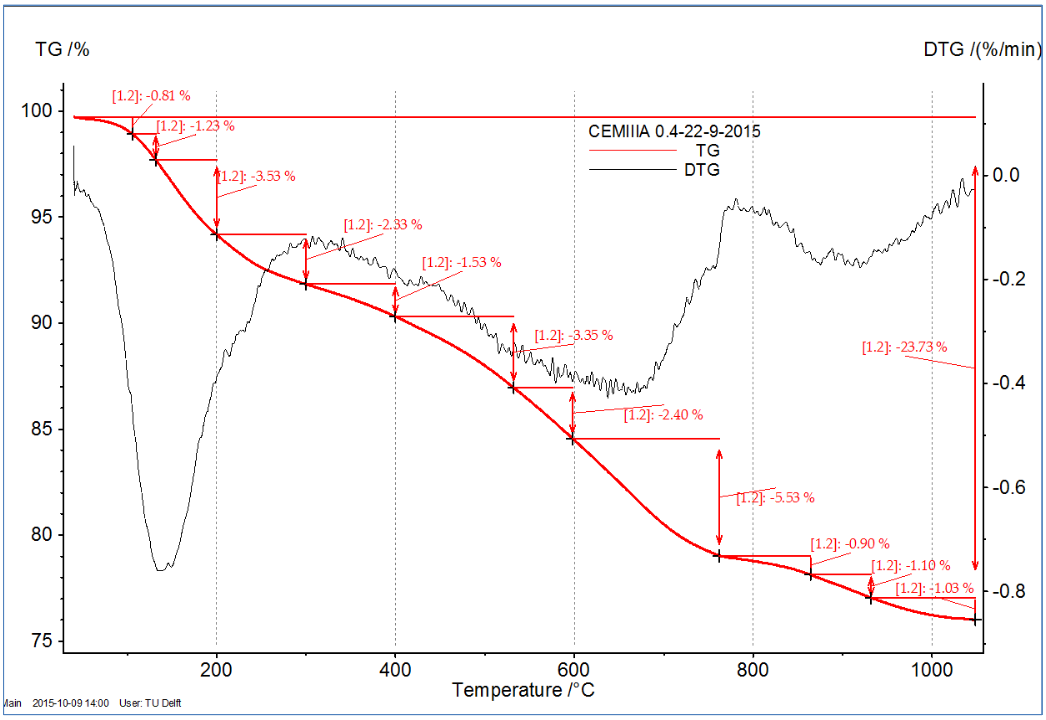

CEM III W/C 0.4

B: RCT28d → Na-MFP

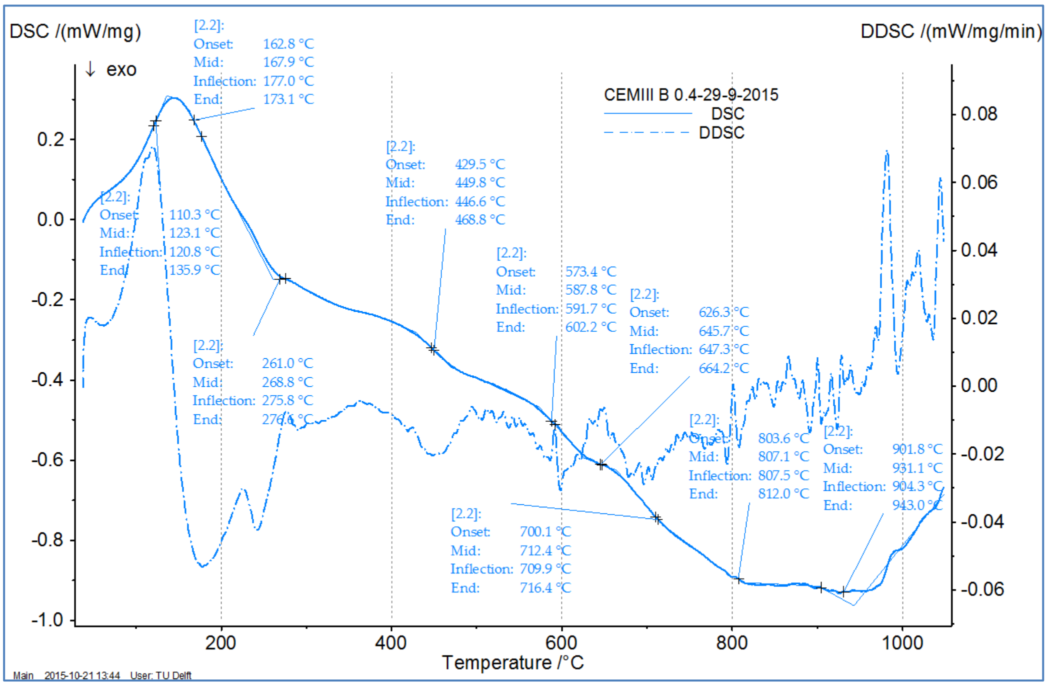

2.
3.
4.

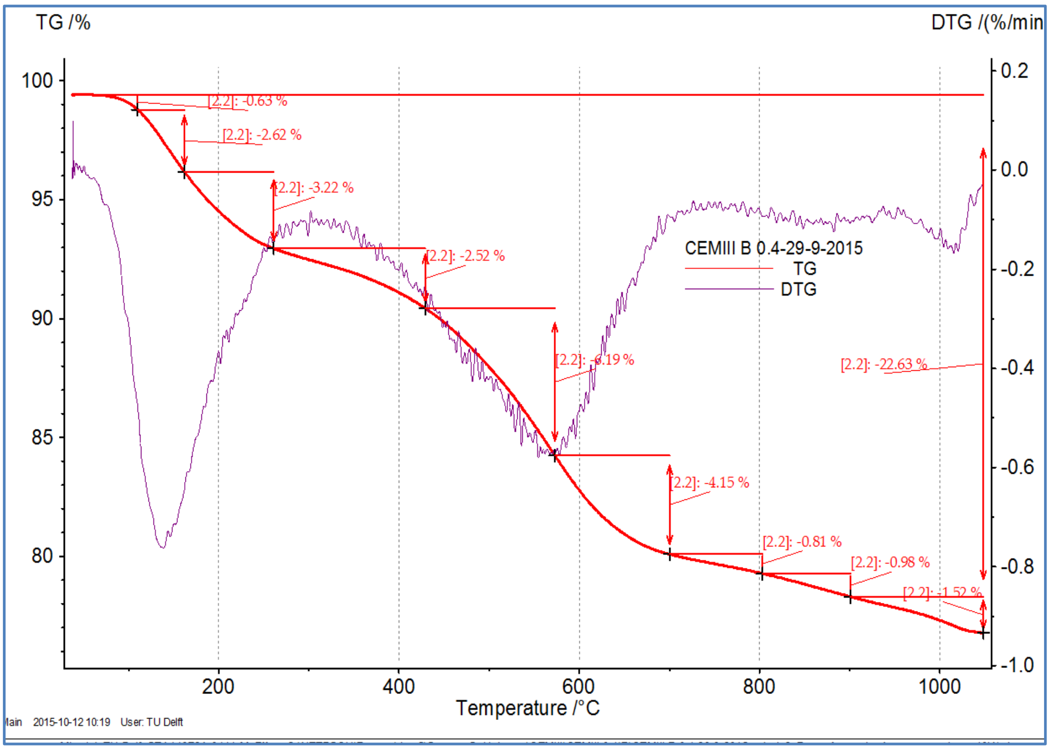

5.
6.

CEM III W/C 0.5

R: Blanc

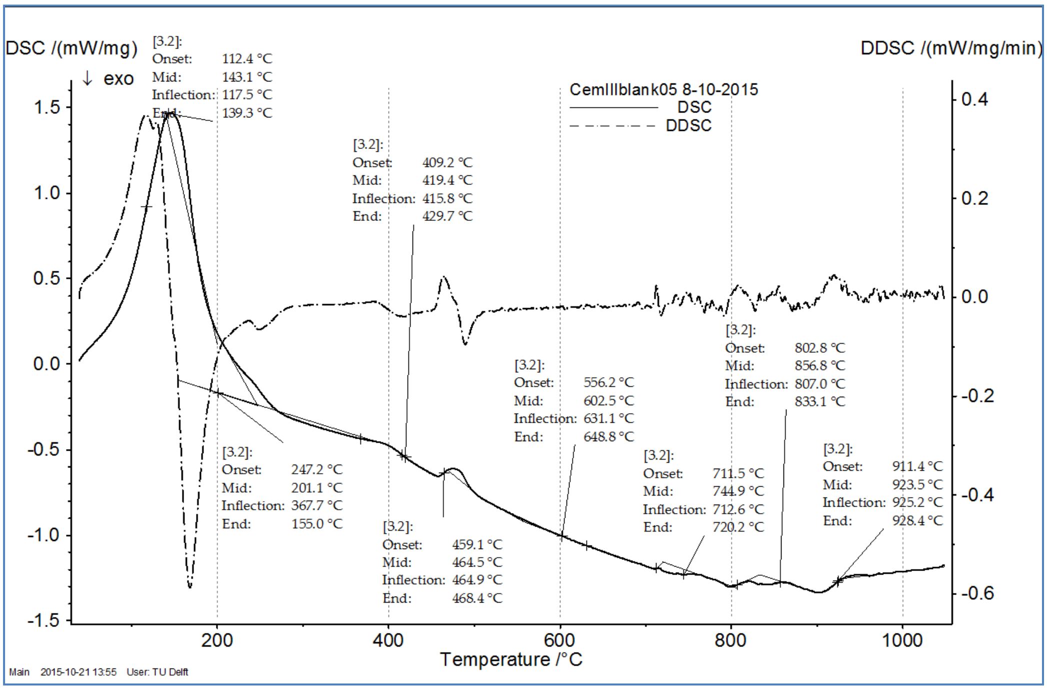

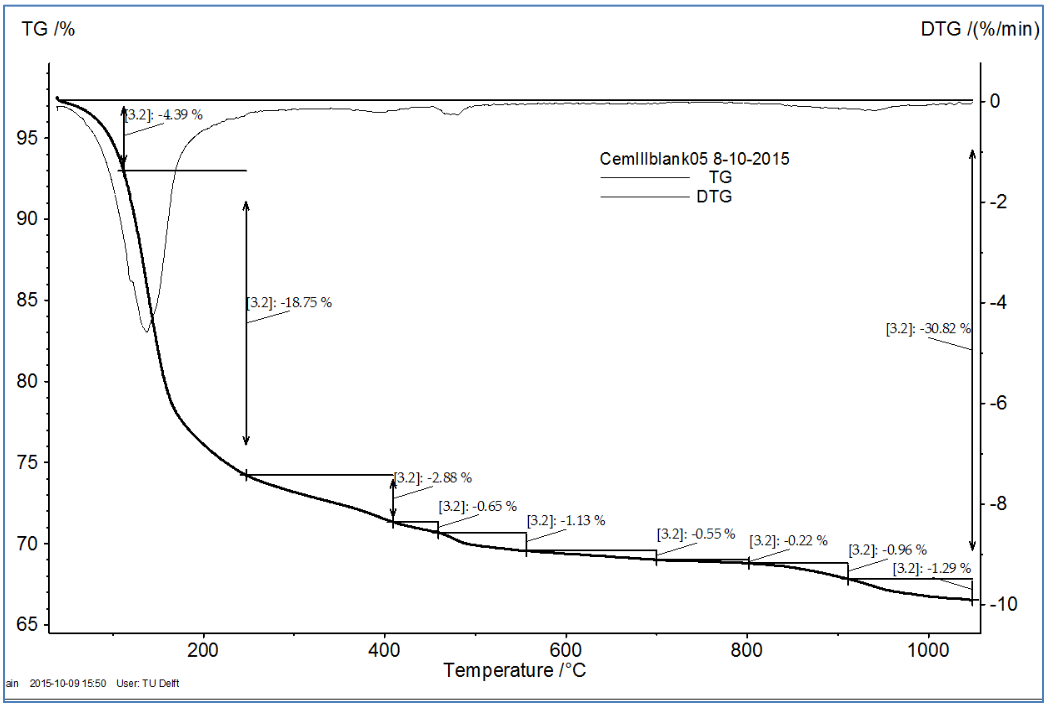

CEM III W/C 0.5

R1CO$_2$: RCT$_{28d}$

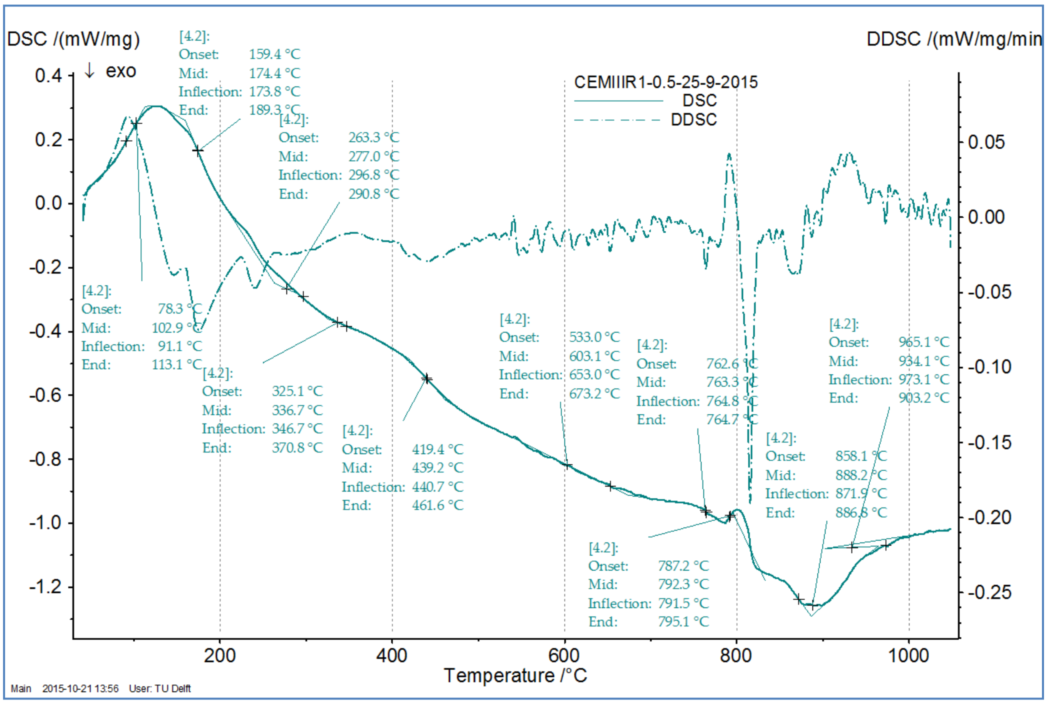

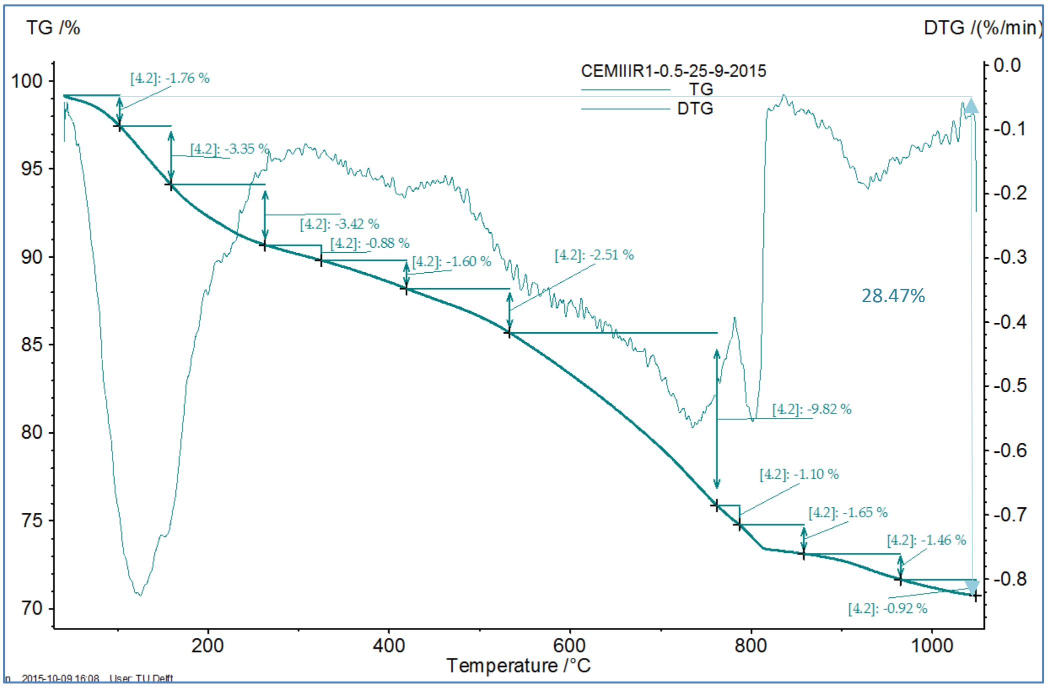

CEM III W/C 0.5

A: Na-MFP → RCT28d

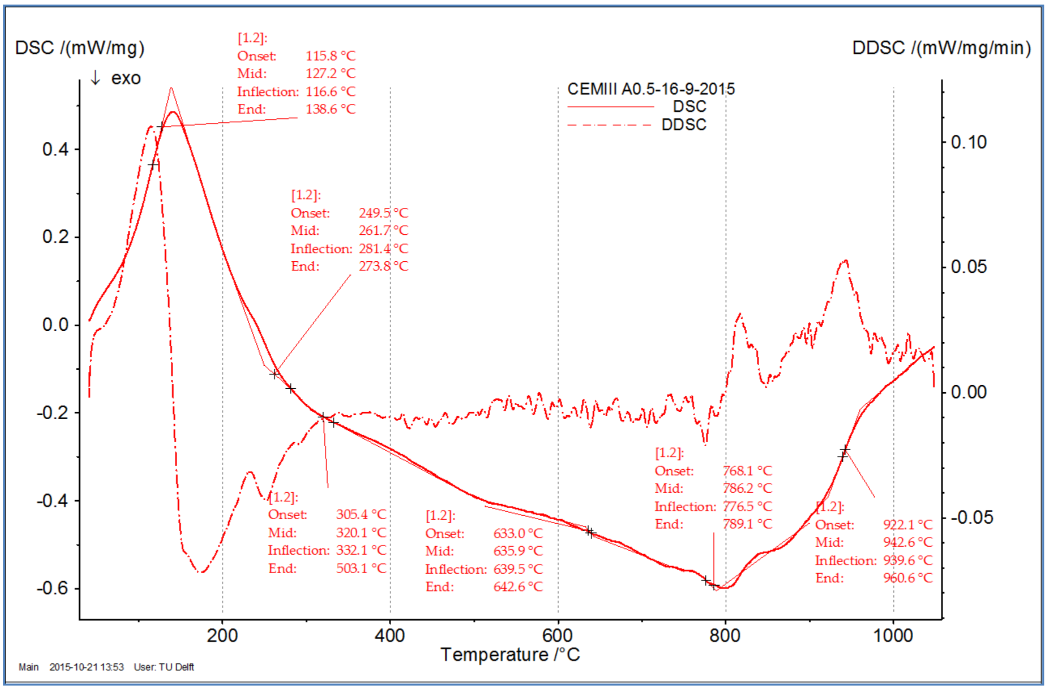

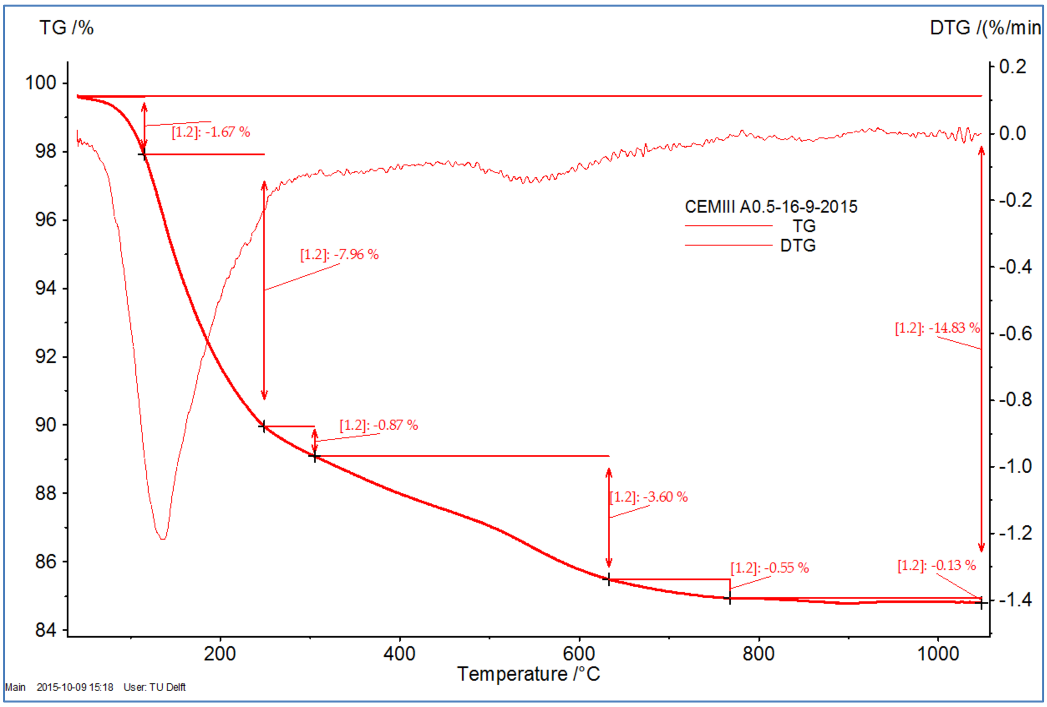

CEM III W/C 0.5

B: RCT28d → Na-MFP

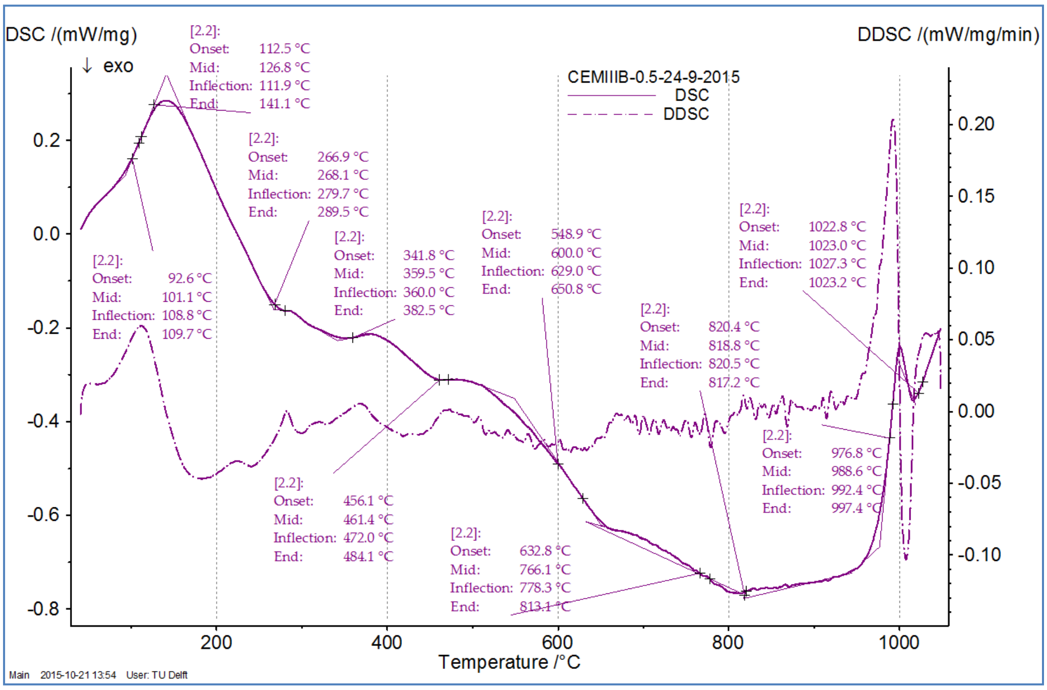

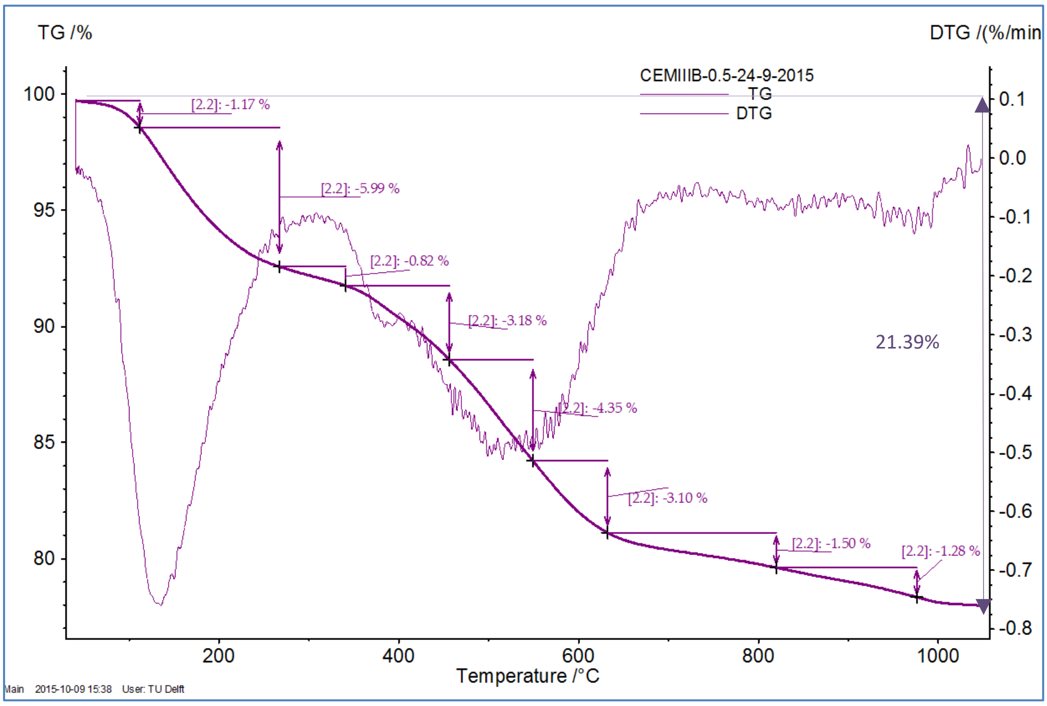

CEM III W/C 0.6

R: Blanc

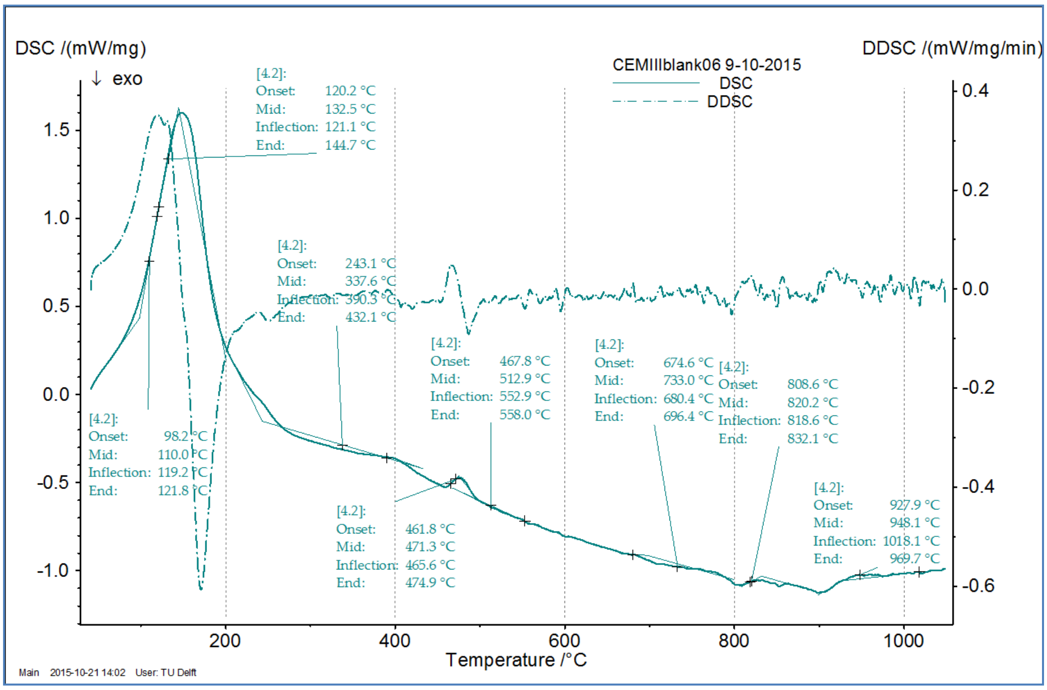

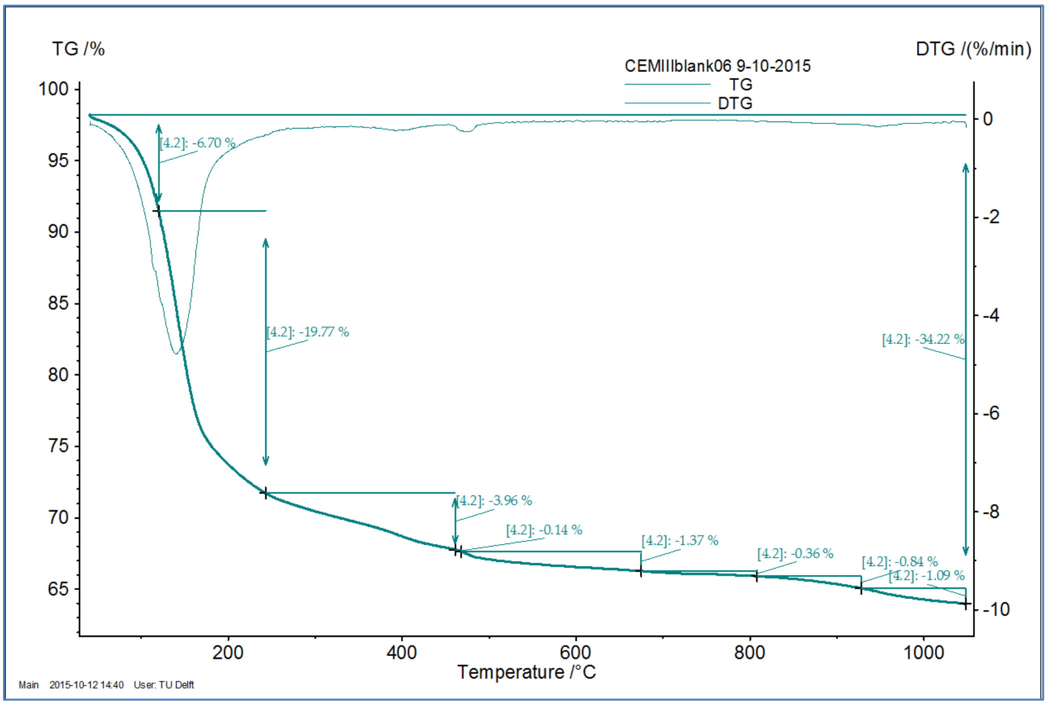

CEM III W/C 0.6

R1CO$_2$: RCT$_{28d}$

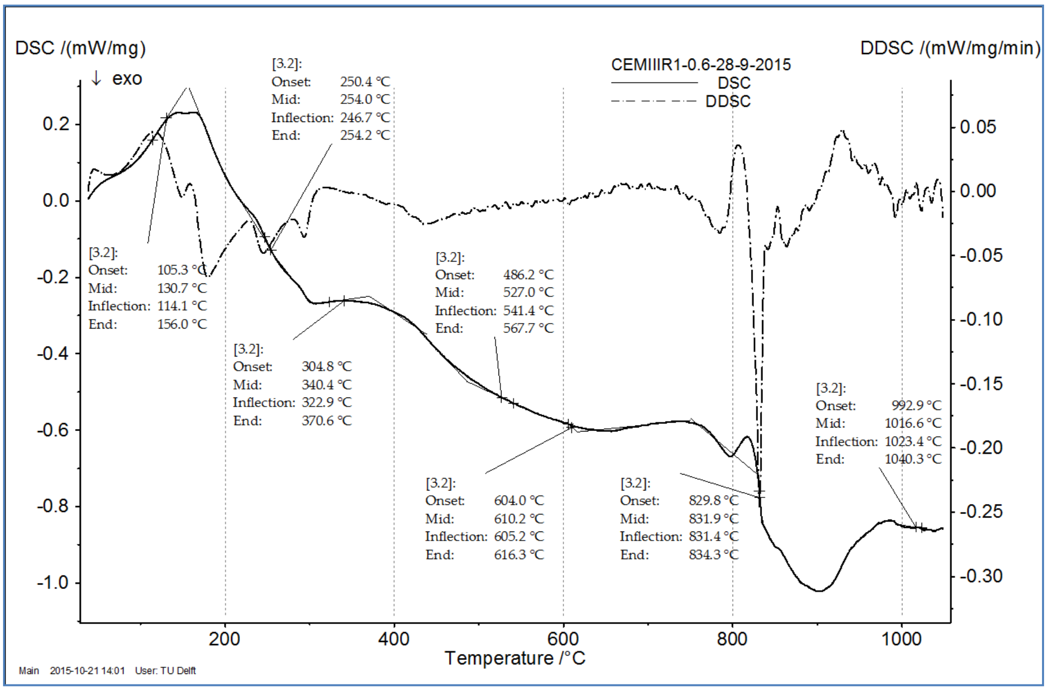

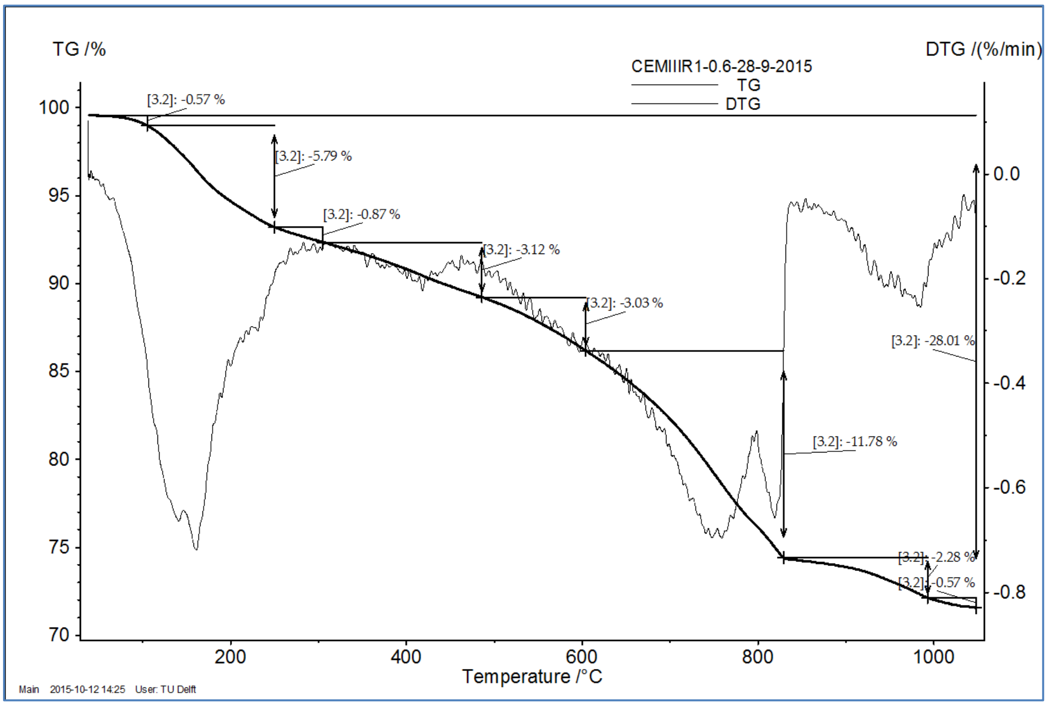

CEM III W/C 0.6

A: Na-MFP → RCT28d

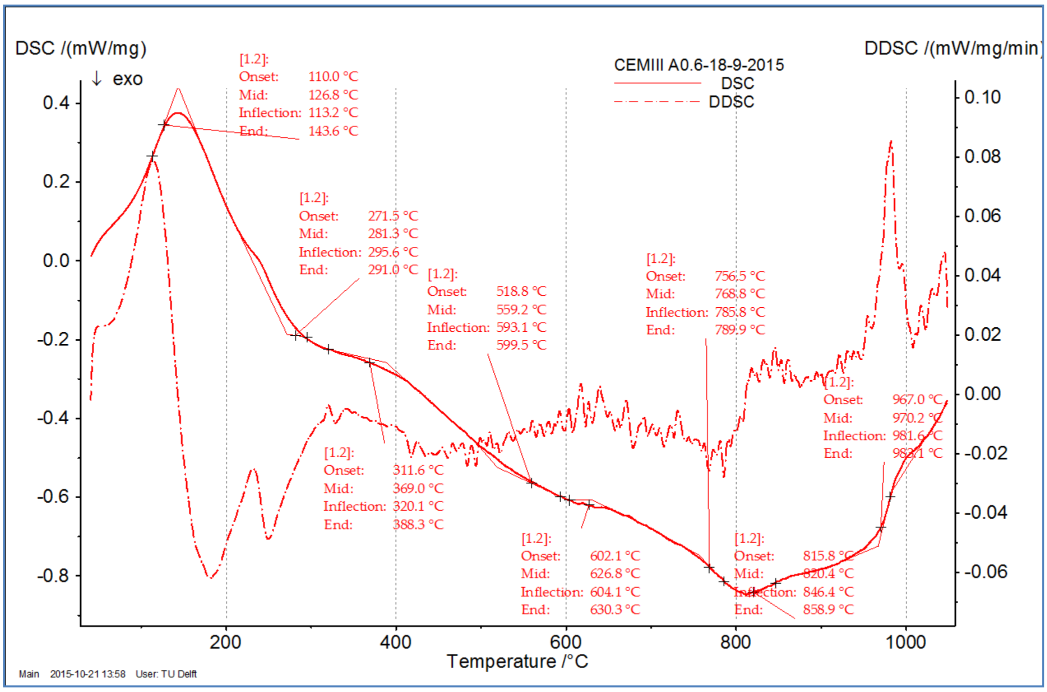

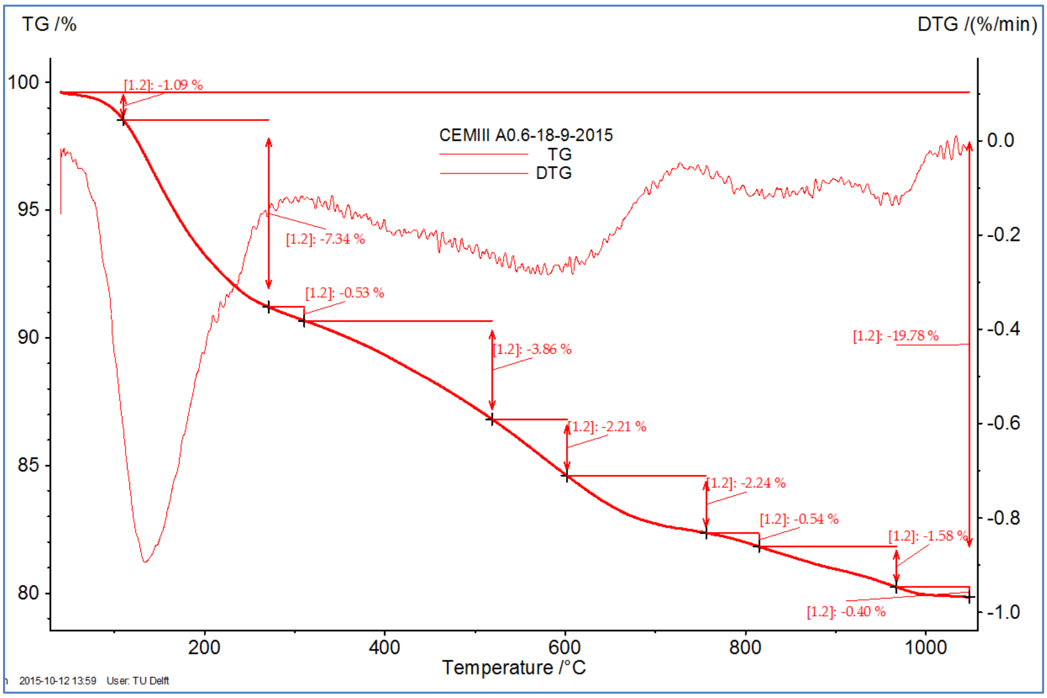

CEM III W/C 0.6

B: RCT28d → Na-MFP

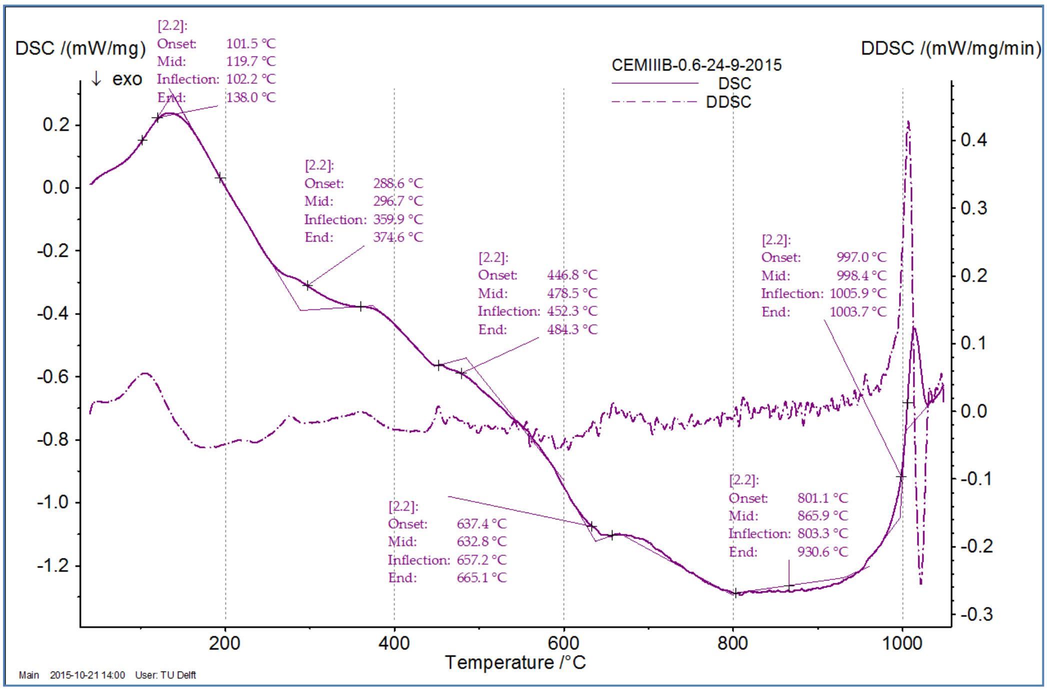

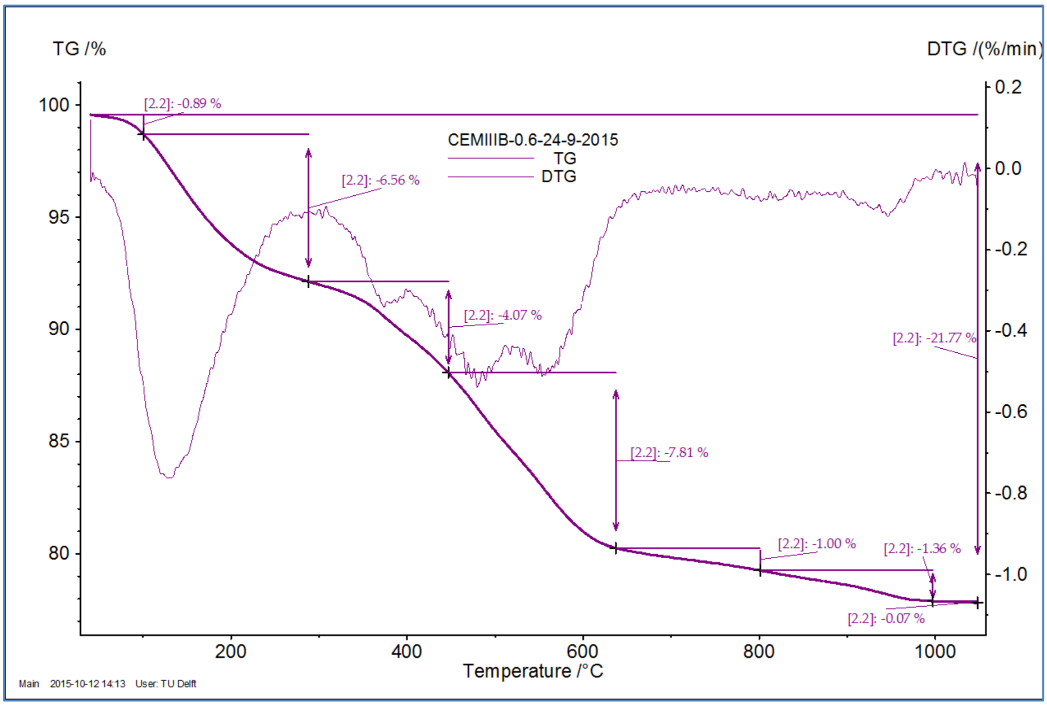

CEM III W/C 0.6

SP MIX W/C 0.4

R: Blanc

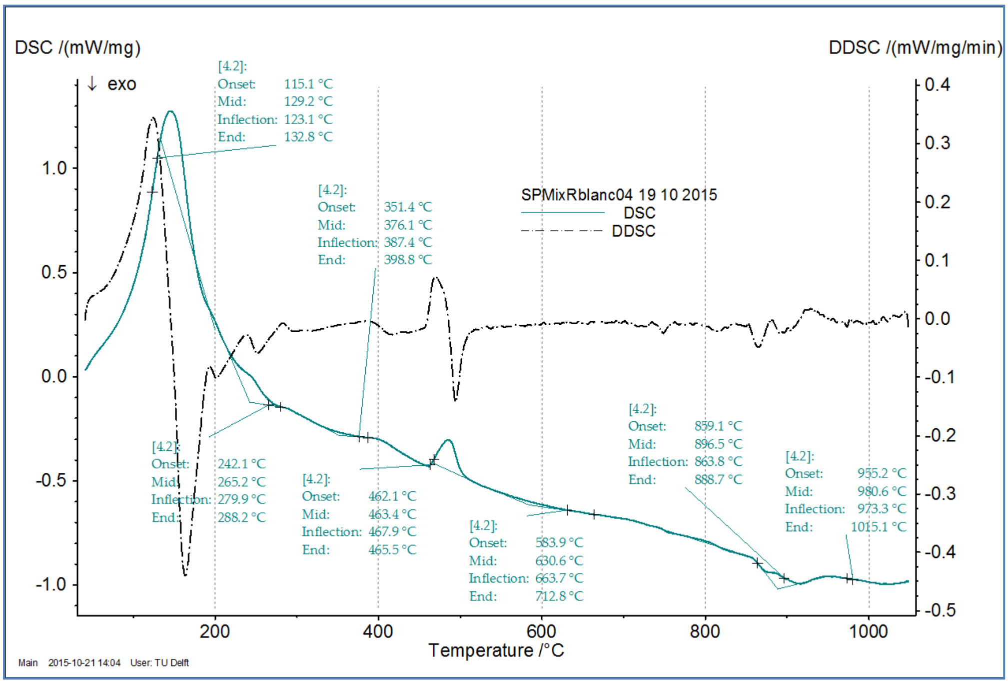

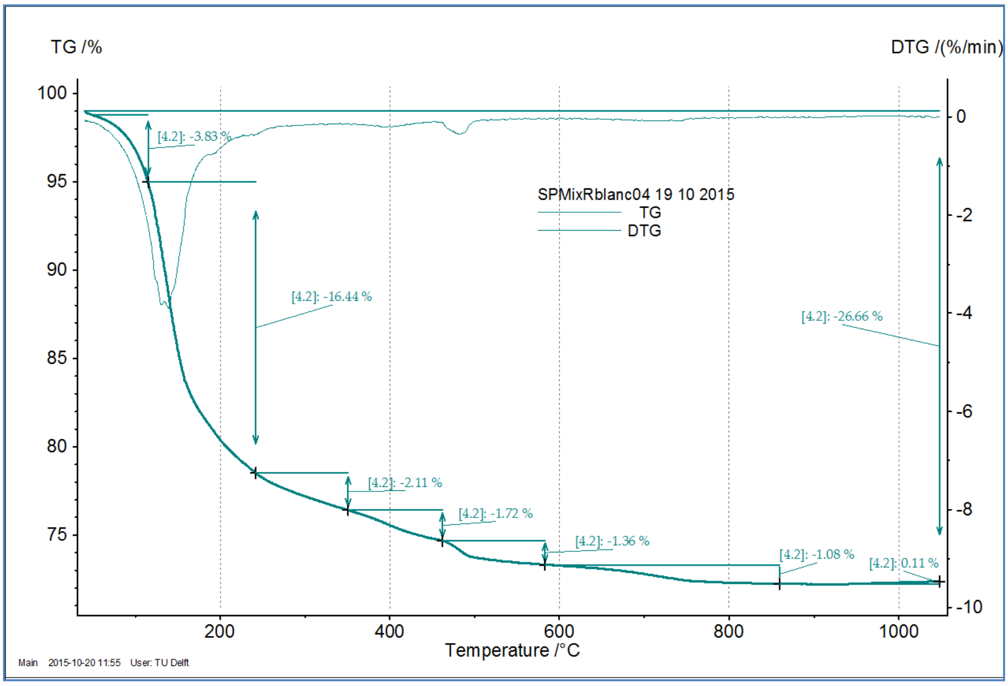

CEM III W/C 0.6

R1co2: RCT28d

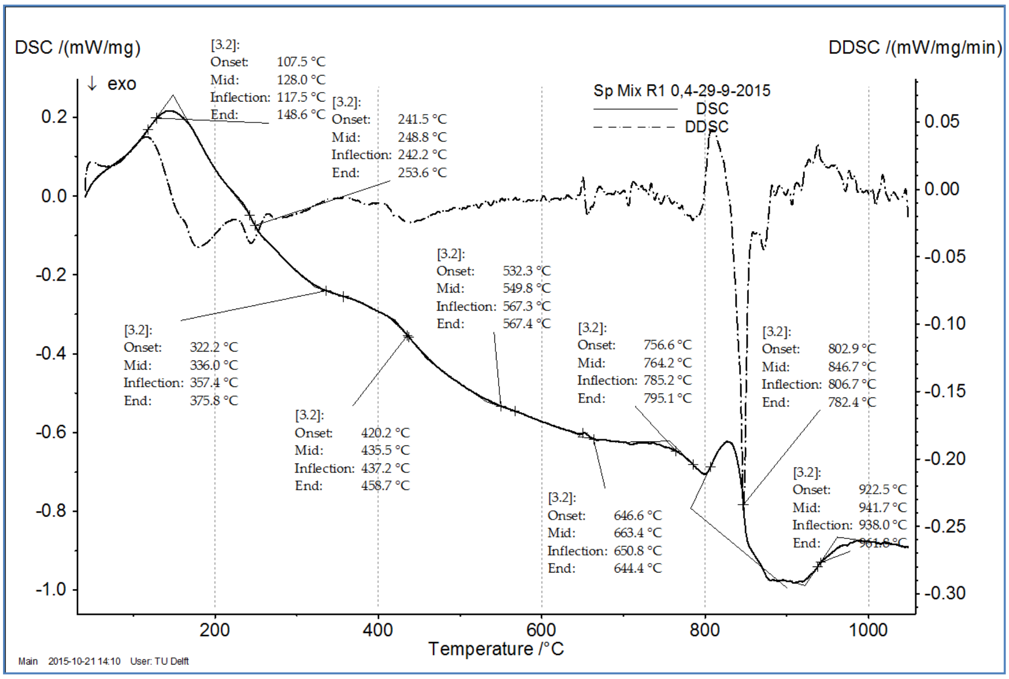

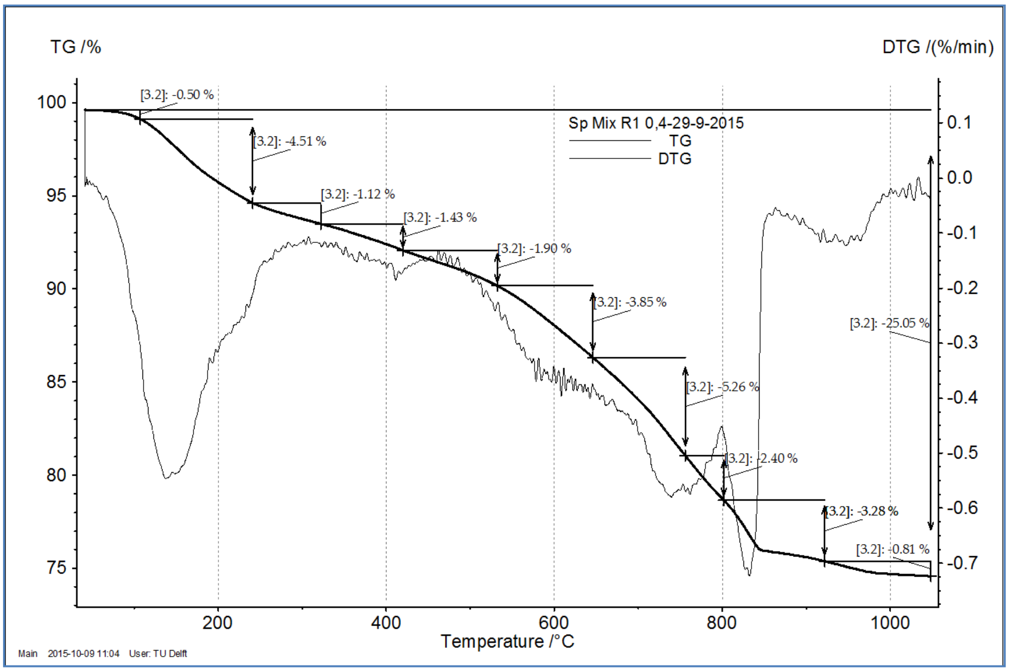

CEM III W/C 0.6

A: Na-MFP →RCT28d

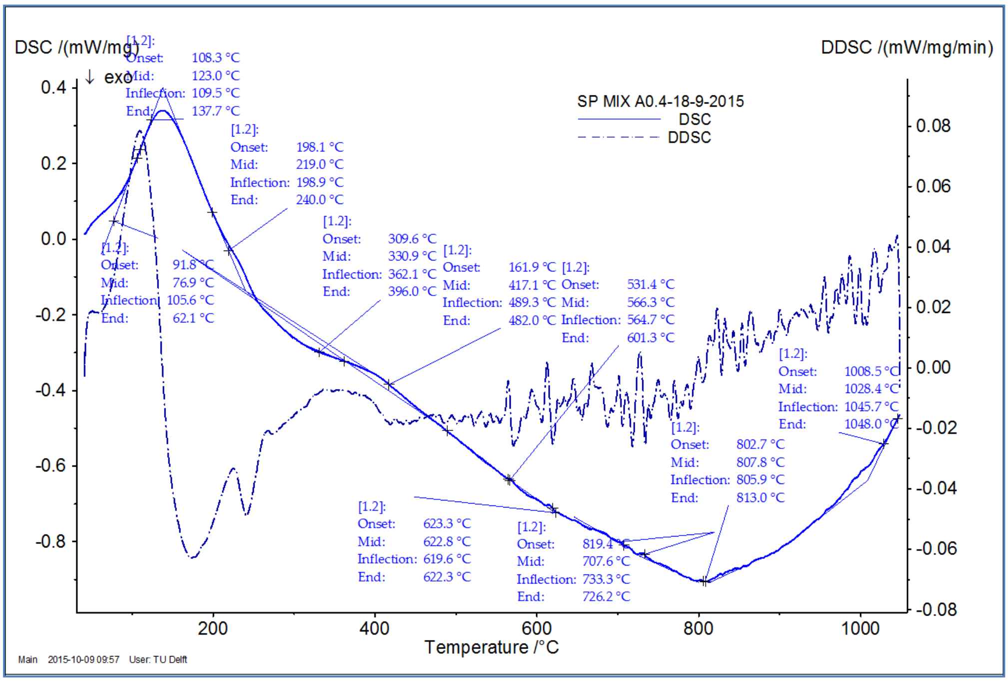

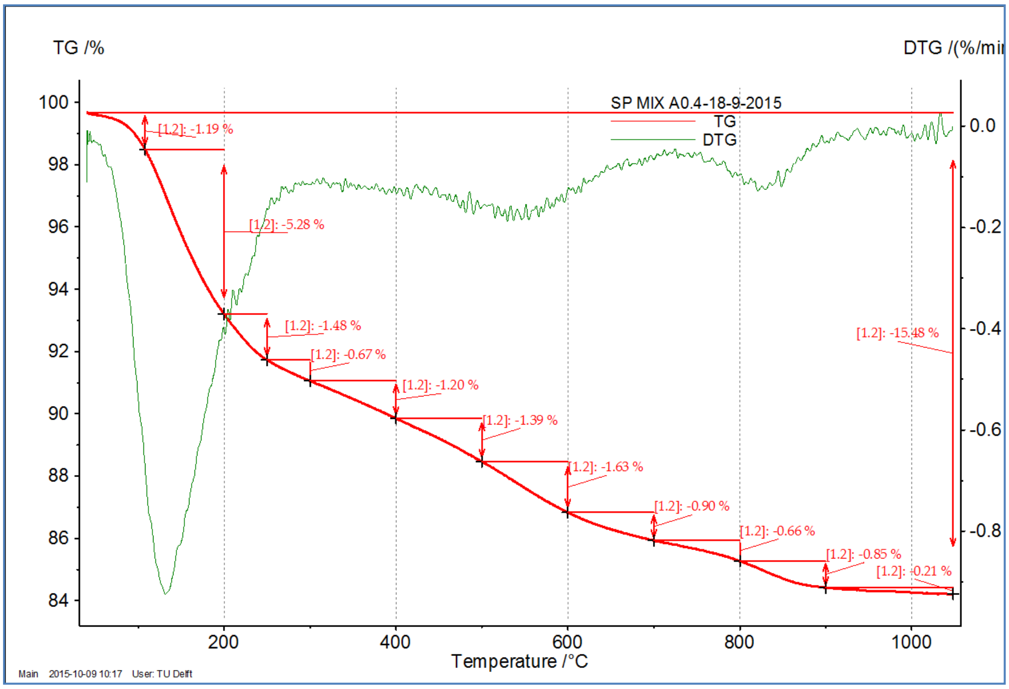

CEM III W/C 0.6

B: RCT28d→Na-MFP

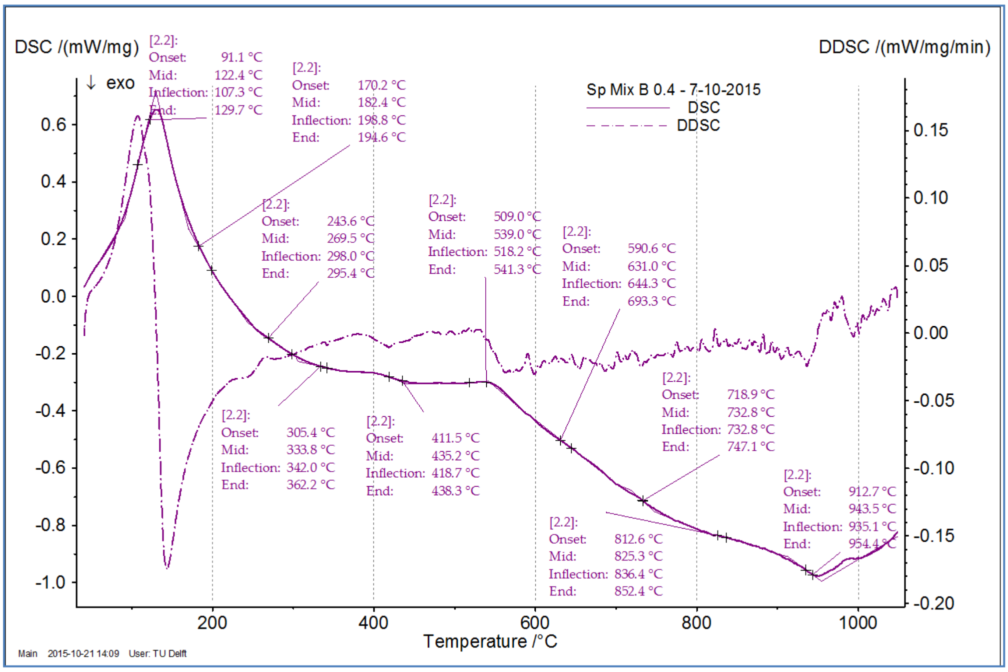

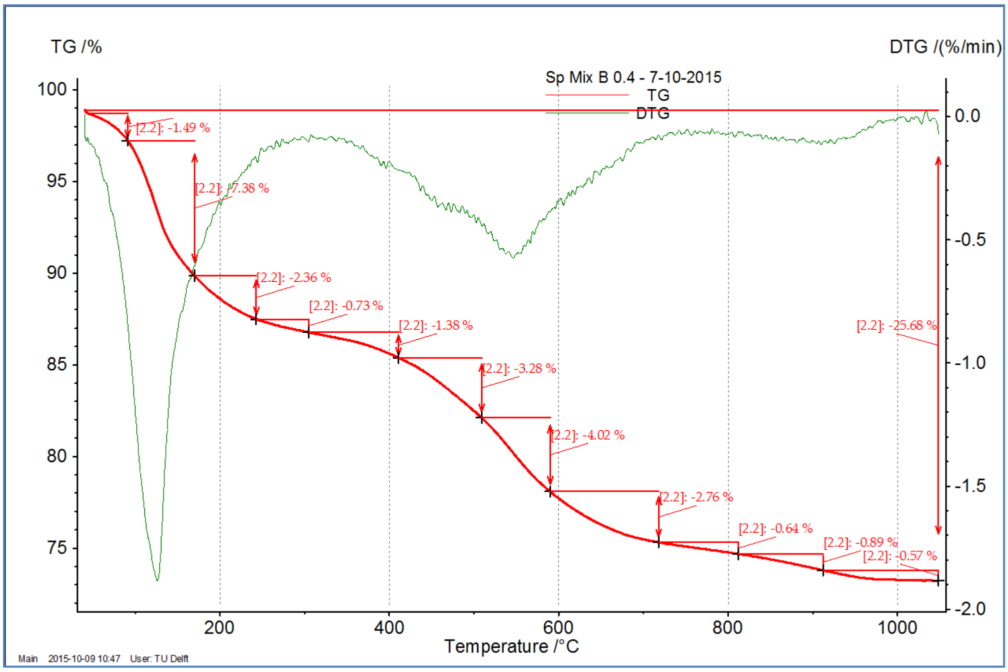

SP MIX W/C 0.5

R: Blanc

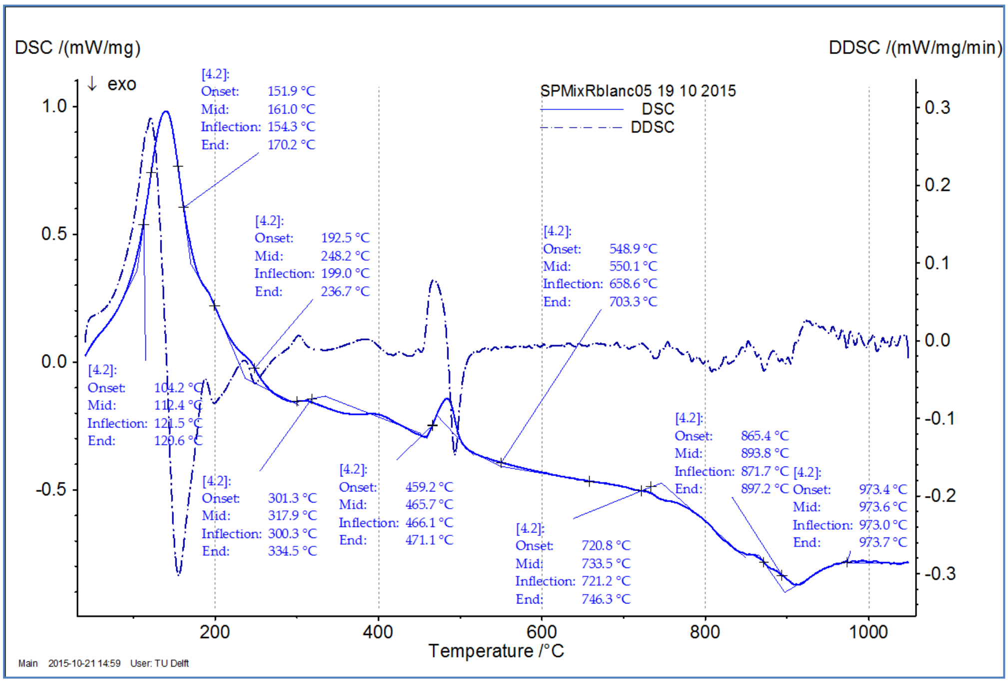

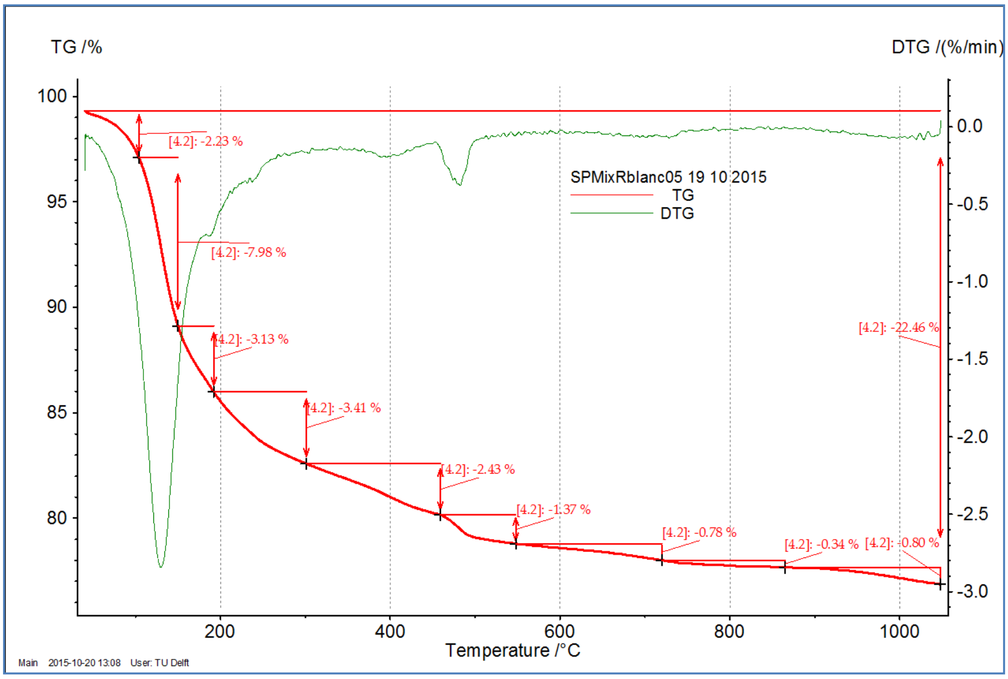

SP MIX W/C 0.5

R1co2: RCT28d

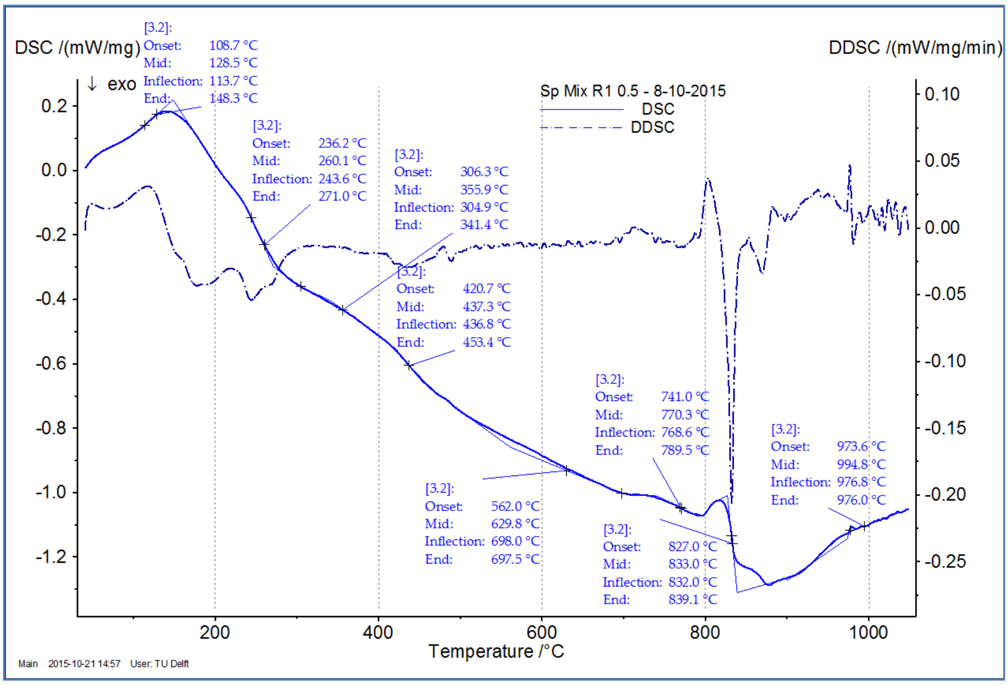

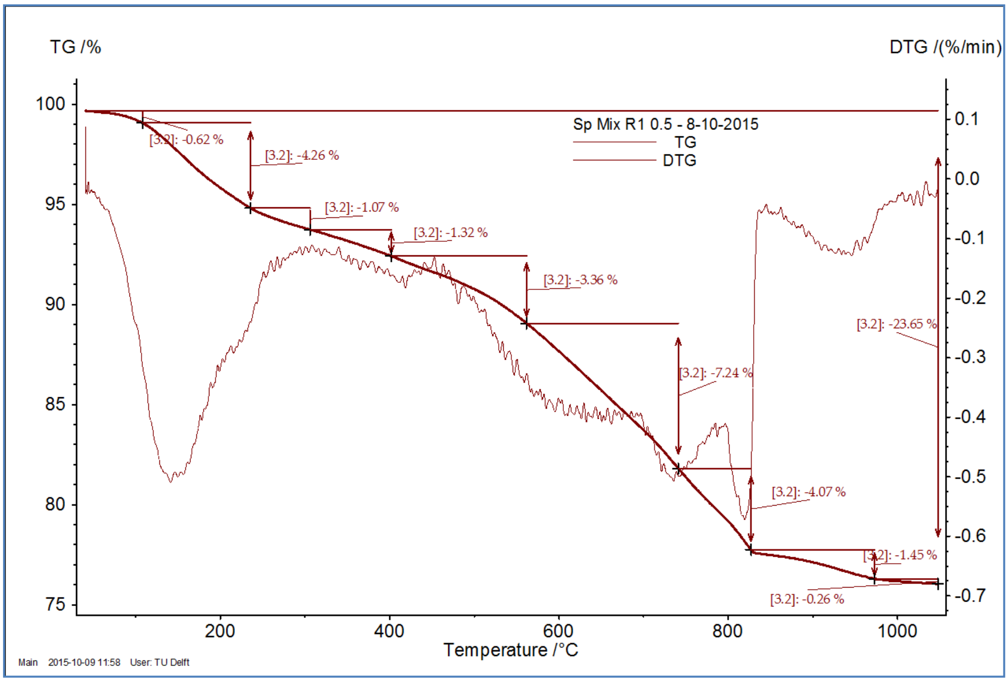

SP MIX W/C 0.5

A:Na-MFP →RCT28d

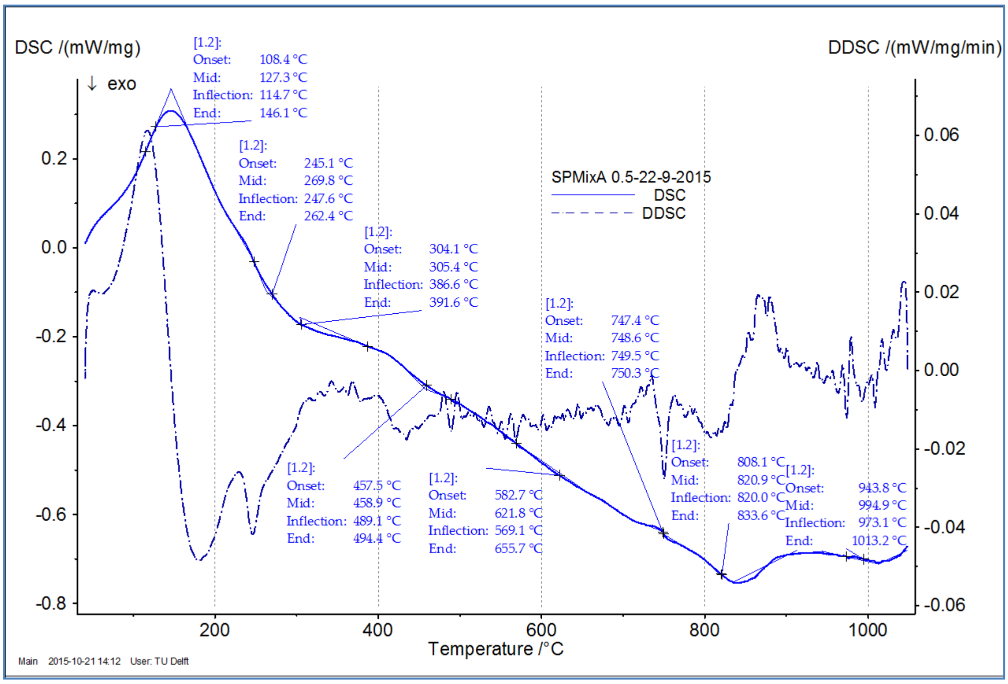

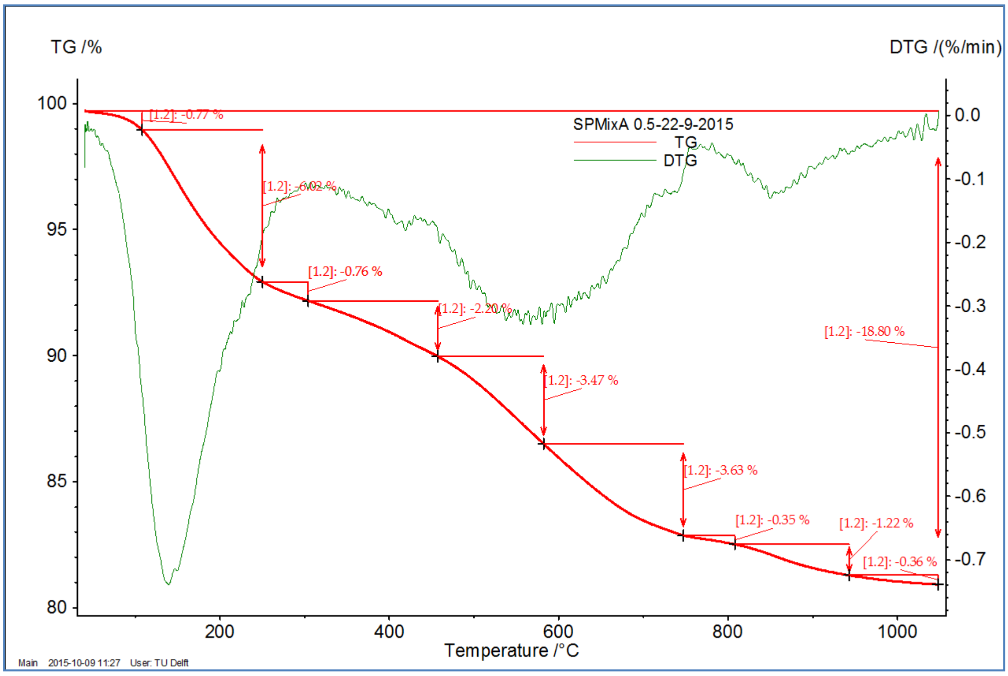

SP MIX W/C 0.5

B: RCT28d→Na-MFP

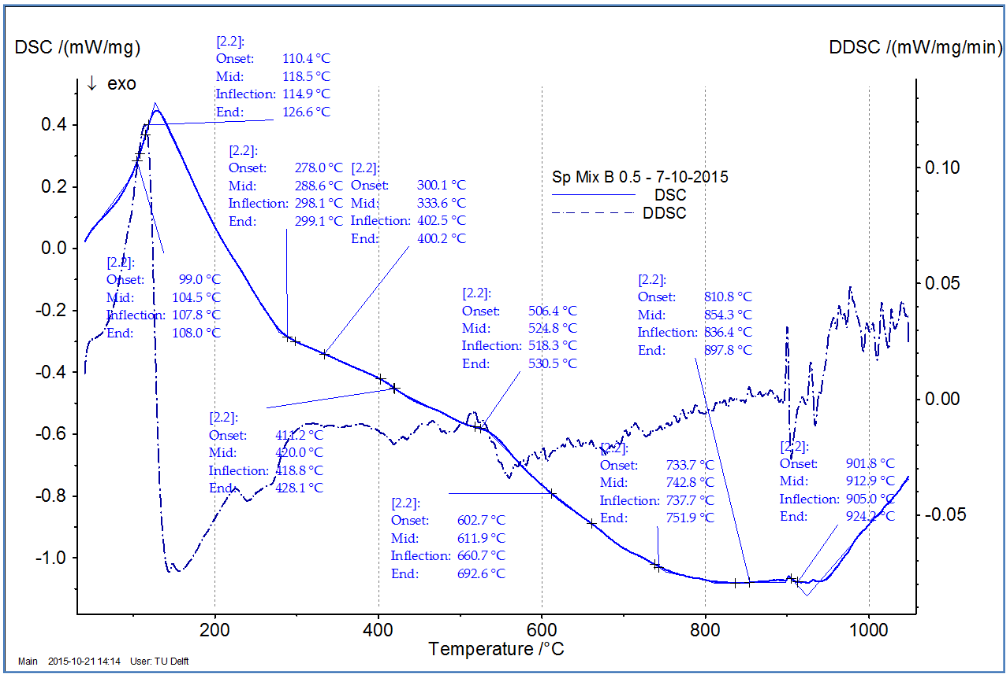

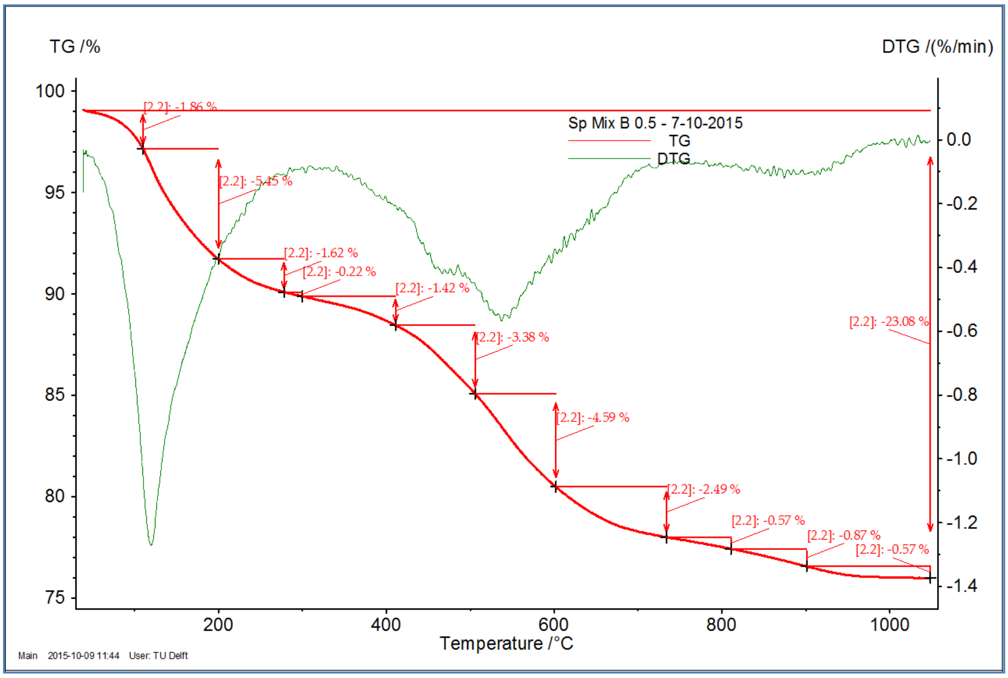

SP MIX W/C 0.6

R: Blanc

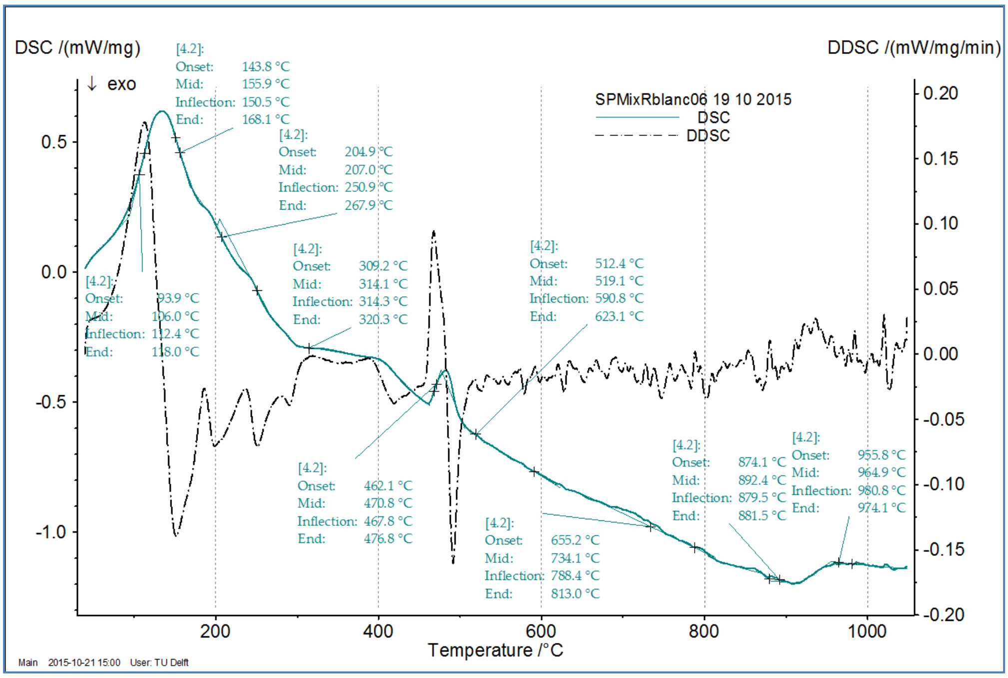

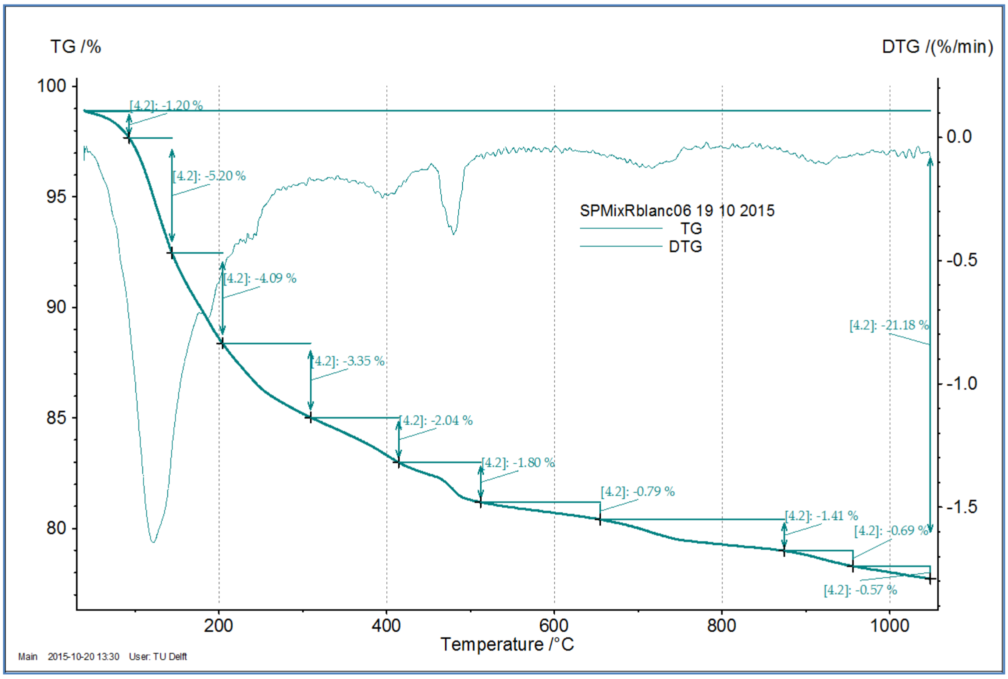

SP MIX W/C 0.6

R1co2: RCT28d

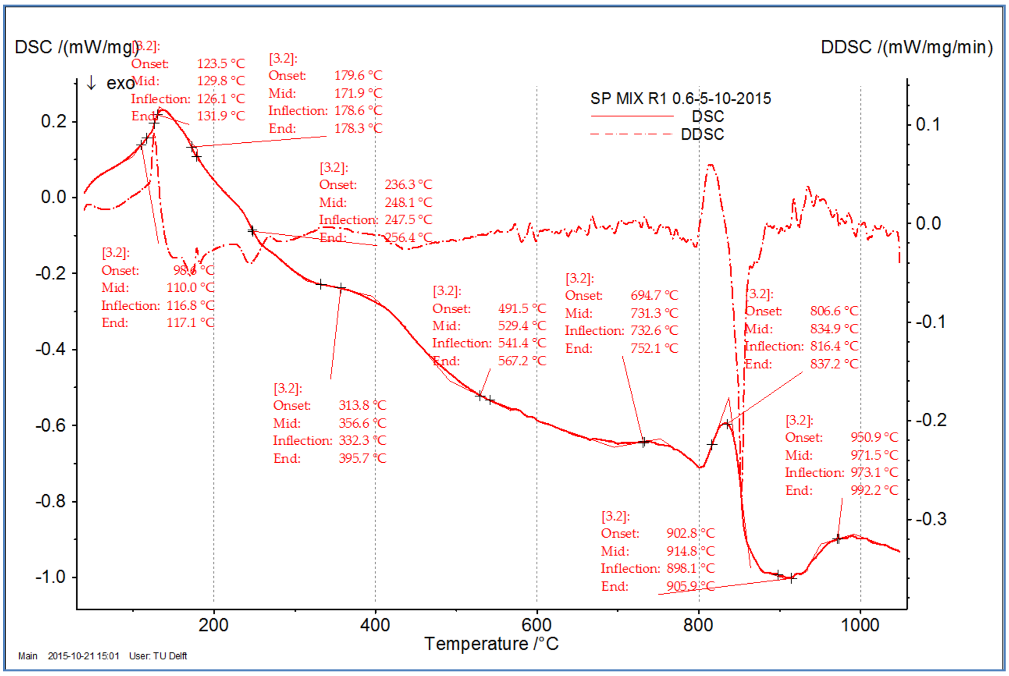

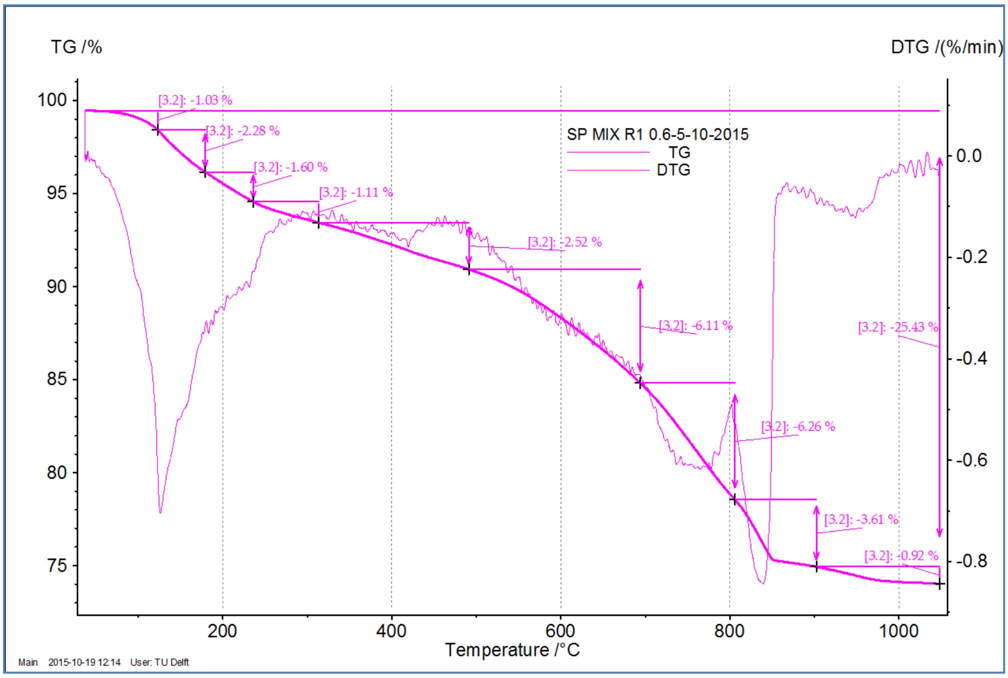

SP MIX W/C 0.6

A: Na-MFP →RCT28d

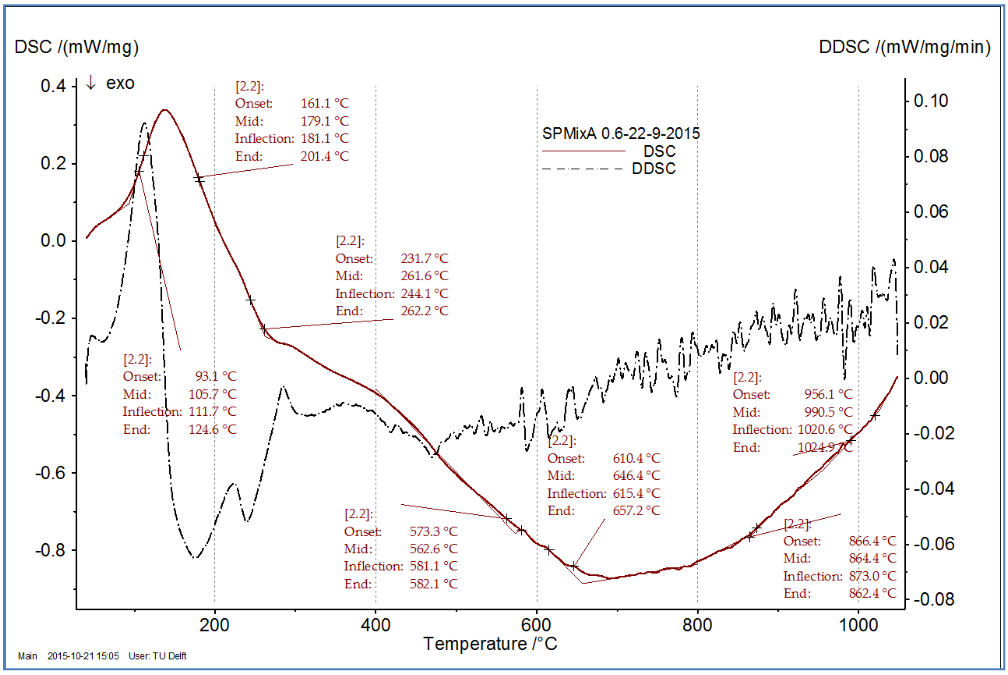

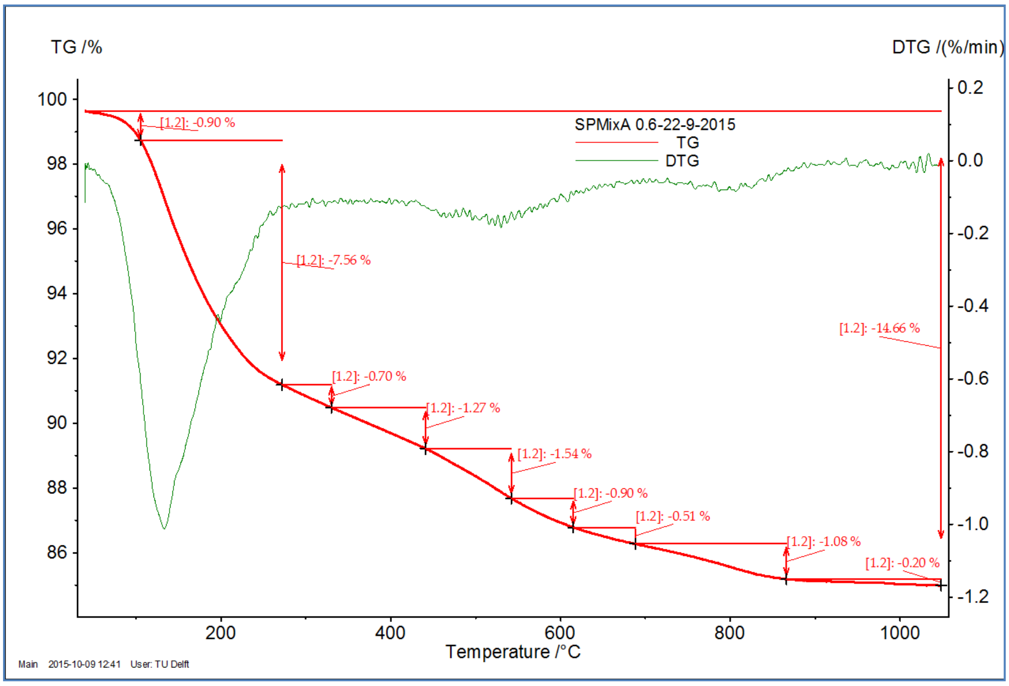

SP MIX W/C 0.6

B: RCT28d→Na-MFP

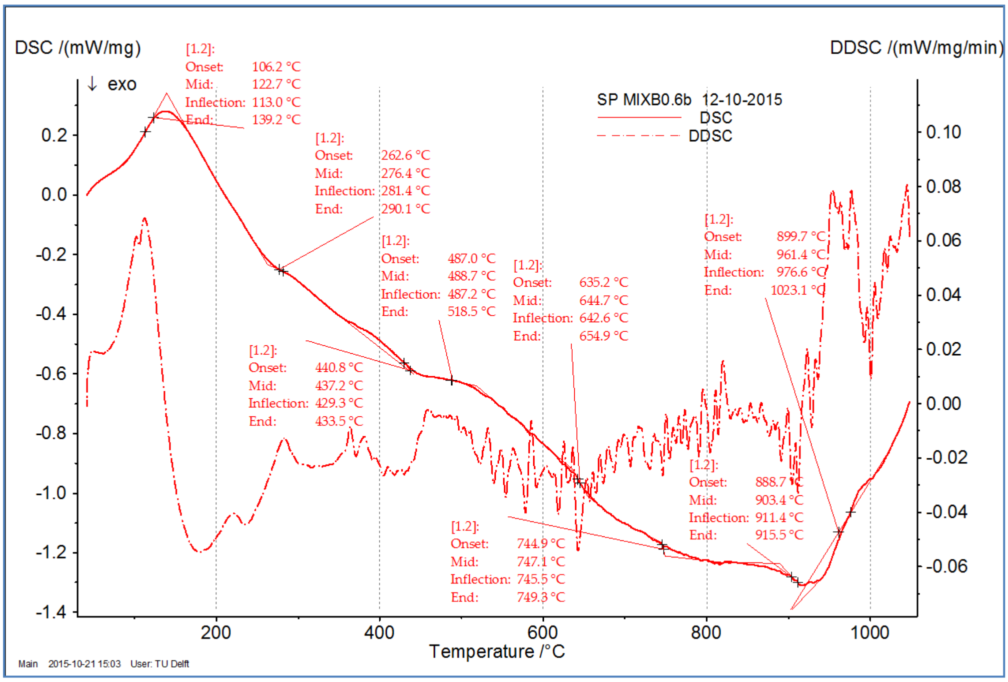

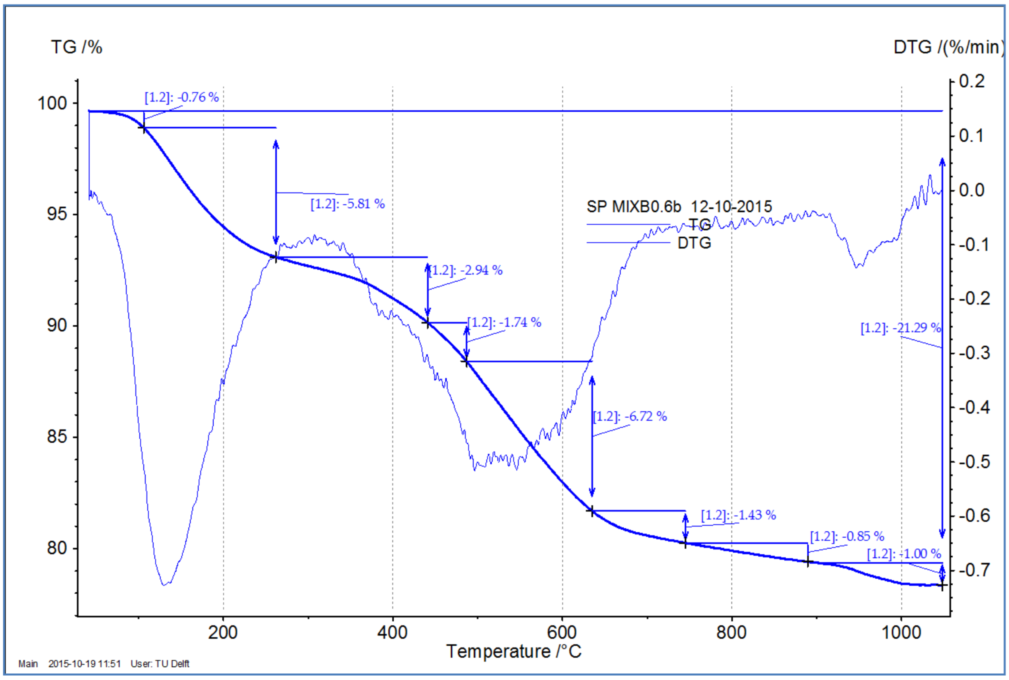

1.22 Analysis DSC/TGA curve-CEM I0.4

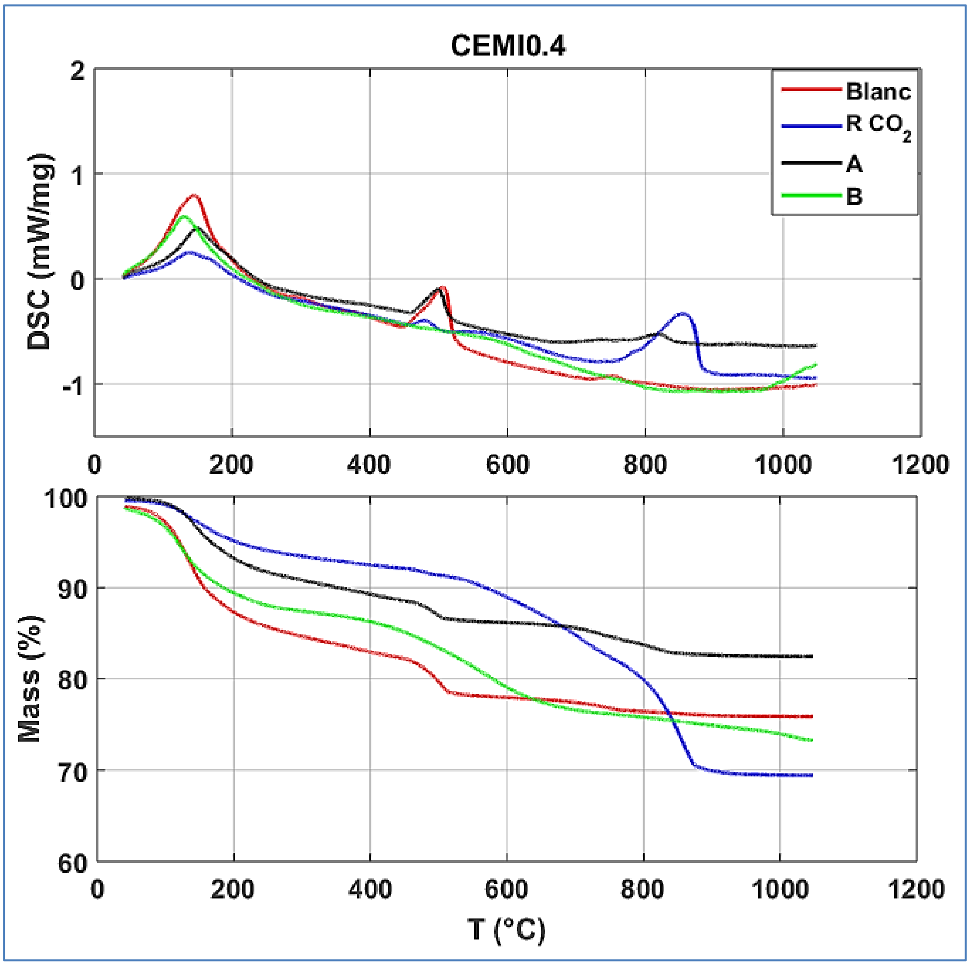

CEMI 0.4			
Sample Treatment	**Temperature interval (T°C)**	**Mass Loss (%)**	**Process**
Blanc	121-247	9.14	P1
	456-550	4.88	P2
	722-857	1.03	P3
R$_{CO2}$(28d)	125-257	4.26	P1
	459-576	2.27	P2
	791-916	10.72	P3
A	112-257	7.32	P1
	461-534	2.01	P2
	802-868	0.99	P3
B	94-267	9.21	P1
	459-622	6.59	P2
	622-831	2.74	P3

	Process
P1	Water loss from C-S-H gels layers and from the dehydration of ettringite
P2	Dehydration of calcium hydrate(CH)
P3	Decarbonation of calcium carbonate (CaCO3).

1.23 Analysis DSC/TGA curve-CEM I 0.5

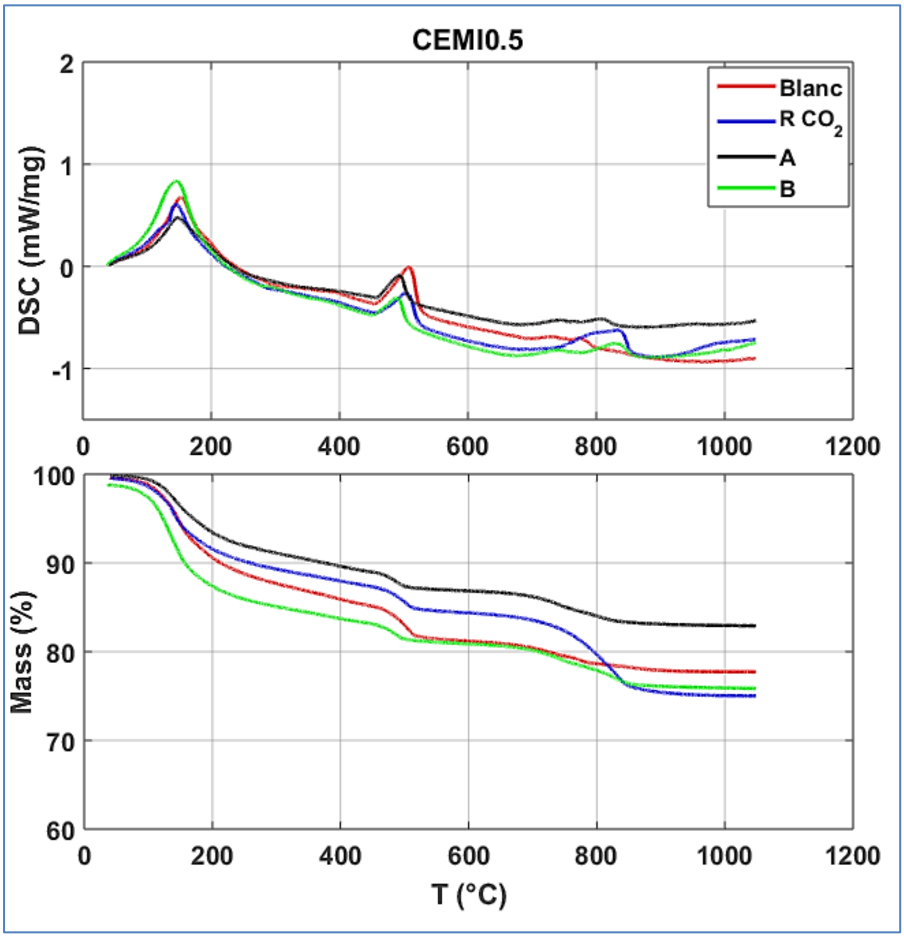

CEMI 0.5			
Sample Treatment	Temperature interval (T°C)	Mass loss (%)	Process
Blanc	121-195	6.75	P1
	460-558	9.48	P2
	701-849	3.15	P3
R_{CO2}(28d)	93-239	8.43	P1
	469-540	2.28	P2
	782-933	5.62	P3
A	112-241	6.89	P1
	459-586	1.95	P2
	817-860	0.41	P3
B	100-249	11.42	P1
	453-557	4.27	P2
	742-899	3.09	P3

	Process
P1	Water loss from C-S-H gels layers and from the dehydration of ettringite
P2	Dehydration of calcium hydrate(CH)
P3	Decarbonation of calcium carbonate (CaCO3).

1.24 Analysis DSC/TGA curve-CEM I 0.6

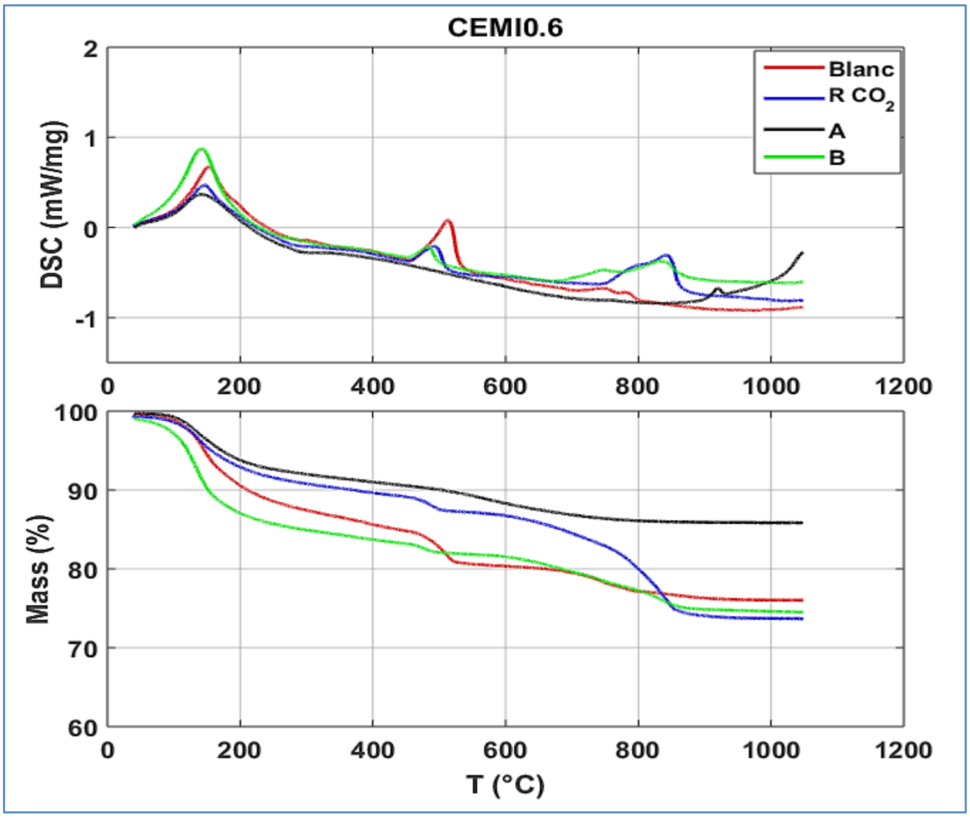

CEMI 0.6			
Sample Treatment	Temperature interval (T°C)	Mass loss (%)	Process
Blanc	104-240	9.83	P1
	466-516	3.2	P2
	717-892	2.86	P3
RCO2	119-269	6.94	P1
	458-508	3.46	P2
	794-898	6.41	P3
A	99-232	6.35	P1
	328-636	3.99	Large Peak for the dehydration of CH
	780-903	0.28	P3
B	119-276	10	P1
	457-581	1.42	P2
	750-877	3.4	P3

	Process
P1	Water loss from C-S-H gels layers and from the dehydration of ettringite
P2	Dehydration of calcium hydrate(CH)
P3	Decarbonation of calcium carbonate (CaCO3).

1.25 Analysis DSC/TGA curve-CEM III 0.4

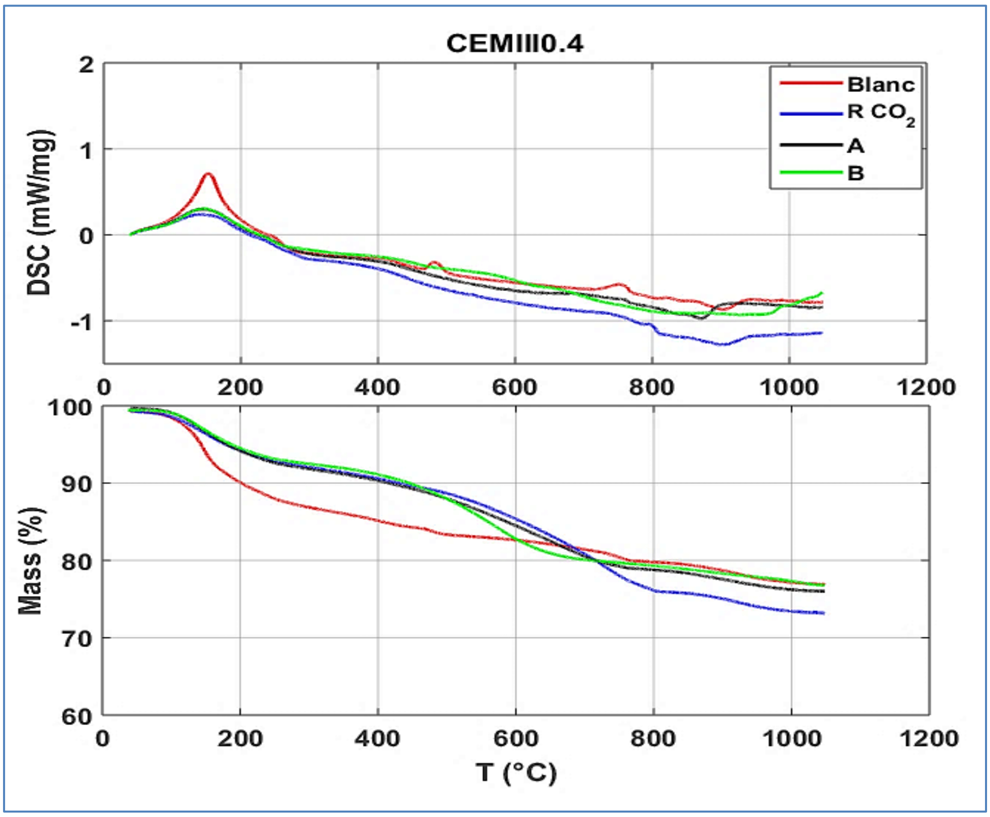

CEMIII 0.4			
Sample Treatment	**Temperature interval (T°C)**	**Mass loss (%)**	**Process**
Blanc	97-274	11.21	P1
	412-468	0.82	P2
	732-803	1.12	P3
	878-973	1.64	Crystallization peak around 905°C, which may be due to a different amorphous phase.
RCO2	108-272	5.87	P1
	400-562	3.77	P2 Large peak
	746-804	2.24	P3
	804-1048	3.84	Crystallization peak around 902°C, which may be due to a different amorphous phase
A	106-200	4.76	P1
	400-598	5.75	P2 Large peak
	762-864	0.9	P3
	864-932	1.1	Crystallization peak around 882°C, which may be due to a different amorphous phase
B	110-261	5.84	P1
	429-700	10.34	P2 large Peak
	700-901	0.98	No peak for carbonation with small loss of mass
	901-1048	1.52	Crystallization peak around 931°C

	Process
P1	Water loss from C-S-H gel layers and from the dehydration of ettringite
P2	Dehydration of calcium hydrate(CH)
P3	Decarbonation of calcium carbonate (CaCO3).

1.26 Analysis DSC/TGA curve-CEM III 0.5

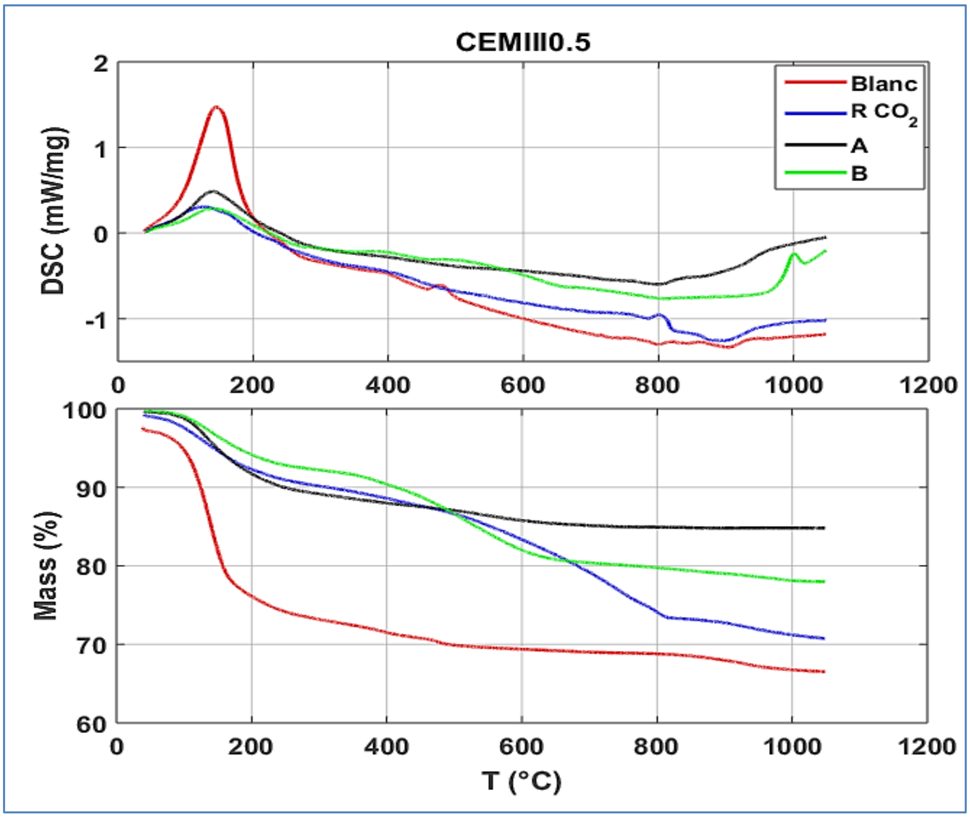

CEMIII 0.5			
Sample Treatment	**Temperature interval (T°C)**	**Mass loss (%)**	**Process**
Blanc	112-247	18.75	P1
	459-556	1.13	P2
	802-911	0.96	P3
RCO2	102-263	6.77	P1
	419-533	2.51	P2
	787-858	1.65	P3
	858-965	1.46	Crystallization peak around 858°C
A	115-249	7.96	P1
	249-768	5.02	Dehydration process without peak
	768-1048	0.13	Crystallization peak around 789°C with very small mass loss
B	**112-267**	5.99	P1
	456-549	4.35	P2
	632-820	1.5	P3
	820- 976	1.28	Crystallization with large peak
	976-1048	0.62	Crystallization with sharp peak around 1000°C with endothermic

	Process
P1	Water loss from C-S-H gel layers and from the dehydration of ettringite
P2	Dehydration of calcium hydrate(CH)
P3	Decarbonation of calcium carbonate (CaCO3).

1.27 Analysis DSC/TGA curve-CEM III 0.6

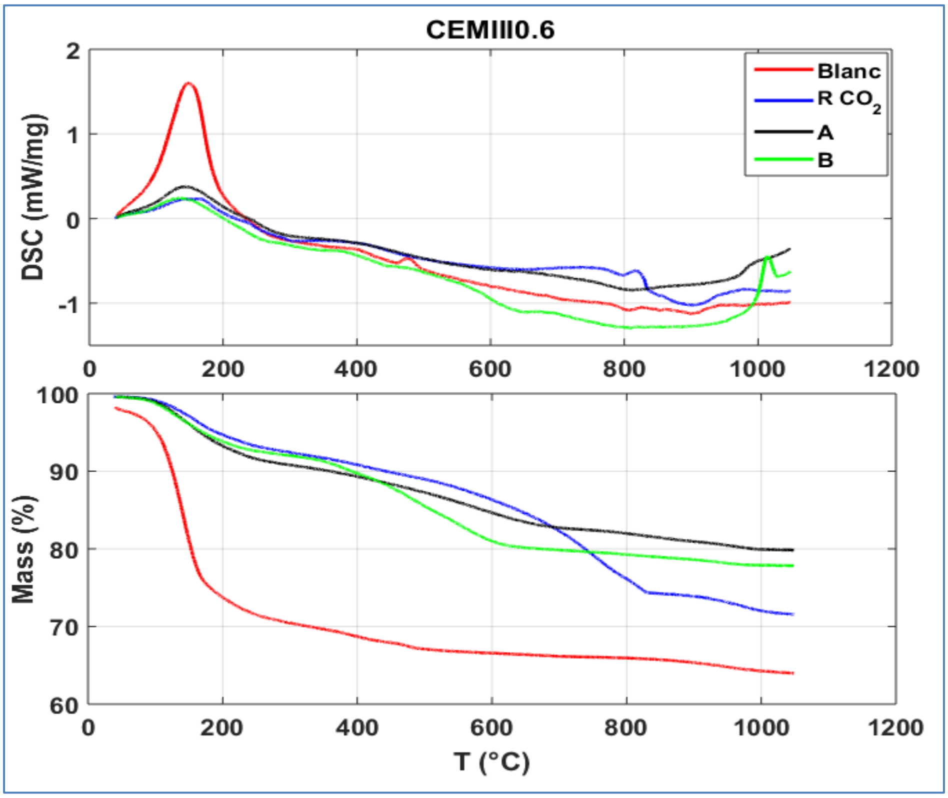

CEMIII 0.6			
Sample Treatment	Temperature interval (T°C)	Mass Loss (%)	Process
Blanc	120-243	19.77	P1
	461-468	0.14	P2 small peak in the DSC Curve
	468-808	1.73	P3
	808-928	0.84	Crystallization around 1000°C-Small peak DSC
RCO2	105-250	5.79	P1
	305-486	3.12	P2
	604-829	14.07	P3
	993-1048	0.98	Crystallization around 993°C-large peak DSC
A	110-271	7.34	P1
	311-519	3.86	P2
	602-815	2.78	P3
	815-967	1.58	Crystallization
	967-1048	0.76	Crystallization with small loss of mass
B	101-288	6.56	P1
	288-637	11.88	P2
	637-801	1	P3
	801-997	1.36	Crystallization
	997-1048	0.49	Crystallization with sharp peak around 1006°C with endothermic

	Process
P1	Water loss from C-S-H gels layers and from the dehydration of ettringite
P2	Dehydration of calcium hydrate(CH)
P3	Decarbonation of calcium carbonate (CaCO3).

1.28 Analysis DSC/TGA curve-SP MIX 0.4

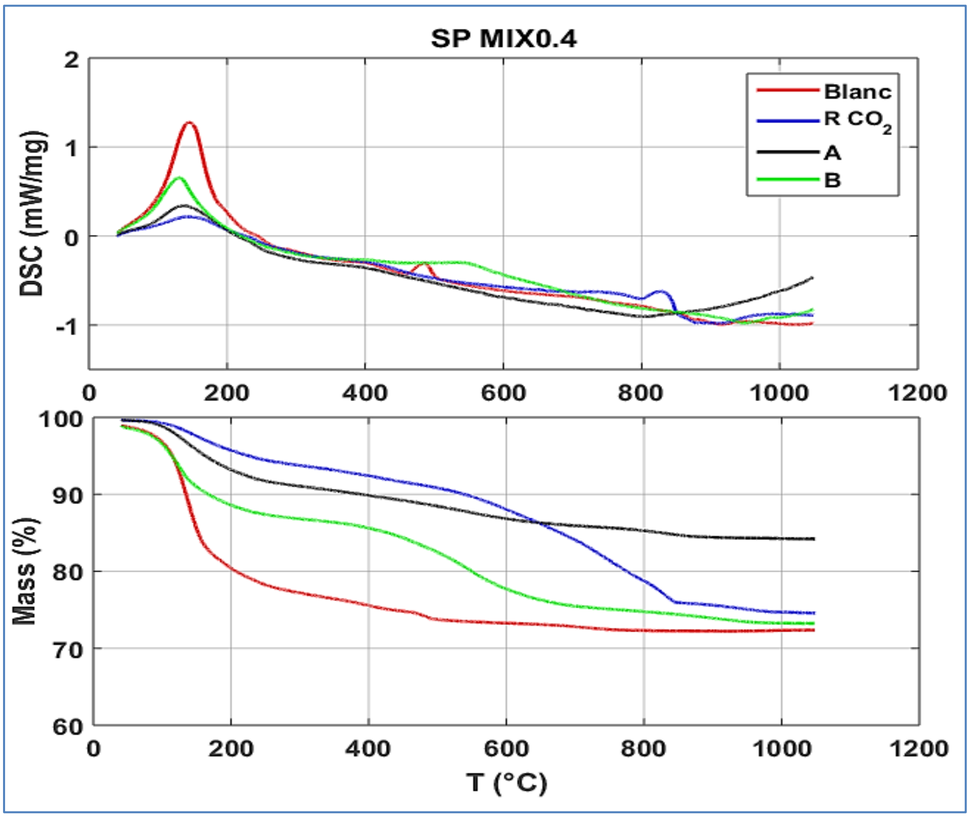

SP MIX 0.4			
Sample Treatment	**Temperature interval (T°C)**	**Mass Loss (%)**	**Process**
Blanc	115-242	16.44	P1
	462-583	1.36	P2
	980	Crystallization with very small mass loss	
RCO2	108-241	4.51	P1
	420-532	1.9	P2
	530-802	11.51	P3
	802-922	3.28	Crystallization around 922**°C**
A	108-250	6.77	P1
	300-800	5.79	P2
	800-1048	1.37	Crystallization around 802 °C
B	91-243	9.74	P1
	305-718	11.45	P2 large peak around 590 °C
	718-912	1.53	P3 small peak
	912-1048	Crystallization around 912 °C with small loss of mass	

	Process
P1	Water loss from C-S-H gels layers and from the dehydration of ettringite
P2	Dehydration of calcium hydrate(CH)
P3	Decarbonation of calcium carbonate (CaCO3).

1.29 Analysis DSC/TGA curve-SP MIX 0.5

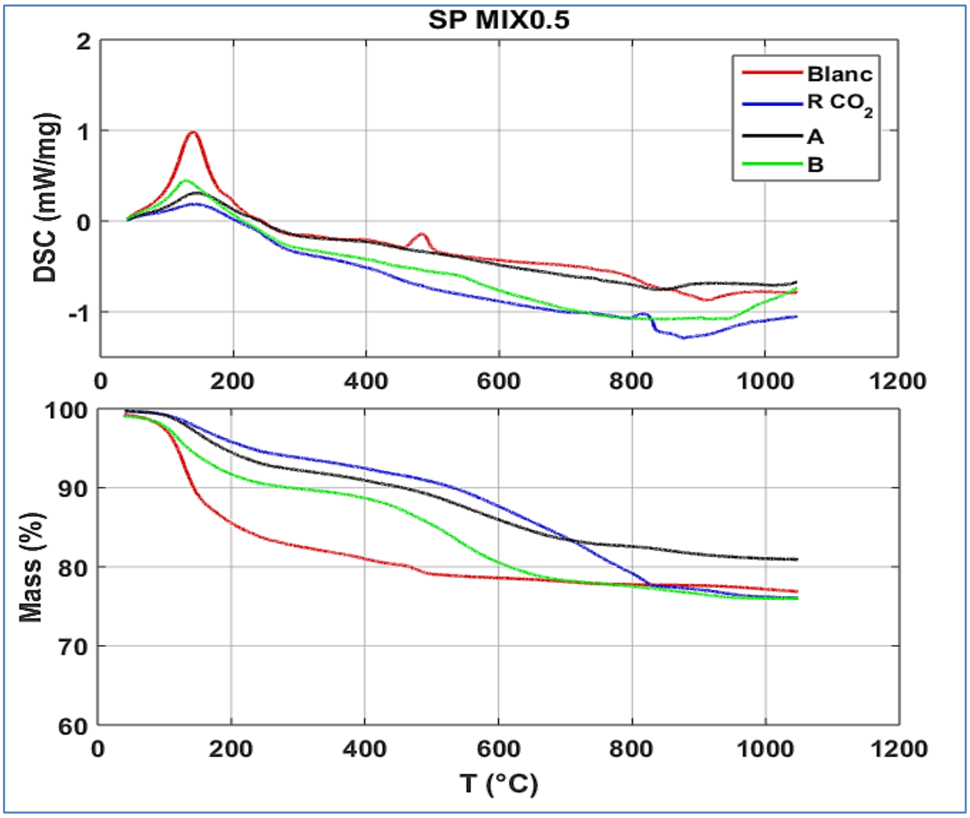

SP MIX 0.5			
Sample Treatment	**Temperature interval (T°C)**	**Mass Loss (%)**	**Process**
Blanc	104-192	11.11	P1
	459-548	1.37	P2
	897-973	Crystallization around 900°C with small mass loss	
RCO2	108-236	4.26	P1
	402-562	3.36	P2
	741-827	4.07	P3
	827-973	1.45	Crystallization around 832°C
A	108-250	6.02	P1
	457-582	3.48	P2
	747-808	0.35	P3
B	110-278	7.07	P1
	411-506	3.38	P2
	No clear peak for decarbonation		
	901-1048	1.55	Crystallization around 901°C

	Process
P1	Water loss from C-S-H gels layers and from the dehydration of ettringite
P2	Dehydration of calcium hydrate(CH)
P3	Decarbonation of calcium carbonate (CaCO3).

1.30 Analysis DSC/TGA curve-SP MIX 0.6

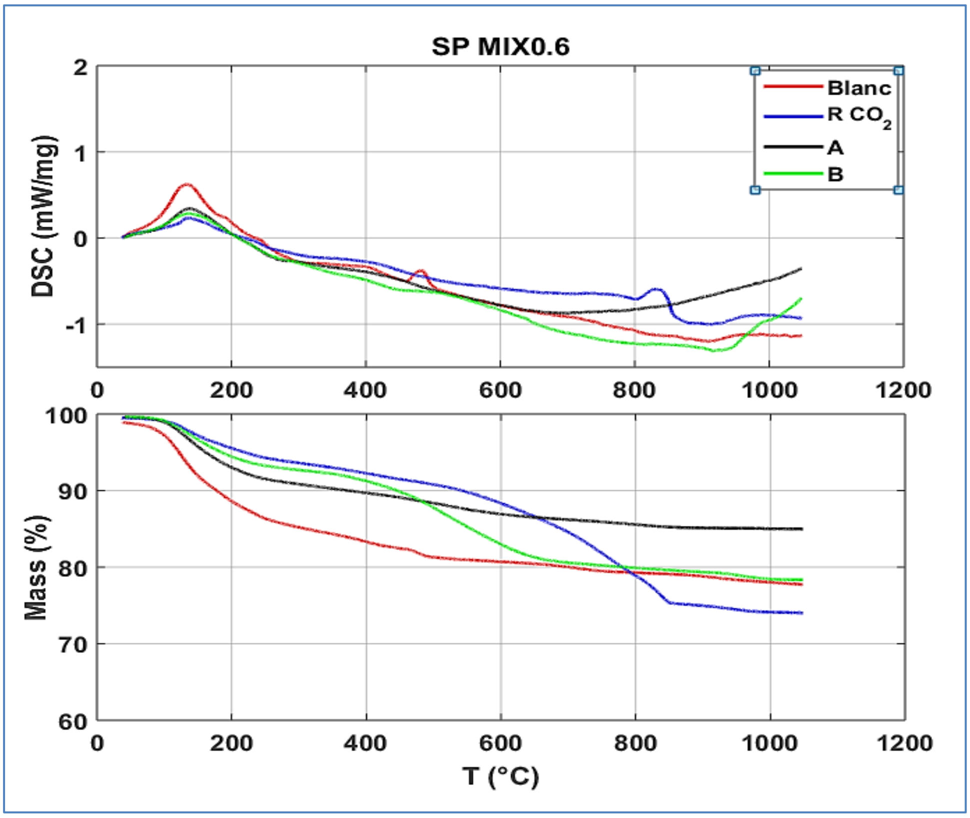

SP MIX 0.6			
Sample Treatment	Temperature interval (T°C)	Mass loss (%)	Process
Blanc	93-204	9.29	P1
	414-512	1.81	P2
	874-956	0.69	P3
RCO2	123-236	3.88	P1
	313-491	2.52	P2
	806-902	3.61	P3
	902-1048	1.46	Crystallization around 902°C
A	105-272	7.56	P1
	441-542	1.53	P2
	615-1048	2.15	Crystallization with multiple small peaks
B	106-262	5.8	P1
	441-487	1.75	P2
	745-889	0.85	P3
	889-1048	1.39	Crystallization around 900°C

	Process
P1	Water loss from C-S-H gel layers and from the dehydration of ettringite
P2	Dehydration of calcium hydrate(CH)
P3	Decarbonation of calcium carbonate (CaCO3).